

**An Experimental Investigation Into The
Passive Oxidation Of Particulate Matter In A
Catalyzed Particulate Filter**

By

Christopher Ryan Hutton

A THESIS

Submitted in partial fulfillment of the requirements

for the degree of

MASTER OF SCIENCE IN MECHANICAL ENGINEERING

MICHIGAN TECHNOLOGICAL UNIVERSITY

2010

Copyright © Christopher Ryan Hutton, 2010

This thesis, “An Experimental Investigation Into The Passive Oxidation Of Particulate Matter In A Catalyzed Particulate Filter”, is hereby approved in partial fulfillment of the requirements of the Degree of MASTER OF SCIENCE IN MECHANICAL ENGINEERING.

DEPARTMENT:

Mechanical Engineering – Engineering Mechanics

Signatures:

Thesis Co-advisor: _____

Dr. John H. Johnson

Thesis Co-advisor: _____

Dr. Jeffrey D. Naber

Department Chair: _____

William W. Predebon

Date: _____

Abstract

To investigate the passive oxidation of particulate matter within a catalyzed particulate filter (CPF), a series of experiments were performed on two engines. A total of ten tests were completed on a Cummins 2002 246 kW (330 hp) ISM and a Cummins 2007 272 kW (365 hp) ISL diesel engine. Five tests were performed on each engine in order to determine if using different engine technologies, which were certified to different emissions regulations, had an impact on the passive oxidation characteristics of the particulate matter (PM) in the CPF.

Prior to performing the experiments a new passive oxidation test method was developed. The new test method requires that the catalyzed particulate filter undergo a loading phase to reach a particulate matter loading of 2.2 ± 0.2 g/L. This initial loading phase was performed in order to ensure that each passive oxidation test was started at the same condition. Once the specified loading was obtained, the engine operating conditions were changed in order to investigate the variables of interest during passive oxidation of PM.

The important parameters when investigating passive oxidation of particulate matter are NO_2 flow rate into the CPF, exhaust temperatures, NO_2 concentration into the CPF, the NO_2/PM ratio in the exhaust, exhaust flow rate and total NO_x concentrations. With this in mind a test matrix was created to provide a wide range of the variables of interest. NO_2 concentrations into the CPF ranged from 45 to 170 ppm, CPF temperatures from 262 to 463°C, and NO_2/PM mass ratios from 6 to 59 during the performed tests.

In order to prepare the CPF for the passive oxidation portion of the test, the filter was loaded with particulate matter to 2.2 ± 0.2 g/L. The average CPF temperatures for this stage of the tests were similar for both engines at 268°C for the ISM and 264°C for the ISL. There was a difference however between the CPF inlet NO_2 concentrations, where on average the ISM had approximately three times more NO_2 than the ISL. The average particulate matter concentration and NO_2/PM ratio on the ISM were 15.4 mg/scm and 11.5 respectively. The average ISL PM concentration and NO_2/PM ratio were 17.4

mg/scm and 3.2. The average calculated reaction rate during loading was $3.04\text{E-}5$ 1/s and $2.45\text{E-}05$ 1/s for the ISL for the ISM respectively.

A statistical analysis of the average reaction rates of PM in the CPF for each engine was performed for the loading portions of the tests. The results show that the reaction rates are not statistically different. However, due to the differing CPF inlet NO_2 /PM ratios they should be and it has been determined that an unmeasured experimental variable differed between engines. A hypothesis is that the structure or composition of the particulate matter differs between engines.

Passive oxidation results show that the reaction rate of particulate matter by NO_2 is dependent upon temperature, NO_2 and NO concentrations along with exhaust flow rates. As temperatures increased the reaction rate also increased. This was the result of two contributions. As the temperature increased, the NO to NO_2 conversion efficiency of the DOC increased therefore increasing the NO_2 at the CPF inlet. This increased conversion efficiency does have an upper limit which is based upon temperature and the space velocity through the DOC. The second reason is that the higher temperature promoted an increased reaction between NO_2 and PM. While NO_2 concentrations are important to the passive oxidation of PM within a CPF, the temperature of the CPF is also a significant variable determining the rate of oxidation. NO_2 concentrations alone are not sufficient to effectively oxidize the particulate matter within the CPF. As an example, ISL Test 1 (CPF average temperature of 252°C and 151 ppm NO_2 at CPF inlet) had one of the highest NO_2 /PM ratios of the performed tests at 47.3:1. The average CPF temperature was the lowest of all testing and as a result, the calculated reaction rate was the lowest of the performed tests.

An important calculated value during the passive oxidation portion of the test is the ratio, NO_2 consumed/ NO_2 available at the inlet of the CPF. For ratios over one, more NO_2 is consumed than what is present at the CPF inlet. This indicates that the production of NO_2 is occurring within the catalyst on the filter substrate wall and the NO_2 is diffusing back into the PM cake layer. This increased NO_2 concentration in the cake layer significantly increases the PM oxidation rate under passive oxidation conditions. To

confirm this finding, Péclet numbers were calculated for the passive oxidation portions of the tests. The Péclet number is a dimensionless parameter group which relates the rate of advection of a substance to the rate of diffusion of the same substance which is driven by a concentration gradient. Péclet values less than one were calculated for each test confirming that the transport of NO_2 within the PM cake layer is diffusion dominated.

While reaction rates were calculated for the loading and passive oxidation portions of the test, a more detailed analysis is not possible with the current reaction rate model. Due to the finding that the Péclet number is near or below one indicates that the diffusion of NO_2 into the PM layer from the substrate wall is occurring. This prohibits the calculation of the pre-exponential factor and activation energy that is possible through using an Arrhenius plot of the reaction rates when the reaction rates were obtained with a constant concentration of an oxidant. A more detailed model with additional information will be needed to determine these values. In order to determine the contribution of passive oxidation to the total reaction rate, the effects of thermal and passive oxidation were determined using the MTU 1-D model.

Acknowledgements

There are several people and organizations that have given me the opportunity to write this thesis. I would like to thank both my professional and personal contacts that have been responsible for this accomplishment.

I would like to thank Dr. John Johnson and Dr. Jeff Naber for providing the opportunity to pursue my Masters degree and Dr. Jason Keith for being on my committee. I also would like to thank Joe Brault and his team at Cummins. This includes Krishna Chillumukuru, Abhijeet Nande, and Rayomand Dabhoiwala. They have been a valuable resource when questions have arisen during testing. I would also like to thank the MTU team members, past and present, who have aided me while testing and during data analysis. This includes Greg Austin, Harsha Shankar, Matt Heath, Ken Shiel, and Kiran C. Premchand. I would also like to extend thanks to the staff at MTU. The people who work here on a daily basis have provided me with information and support during the two years that I have been pursuing my Masters degree and without them it would not have been possible to finish in this timeframe.

Personally I would like to thank Dr. Christopher Mehall and Andreas Koutouzos for being there to support me when things were tough. Without the both of you I can truly say I would not be where I am today.

For financial support I would like to extend my appreciation to Cummins Inc. for the funding they provided for my fellowship and also to the U.S. Department of Energy for providing financial support, on contract no. DE-EE0000204, for this thesis.

Abbreviations

act.: Actual

C_{in} : Engine out PM concentration (mg/std. m^3)

CO : Carbon monoxide

CO₂ : Carbon dioxide

CPF: Catalyzed particulate filter

DOC: Diesel oxidation catalyst

EGR: Exhaust gas recirculation

HC : Hydrocarbons

m_C : Calculated clean mass of the CPF

m_{Load} : Measured mass of the CPF after a nominal CPF loading of 2.2 g/l is achieved

m_{Ret-Ld} : Calculated PM mass retained in the CPF after Stage 2 loading

m_{Ret-PO} : Calculated PM mass retained in the CPF after Passive Oxidation

m_{Ret-S1} : MTU 1-D model predicted PM mass retained in the CPF after Stage 1 loading

m_{Ret-S3} : Calculated PM mass retained in the CPF during Stage 3 loading

m_{s3} : MTU 1-D model predicted PM mass retained in the CPF during Stage 3 loading, [g]

m_{stage1} : Measured mass of the CPF after Stage 1 loading

m_{stage3} : Measured mass of the CPF after Stage 3 loading

NMHC: Non-methane hydrocarbons

NO : Nitrogen monoxide

NO₂ : Nitrogen dioxide

NO_x : The sum of nitrogen monoxide and nitrogen dioxide

O₂: Oxygen

Q : Exhaust volumetric flow rate (std. m³/sec)

RR_o : Global reaction rate for PM oxidation (s⁻¹)

scm: Standard cubic meters @ 25°C and 101.325 kPa

t_{eff} : Time of passive oxidation (s)

η_f : Filtration efficiency of the CPF

Table of Contents

Abstract	iii
Acknowledgements	vi
Abbreviations	vii
List of Figures.....	xiv
List of Tables.....	xviii
Chapter 1 Introduction	1
1.1 Introduction	1
1.2 Research Goals	3
1.2.1 Experimental Objectives.....	4
1.2.2 Modeling Objectives.....	4
1.3 Overview of Thesis	5
Chapter 2 Background and Literature Review	7
2.1 Diesel Emissions.....	7
2.2 Diesel Oxidation Catalyst.....	8
2.3 Catalyzed Particulate Filter	14
2.4 Active Regeneration.....	16
2.5 Passive Regeneration.....	17
2.6 Experimental and Modeling Results	22
2.7 Global Reaction Rate and Activation Energy.....	27
2.8 Summary	32
Chapter 3 Experimental Setup and Procedures	33

3.1 Test Cell and Components	33
3.1.1 Engines and Dynamometer.....	33
3.1.2 Diesel Oxidation Catalyst and Catalyzed Particulate Filters	36
3.1.3 Engine and Aftertreatment Layout.....	38
3.1.4 Fuel Properties	39
3.2 Measurement Systems and Procedures.....	40
3.2.1 Data Acquisition System	41
3.2.2 Temperature.....	42
3.2.2.1 DOC Thermocouple Layout	42
3.2.2.2 CPF Thermocouple Layout	45
3.2.3 Pressure	46
3.2.4 Air and Fuel Flow	47
3.2.5 Gaseous Emissions.....	48
3.2.6 Particulate Matter	50
3.2.7 Particle Size Distribution	51
3.2.8 PM Mass Retained in the CPF	54
3.3 Passive Oxidation Test Procedure-Overall Approach.....	56
3.4 Passive Oxidation Test Matrix	59
Chapter 4 Experimental Results	63
4.1 Emissions Analyzer Comparison	63
4.2 PM Concentrations	66
4.3 Gas Temperature Analysis	69
4.3.1 DOC Temperatures	69
4.3.2 CPF Temperatures.....	73

4.4 Stage 1 Loading.....	77
4.4.1 Gaseous Emissions.....	77
4.4.2 Pressure Drop Profiles	82
4.5 Stage 2 Loading.....	85
4.5.1 Gaseous Emissions.....	86
4.5.2 Particle Size Distribution	88
4.5.3 Reaction Rates and NO ₂ /PM Ratios	91
4.6 Passive Regeneration.....	95
4.6.1 Gaseous Emissions.....	96
4.6.2 Reaction Rates and NO ₂ /PM Ratios	96
4.6.3 Pressure Drop Profiles	104
4.7 Stage 3 Loading.....	106
4.7.1 Gaseous Emissions.....	106
4.7.2 Pressure Drop Profile	109
4.8 Overall Pressure Drop Profiles	111
4.9 CPF Comparison Test	115
Chapter 5 Summary and Conclusions	121
5.1 Summary	121
5.1.1 NO and NO ₂ Emissions Measurement.....	121
5.1.2 PM Concentrations and CPF Filtration Efficiency	122
5.1.3 Temperature Analysis	123
5.1.4 Stage 1 and Stage 2 Loading.....	124
5.1.5 Passive Oxidation.....	125
5.1.6 Stage 3 Loading	127

5.1.7 CPF Comparison Test.....	128
5.2 Conclusions	129
5.3 Recommendations	131
References	133
Appendix A. CPF Mass Balance	138
Appendix B. Engine Dynamometer Supplementary Data	141
Appendix C. Differential Pressure Transducer Calibration.....	143
Appendix D. Air Flow Calculations Using the Laminar Flow Element (LFE)	147
Appendix E. Development of Particle Size Distribution Measurement Technique.....	152
Appendix F. CPF Weighing Procedure	165
Appendix G. Passive Oxidation Test Procedure	168
Appendix H. NO ₂ Stoichiometric Reaction with Carbon	177
Appendix I. PM Concentrations	178
Appendix J. Additional Temperature Profiles	179
Appendix K. Gaseous Emissions Summary.....	180
Appendix L. DOC NO to NO ₂ Conversion Efficiencies	190
Appendix M. Particle Size Distribution Data	192
Appendix N. Mass Balances	202
Appendix O. NO ₂ Calculations	208
Appendix P. Filter Wall Velocities	210

Appendix Q.	Pressure Drop Profiles.....	212
Appendix R.	Relative Humidity to Absolute Humidity.....	217
Appendix S.	Standard Operating Procedures.....	218
Appendix T.	Persmissions to Use Copyrighted Material.....	220

List of Figures

Figure 2.1: Representative Conversion Efficiency of Reactants Across DOC [8]	10
Figure 2.2: Example of DOC Flow Through Channel.....	10
Figure 2.3: Example of CPF Wall Flow Structure.....	10
Figure 2.4: CPF NO to NO ₂ Conversion Efficiency Based upon Catalyst Material and Loading, [13].....	12
Figure 2.5: Reduction of NO ₂ by CO and HC, “X” indicates conversion [8].	14
Figure 2.6: Passive Regeneration Testing at 350°C and 505°C, [14].	23
Figure 2.7: Balance Point Temperature Testing Performed in Reference [20] with a DOC and DPF.	24
Figure 2.8: Transient Passive Regeneration Testing Performed in Reference [12].	25
Figure 2.9: Percent of Thermal Oxidation at Different DPF Inlet Temperatures, [25].	27
Figure 3.1: Heavy Duty Diesel Test Cell (North End).....	34
Figure 3.2: Exhaust Routing Used for Testing on the 2007 ISL	37
Figure 3.3: Exhaust Routing Used for Testing on the 2002 ISM, Picture from [33].....	39
Figure 3.4: Quadrant Definition within DOC	43
Figure 3.5: DOC Thermocouple Layout #1	43
Figure 3.6: DOC Thermocouple Layout #2, ISL	44
Figure 3.7: CPF Thermocouple Layout	45
Figure 3.8: Overview of the Four Main Stages of the Passive Oxidation Test Procedure	57
Figure 4.1: PM Concentration Variation Due to Absolute Humidity.....	68
Figure 4.2: DOC Radial Temperature Distributions.....	70
Figure 4.3: Magnitudes of Radial Temperature Differences in Quadrant II	71
Figure 4.4: Comparison of Radial Temperature Profiles for DOC Quadrant II and III.....	72
Figure 4.5: DOC Axial Temperature Profiles.....	73
Figure 4.6: CPF Temperature Profiles during ISL Test 3 Passive Oxidation	74
Figure 4.7: Average Temperature Profiles during Passive Oxidation for ISL Test 3.....	75

Figure 4.8: Radial Temperature Differences during Three Engine Operating Conditions.....	76
Figure 4.9: Summary of Gaseous Emissions during ISM Stage 1 Loading, 1800 rpm and 300 Nm	78
Figure 4.10: Summary of Gaseous Emissions during ISL 365 Stage 1 Loading, 2100 rpm and 195 Nm	79
Figure 4.11: NO to NO ₂ Conversion Efficiencies for Stage 2 Loading	81
Figure 4.12: NO to NO ₂ Conversion Efficiencies for Passive Oxidation	82
Figure 4.13: ISM CPF Pressure Drop Profiles during Stage 1	83
Figure 4.14: ISL CPF Pressure Drop Profiles during Stage 1	83
Figure 4.15: ISM vs. ISL Pressure Drop Comparison	85
Figure 4.16: Summary of Gaseous Emissions during ISM Stage 2 Loading	87
Figure 4.17: Summary of Gaseous Emissions during ISL Stage 2 Loading	88
Figure 4.18: Particle Size Distribution Weighted by Number for the ISM at 1800 rpm and 300 Nm.....	90
Figure 4.19: Particle Size Distribution Weighted by Volume for the ISM at 1800 rpm and 300 Nm.....	90
Figure 4.20: Mass Values Used in Determining Error Bars for the Reaction Rate Plot ..	93
Figure 4.21: Stage 2 Loading Reaction Rates	94
Figure 4.22: Average Particulate Matter Reaction Rates	97
Figure 4.23: Visual Depiction of NO ₂ Production	100
Figure 4.24: NO ₂ Production Trend	101
Figure 4.25: Pressure Drop Comparison of ISM Test 3 and ISL Test 4.....	104
Figure 4.26: Pressure Drop Profiles during Passive Oxidation on the 2002 ISM.....	105
Figure 4.27: Pressure Drop Profiles during Passive Oxidation on the 2007 ISL.....	105
Figure 4.28: Summary of Gaseous Emissions during ISM Stage 3 Loading	108
Figure 4.29: Summary of Gaseous Emissions during ISL Stage 3 Loading	108
Figure 4.30: CPF Pressure Drops for ISM Stage 3 Loading	109
Figure 4.31: CPF Pressure Drops for ISL Stage 3 Loading	110

Figure 4.32: ISM Test 3 and 4 Pressure Drop Profile	112
Figure 4.33: ISL Test 2 and 3 Pressure Drop Profile	113
Figure 4.34: ISL Test 1 Pressure Drop Profile	114
Figure 4.35: PM Mass Retained after Regeneration	114
Figure 4.36: Pressure Drop Comparison of Stage 2 and 3 Loading	115
Figure 4.37: ISL Test 2 and ISL Test 3 Pressure Drop Comparisons	117
Figure 4.38: ISL Test 2 and ISL Test 3 Aligned for Data during Passive Oxidation (Test 2 data was moved 21 min. earlier) Pressure Drop Comparisons.....	117
Figure 4.39: ISL Test 2 and ISL Test 3 Normalized Pressure Drops	119
Figure 4.40: ISL Test 2 CPF Temperatures	120
Figure 4.41: ISL Test 3 CPF Temperatures	120
Figure A.1: Control Volume for CPF Mass Balance	138
Figure B.1: Engine Dynamometer Dimensions (in.)	141
Figure B.2: Engine Dynamometer Torque (red) and Power Curve (blue)	142
Figure C.1: Calibration of LFE Differential Pressure Transducer through Labview.....	144
Figure C.2: Calibration of CPF Differential Pressure Transducer through Labview	145
Figure C.3: Calibration of DOC Differential Pressure Transducer through Labview	145
Figure D.1: Viscosity Correction Factor Plot	149
Figure E.1: Comparison of Old and New Carbon	152
Figure E.2: Dilution Ratio Function	153
Figure E.3: Variation of Dilution Ratio Dependent upon Sampling Location	155
Figure E.4: Dilution Process	156
Figure E.5: Background Particles in the Compressed Air	157
Figure E.6: Incorrect Method for Determining Thermodenuder Losses	160
Figure E.7: Method for Determining Thermodenuder Losses DCPF, Not Compensating for Dilution Ratio	161
Figure E.8: Method for Determining Thermodenuder Losses UDOC, Not Compensating for Dilution Ratio	161

Figure E.9: Method for Determining Thermodenuder Losses DDOC, Not Compensating for Dilution Ratio	162
Figure F.1: Cummins 2007 ISL After-treatment System	165
Figure G.1: Schematic Overview of Passive Oxidation Test Procedure	176
Figure J.1: Radial Temperature Profiles during Passive Oxidation for ISL Test 5	179
Figure J.2: Radial Temperature Profiles during Stage 2 for ISL Test 5.....	179

List of Tables

Table 1.1: History of U.S. EPA Heavy Duty Diesel Emissions Standards (g/bhp-h)	2
Table 2.1: Gas Feed Used During Reduction Experiment Shown in Figure 2.5 [8]	13
Table 2.2: Activation Energies for NO ₂ Oxidation of PM	31
Table 3.1: Engine Specifications	35
Table 3.2: DOC and CPF Specifications	36
Table 3.3: ULSD Fuel Properties Used During Testing.....	40
Table 3.4: Heating Value, Hydrogen and Carbon Content Testing Performed by Paragon Laboratories	40
Table 3.5: Summary of National Instrument's Hardware.....	41
Table 3.6: DOC, CPF and Exhaust System Thermocouple Specifications	42
Table 3.7: Pressure Transducer Specifications	46
Table 3.8: Semtech DS Emissions Bench Specifications	49
Table 3.9: Pierburg Emissions Bench Specifications	49
Table 3.10: Span Gas Values	49
Table 3.11: Selected Engine Operating Conditions	61
Table 3.12: Passive Oxidation Test Matrix with Experimental Values	62
Table 4.1: Post CLD repair Testing Engine Out Emissions.....	65
Table 4.2: Emissions Analyzer Comparison Test Results (wet measurements).....	65
Table 4.3: Experimental PM Concentrations.....	67
Table 4.4: Test Cell Conditions during Passive Oxidation Testing.....	68
Table 4.5: Calculated CPF Filtration Efficiencies	69
Table 4.6: Comparison of Stage 1 Emissions from ISM (1800 rpm and 300 Nm) and ISL (2100 rpm and 195 Nm)	78
Table 4.7: Conversions Efficiencies across the DOC for Stage 1 Loading	80
Table 4.8: NO to NO ₂ Conversion Efficiencies during Performed Testing	80
Table 4.9: Comparable Passive Oxidation Tests	81

Table 4.10: T-Statistic and 99% Confidence Interval for Stage 1 Pressure Drop Comparison.....	84
Table 4.11: Comparison of Stage 2 Emissions from ISM and ISL	87
Table 4.12: Conversions Efficiencies Across the DOC for Stage 2 Loading.....	88
Table 4.13: Stage 2 Loading Reaction Rates	92
Table 4.14 : T-Statistic and 99% Confidence Interval for Stage 2 Reaction Rate Comparison.....	94
Table 4.15: Passive Oxidation NO ₂ /PM Ratios and Percent PM Oxidized	97
Table 4.16: NO ₂ Concentrations during Passive Regeneration Portions of Completed Tests.	98
Table 4.17: Simulation Results of Selected Passive Oxidation Testing from Reference [41].....	103
Table 4.18: Selected variables during ISM Test 3 and ISL Test 4 Comparison.....	103
Table 4.19: Exhaust Mass Flow Rates and CPF Average Temperatures.....	104
Table 4.20: Comparison of Stage 3 Emissions from ISM and ISL	107
Table 4.21: Conversions Efficiencies across the DOC for Stage 3 Loading	109
Table 4.22: PM Concentrations for Stage 3 Loading	110
Table 4.23: Summarized Passive Oxidation Values	116
Table C.1: Differential Pressure Transducer Scaling Factors	146
Table D.1: Density Correction Factor Table for Humid Air (Meriam Instruments Manual).....	150
Table E.1: Dilution Ratios Based upon Sample Location.....	154
Table G.1: Engine Speed and Load for Initial Engine Warm Up	169
Table G.2: Engine Speed and Load for Stage 2 Engine Warm Up	172
Table L.1: Tabulated DOC NO to NO ₂ Conversion Efficiencies.....	191

Chapter 1 Introduction

1.1 Introduction

Over the course of the last century, the diesel engine has become a popular engine in many stationary and mobile vehicles. In the United States the majority of on-road diesel engine usage is in medium and heavy duty applications. The thermodynamic efficiency of greater than 40% of a diesel engine makes it the preferred powerplant for heavy-duty vehicles.

However, with the increased usage of this engine, concerns developed about the possible health related effects that excessive exposure to exhaust emissions could cause. Along with the negative impact on human health of diesel exhaust exposure, the ever increasing environmental awareness of the public has driven regulations that decrease the tailpipe emissions from diesel engines. The United States regulatory agency that is responsible for developing the emission standards for diesels is the Environmental Protection Agency (EPA). Over the course of many years the allowable tailpipe emissions from heavy-duty diesel powered vehicles have been reduced drastically. The time history of these reductions for heavy duty on-road applications can be seen in Table 1.1.

Starting in 2007, an order of magnitude reduction, 0.10 to 0.01 g/bhp-h, was required by manufacturers to meet the particulate matter (PM) standards that were specified for that year. The two other standards that were reduced by a significant amount were oxides of nitrogen (NO_x) and non-methane hydrocarbons (NMHC). The reductions in emissions for these species were implemented over the next three years on an incremental basis with the final regulations being implemented in 2010. To meet the EPA standards, engine manufacturers have addressed the issue by several different methods.

Table 1.1: History of U.S. EPA Heavy Duty Diesel Emissions Standards (g/bhp-h)

	1991-1993	1994-1997	1998-2003	2004-2006	2007 Standard	Phase-In Model Year			2010 Standard
						2007	2008	2009	
NO _x	5.0	5.0	4.0	2.0**	2.0	1.0	1.0	1.0	0.20
NO _x + NMHC	-	-	-	2.4*	-	-	-	-	-
NMHC	-	-	-	0.5**	1.4	0.7	0.7	0.7	0.14
HC	1.3	1.3	1.3	-	-	-	-	-	-
CO	15.5	15.5	15.5	15.5	15.5	15.5	15.5	15.5	15.5
PM	0.25	0.10	0.10	0.10	0.01	0.01	0.01	0.01	0.01
Formaldehyde	-	-	-	-	0.01	0.01	0.01	0.01	0.01

* option #1 for 2004-2006 NO_x emissions regulations

** option #2 for 2004-2006 NO_x emissions regulations

The engine hardware and control strategy has changed over the course of the years to meet the emissions standards listed in Table 1.1. Parameters such as injection timing and exhaust gas recirculation flow have been adjusted to tailor the engine exhaust emissions to meet federal emissions standards. Another strategy that has been employed is the addition of engine components that are highly adjustable. This would include variable geometry turbochargers and electronically controlled fuel injectors [1].

Even with the technological advancement of engine components and control strategies, manufacturers have been required to develop other solutions to meet emissions standards. An effective method for meeting the 2007 PM standards was the use of a diesel particulate filter or catalyzed particulate filter (CPF). The filtration efficiency of these filters can approach 99%. Although effective, there is an additional cost associated with the use of these filters both at the time of implementation and during engine operation.

The CPF is generally used with a diesel oxidation catalyst (DOC) and installed into the exhaust as a system. The DOC is connected upstream of the CPF in the exhaust system and serves many functions. As the exhaust stream passes over the precious metal washcoat within the DOC, chemical reactions occur oxidizing the CO, HC, and NO. Another important function of the DOC is the oxidation of hydrocarbons (HC) that

are injected upstream of the DOC to create an exotherm during an active regeneration of the CPF. The temperature increase generated by this reaction is used to periodically oxidize the PM retained in the CPF thereby reducing back-pressure experienced by the engine and improving performance.

While introducing HC into the exhaust stream is effective at oxidizing the PM in the CPF, the fuel used during this process does not produce useful work. By passively oxidizing the PM within the CPF the frequency of active regenerations will be reduced. This reduction in active regenerations will decrease the fuel penalty experienced during this filter clean out strategy. Passive oxidation occurs through a chemical reaction involving gaseous NO_2 and solid PM within the CPF. This method of filter regeneration is preferred since it uses combustion by-products to oxidize the PM within the CPF thus reducing the necessity of HC dosing and the associated fuel penalty.

Passive oxidation (PO) of PM within the CPF will not eliminate the need to perform active regenerations but, by fully understanding the important variables responsible for passive oxidation of PM, operating strategies can be developed to maximize the use of this technology reducing the need for active regenerations. A thorough explanation of the PO process and its dominant variables will be discussed within this thesis.

1.2 Research Goals

The main goals of the research is to develop a test procedure to collect, characterize and then to analyze the PM passive oxidation data and determine the impact of using different engine technologies on the passive oxidation of particulate matter. Along with the experimental portion of the research, a modeling effort will follow which will use the data collected from the experiments to calibrate a 1-D CPF computer simulation program. The objectives for the simulation portion of the research are also listed below but will not be addressed within this thesis as they are the responsibility of modeling team associated with the DOE project.

1.2.1 Experimental Objectives

- Develop a test procedure to collect high quality data that can support the modeling effort and PM oxidation analysis effort
- Using a Cummins 2002 ISM and a 2007 ISL, determine if the PM created by these engines oxidizes passively in a similar manner
- After the experiments are performed on the 2002 ISM, install the 2007 ISL
- Determine the PM reaction rates at the selected operating conditions based upon the filter loading, temperature, and NO_2/PM ratio
- Quantify the effects that temperature has on passive PM oxidation rates
- When performing tests with the same the engine using the same exhaust flow rate and temperature, determine if using a different catalyzed particulate filter has an impact on the pressure drop, reaction rate, and PM loading characteristics produced by the engine

1.2.2 Modeling Objectives

- Calibrate the MTU 1-D 2-Layer CPF model to determine if different calibration parameters are needed to accurately model the experimental data
- Determine at what temperature thermal oxidation becomes the dominant pathway for PM oxidation
- Calculate the passive, thermal, and total reaction rate during the experiments using the simulation model and compare these values with the experimentally determined reaction rates
- Quantify the effects that the NO_2/PM ratio, temperature, PM concentration, and exhaust flow rate have on passive PM oxidation rates
- Fit the data to a reaction rate model to determine the activation energy required to passively oxidize PM within a CPF and compare the calculated value to previously published and utilized models

- Determine the contribution of the wall, cake and the channel pressure drops along with the percentages of thermal and passive oxidation out of the total reaction rate
- Develop an understanding of NO₂ back diffusion on the PM passive oxidation rate

1.3 Overview of Thesis

This chapter provides an introduction to the material which will be included within the body of the thesis. A short introduction of the emission regulations dictated by the EPA and the history of steadily decreasing limits is shown in Table 1.1. Several methods that have been used to partially reduce engine out emissions have been introduced. The purpose of the aftertreatment system is explained and the main functions of this system are discussed along with the individual objectives of this research.

Chapter 2 provides information so the reader can understand why research in this area is important. Background information was collected from previous research conducted at Michigan Technological University (MTU) along with technical articles from different sources. This information will be used to support findings in the literature and will include an explanation of the operating principles and characteristics of the DOC and CPF.

Chapter 3 explains the test cell layout and experimental procedure used during tests. An overview of the testing facilities and its capabilities will be presented, including details of the ISM and ISL engines. The description of the test cell will include an explanation of the various items used for monitoring and recording the data during experiments. The specific instruments and methods used to determine fuel flow, exhaust flow and PM concentrations will be discussed. Also included in this section will be new procedures that have been developed and implemented into the testing process during this research. An explanation will be provided on how the test matrix was developed along with difficulties encountered during the implementation of the test matrix.

Chapter 4 will detail the results of the experiments. An explanation of how the data were collected and analyzed will be provided. This will include a number of difficulties encountered while collecting data. The mass balances used for the experimental process will be presented and discussed.

Chapter 5 provides a summary of the test results. Conclusions based on the analyzed data are discussed. Recommendations on how to improve the test process are presented along with supporting information to justify these suggestions.

Chapter 2 Background and Literature Review

The purpose of this chapter is to provide the reader with knowledge of diesel engine emissions and the passive oxidation of particulate matter (PM) by NO_2 within a catalyzed particulate filter (CPF). This will include a brief history of the specific aftertreatment system which includes a diesel oxidation catalyst (DOC) and a CPF. The prevalent reactions that occur within the DOC and CPF will be introduced along with an explanation of the operating principles used within these devices. After reviewing Chapter 2 the reader will be able to understand why certain parameters including temperature, NO_2 concentration, NO_2 flow rate (mg/min) into the CPF along with the NO_2/PM ratio of the exhaust, were varied during testing to investigate the change in passive oxidation rates.

2.1 Diesel Emissions

Over the course of a century, the diesel engine has developed into a reliable power plant which has been used in many applications including passenger cars, heavy duty trucks, and mobile power generation. While the technology used on this engine has steadily changed, so have the regulations that limit the amount emissions that the engine can produce. As shown in Table 1.1, the heavy duty (HD) diesel emissions standards have become more restrictive over time. This has created many challenges for engine manufacturers. In order to meet the emission standards, the original equipment suppliers have approached the challenge by two methods, on engine and post engine emissions treatment.

The emissions from a diesel engine are of two types, e.g. gaseous and particulate emissions. The gaseous species of interest are CO, CO_2 , HC, H_2O , NO_x ($\text{NO} + \text{NO}_2$) and O_2 . Currently only, CO, HC, and NO_x are regulated by the U.S. 2010 HD emissions standards. Also regulated is the particulate matter (PM) from the engine which can vary in size with diameters ranging from 0.010 to 1.0 μm [2]. Although the PM from the engine

varies in size and can be measured, the 2007 emission standard for PM is based on the mass of particles exiting the aftertreatment system and allows a maximum 0.01 g/bhp-h. In addition to the current regulations, there is a recent proposal by EPA and NHTSA to regulate fuel consumption and CO₂ emissions.

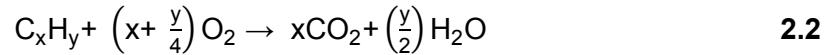
The very small particles from diesel exhaust have been shown to increase certain health risks so a conscious effort has been made to reduce the amount of particles entering the atmosphere through the use of a diesel particulate filter. The filter is very effective at removing PM from the exhaust stream and can achieve filtration efficiencies up to 99% [3]. Continuous removal of these particles from the exhaust can result in an increased engine backpressure due to the trapped particles acting as a flow restriction to the exhaust. This increased flow restriction decreases performance and reduces fuel economy [4, 5]. In order to avoid the aforementioned penalties, a method is required to periodically clean out the filter.

Two methods to perform the clean out of the CPF are active and passive regeneration. Active regeneration is a method that introduces additional hydrocarbons into the exhaust system either by late in-cylinder post injection or by an auxiliary fuel injector mounted in the exhaust system. The additional hydrocarbons are used to increase the temperature of the exhaust above 500°C to promote PM oxidation within the CPF, a detailed description of this process can be found in section 2.4. The second method, which is termed passive oxidation, uses NO₂ from the engine exhaust to oxidize the PM within the CPF. This oxidation reaction occurs at temperatures less than that of active regeneration, 250°C to 400°C, and is directly dependent upon engine operating conditions due to the NO₂ and temperature dependency. Passive regeneration is discussed in detail in section 2.5.

2.2 Diesel Oxidation Catalyst

The DOC is the first part of the aftertreatment system and therefore is exposed to the engine out exhaust gas stream. The main function of the DOC is to convert engine out

exhaust gas species (HC, CO) into CO₂ and H₂O and convert NO to NO₂. This occurs by exhaust gases flowing over a precious metal catalyst which promotes certain chemical reactions. Three main global reactions occur within the DOC and are listed below in equations 2.1-2.3 [6, 7] where the x and y refer to the average molecules of carbon and hydrogen in the diesel fuel respectively.



The reactions occurring across the DOC do not always go to completion. For equation 2.1 and 2.2, less than 100% conversion efficiency of the reactants to the products is often seen. A representative figure of the conversion efficiencies of the above equations can be seen in Figure 2.1, [8]. The conversion efficiency across the DOC can be dependent upon many factors. The reactant inlet concentrations, catalyst loading or type, residence time, temperatures of the exhaust gas and DOC along with competition for reactant sites on the DOC by other species all play a role in determining the conversion efficiencies. As an example, the conversion of NO to NO₂ is limited at temperatures below 350°C by reaction kinetics and by thermodynamics at higher temperatures. This is visualized by the peak of the NO to NO₂ conversion efficiency in Figure 2.1.

The DOC used for the performed experiments was of a flow through monolith design constructed of cordierite with 62 cells/cm² (400 cells/in²). Two representative channels of this design can be seen in Figure 2.2. The reactions represented by equations 2.1-2.3 which occur within the DOC can also occur within the CPF. Due to this similarity, an investigation into the conversion efficiencies of different support structures was performed in reference [9]. The flow through design was compared with a wall flow structure, shown in Figure 2.3, to determine which design had the largest conversion

efficiency of HC. The comparison showed that the two structures had different mass flow processes.

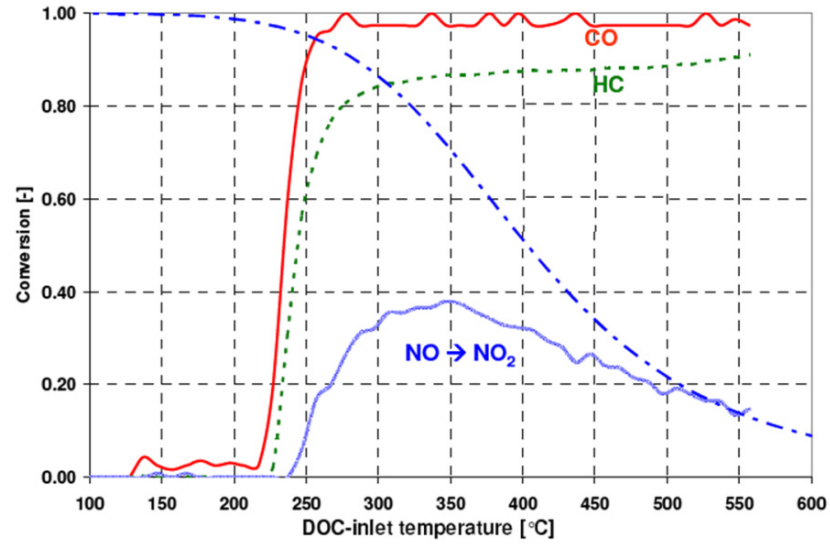


Figure 2.1: Representative Conversion Efficiency of Reactants Across DOC [8]



Figure 2.2: Example of DOC Flow Through Channel

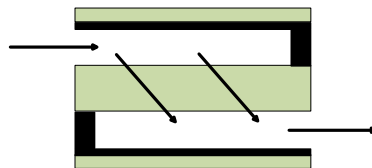


Figure 2.3: Example of CPF Wall Flow Structure

The flow through channel transports reactants via a diffusion process while the wall flow filter uses convection [9]. The method of mass transfer directly affects the residence time of the species and therefore the conversion efficiency. With similar catalyst loading and volume for the two structures, the additional residence time provided by the flow through design increased HC conversion efficiencies up to 22% under the same operating conditions [9]. Researchers in reference [6] found similar results and demonstrated that the exit CO concentration from a DOC (flow through design) was lower than that of a CPF (wall flow design) when both devices had similar catalysts loading and dimensions. The results from these studies can be extended to other reactions within the DOC such as the conversion of NO to NO₂.

For the current study, the rate of PM passive regeneration is dependent upon NO₂ concentrations and temperature, therefore the most important reaction is represented by equation 2.1. Since engine out NO₂ ranges in concentration from 5-15% of the total NO_x [10, 11, 12], it is important to be able to catalytically increase the NO₂ concentration of the exhaust through the use of a DOC. Experiments have been performed to determine if the use of a DOC was required in an aftertreatment assembly [6]. It was demonstrated that for similar PM loadings of the filter, the regeneration efficiency during HC dosing of a system with only a CPF was higher than that of a system with a DOC and CPF. However, since the species that usually are oxidized within the DOC were being oxidized within the CPF, higher temperatures and different temperature gradients were experienced in the CPF without a DOC.

As a result of these differences, the PM distribution in the filter that did not use a DOC was non-uniform and concentrated towards the front of the filter after the active regeneration event [6]. Although passive regeneration is an efficient way to oxidize PM, the need for an alternative way to periodically completely clean the CPF is necessary, because in most applications the passive oxidation of PM is not sufficient to keep the filter clean. The chosen method is active regeneration and the maldistribution of PM is avoided because engine manufacturers routinely employ the use of a DOC in manufactured aftertreatment systems that use HC dosing.

The design of the substrate can have an effect on the conversion efficiencies of gaseous reactants across the DOC. Also, direct comparisons can be made between results obtained on a DOC and CPF. In reference [13], a comparison was made between two catalytic coatings, platinum and palladium used on a CPF. Although expensive, platinum is widely used as the catalytic coating on both the DOC and CPF. A less costly option is palladium, but this material has shown to be less robust than platinum [13]. Results from testing in reference [13] can be seen in Figure 2.4. The data demonstrates how changing catalyst material and loading can affect the conversion efficiencies across a DOC. Since NO_2 concentrations into the CPF are extremely important, the catalyst type and loading should be optimized in order produce high conversion efficiencies while also keeping costs down.

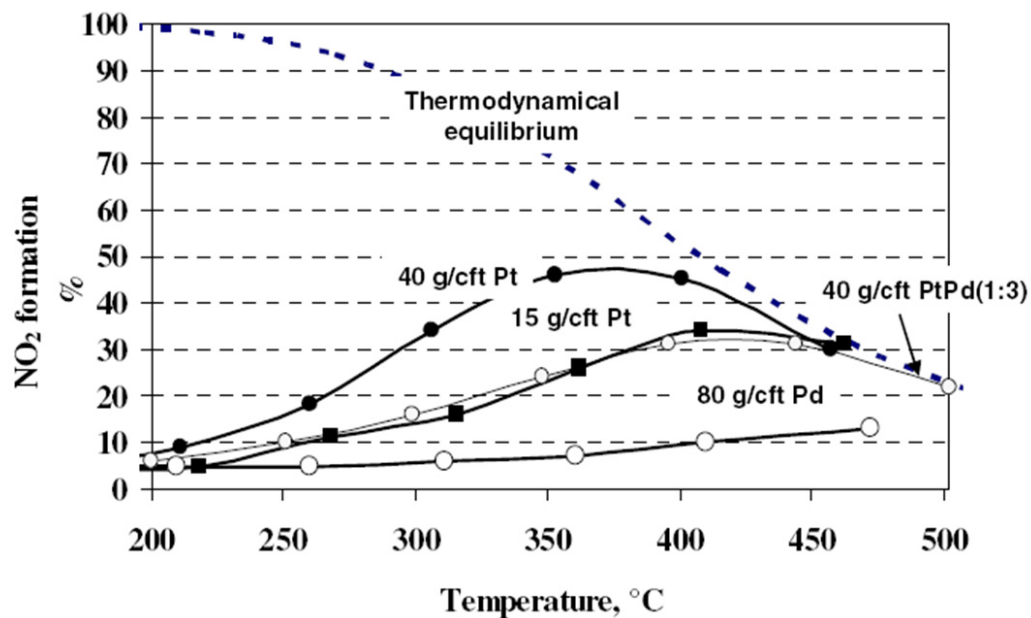


Figure 2.4: CPF NO to NO_2 Conversion Efficiency Based upon Catalyst Material and Loading, [13].

Since the production of NO_2 is an important function of the DOC in diesels, mechanisms that reduce or prevent this reaction from occurring need to be determined. Competition for catalytic sites can be a significant factor in the reduction of NO_2 . Results shown in

references [8, 14] demonstrate that HC dosing in the engine exhaust significantly reduces the amount of NO₂ produced by the DOC. This reduction of conversion efficiency is attributed to the increased HC concentrations competing for catalytic sites and the increased temperature of the DOC which thermodynamically limits the reaction of NO to NO₂ [8, 12, 15].

The NO₂ concentration can also be decreased in the presence of reductants [8] at engine out concentrations experienced during normal engine operation. Testing on a reactor with an inlet gas stream composed of the species and concentrations listed in Table 2.1 showed that in the presence of HC and CO, NO₂ is reduced to NO. This can be seen in Figure 2.5 where at the beginning of the test, represented by the left side of the figure, the NO₂ is immediately reduced to approximately 10 ppm. Figure 2.5 also shows that the oxidation of CO and HC are complete before the oxidation of NO to NO₂ is completed. This indicates that there is a reaction preference within the catalyst. After the oxidation of CO and HC, the oxidation of NO to NO₂ is completed. Total NO_x concentration at the end of the test is approximately 80 ppm but originally 100 ppm of NO₂ was in the gas feed. This indicates that some losses occurred during the initial reduction of NO₂ to NO by the HC and CO, this is hypothesized to be the reduction of the NO_x to N₂ [8]. This loss of NO₂ increases as a DOC ages, possibly due to the decreased conversion efficiency across the DOC of CO and HC [8].

Table 2.1: Gas Feed Used During Reduction Experiment Shown in Figure 2.5 [8]

Species	Concentration
NO ₂	100 ppm
C ₂ H ₄	300 ppm C1
CO	1000 ppm
H ₂	333 ppm
H ₂ O	4.5%
CO ₂	5%
N ₂	Balance

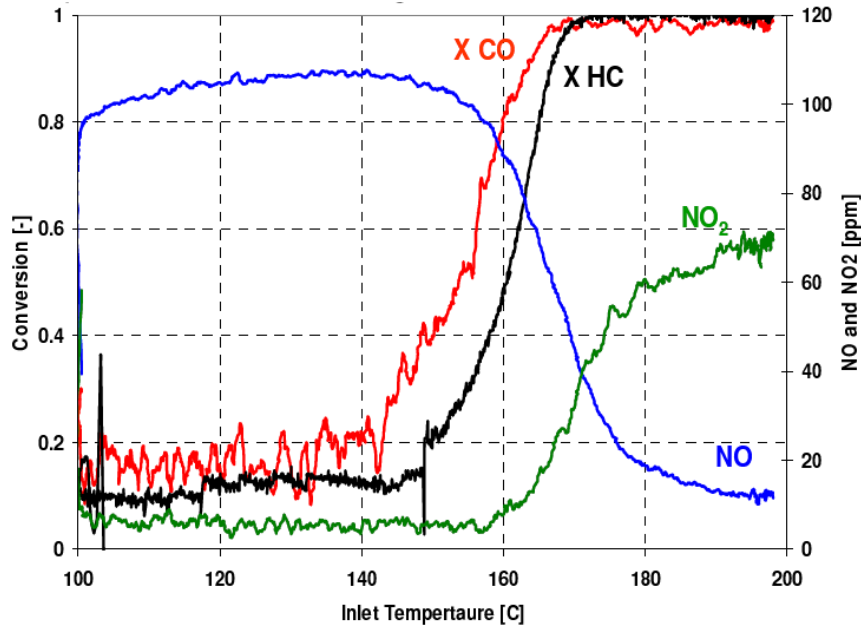


Figure 2.5: Reduction of NO_2 by CO and HC, “X” indicates conversion [8].

2.3 Catalyzed Particulate Filter

The second component in the aftertreatment system is a diesel particulate filter. The filter used during experiments is a wall flow through design manufactured from a ceramic material called cordierite. The filter is coated with a catalyst to promote oxidation of certain gaseous species. If catalysts are applied to the ceramic substrate, the filter is then termed a catalyzed particulate filter (CPF).

The CPF has several functions, one of which is to filter the PM in the exhaust stream. This is accomplished by collecting the engine out PM to ensure that the concentration of PM is below 0.01 g/bhp-h. As with the DOC there are several reactions that take place in the CPF, equations 2.1-2.3 occur if there are reactants available. Aftertreatment systems with a DOC oxidize the majority, if not all, of CO coming from the engine so this reaction in the CPF is negligible under most normal engine operating conditions. During active regenerations with post turbocharger HC injection, average HC concentrations in the

range of 3000-4500 ppmC1 can be experienced at the CPF inlet dependent upon the fuel type, exhaust flow rate and required CPF inlet temperature [16]. Therefore, the HC and CO chemical reaction represented by equations 2.2 and 2.3 are important during this operating condition.

The oxidation of NO to NO₂ can occur within the CPF, dependent upon operating conditions of the system. Additional reactions occur within the filter to oxidize the trapped PM and will be discussed in section 2.5. Experimentation performed in reference [3] showed that along with the significant reduction in particulate matter, the use of a CPF also reduced unregulated chemical compounds including formaldehyde, acetaldehyde and fluoranthene [3].

The addition of a DOC and CPF in the exhaust stream does have some drawbacks. Both of these devices act as a flow restriction which can increase the back pressure on the engine and increase fuel consumption. This effect is minor when considering the DOC but the flow restriction created by the CPF can be significant as the filter reaches high levels of loading. The CPF pressure drop varies depending on the mass of PM in the filter wall and cake layer, and the exhaust flow rate.

A CPF that is completely clean generates a pressure drop from friction and drag as the exhaust flow passes through the filter inlet channels, outlet channels, and wall. The initial pressure drop across a clean CPF is non-linear and is shown to be a result of deep bed filtration [17] with PM in the wall. This initial non-linear pressure drop transitions to a liner pressure drop as a cake layer of PM is formed on the CPF inlet channels. After the PM cake layer is formed, under steady operating conditions, the pressure drop will continue to be an increasing linear function in most cases unless the flow rate changes or a point is reached where the mass retained in the CPF is constant and the incoming PM is equal to the PM oxidized.

Ash collected, that is a byproduct of engine oil consumption, in the CPF can affect the pressure drop across the CPF. It has been shown that the accumulation of ash does generate a flow restriction in the CPF which increases engine backpressure. The

additional back pressure generated by the collected ash is not solely dependent upon the mass of the ash but also depends upon the chemical characteristics and size of the deposits [18].

2.4 Active Regeneration

The integration of a particulate filter into the exhaust system was an extremely important step in meeting the emission standards. However, due to the high efficiency of the filter it does require periodic cleaning via active regeneration since passive oxidation is not sufficient in most applications to completely oxidize the PM in the CPF. There are two driving factors for this periodic maintenance. First, as the filter collects PM, the backpressure on the engine increases which increases fuel consumption and decreases performance. Second, if the filter collects an excessive amount of PM it is possible for a runaway regeneration to occur. When this event occurs during low flow rates, localized high temperatures result which can damage the ceramic substrate or catalytic coating and lead to filter failures.

Several researchers at MTU have performed experiments using active regeneration [4, 16, 19], so the topic will not be covered in detail within this thesis. The interested reader is referred to the referenced publications. What will be provided is an introduction to the topic and how it relates to passive regeneration which is the subject of the thesis. Active regeneration of the CPF increases the temperature of the CPF via HC dosing into the exhaust stream prior to the DOC. This dosing of fuel can be performed through the use of an auxiliary injector or by late in-cylinder dosing. The additional hydrocarbons are oxidized across the DOC to increase the temperature of the exhaust to above 550°C and therefore the temperature of the CPF. This increased temperature thermally oxidizes the collected PM in the filter with O₂ and after a period of 10 to 15 minutes provides for a clean filter.

The PM is oxidized by thermal oxidation, this method refers to the direct oxidation of PM by oxygen [17]. This method of oxidation starts to occur as the exhaust temperature

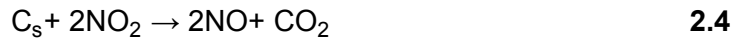
reaches approximately 500°C [20]. Due to the high temperatures involved, this method is very effective at cleaning out the CPF. Unfortunately this strategy increases fuel consumption since the hydrocarbons oxidized to generate the increased temperatures in the system do not produce any useful work. Simulations performed in reference [21] showed that the fuel penalty associated with performing an active regeneration was larger than the fuel penalty associated with increased engine backpressure from a loaded filter. Active regenerations are necessary however since high PM loading of the CPF can result in runaway regenerations.

To maximize the use of fuel injected into the exhaust, it has been shown that the largest amount of PM is oxidized with the least amount of fuel when higher CPF inlet temperatures and PM loadings are used for active regenerations [4, 16, 19, 21]. This combination of variables provides for a faster reaction rate thereby oxidizing the most PM with the least amount of fuel. After cleaning the filter, the pressure drop is reduced and fuel consumption decreases. On some occasions only a portion of the PM is removed from the filter, this is termed a partial regeneration. If a partial regeneration is performed, the resultant pressure drop can be less than that of a clean filter that has PM in the substrate wall due to the filtration effect provided by the PM cake layer on the inlet channels of the CPF [4, 16]. This further reduction of backpressure allows for the opportunity of decreased fuel consumption.

2.5 Passive Regeneration

Passive regeneration is the oxidation of PM by the gaseous species NO₂. This type of PM oxidation is the dominant mechanism over the temperature range of 250 - 400 °C [11]. The reactions associated with this process are shown by equations 2.4-2.5. By using a diesel particulate filter without a catalytic coating, researchers in [20] showed that the reaction represented by equation 2.4 was dominant. This was demonstrated by the very low levels of CO concentrations downstream of the diesel particulate filter during regeneration events. This conclusion could not have been made if a catalyzed

particulate filter was used during the study. If the experiment was performed while using a CPF and if equation 2.5 was dominant oxidation reaction, the catalyst coating would have oxidized the CO into CO₂ reducing downstream CO concentrations obscuring the results of the experiment and possibly leading to the conclusion that equation 2.4 was the dominant oxidation method.



During the development of the aftertreatment assembly, several combinations of components were tested. Some examples include a DOC with an un-catalyzed diesel particulate filter, a CPF only, and the combination that was used during this testing, a DOC and CPF. The combination of a DOC and CPF is widely used for on-road vehicles as it allows a wide range of operating conditions with the versatility of both passive and active regeneration capabilities.

The reactions represented by equations 2.4 and 2.5 which depict passive regeneration, involve two main components, carbon in the form of PM and gaseous NO₂. Depending upon the operating conditions of the engine, fuel type used and combustion fundamentals, the PM exiting the engine will vary in structure. An example is PM that contains adsorbed hydrocarbons. These hydrocarbons are combustion by-products that result from incomplete combustion of diesel fuels and lubricating oils. The structure of the PM exiting the engine and measured in a dilution tunnel has been shown to vary based upon the quantity of soluble organic fraction adsorbed on the particles [22]. Additionally, a comparison of the engine out PM from a 2004 and 2007 Cummins ISX showed that for the 2004 engine 44% of the total PM mass emitted was organic while the fraction of organic mass for the 2007 engine was only 35% [23]. The remainder of the PM consisted of sulfate, nitrate and ammonium ions, elemental carbon and trace metallic compounds.

The passive regeneration of PM is achieved through two mechanisms. The gaseous NO₂ travels into the PM cake layer via the exhaust gases and the PM is in direct contact

with the catalyst that is deposited on the ceramic substrate. While passive regeneration is a very efficient method to reduce the CPF PM loading, it does take place as a localized reaction and therefore can lead to heterogeneous PM distributions [24, 25]. To expand on this statement, it has been shown that the flow through a CPF is not uniform and can vary based upon filter loading and history. Since the PM reaction with NO₂ is flow rate dependent, areas within the filter that experience higher flow rates will also experience higher PM oxidation rates possibly leading to a PM distribution that is not homogeneous.

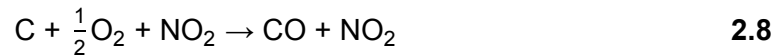
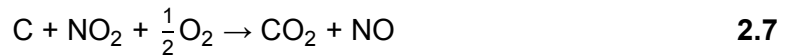
Since the concentration of NO₂ can vary within the CPF as it passes through the PM cake layer and wall, there is the possibility of NO₂ diffusion from areas of low concentration to areas of high concentration. This flow of NO₂ against the exhaust flow is termed back diffusion of NO₂ or NO₂ turn-over. This phenomenon is dependent upon the local Péclet number within the PM layer and substrate wall [26, 27]. There are two Péclet numbers referenced in literature, one used in the transfer of heat and the other which is used in diffusion calculations. The Péclet number in this instance is a dimensionless parameter group which relates the rate of advection of a substance to the rate of diffusion of the same substance which is driven by a concentration gradient. The Péclet number is shown in equation 2.6. The characteristic length L, is the thickness of the PM cake layer, V is the wall velocity and D is the mass diffusion coefficient which can be obtained through the modeling efforts associated with the performed experiments or published literature.

$$Pe_L = \frac{LV}{D} \quad 2.6$$

This topic is routinely discussed in modeling papers as it could be a contributor to local NO₂ concentrations and therefore PM oxidation. Experimentally, the determination of this event is difficult due to the lack of information on the mass diffusion coefficient and local velocities in the PM and wall. Simulations performed in references [26, 27] resulted in calculated Péclet numbers of 0.2-2.5 [26] and 0.03 [27]. A value less than 1 would indicate that the diffusion process is possible and the NO₂ could be reacting with PM upstream of the substrate wall. When calibrating the simulation model in reference [10]

with experimental engine data, it was shown that when NO₂ back diffusion was included in the model, the calculated reaction rates more closely matched the experimental rates. When this additional term was excluded from the calculations there was a significant difference between the experimental and simulated rates.

Additional contributions to the oxidation of PM can occur from gaseous species besides NO₂. Due to the implementation of the DOC in the aftertreatment system however, the concentration of hydrocarbons entering the CPF during passive regeneration is minimal and provides no significant contribution to the regeneration of PM [12]. CO concentrations were frequently zero entering the CPF during performed tests so negligible contribution was received from this species. Since oxygen is in excess within diesel engine exhaust and while the reactions represented by equations 2.4 and 2.5 form the basis for passive regeneration, researchers have suggested additional cooperative reactions that contribute to passive regeneration [11, 12], two of which are shown by equation 2.7 and 2.8. The total regeneration of PM by NO₂ is the sum of reactions equations 2.4, 2.5, 2.7, and 2.8 [11]. Equations 2.7 and 2.8 differ from 2.4 and 2.5 by the addition of the oxygen term on the reactant side.



While performing experiments at 300°C, with a reaction atmosphere that contained 10% O₂, the carbon NO₂ reaction was about twice as fast [12] when compared to an experimental atmosphere with no O₂. This can be contributed to the reactions represented by equations 2.7-2.8. This is not a result of the oxygen directly acting with the PM as 300°C is below the minimal threshold required for thermal PM oxidation to occur. At this temperature the appearance of O₂ is more important in the formation of NO₂ by the DOC as shown by equation 2.1 [28] which provides additional NO₂ to support the NO₂ and PM reaction.

Since the filtration efficiency of the CPF approaches 99%, another variable to consider during passive regeneration is the accumulation of ash and the effects it may have on this process. Ash accumulation occurs over extended engine operating periods and is the product of oil consumption during combustion. Effects to minimize ash production have led to the development of oils with low ash content. A review of the relevant literature provides opposing opinions on to whether or not ash affects the performance of the CPF during passive regeneration.

An extended review of several published papers in reference [18] showed that changes in balance point temperatures could result due the accumulation of ash generated through the combustion of oils with different additives. The balance point temperature (BPT) is defined as a period of engine operation which provides a specific temperature, PM concentration and concentration of gaseous emissions to the CPF which provides for a pressure drop profile that is constant [12, 20]. The BPT is also dependent upon the PM loading of the filter. A different but equivalent definition is the period when PM accumulation in the filter is equal to the rate of PM oxidation. Contrast the review performed in reference [18] with an extended real world experiment performed in reference [29] where it was determined, for the time period of the test, that no significant reduction in regeneration performance was experienced.

Another factor affecting passive regeneration of PM within a CPF is the PM contact with the filter substrate. Research in reference [30] has shown that the geometry of the substrate wall and catalytic coating deposited on this surface plays a large role in PM oxidation. The authors stress that the physical contact of the PM and coating is just as important as the type of coating used. PM in close proximity of the catalytic coating has a higher possibility of being oxidized by the NO_2 generated from the catalytic surface. This idea could be expanded to include the size and distribution of the particulate matter. If the generated PM from the engine was such that it promoted tighter contact with the substrate wall then a faster reaction rate should be observed.

2.6 Experimental and Modeling Results

After a review of the available literature, experimental research into passive regeneration has consisted of micro reactor studies, balance point temperature determinations, transient driving cycle simulation and passive regeneration of a loaded filter at a constant temperature. The majority of the collected data has been used to aid in modeling efforts. The concept of developing a simulation model to aid in the design, sizing, control, and installation of aftertreatment systems for specific engines is appealing from a cost standpoint. Also, calibrated models can be used for other tasks such as on-board diagnostics for installed systems. Since the experimental research for this thesis was focused on engine experiments, the reviewed literature for this section will concentrate on similar results.

The first set of experiments that will be reviewed is testing completed with two aftertreatment configurations. The first configuration uses only a CPF while the second configuration employs a DOC and a DPF. An example of the steady state passive regeneration tests from reference [14] can be seen in Figure 2.6. At 350°C, the DOC and DPF performed slightly better than the CPF. This can be attributed to the NO to NO₂ conversion across the DOC which provides for a higher concentration of NO₂ at the DPF inlet enabling higher reaction rates. The catalyzed particulate filter performed similar to the DOC and DPF even though the inlet NO₂ concentration was less. This unexpected performance could be due to NO₂ production in the CPF and the subsequent back diffusion of NO₂ into the PM cake layer.

At the 505°C testing, the regeneration performance of CPF is better than the DOC and DPF as viewed in Figure 2.6 by the pressure drop profile. This can be attributed to two reasons. At this temperature the DOC conversion efficiency of NO to NO₂ is low limiting NO₂ availability and at 505°C, the oxidation mechanism is dominated by the presence of O₂ and the PM contact with the catalytic coating of the filter [14].

The next reviewed paper compared three aftertreatment configurations. Configuration one was a CPF, configuration two was the combination of a DOC and a DPF while the third configuration consisted of a DOC and CPF. Balance point temperatures from testing performed in [20], an example of which can be seen in Figure 2.7, showed the lowest BPT from the combination of a DOC and CPF. The ranking of the configurations in reference [20] were as follows, DOC & CPF → DOC & DPF → CPF. The BPT can be used as an approximation to determine low temperature performance of the system which is dominated by passive regeneration. This testing showed that the most efficient combination of components was a DOC and CPF. The increased low temperature performance can be attributed to the catalytic coating applied to both the DOC and CPF which promotes the oxidation of NO to NO₂ and therefore the passive oxidation of PM.

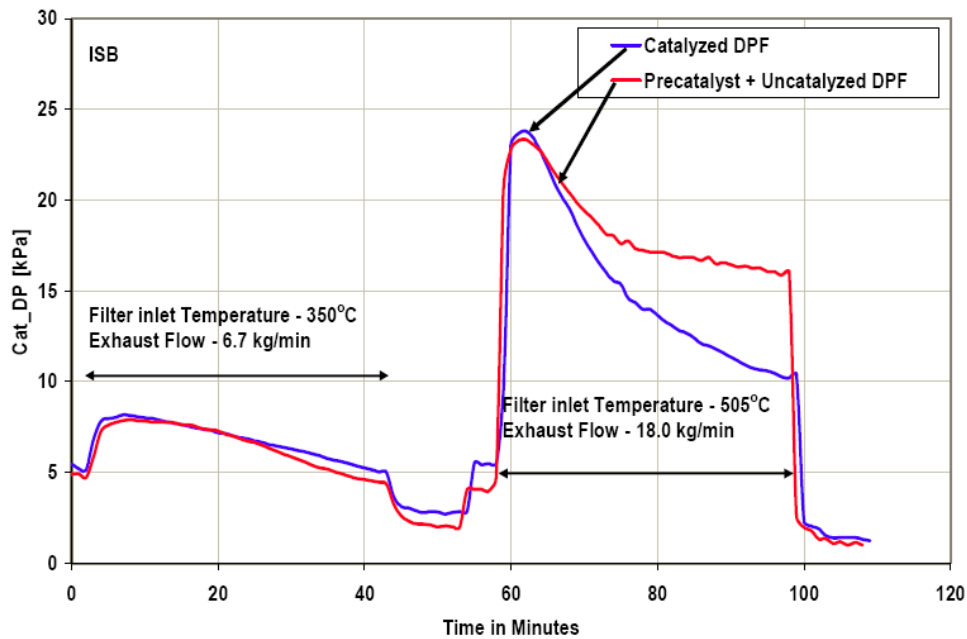


Figure 2.6: Passive Regeneration Testing at 350°C and 505°C, [14].

Similar testing in reference [12] added an additional configuration to the test sequence. The fourth configuration consisted only of a DPF. The temperature profiles and calculated PM loadings for the filters during the performed transient testing can be seen in Figure 2.8. As expected the DOC and CPF system, “CCRT” in Figure 2.8, performed

the best with the total rankings as follows, DOC & CPF → CPF → DOC & DPF → DPF. This rating can once again be attributed to the additional NO₂ provided by the DOC and CPF and the PM contact with the catalytic coating within the CPF.

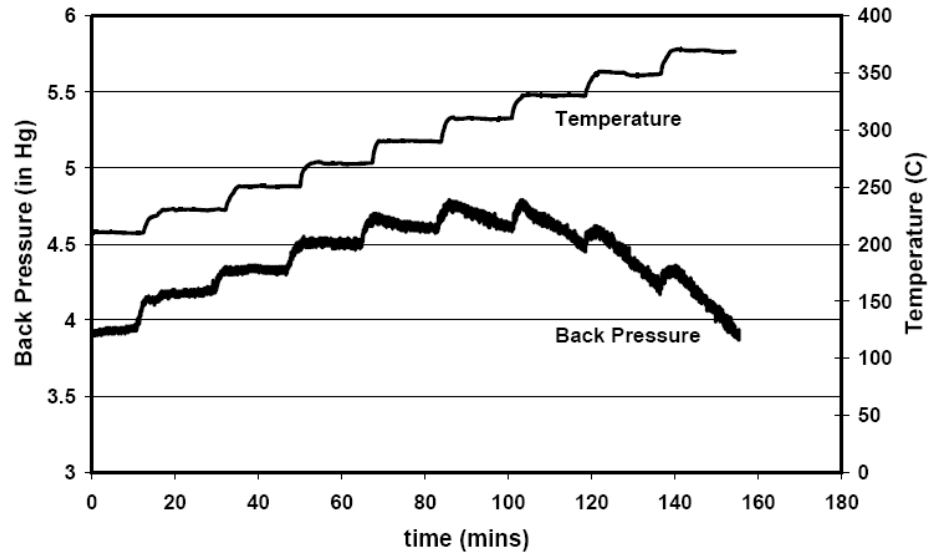


Figure 2.7: Balance Point Temperature Testing Performed in Reference [20] with a DOC and DPF.

Previous passive regeneration testing performed at Michigan Technological University is reported in reference [15]. Testing consisted of loading a clean CPF at steady state operating conditions at various engine loads. Several aftertreatment configurations were used during this research which included reformulated production catalysts for comparison with earlier versions of the same components. A comparison of the new and old formulation is not directly applicable to the passive regeneration testing performed for this thesis. However, the steady state loading portions of the experiments using two configurations for the aftertreatment system provide useful information. Configuration one was a DOC and CPF, while configuration two was only a CPF.

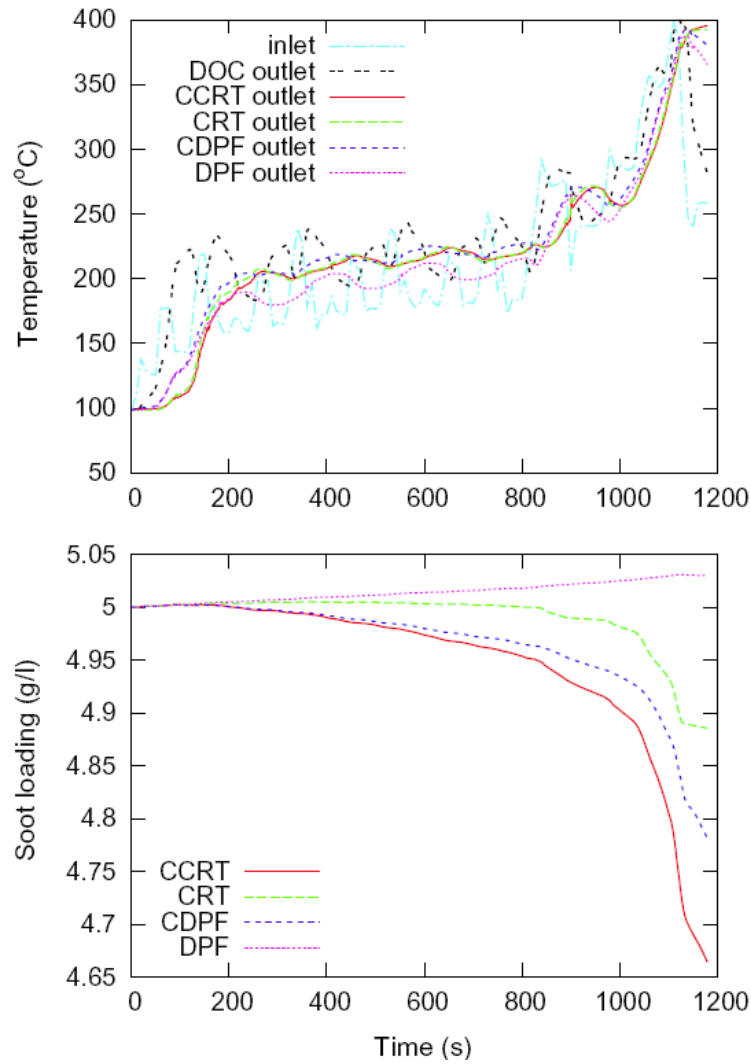


Figure 2.8: Transient Passive Regeneration Testing Performed in Reference [12].

Testing of the two configurations showed results similar to above, the DOC and CPF configuration was superior to the CPF only configuration in the area of passive regeneration. Several important conclusions were derived from this testing which include the items listed below [15].

- At temperatures below 400°C, passive oxidation occurs only through the reaction of NO_2 with PM.

- At higher loads, PM oxidation increases due to higher exhaust temperatures.
- When the engine is operated at high loads and exhaust temperatures, the initial reduction in pressure drop across the CPF is due to the oxidation of PM within the wall of the filter substrate.
- Maximum filtration efficiency provided by the CPF is due to the PM cake layer.

The last reviewed paper consisted of experiments performed in two configurations at John Deere with the data compiled by the authors of reference [25]. Configuration one was a DOC and a DPF, configuration 2 consisted only of a DPF. These experiments were used to calibrate the MTU 1-D DPF model [25] which then allowed a study of several variables of interest. A total of 20 tests were performed, 8 using the DOC and DPF configuration and 12 using only a DPF. The experiments were performed with a clean filter which was loaded using different engine loads at steady operating conditions for a specified period of time.

Several of the results from this study are relevant to the performed experiments. The knowledge of the NO_2/PM ratio is important due to the fact that it provides a quick estimate on whether a clean DPF will be gaining or losing mass. The stoichiometric ratio of NO_2/PM is 7.67:1 by mass and if the temperature of the system is such that it will promote passive oxidation, knowledge of the NO_2/PM can be used to predict mass accumulation or depletion. With a loaded filter, the NO_2 flow rate is more important than the NO_2/PM ratio. An explanation for this statement is best discussed through an example. If two engine operating conditions produced the same NO_2/PM ratio, which was greater than 7.67 to 1 by mass, but had different exhaust flow rates which correspond to NO_2 flow rates into the DPF, the operating condition with the higher exhaust flow rate would oxidize the PM within the DPF faster due to the larger flow rate of excess NO_2 into the DPF [25].

It was shown in reference [25] that temperatures played an important role in the passive regeneration of PM, with higher temperatures oxidizing PM at a faster rate. A set of simulations were performed with different DPF inlet temperatures and the results can be seen in Figure 2.9. This part of the paper was focused on determining what portion of

the reaction rate was due to thermal oxidation at the different DPF inlet temperatures. The results in Figure 2.9 show that at 400°C, approximately 1% of PM oxidation is the result of thermal oxidation. Therefore under 400°C, oxidation is dominated by passive regeneration.

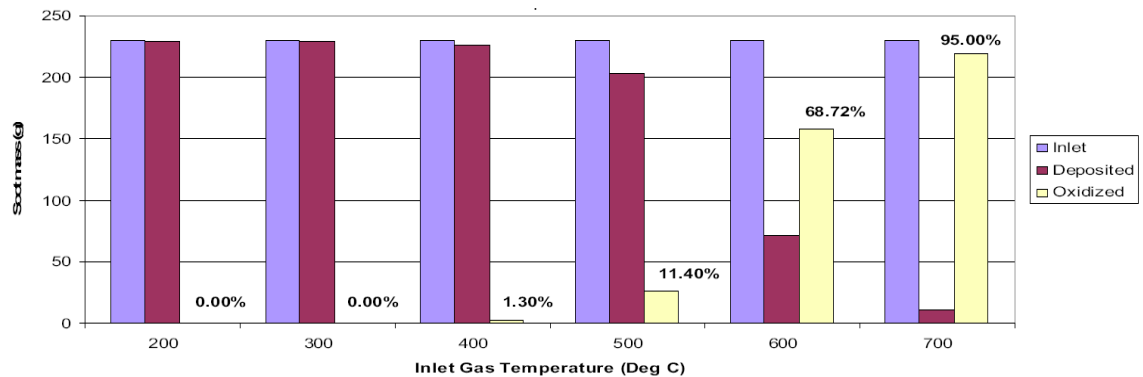


Figure 2.9: Percent of Thermal Oxidation at Different DPF Inlet Temperatures, [25].

2.7 Global Reaction Rate and Activation Energy

One of the objectives of this research is to determine the average global reaction rate for the performed tests. This was performed for loading and the passive oxidation portion of the test. Loading presented an ideal opportunity to calculate a reaction rate since there was a direct mass measurement before and after this stage of the test. An important input for the reaction rate equation are the beginning and ending PM mass values within the CPF and the direct mass measurement gives the most accurate values for this parameter.

The reaction rate for the passive oxidation portion of the test was calculated using the mass measurement of the CPF at the end of loading and the mass measurement at the end of the test minus the mass deposited into the CPF during the last 30 minutes of the test. The mass deposited in the CPF during the last 30 minutes of the test is a

calculated value obtained from performing a simulation of the stage with the actual test conditions using the MTU 1-D CPF model. While not a direct mass measurement, it is felt that the model accurately estimates the PM deposition for this short time frame under steady state conditions.

In order to determine a global reaction rate for the performed experiments, a mass balance is derived for the amount of PM in the filter at any given time. The control volume used for this mass balance and several of the intermediate steps involved in deriving the final equation can be seen in Appendix A. The assumptions used for this derivation are as follows.

1. The temperature of the system remains constant
2. For the purpose of this derivation, the gaseous species at the inlet of the CPF remain constant
3. The reaction rate during PM oxidation remains constant due to 1 and 2
4. The PM concentration in the exhaust remains constant
5. The exhaust volumetric flow rate remains constant
6. The filtration efficiency of the CPF remains constant

From the assumptions listed above, this equation can only be used for conditions of steady state operation. The differential equation for the mass balance is shown by equation 2.9 with the parameters of interest listed below. The solution of this differential equation is given by equation 2.10, which allows for the determination of RR_o . The basis for this mass balance was derived from the work in reference [31].

$$\frac{dm}{dt} = \dot{m}_{in} - \dot{m}_{out} - m_{start} RR_o \quad 2.9$$

$\frac{dm}{dt}$ = Change of mass over time, (g/s)

\dot{m}_{in} = PM mass flow rate into CPF (g/s)

\dot{m}_{out} = PM mass flow rate out of CPF (g/s)

m_{Start} : PM mass retained in the CPF at the beginning of the test, (g)

RR_o = Global reaction rate, (1/s)

$$m_{Stop} = \frac{Q_{exh} * C_{in} * \eta_f}{RR_o * 1000} \left[1 - e^{(-RR_o * t_{eff})} \right] + m_{Start} * e^{(-RR_o * t_{eff})} \quad 2.10$$

η_f = Filtration efficiency of the filter

C_{in} = Particulate matter concentration in the exhaust, (mg/std m³)

Q_{Exh} = Standard volumetric flow rate of exhaust, (std. m³/sec)

t_{eff} : Time of passive oxidation, (s)

m_{Stop} : PM mass retained in the CPF at the end of the test, (g)

m_{Start} : PM mass retained in the CPF at the beginning of the test, (g)

By using equation 2.10 and the required inputs, the global reaction rate can be determined. The formula for the passive oxidation RR_o can be seen in equation 2.11 and includes several inputs such as the NO₂ concentration, a pre-exponential factor (A), activation energy (E_a) and temperature. This equation has been obtained from reference [32] where in the original equation the partial pressure of NO₂ was used. The partial pressure of NO₂ can be converted into parts per million (ppm) which is a common unit of measurement for emissions analyzers.

$$RR_o = [NO_2]A \cdot e^{\left(\frac{-E_a}{R \cdot T_R}\right)}$$

2.11

$[NO_2]$ = Concentration of NO_2 , (ppm)

A = Pre-exponential factor, (1/s)

E_a = Activation energy, (J/gmol)

R = Universal gas constant, (J/gmolK)

T_R = Average temperature in CPF during passive regeneration, (K)

For the majority of the performed tests on the ISM and ISL the NO_2 concentration within the PM layer did not remain constant. This was indicated by the NO_2 consumed during the passive oxidation portion of the test. In most cases the NO_2 consumed was greater than what was available at the CPF inlet, this indicates an NO_2 concentration that varies across the PM cake layer. The additional required NO_2 was supplied by back diffusion from the CPF substrate after oxidation of NO to NO_2 .

Due to the varying NO_2 concentrations, the assumptions that were used in references [33, 34] no longer hold which prevents the calculation of an accurate E_a and A. A more detailed model such as the MTU 1-D CPF model will be required to accurately determine these values. While the parameter A and E_a cannot be accurately determined, this method does provide for an average reaction rate for the test and allows for the calculation of the PM oxidation rate using equation 2.12. Previous research in this area has allowed the determination of the activation energy for the passive oxidation of PM by NO_2 by other researchers. A partial list of the activation energies found in the literature can be seen in Table 2.2

$$\frac{dm_{ox}}{dt} = RRo \cdot m(t)$$

2.12

$\frac{dm_{ox}}{dt}$ = PM oxidation Rate, (g/s)

RRo = Global reaction rate of PM in the CPF, (1/s)

m (t) = PM in the CPF at time t, (g)

Table 2.2: Activation Energies for NO₂ Oxidation of PM

Reference Name	Reference #	Arrhenius Model Used	Activation Energy	Pre-exponential Factor	Temperature Range of Testing	Test Condition/PM Type
Mejdi et al.	[11]	S. Arr	52.2 kJ/mol	51.4 1/s	300°C - 400°C	catalyzed reactor experiments, carbon black
Dabhoiwala et al.	[15]	M. Arr	73 kJ/mol	0.5-3.0 m/s*K	273°C - 475°C	catalyzed filter, diesel exhaust sample
Triana et al.	[25]	M. Arr	122 kJ/mol	100 m/s*K	286°C - 429°C	un-catalyzed filter, diesel exhaust sample
Messerer et al.	[28]	S. Arr	115.5 kJ/mol	1.19E6 1/s	275°C - 450°C	catalyzed reactor experiments, light duty diesel PM
Messerer et al.	[28]	S. Arr	98.3 kJ/mol	0.736E5 1/s	300°C - 400°C	catalyzed reactor experiments, heavy duty diesel PM
Kandylas et al. (2002)	[35]	M. Arr	40 kJ/mol	0.028 mol*K/m ² *s	250°C - 450°C	un-catalyzed filter, diesel exhaust sample
Yamamoto et al.	[36]	S. Arr	79.5 kJ/mol	146 1/s	400°C - 500°C	catalyzed reactor experiments, carbon black

Note:

S. Arr: Standard Arrhenius Behavior for Thermal Oxidation of PM

M. Arr: Modified Arrhenius behavior for Thermal Oxidation of PM

In addition to the passive oxidation of PM, at temperatures above 400°C, thermal oxidation contributes to the overall oxidation rate. The equation for thermal oxidation of PM is similar to that of passive oxidation and is shown by equation 2.13. As described in references [33, 34], when the oxygen concentration is in excess and constant, it can be combined with the pre-exponential factor thereby simplifying the equation.

$$RRo = [O_2]A \cdot e^{\left(\frac{-E_a}{R \cdot T_R}\right)}$$

2.13

[O₂] = Concentration of O₂, (ppm)

2.8 Summary

Several different methods have been used to investigate the passive oxidation of PM by NO₂. Research has consisted of micro reactor studies, balance point temperature determinations, transient driving cycle simulation and passive regeneration of a loaded filter at a constant temperature. The performed experiments for this thesis approached the topic of interest in a different manner by beginning the passive oxidation portion of each test with a CPF PM loading of 2.2 ± 0.2 g/L. Keeping this baseline condition constant allows a closer look at the variables of interest.

The parameters of interest for passive oxidation which are exhaust temperature, NO₂ flow rate into the CPF, NO₂ concentration and the NO₂/PM ratio were varied from the baseline condition to determine what affect each of the variables had on passive oxidation. Some of this analysis will be derived through the use of the MTU 1-D CPF model. Due to this unique approach, new information has been identified experimentally. The calculated ratio of NO₂ consumed/NO₂ available at the CPF inlet has demonstrated that during the passive oxidation test conditions, more NO₂ has been used than what is available at the CPF inlet. This lead to a further investigation of the Péclet number and calculated values for the performed experiments show that the transport of NO₂ is diffusion dominated. This transportation of NO₂ against the exhaust flow allows for the increased NO₂ consumption. This may be the first time this has been experimentally verified and will need to be addressed in the modeling of CPF.

Chapter 3 Experimental Setup and Procedures

The heavy duty diesel test cell on the campus of Michigan Technological University was used for the passive oxidation testing. The test cell is separated into two separate rooms. The control room contains the controls for the engine and dynamometer along with the Pierburg emissions bench and desktop computers. The second room contains the engine, engine dynamometer, data acquisition system, fuel balance and a laminar flow element used to measure air flow. This arrangement provides a safe, comfortable work environment for performing experiments.

3.1 Test Cell and Components

The engine test cell has several different components that will be described. A picture of the test cell and the currently installed engine can be seen in Figure 3.1. The room is kept under a negative pressure of approximately 0.5 hPa (0.2 in H₂O) which provides for a fresh supply of air to the room and ventilates fumes that might escape from the exhaust. The engine exhaust system is maintained on average, at a vacuum of 8.7 hPa (3.5 in H₂O). This provides for the removal of engine exhaust but has been shown to dilute the gaseous emission samples downstream of the diesel oxidation catalysts by drawing fresh air into the exhaust system. The ambient temperature of the test cell cannot be independently controlled and as such the temperature and relative humidity vary from test to test.

3.1.1 Engines and Dynamometer

The engine and engine dynamometer are mounted to an engine test bed manufactured by Lake Shore Inc. located in Iron Mountain MI. The test bed consists of a large machined steel plate with t-slots that are integrated within the design to allow for the attachment of the engine and dynamometer. The machined plate is supported by four

large pneumatic lift devices that are pressurized to 690 kPa (100 psig). The lift devices maintain the test bed height while also isolating the building from vibrations generated from the engine.

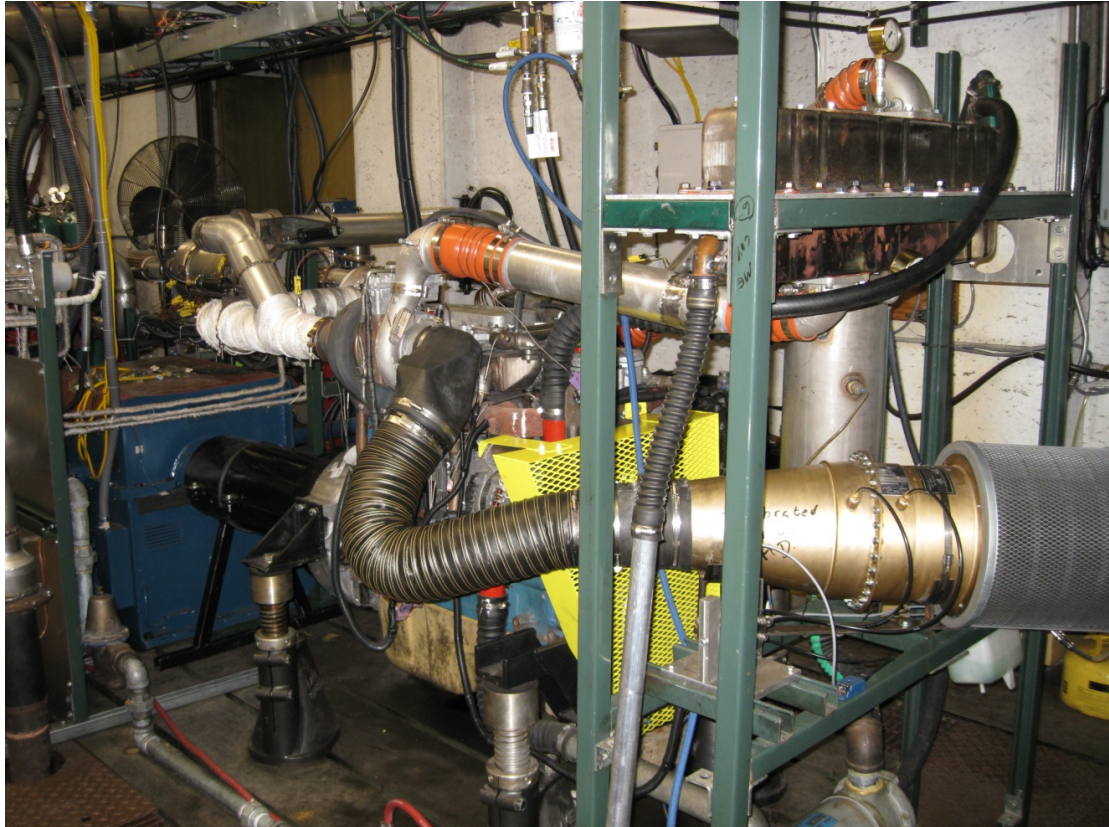


Figure 3.1: Heavy Duty Diesel Test Cell (North End)

Two different engines were used in the experiments. Five tests were conducted on a 2002 Cummins 10.9 L 346 kW (330 hp) ISM. After the completion of the first five tests, the ISM was replaced by a 2007 Cummins 8.9 L 272 kW (365 hp). Five additional tests were performed on this engine. The replacement of the engine was a planned component of the test matrix and provided for the opportunity to obtain data from two different engine platforms. This allowed for the comparison of the different technologies used by the engines since the ISM was certified for 2002 emissions standards while the

ISL met the 2007 regulations shown in Table 1.1. The specifications for the engines used during the performed tests are listed in Table 3.1.

Table 3.1: Engine Specifications

Model	Cummins ISM-246 kW (330 hp)	Cummins ISL-272 kW (365 hp)
Year of Manufacture	2002	2007
Cylinders	6, inline	6, inline
Bore& Stroke	125 mm x 147 mm	114 x 144.5 mm
Displacement	10.8 L	8.9 L
Aspiration	Turbo Charged	Turbo Charged
Aftercooling	Cummins Charge Air Cooler	Cummins Charge Air Cooler
Turbocharger	Variable Geometry Turbine (Holset)	Variable Geometry Turbine (Holset)
Rated speed and Power	2100 rpm and 246 kW	2100 rpm and 272 kW
Peak Torque	1697 Nm @ 1200 rpm	1695 Nm @ 1400 rpm
Common Rail pressure (peak)	179 MPa	160 MPa
EGR system	Electronically controlled and cooled	Electronically controlled and cooled

The engine dynamometer installed in the test cell is a Dyne Systems Dynamatic model 8121 wet gap / low inertia eddy current dynamometer. The maximum power capacity of the dynamometer is 373 kW (500 hp) from 1750-6000 rpm. Maximum torque is limited to 2035 Nm (1501 ft-lb) at 1750 rpm and decreases inversely as rpm increases. This dynamometer is water cooled and has a coolant requirement of 38 L/min (10 gpm) per 75 kW (100 hp). The maximum inlet water temperature is 32°C with a maximum coolant outlet temperature of 60°C. The coolant inlet pressure requirements are 380-690 kPa (55-100 psig). The torque and power curve for this dynamometer along with dimensions can be found in Appendix B.

The engine speed and torque were regulated by a Digalog Model 1022A dynamometer controller. This controller has two operating modes, “Speed” and “Load” control. For the passive oxidation testing performed, the controller was operated in the “Speed” mode. This mode allows the operator to set the engine speed and then vary the load placed on the engine by either increasing or decreasing the fuel supplied to the engine through the use of a manually controlled rheostat.

3.1.2 Diesel Oxidation Catalyst and Catalyzed Particulate Filters

A Cummins 2007 aftertreatment system was used during testing completed on the ISL and ISM. This consisted of a diesel oxidation catalyst (DOC) and a catalyzed particulate filter (CPF). One DOC was used for testing on both engines but each engine had a dedicated CPF for the tests performed on that engine. The part numbers on the two different filters were the same and the specifications for the DOC and the CPF's used in this study can be seen in Table 3.2.

Table 3.2: DOC and CPF Specifications

Specification	DOC	CPF
Part #	EPN Q621300	EPN Q623316
Substrate	Cordierite	Cordierite
Cell geometry	Square	Square
Diameter (mm)	267	267
Length (mm)	102	305
Total Volume (L)	5.7	17.1
Cell Density (cells/cm ² , cells/in ²)	62, (400)	31, (200)
Cell Width (mm)	1.09	1.49
Frontal Area (%)	81	69
Channel Wall Thickness (mm)	0.114	0.305
Wall density (g/cc)	N/A	0.45
Specific heat (J/kg K)	N/A	891
Thermal conductivity (W/ m*K)	N/A	0.84
Porosity (%)	35	52
Mean Pore Size (micron)	N/A	13

In order to ensure that the CPF is at the same state during each test, an active regeneration is performed prior to the start of each test. The current method of active regeneration consists of using an auxiliary fuel injector mounted within the exhaust system immediately after the turbocharger outlet. The injector location can be seen in the lower right of corner of Figure 3.2.

The doser injector assembly was obtained from Cummins NPower with a manufacturer part number of P4966472_ASSY. This is a Mid Flow fuel injector with a maximum flow rate of 4 ml/sec @ 7 bar. This injector is compatible with the following fuels; #1 diesel, #2

diesel, kerosene and 20% biodiesel. The injector in the MTU test cell is provided with a 690 kPa (100 psig) fuel supply that is delivered via an aftermarket electronic fuel pump. The fuel pump is manufactured by Walbro and has a manufacturer part number of CSL 392. The fuel pressure regulator is manufactured by Weldon Pumps with a part number of 2040.

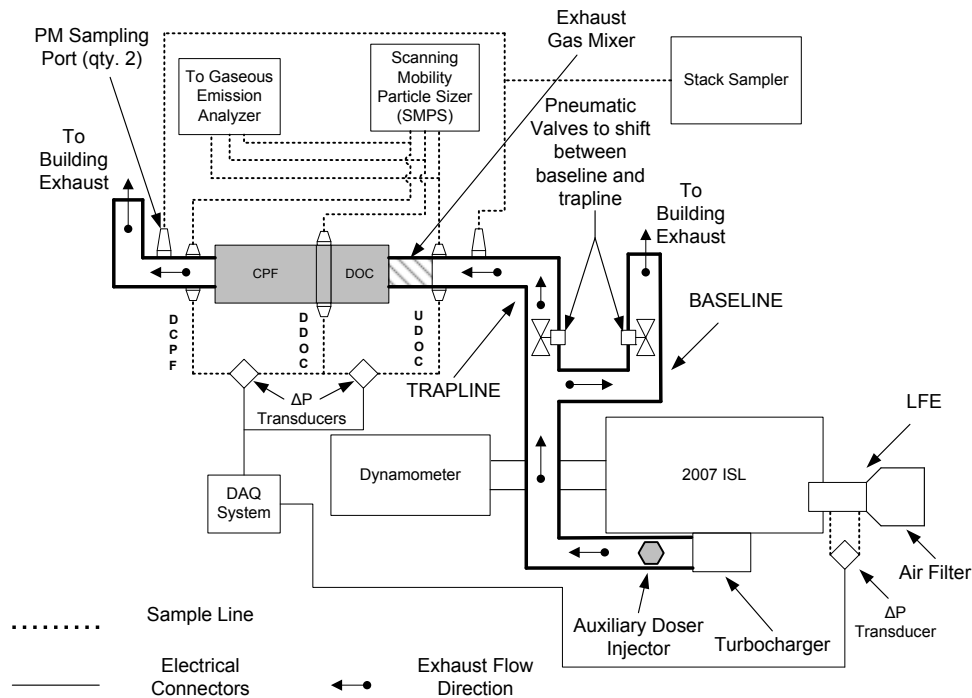


Figure 3.2: Exhaust Routing Used for Testing on the 2007 ISL

The doser injector is controlled via software from the control room for the test cell. This system is controlled by the user who adjusts the duty cycle of the injector located after the turbo charger to obtain the specified CPF inlet temperature, which for clean outs is 600°C. For the ISM, in-cylinder dosing was not available and this method for active regenerations was required to be used. The 2007 ISL has in-cylinder dosing capabilities but in order to maintain consistency across engine platforms it was decided to use the auxiliary doser to perform clean outs of the CPF for both engines.

3.1.3 Engine and Aftertreatment Layout

The engine exhaust system used over the course of testing has changed. The tests completed on the ISM used an exhaust system in which the diameter of the pipe varied from 4 in. to 6 in. throughout the length of the system. The inlet of the DOC and exit of the CPF used standard factory dimensions of approximately 4 in. Upon installation of the ISL, new exhaust was routed with a 4 in. diameter pipe for the entire length of the system to ensure consistent flow throughout.

The layout of the exhaust system used on the ISM can be seen in Figure 3.3. This system provides two paths for the exhaust to travel. For start up of the engine and during warm up periods the exhaust travels through the “baseline”. By allowing the engine to warm up completely before the exhaust is allowed to pass through the aftertreatment system, variability during testing is reduced. Once the engine operation has stabilized at the selected conditions, two pneumatically controlled valves are actuated. The first valve closes the baseline while the second valve opens the “trapline” allowing exhaust to pass through the DOC and CPF.

Upon installation of the 2007 ISL a new exhaust routing was designed. The current exhaust layout can be seen in Figure 3.2. Operationally this system performs in the same manner as the exhaust system installed on the ISM. As mentioned above a 10.2 cm (4 in.) diameter steel aluminized pipe was used for the exhaust to promote a consistent flow throughout the system. Other modifications include a shorter baseline and electronically actuated valves for switching between the different gaseous sampling locations. The actuation of the solenoid valves is accomplished through a program created in Labview 8.6.

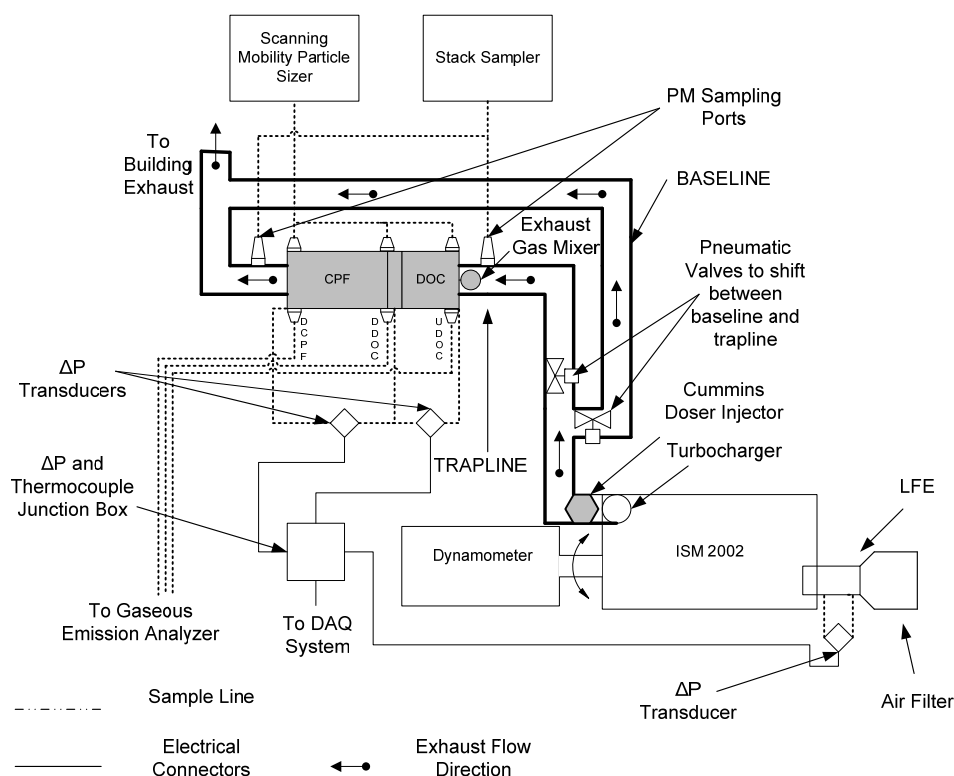


Figure 3.3: Exhaust Routing Used for Testing on the 2002 ISM, Picture from [33]

“Reprinted with permission from Reference [33], © 2010 Greg Austin. See Appendix T for documentation of permission to republish this material.

3.1.4 Fuel Properties

For the passive oxidation testing performed, only one batch of fuel was ordered. A quantity of 3300 gallons was ordered from Krans Oil (Dollar Bay, MI). The fuel was a summer blend of Ultra Low Sulfur Diesel (ULSD) with 7 ppm of sulfur. Fuel testing was performed by Cummins and the results from two independent tests are shown in Table 3.3. A separate set of tests were performed which obtained the heating value of the fuel, hydrogen and carbon content of the fuel. The results of this testing is shown in Table 3.4.

Table 3.3: ULSD Fuel Properties Used During Testing

Sample	Sulfur	Viscosity @ 40°C	API	Spec.	Cetane	IBP	10%	50%	90%	FBP	WATER	ICP for Metals
	(ppm)	(cSt)	Gravity	Gravity	Index		°C				(ppm)	(ppm)*
1	7	2.125	35.8	0.8458	39.93	168	194	245	303	341	103	<1
2	7	2.455	35.7	0.8463	39.73	168	194	245	302	339	80	<1

*All metal were less than 1ppm

IBP: Initial Boiling Point

FBP: Final Boiling Point

Table 3.4: Heating Value, Hydrogen and Carbon Content Testing Performed by Paragon Laboratories

Carbon	Hydrogen	API Gravity @ 15.6°C	Density @ 15.6°C	Spec. Gravity @ 15.6°C	Gross Heating Value		Net Heating Value	
(Wt%)	(Wt%)	°API	g/mL	-	(Mj/kg)	(BTU/lb)	(Mj/kg)	(BTU/lb)
86.94	13.06	35.6	0.8457	0.8465	45.6	19595	42.8	18403

3.2 Measurement Systems and Procedures

Prior to creating and beginning the test matrix for passive oxidation testing, a literature review was performed which is discussed in Chapter 2. From this review, it was determined that several key variables were important to the understanding of passive oxidation of PM in a CPF. The most important factors involving passive oxidation are the temperature and NO₂ flow rate (mg/scm) into the CPF along with the NO₂/PM ratio of the exhaust. Measuring and recording of these variables required several different sensors and the collection of these signals into one location. Hardware and software from National Instruments were selected for the data acquisition and processing of these signals.

3.2.1 Data Acquisition System

Over the course of the test matrix, two different sets of hardware were used from National Instruments (NI) to acquire, visualize, and record the data. The testing performed on the ISM used two 16 channel SCXI modules which contained signal conditioning and filtering to acquire temperatures. Along with the thermocouple data, analog voltages were recorded in this system by a 6052-NE multifunction I/O DAQ board. The software used for this signal acquisition was Labview version 6.1 which recorded the data every three seconds.

Prior to testing on the ISL, a new data acquisition system was purchased and installed in the test cell. The new system uses a NI cDAQ-9178 capable of multiple inputs and outputs. This system is connected to a desktop computer via a USB cable and is located within the test cell to minimize the length of sensor wires which reduces the possibility of signal noise. A summary of the National Instrument's hardware that was installed in the test cell is shown in Table 3.5.

Table 3.5: Summary of National Instrument's Hardware

Module	# of Channels	Measurement	Maximum Sample Rate	Actual Sample Rate	Hardware Filtering	Filter Type	Software Filtering	Filter Type
NI 9205	32 SE	Analog Voltage Input	Aggregate 250 kS/s	4 kS/s	NO	N/A	Yes	Lowpass Butterworth 2nd order 10 Hz cutoff frequency
NI 9213	16	T/C Module	83 S/s	100 S/s	YES	Differential filter	None	N/A
NI 9237	4	Analog Voltage Input, bridge Sensor	Using internal timebase: 1613S/s to 50 kS/s. Using external timebase: 390.625S/s to 51.3kS/s. In general the rate is: fm/256/n (n=1..31)	2.5 kS/s	YES	Analog and digital filtering	Yes	Lowpass Butterworth 2nd order 30 Hz cutoff frequency
NI 9401	8	TTL Digital Input/Output Module	Max Input Switching Freq 9 MHz	4 S/s (output)	NO	N/A	No	N/A
NI 9472	8	Digital Output	N/A	N/A	N/A	N/A	N/A	N/A
NI 9203	8	Current Input	200 kS/s	Not Used	N/A	N/A	N/A	N/A

3.2.2 Temperature

Temperatures throughout the aftertreatment system and test cell exhaust routing were measured using Type K thermocouples (T/C) which are ungrounded and use shielded wire. Engine temperatures including exhaust manifold, oil and coolant were measured using Type E thermocouples which were supplied with the engine when it was delivered from Cummins Inc. Three different size thermocouples were used on the engine and aftertreatment system depending on the location measured. The information for the Type K thermocouples is listed in Table 3.6. Products from Omega engineering were used during testing on the ISM while thermocouples from Watlow were used for testing with the ISL. While it is important to measure and record temperatures for the engine, these values are only used to ensure consistent engine operation between tests while the focus of the tests conducted are on the temperatures in the exhaust and aftertreatment system.

Table 3.6: DOC, CPF and Exhaust System Thermocouple Specifications

Location	Type	Diameter	Length	Omega #	Body Material	Watlow #	Body Material
DOC	K	0.020"	12"	KMQSS-020U-12	Stainless Steel	AX1078701	Inconel
CPF	K	0.032"	12"	KMQSS-125U-6	Stainless Steel	AX1078801	Inconel
Engine exhaust	K	0.125"	6"	KMQSS-032U-12	Stainless Steel	ACGF00Q060U4000	Inconel

3.2.2.1 DOC Thermocouple Layout

In order to determine the radial and axial temperature gradients within the DOC, two different T/C layouts were used during testing on the ISL. The individual quadrants within the DOC are labeled as shown in Figure 3.4. The first T/C layout used for testing on the ISL, which was also used on the ISM, can be seen in Figure 3.5. This distribution of thermocouples was specifically created to look at the radial temperature gradients within the DOC substrate. Passive oxidation testing on the ISM and ISL implemented the use of an uninsulated DOC. Prior testing at MTU used a DOC that was insulated so it was deemed important to investigate the temperature distribution within the DOC substrate since it has a direct effect on conversion efficiencies across the DOC.

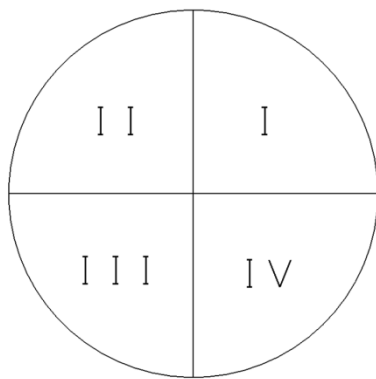


Figure 3.4: Quadrant Definition within DOC

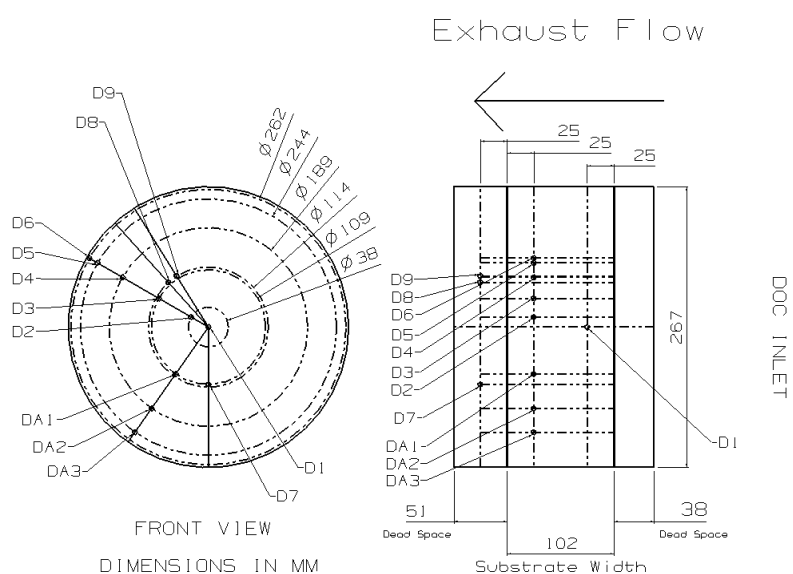


Figure 3.5: DOC Thermocouple Layout #1

In Figure 3.5 the thermocouples listed as D1-D6 and DA1-DA3 are 0.51 mm (0.020 in.) in diameter and are positioned in the DOC substrate. D7-D9 are 0.125 in. thermocouples that measure the exhaust “gaseous” temperatures and are located in the space after the DOC substrate but before the CPF. The radial distribution of temperature is provided by the thermocouples labeled D2-D6 located in quadrant II and the thermocouples DA1-DA3 in quadrant III. These set of thermocouples provides a set of data to investigate the radial temperature gradients within the DOC.

Although the positioning is different, the same number of thermocouples are used in the second DOC thermocouple layout for the ISL which can be seen in Figure 3.6. The general placement, 0.020 in. thermocouples in the substrate and 0.125 in. placed in the gas stream, remains consistent but there are less thermocouples in the radial direction within quadrant II. This layout was developed to look at thermal gradients in the axial direction while also providing a way to compare temperatures in different quadrants.

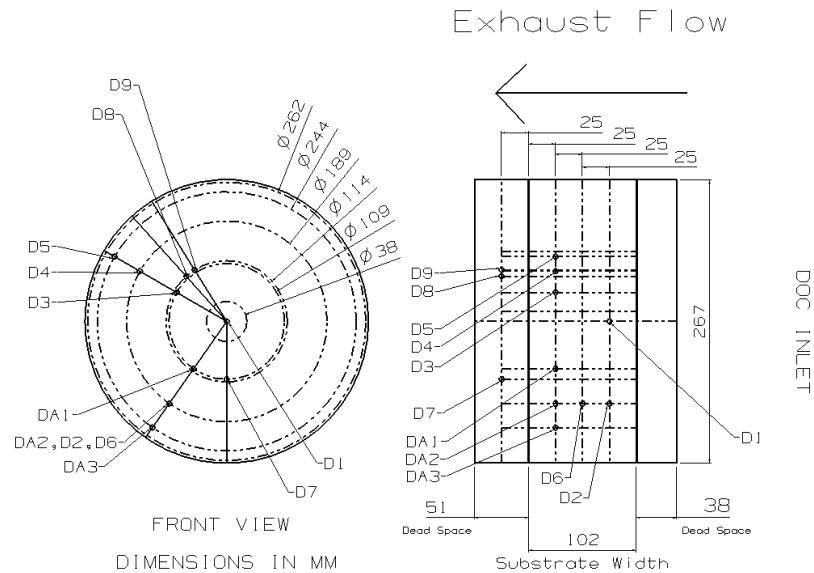


Figure 3.6: DOC Thermocouple Layout #2, ISL

When installed, the DOC is situated as shown in Figure 3.6 with the 0.020 in. thermocouples residing in quadrants II and III. It is possible to experience radial temperature gradients that differ between the two quadrants if the flow through the DOC is not symmetric or if there is an inherent preferred direction of heat transfer in the DOC. There are three sets of matched thermocouples located in two separate quadrants, D3 and DA1, D4 and DA2 and D5 and DA3 which have been installed to investigate if a preferential heat transfer occurs.

The T/C distribution shown in Figure 3.6 also allows for the investigation of axial temperature gradients. The thermocouples DA2, D2 and D6 are located at a radial distance of 95 mm from the center of the DOC substrate and reside in quadrant III. The

thermocouples are equally spaced along the length of the substrate allowing a close look at the axial temperature distribution during steady state loading and passive oxidation testing. An analysis of the temperatures from two previously discussed T/C layouts will be detailed in section 4.3.1.

3.2.2.2 CPF Thermocouple Layout

In order to evaluate the radial and axial temperature gradients with the CPF, the T/C layout in Figure 3.7 was used during passive oxidation testing. This figure only shows the CPF substrate and the position of the 0.032 in. Watlow thermocouples. When packaged for use in an aftertreatment assembly, the substrate is surrounded by a stainless steel cylindrical cover (can) which provides for attachment points to other aftertreatment components and protection from foreign objects.

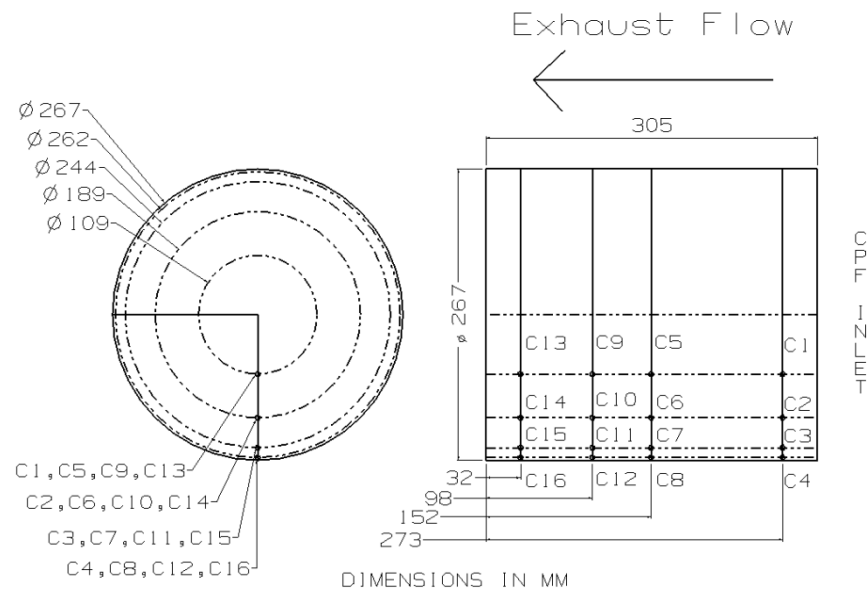


Figure 3.7: CPF Thermocouple Layout

Testing that was previously performed at MTU [33, 34], used a similar T/C layout but did not have the additional thermocouples located near the periphery of the CPF. The

thermocouples labeled C4, C8, C12 and C16 were included to gain a better understating of the temperature gradients involved while using an uninsulated CPF. Testing performed in references [33, 34] used an insulated CPF can which reduced heat transfer to the test cell and as a result the radial temperature gradients are expected to be less. The T/C placement allows for the volume averaged temperature of the CPF substrate. The calculation method for determining the volume averaged temperature can be found in references [33, 34].

3.2.3 Pressure

Pressure measurements were monitored by four different sensors. Three of these sensors were differential pressure transducers of the wheatstone bridge type. The fourth pressure transducer was used to measure the barometric pressure of the test cell. The specifications of the pressure transducers can be seen in Table 3.7. The output for the differential pressure transducers is in mV/V. When the sensor is at its maximum capacity it will provide one mV of output for every volt that is used as an input. As an example when using a 10 V power supply, if the 3.5 kPa sensor is pressurized so it experiences a differential pressure of 3.5 kPa, the output will be 10.01 mV. The raw signals from these sensors are passed into the NI hardware which then applies both hardware and software filtering to process the signal. The characteristics of the applied filtering is shown in Table 3.5.

Table 3.7: Pressure Transducer Specifications

Measured Value	Manufacturer	Part #	Sensor Type	Range of Sensor	Units	Sensor Output	Response Time
DP across LFE	Sensotech	AD111AN	Differential Pressure	0.0-3.5	kPa	1.001 mV/V	< 1 ms
DP across DOC	Sensotech	AD111AR	Differential Pressure	0.0-13.8	kPa	1.506 mV/V	< 1 ms
DP across CPF	Sensotech	AD111AV	Differential Pressure	0.0-68.9	kPa	2.005 mV/V	< 1 ms
Barometric Pressure	Omega Engineering	PX419-26B5V	Barometer	26.00-32.00	In Hg	0-5 V	< 1 ms

After the refurbishment of the test cell and the installation of the new National Instruments hardware, the differential pressure transducers were implemented with the scaling factors used for testing on the ISM. After some initial testing, it was determined that the flow rates calculated using the differential pressure values measured across the

LFE were in error. This was traced back to the scaling factors used for the DP sensors. To rectify this situation, a calibration of the DP sensors was performed through Labview. The calibration procedure and some background information can be found in Appendix C.

3.2.4 Air and Fuel Flow

Air flow measurements are performed through the use of a laminar flow element (LFE) manufactured by Meriam Instruments (Cleveland, Ohio). The instrument model number is 50MC2-6F and has the capability of handling a differential pressure up to 138 kPa (20 psig) and a maximum temperature of 65°C. The maximum calibrated flow rate for this device is 26.9 std. m³/min. This instrument is paired with the 0.5 psid differential pressure gauge listed in Table 3.7. When there is air flow across the LFE, a pressure drop is generated across the device and is measured by the pressure transducer. The wheatstone bridge within the sensor then provides a corresponding voltage to the Labview program which is used with several formulas to determine airflow.

The formula for calculating the airflow with the LFE has several inputs. Along with the pressure drop from the differential pressure transducer, the test cell temperature, relative humidity and barometric pressure are required for the calculation. The program in Labview calculates several values with these inputs. The actual (m³/s) and standard (standard m³/s) volumetric flow rates are calculated and recorded. The temperature and pressure used for the standard calculations are 25°C and 101.325 kpa respectively. Also calculated are the air mass flow rate (kg/min) and the exhaust mass flow rate (kg/min). The exhaust mass flow rate is calculated by adding the mass air flow rate and the fuel flow rate from the fuel measuring device. The formulas used for these calculations can be found in Appendix D.

Fuel flow is measured by a fuel mass balance (scale) manufactured by AVL (Plymouth, MI) with a manufacturer part number of 703G. This measuring device is controlled by an electronic control unit also made by AVL which carries the part number

711A. The control unit allows for the selection of a single or multiple measurement cycle. By using both the scale and the control unit, the time required to use a measured amount of fuel is determined.

A simplified explanation of the operating principle is as follows. The control unit allows the selection of three weights, 0.2, 0.4 and 0.8 kg. Once the mass is selected, the reservoir attached to the scale is filled with the appropriate amount of fuel which corresponds to the user's selection, this is the beginning of the measurement cycle. As the engine is operated and the measured quantity of fuel is consumed, the arm of the balance beam for the scale reaches a limit switch which provides a signal to control unit indicating that the measurement cycle has ended. When measuring continuous fuel usage the cycle repeats, for single measurements the cycle is over. From the selected mass of fuel (kg) and the time required to use this fuel (s) the mass flow rate of the fuel used by the engine can be calculated. For the performed tests, continuous fuel usage was monitored with the mass selector set at 0.4 kg.

3.2.5 Gaseous Emissions

Over the course of accumulating data, two different emissions analyzers were used. The Pierburg emissions bench which is manufactured by AVL North America (Plymouth, MI) was out of service during the passive oxidation testing on the ISM so an alternative analysis method was required. The analyzer used as a temporary replacement for the Pierburg was a Semtech DS from Sensors Inc. (Saline, MI). The specifications for this analyzer can be seen in Table 3.8.

During refurbishment of the test cell, the Pierburg emissions bench was repaired and has been used on all of the subsequent passive oxidation tests performed on the ISL. The specifications for the Pierburg emissions bench can be seen in Table 3.9. Over the course of testing many span gases were required to perform calibrations of the analyzers prior to testing with the emission instruments. A list of the gases used during passive oxidation testing on the ISM and the ISL can be found in Table 3.10. Gases with

a numerical value next to the concentration were consumed during testing and a replacement gas was obtained in order to allow for the continuation of testing.

Table 3.8: Semtech DS Emissions Bench Specifications

	O ₂	CO	CO ₂	NO	NO ₂	THC
Range	0 - 25%	0 - 8%	0 - 20%	0 - 2,500 ppm	0 - 500 ppm	0 - 40,000 ppmC
Resolution	0.1%	10 ppm	0.01%	1 ppm	1 ppm	1 ppmC
Accuracy	±1%	±3% of reading or ± 50 ppm	±3% of reading or ± 0.1%	±3% of reading or ± 15 ppm	±3% of reading or ± 10 ppm	±2.0% of reading or ±5 ppmC
Repeatability	±0.25 % of reading or 0.3 % oxygen whichever is greater	±2 % of reading or 20 ppm	±2 % of reading or ±0.05 %	±2 % of reading or 5 ppm	±2 % of reading or 5 ppm	±1.0 % of reading or ±2 ppmC
Analyzer Type	Electrochemical	NDIR	NDIR	NDUV	NDUV	FID
Measurement Type	Dry	Dry	Dry	Dry	Dry	Wet

Table 3.9: Pierburg Emissions Bench Specifications

	O ₂	CO	CO ₂	NO _x	NO	THC
Range	0 - 25%		0 - 20%	0 -10,000 ppm		0 -20,000 ppm C3
Resolution	15 ppm	125 ppb	15 ppm	35 ppb		30 ppb
Accuracy	Not Available					
Repeatability	≤ 0.5 % of the measuring value + 2x detection limit	≤ 0.5 % of the measuring value + 2x detection limit	≤ 0.5 % of the measuring value + 2x detection limit	≤ 0.3 % of the measuring value + 2x detection limit		≤ 0.5 % of the measuring value + 2x detection limit
Analyzer Type	Paramagnetic	IRD	IRD	CLD	CLD	FID
Measurement Type	Dry	Dry	Dry	Wet	Wet	Wet

Table 3.10: Span Gas Values

Analyzer	Measured gas	Span Gas	Concentration	Units
P,S	THC	C ₃ H ₈ , Balance N ₂	93 and 3200	ppm C1
P,S	CO	CO, Balance N ₂	300	ppm
P,S	CO ₂	CO ₂ , Balance N ₂	14.02	%
P	NO _x , NO	NO, Balance N ₂	515	ppm
P,S	O ₂	O ₂ , Balance N ₂	(1) 20.91, (2) 12.94	%
S	NO	NO, Balance N ₂	515	ppm
S	NO ₂	NO ₂ , Balance Air	(1) 254, (2) 252	ppm

P-Pierburg

S-Semtech DS

Gaseous emissions testing on the ISM and ISL consisted of sampling raw exhaust gas from three locations in the aftertreatment system. The sampling locations can be seen

in Figure 3.2 and are UDOC, DDOC, and DCPF. During testing on the ISM, the sampling locations were selected manually by three separate ball valves. When activated, the ball valves directed compressed air at 690 kPa (100 psig) to sampling valves which then opened the sampling pathway to the emissions analyzer. For testing on the ISL, the switching of sampling locations was automated through the Labview program. Electric solenoid valves control the airflow to the sampling valves and are turned on or off by the user.

After the exhaust gas is removed from the specific sampling location, it passes through a filter that is maintained at 185°C. The exhaust sample then flows to the emissions bench by a 30 ft long sample line that is also heated to 185°C. From this point, the non-diluted, heated exhaust gas is divided and sent to the individual analyzers or to a chiller which will cause the water in the exhaust sample to condense. A “dry” sample is required for some of the individual analyzers to function properly. A comparison of the recorded values from Pierburg emissions bench and the Semtech analyzer will be provided in Chapter 4.

3.2.6 Particulate Matter

The hardware used for Particulate Matter (PM) measurements was a manual sampling train from Andersen Instruments Inc. (Smyrna, GA). Raw, heated (260°C - 480°C) exhaust was drawn through a Pall Corporation (Ann Arbor, MI) type A/E 47 mm glass fiber filter type. This was done multiple times over the course of the individual tests, both during loading and the passive oxidation portions of the test to gain an average PM concentration. The particulate matter concentrations were measured in the same manner on both the ISM and ISL. The two sampling locations used for this measurement were UDOC and DDOC which can be seen in Figure 3.2. Measurements taken UDOC were for five minute time intervals, while sampling DCPF was required to be performed for 1 hour in order to obtain a measurable amount of mass due to the high filtration efficiency of the CPF. The scale used for this measurement is a Mettler Toledo

model #UMT2 with a readability of 0.1 µg and repeatability of ± 0.25 µg. The experimental PM concentrations will be discussed in Chapter 4.

The average PM concentrations are used in several calculations during post processing of the data. The concentrations are used in the experimental mass balances and the MTU 1-D CPF model also uses these values as an input. Additionally, the steady state filtration efficiency of the CPF can be calculated by using the samples taken UDOC and DCPF. The average PM concentration is calculated from the samples taken UDOC during loading. This average along with the PM concentration DCPF is used to determine the filtration efficiency by using eq. 3.1. Additional information on this process can be found in references [19, 37].

$$\eta_f = \frac{C_{in} - C_{out}}{C_{in}} \times 100 \quad 3.1$$

η_f = Filtration efficiency of the CPF

C_{in} = CPF inlet concentration (mg/scm)

C_{out} = CPF outlet concentration (mg/scm)

3.2.7 Particle Size Distribution

Although the filtration efficiency of the CPF can approach values as high as 99%, particles do pass through the wall flow filter, exit into the exhaust and then into the ambient air during the operation of the engine. A set of four instruments were used to measure the particle size distribution (PSD) exiting the CPF. Collectively the group of three instruments manufactured by TSI Inc. (Shoreview, MN) is termed a Scanning Mobility Particle Sizing (SMPS) system. Sampling occurs at three locations in the aftertreatment system, UDOC, DDOC, and DCPF.

The first of the four instruments is a mini dilution system that was designed and manufactured in-house at MTU. This dilution system uses filtered, compressed air heated to a temperature of 200°C and is used to condition the exhaust gas. The average

dilution ratio used was 10:1 but over the course of testing was found to vary dependent upon two separate factors. First, the inlet compressed air pressure is used to directly control the dilution ratio. Experimentation has shown that the second factor affecting the dilution ratio is the exhaust mass flow rate and the resulting pressure drop across the aftertreatment components. This variation of dilution ratio is compensated for during post processing of the PSD data.

The remaining three instruments for the measurement of PSD are manufactured by TSI Instruments Inc. and include a model 3065 low flow thermodenuder (TD), model 3071A electrostatic classifier (EC) and a model 3025A condensation particle counter (CPC). After passing through the dilution system the exhaust sample passes into the TD which is a second source of sample conditioning. The TD removes any remaining volatile components before delivering the sample to the EC [38]. After traveling through the TD, the exhaust sample is transported to the EC and then to the CPC which measures the size distribution characteristics of the sample [39].

Data were collected with the TD heated to a temperature of 230°C. By heating the TD to this temperature, a more consistent sample is provided to the EC by ensuring that hydrocarbons and soluble organic fraction (SOF) present in the sample remain in gaseous form [39]. The activated carbon used within the TD removes the HC molecules from the exhaust gas as it passes through TD therefore providing a “dry” sample to the EC.

The acquisition of the PSD was acquired with the software programmed with an up scan time of 180 seconds and a down scan time of 60 seconds. The diluted sample flow rate used during this study was 0.7 lpm. Corrections were made to the data for losses due to the use of the thermodenuder using methods developed in reference [38] and to account for the dilution ratio used during sampling. This procedure provides the PSD weighted by number or volume for the selected sampling location. Due to a failure of the EC, PSD data were only acquired while testing on the ISM. A summary of the steps necessary to accurately acquire particle size data is detailed below. The development of this process

can be found in Appendix E. The following procedure is used to collect PSD data during steady state engine testing.

1. Prior to measuring PSD data, determine the experimental dilution ratios that are being used at each of the three sample locations, UDOC, DDOC and DCPF.
2. These dilution ratios should be measured while using the identical engine operating conditions that are to be used during the steady state testing.
3. Determine the concentration of particles in the compressed air (C_{CA}) used for the dilution system by measuring the size distribution within the air.
4. Record the PSD data during testing using the dilution system and thermodenuder at all sampling locations when measuring a “dry” sample. This method allows for consistent conditioning of the sample before measurement.
5. After the collection of raw data has been performed, the first step of post processing is accounting for losses created by the use of the thermodenuder using equations 3.2 and 3.3 [38].

$$TP(\%) = a \cdot T(^{\circ}C) + b \cdot D(nm) + c \quad 3.2$$

$$T_{Loss} = 1 - \frac{TP}{100} \quad 3.3$$

TP = % of particles passing through thermodenuder

$a = -0.0864 (^{\circ}C^{-1})$

$b = 0.0108 (nm^{-1})$

$c = 91.9$

D = diameter of the particle (nm)

T_{Loss} = Losses created by use of the thermodenuder in fraction form

After accounting for losses, the dilution ratio at each location needs to be accounted for by using equation 3.4.

$$C_{\text{Exhaust}} = \frac{(D_R + 1)D_{\text{cpc}}}{[1 - T_{\text{Loss}}]} - D_R C_{\text{CA}} \quad 3.4$$

C_{Exhaust} = Actual particle concentration in exhaust, (particles/cm³ or nm³/cm³)

D_{cpc} = Recorded particle of CPC counter, (particles/cm³ or nm³/cm³)

T_{Loss} = Thermodenuder losses in fraction form. “0.9 not 90%”

C_{CA} = Concentration of particles in compressed air used for dilution,
(particles/cm³ or nm³/cm³)

D_R = Dilution ratio

3.2.8 PM Mass Retained in the CPF

In order to perform a mass balance for the performed experiments, the CPF is weighed multiple times during testing. Throughout all of the testing on the 2002 ISM and 2007 ISL the same scale was used for the weighing process. The scale used for the mass measurement was an Ohaus Ranger model 35LM with a readability of 0.1 g, and a repeatability of ± 0.3 g.

From experimentation and analysis performed in reference [33], it has been shown that the mass of the CPF can be heavily influenced by the temperature that it is weighed at. As such, great care was taken to ensure that the CPF was weighed at approximately the same temperature during each stage of the test. The CPF was weighed while it was in a vertical orientation with two steel caps attached to the ends. The ends are capped to prevent flow through the channels during the weighing process. This prevents the lifting phenomenon that could be created from the shear force generated by the flow of air through the channels of the filter [33].

To ensure that the CPF is weighed at the same temperature throughout the test process, temperature measurements are recorded prior to weighing at each of the locations shown in Figure 3.7. When performing tests at the same engine operating conditions, temperature variation within the CPF does occur when the tests occur on different days. This can be attributed to changes in the test cell conditions such as the ambient temperature and relative humidity. These parameters vary due to the fact that the test cell does not have the ability for climate control.

The individually measured substrate temperatures within the CPF can vary widely. As an example, measured temperatures within the CPF at a given time after operating at 2100 rpm and 195 N can range from 180°C to 290°C. Due to the temperature gradients, it is not practical to specify an average CPF temperature at which weighing occurs for every test. The preferred approach is to ensure that the individual temperature measurements, shown in Figure 3.7 by the thermocouple locations, vary by no more than $\pm 15^{\circ}\text{C}$ during the different portions of the test.

Along with the measured temperatures within the CPF substrate, one thermocouple is placed in each of the end caps which allows for the measurement of the air trapped under each of the caps. After the temperatures are recorded, the mass of a calibration weight is measured as a calibration check to ensure that the mass measurements from test to test are repeatable. If the mass of the calibration weight is consistent with previous testing, the mass of the CPF is measured three times and an average of the three masses is used for calculation purposes. If the individual temperatures of the CPF vary by more than $+15^{\circ}\text{C}$ between the mass measurements for the different portions of the test, the CPF is allowed to cool and the temperatures and mass measurements are performed again. The detailed mass measurement procedure can be found in Appendix F.

3.3 Passive Oxidation Test Procedure-Overall Approach

The main objective of passive oxidation testing is to determine the reaction rate that occurs during the test. In order to accomplish this, a combination of modeling and several mass measurements are required. Modeling is used as a substitute when mass measurements are subject to errors. This error is due to difficulties in obtaining accurate mass measurements of the CPF at elevated temperatures as described in 3.2.8. The MTU 1-D CPF model is used to predict the deposition of PM in the CPF during the first and last thirty minutes of the test.

By using the model to simulate the first 30 minutes of the test, the clean weight of the CPF can be predicted without having to measure the mass of the CPF at elevated temperatures where there is potential for error. This provides the clean weight of filter which is used in the remainder of the calculations to determine the CPF loading and reaction rates during the test. By using the model for the last 30 minutes of the experiment, the PM deposited during this time can be determined which then allows the calculation of the reaction rate during the passive oxidation portion of the test. A full description of the test procedure along with the calculations used in the mass balance is discussed in Appendix G while a brief summary of the process is described in the following paragraphs.

Passive oxidation testing is broken up into four parts. An example of the pressure drop profile and estimated particulate matter (PM) retained in the CPF during the four parts can be seen in Figure 3.8. The four separate parts are listed in the following paragraphs with an explanation of what occurs during each portion of the test.

1. Stage 1 (S1): This immediately follows the clean out of the filter. The engine is operated at loading conditions for thirty minutes to ensure that the CPF has returned to a repeatable temperature for weighing.
2. Stage 2 (S2): The engine is operated at the Stage 1 loading conditions until a catalyzed particulate filter (CPF) loading of 2.2 ± 0.2 g/L is achieved.

3. Passive Oxidation (PO): The engine operating conditions are changed to obtain a specified exhaust mass flow rate $\pm 5\%$ and diesel oxidation catalyst (DOC) inlet temperature $\pm 10^\circ\text{C}$. After a predetermined amount of time or prior to the pressure drop profile across the CPF becoming horizontal, the PO portion of the experiment is halted and the transition is made to Stage 3 loading.
4. Stage 3 (S3): This immediately follows the passive oxidation stage and the engine is returned to the conditions that were used during Stages 1 and 2 loading. Operating in this manner for 30 minutes allows the CPF to return to a similar temperature that was seen at the end of Stage 1. This strategy improves the consistency of the CPF weighing procedure.

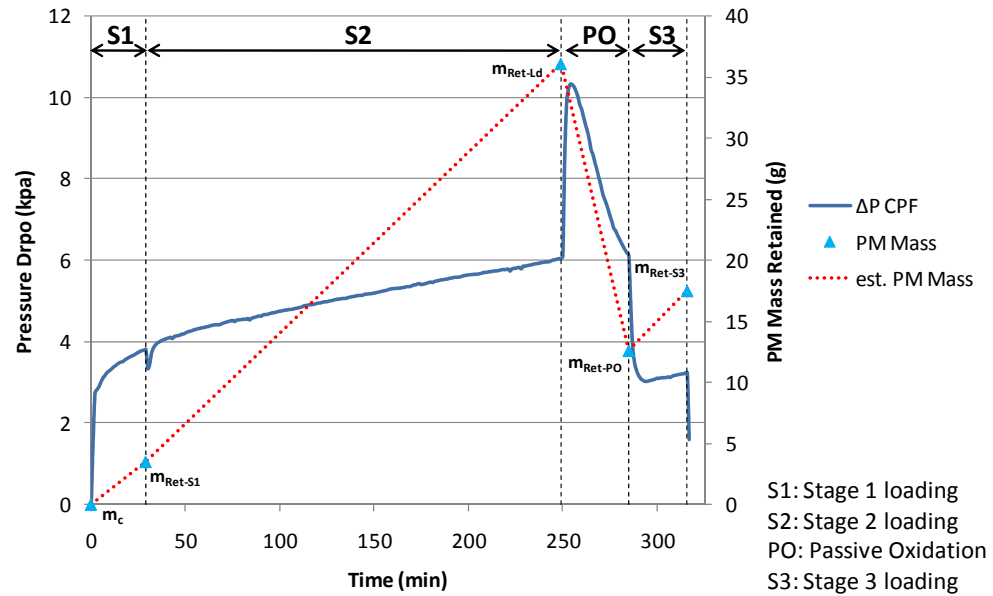


Figure 3.8: Overview of the Four Main Stages of the Passive Oxidation Test Procedure

The test begins by performing a clean out of the CPF. After it has been determined that the filter is clean, by observing a horizontal pressure drop profile during the clean out, Stage 1 loading is performed for 30 minutes which allows the CPF to reach a stable, repeatable temperature. After the completion of Stage 1 loading, the CPF is removed from the exhaust system and weighed on a scale with a resolution of 0.1 g and a repeatability of ± 0.3 g. The mass of the CPF is recorded and the aftertreatment assembly is reassembled allowing the system to be prepared for Stage 2 loading. Assembly and disassembly of the after treatment system should be done in a consistent manner which will allow for approximately the same amount of time to pass before the CPF is weighed, thus providing a consistent temperature of the CPF.

Stage 2 loading uses the same engine operating parameters as Stage 1 but is performed until the CPF reaches a nominal target loading of 2.2 ± 0.2 g/L. The time required to reach the specified CPF loading is predicted by two different methods. First, the MTU 1-D CPF model is used to predict the time required for loading. A second estimate is provided by the experience gained from performing previous passive oxidation testing at the Michigan Technological University test cell. After performing several tests, an estimate for the loading time can be generated by reviewing the loading times of previous tests. The actual CPF loading is determined by disassembling the aftertreatment system and weighing the CPF. If the CPF loading of 2.2 ± 0.2 g/L is confirmed, the aftertreatment assembly is reassembled and the experiment proceeds to the Passive Oxidation (PO) portion of the test. If the loading of the CPF is below the specified value by more than 0.2 g/L, additional loading is performed until the nominal loading value is obtained.

In most cases, the PO portion of the test is performed at engine operating conditions different from those used for loading, however some tests will use the same conditions for both loading and passive oxidation. The MTU 1-D CPF model is used to predict the amount of time that the engine remains at the PO conditions to ensure that the balance point of the system is not reached. A description of the balance point can be found in the Passive Regeneration section in Chapter 2. In addition, the pressure drop profile across the CPF is monitored to ensure that the balance point is not reached. When the system

reaches the balance point, the rate of change of PM within the CPF is zero which prevents the calculation of an accurate reaction rate. When it has been determined that a sufficient amount of time has passed, the PO portion of the test is ended and Stage 3 loading is initiated.

Stage 3 loading is performed at the same engine operating conditions as Stage 1 and 2. The main purpose of Stage 3 loading is to allow the CPF to reach a stable, repeatable temperature. It is an important modeling objective to see if the CPF 1-D model can simulate loading, passive oxidation and the Stage 3 part of the test, so this stage is also important for the calibration of the 1-D CPF model since it signifies the end of the test and provides the final condition for the model to replicate. Stage 3 is performed for about thirty minutes allowing the CPF to reach a similar temperature to what was experienced in Stage 1 and 2. After Stage 3 is completed the aftertreatment assembly is removed from the exhaust system and disassembled which allows the CPF to be weighed. This is the last stage of the test and a detailed explanation of each stage of the testing process can be found in Appendix G.

3.4 Passive Oxidation Test Matrix

In order to determine the dominant factors in passive oxidation of PM in a CPF, a series of tests were created which covered a range of engine operating conditions. From the literature review, it has been determined that the important factors involving passive oxidation are the CPF temperature, NO_2 concentration and flow rate into the CPF, in addition to the NO_2/PM ratio into the CPF.

Preliminary calculations of the reactions concerning passive oxidation of PM by NO_2 in the CPF have been undertaken to determine what the stoichiometric ratio of NO_2/PM would be. When calculated on a mass basis, the stoichiometric ratio of NO_2/PM is 7.67 to 1. This calculation can be seen in Appendix H. This information is important in determining the correct engine operating conditions to ensure that the selected conditions will provide data that uses NO_2/PM ratios that are both above and below this

stoichiometric ratio. Collecting data from conditions above and below the stoichiometric ratio will be necessary to allow for an accurate representation of an on-road operating engine and the reaction rates experienced during this operation.

The test matrix was completed using two engines, a Cummins 2002 246 kW ISM and a Cummins 2007 272 kW ISL. Through the use of two different engine technologies a wider range of operating conditions were available for testing over a range of NO₂ concentrations, NO₂ flow rates and NO₂/PM ratios. In order to obtain an accurate comparison of the results across engines, two of the parameters were kept constant during testing. These were DOC inlet temperature and exhaust mass flow rate.

Preliminary data were gathered from engine maps provided by Cummins to select the initial test conditions. The information from these engine maps allowed the selection of various engine loads and speeds to vary DOC inlet temperatures and exhaust mass flow rates. With this information, testing was performed on the engines to verify the necessary engine operating conditions required to obtain a specified exhaust mass flow rate and DOC inlet temperature. This testing was termed “Point Validation” and consisted of a full day of testing.

Goals for the specified engine operating conditions were as follows. The DOC inlet temperature was maintained at +/- 10°C and the exhaust mass flow rate was +/- 5% of the specified value. During the point validation portion of the testing, the engine load and speed were adjusted to obtain the necessary exhaust flow rate and DOC inlet temperature. The engine was operated until steady state was achieved and then measurements were gathered to be used for the pre-test modeling effort. This included gaseous emissions, PM concentrations, temperatures, flow rates and pressure drops across the DOC and CPF.

The engine speed and loads determined during point testing which provided for the specified exhaust mass flow rate and DOC inlet temperature can be viewed in Table 3.11. Each set of conditions was given a reference letter to simplify future discussions. The temperatures and flow rates listed in this table are target values.

During the actual experiments, the load and speed are set to the values previously determined during point validation testing and all other parameters are allowed to find their steady state values for the day.

This method was chosen because it allows for a more consistent engine operation between experiments. By trying to exactly match the flow rate and temperatures in Table 3.11 on test days, it was found that this sometimes required a significant change to the engine speed and load which resulted in the engine operating in a different portion of the calibration map. When the engine changed operating points on the engine map other variables would change at the same time requiring an adjustment to the test plan for the day negating all of the preliminary test planning.

Table 3.11: Selected Engine Operating Conditions

ISM 246 kW						
Ref. #	Temp	Flow	Speed	Torque	DOC Space Velocity	CPF Space Velocity
	°C	kg/min	rpm	Nm	1/hr	1/hr
A	260	5.2	1080	320	94k	76k
B	274	12.8	1800	300	230k	186k
F	371	6.8	1130	580	148k	120k
H	427	14.5	1300	1160	330k	267k
J	482	17.2	1270	1500	418k	339k

ISL 272 kW						
Ref. #	Temp	Flow	Speed	Torque	DOC Space Velocity	CPF Space Velocity
	°C	kg/min	rpm	Nm	1/hr	1/hr
A	260	5.2	1200	275	94k	76k
B	274	12.8	2100	195	230k	186k
F	371	6.8	1290	540	148k	120k
H	427	14.5	1510	1045	330k	267k
J	482	17.2	1650	1250	418k	339k

With the experimental engine operating conditions determined, a test matrix was created which provided for a wide range of NO₂ and exhaust mass flow rates, DOC inlet temperatures and NO₂/PM ratios. The test matrix of the experiments performed for this thesis with the experimental values of engine speed and load can be seen in Table 3.12. Other recorded values such as the gaseous emissions, PM concentrations, temperatures and experimentally determined reaction rates will be detailed in Chapter 4.

Table 3.12: Passive Oxidation Test Matrix with Experimental Values

ISM 256 kW																
	Test Condition	Reference Point	Average CPF Temp.	Engine Speed	Engine Torque	CPF Loading at End of Stage	Exhaust Flow	DOC Space Velocity	CPF Space Velocity	Engine out PM Conc.	NOx Conc. into CPF	NOx Conc. into CPF	NO2 Conc. into CPF	NO2 Conc. into CPF	NOx/PM	NO2/PM
			°C	rpm	Nm	g/L	kg/min	1/hr	1/hr	mg/scm	ppm	mg/scm	ppm	mg/scm	-	-
Test 1	Loading	B	270	1800	300	2.2	13.1	244k	196k	15.1	192	361	94	177	23.9	11.7
	Passive Ox.	F	327	1170	510	2.0	6.8	140k	114k	32.1	220	414	138	259	12.9	8.1
Test 2	Loading	B	272	1800	300	2.1	13.2	246k	198k	15.7	192	361	88	165	23.0	10.5
	Passive Ox.	F	348	1130	580	1.5	6.8	145k	118k	30.6	245	461	112	211	15.1	6.9
Test 3	Loading	B	270	1800	300	2.2	13.0	241k	194k	14.9	191	359	95	179	24.1	12.0
	Passive Ox.	H	411	1300	1160	0.3	14.4	338k	268k	5.4	460	865	168	316	160.1	58.5
Test 4	Loading	B	272	1800	300	2.3	12.7	236k	190k	15.7	193	363	99	186	23.1	11.9
	Passive Ox.	J	463	1270	1500	0.6	16.9	423k	335k	7.1	411	773	86	162	108.8	22.8
Test 5*	Loading	F	351	1780	600	1.1	6.8	151k	117k	39.2	281	528	158	297	13.5	7.6
	Loading	F	358	1780	600	1.1	6.7	146k	117k	39.2	289	543	163	306	13.9	7.8

*ISM Test 5 was performed at different operating conditions during loading than other tests

ISL 272 kW																
	Test Condition	Reference Point	Average CPF Temp.	Engine Speed	Engine Torque	CPF Loading at End of Stage	Exhaust Flow	DOC Space Velocity	CPF Space Velocity	Engine out PM Conc.	NOx Conc. into CPF	NOx Conc. into CPF	NO2 Conc. into CPF	NO2 Conc. into CPF	NOx/PM	NO2/PM
			°C	rpm	Nm	g/L	kg/min	1/hr	1/hr	mg/scm	ppm	mg/scm	ppm	mg/scm	-	-
Test 2	Loading	B	266	2100	200	2.2	13.2	243k	195k	17.2	85	160	34	64	9.3	3.7
	Passive Ox.	F	359	1290	550	0.9	7.7	165k	136k	6.9	206	387	117	220	56.1	31.9
Test 1	Loading	B	270	2100	200	2.4	13.4	247k	200k	18.5	79	149	30	57	8.0	3.1
	Passive Ox.	A	252	1200	280	2.4	5.6	100k	83k	6.0	283	532	151	284	88.7	47.3
Test 4	Loading	B	266	2100	200	2.2	13.1	241k	193k	17.6	80	150	30	57	8.5	3.2
	Passive Ox.	H	409	1520	1040	1.1	15.1	348k	277k	6.5	200	376	73	137	57.8	21.1
Test 5	Loading	B	260	2100	200	2.2	13.2	237k	193k	16.4	93	175	33	62	10.7	3.8
	Passive Ox.	J	437	1650	1250	1.2	18.0	423k	337k	13.3	174	327	45	85	24.6	6.4
Test 3	Loading	B	265	2100	200	2.2	13.3	241k	196k	17.5	83	156	30	56	8.9	3.2
	Passive Ox.	F	365	1290	560	0.9	7.7	162k	137k	7.0	223	419	116	218	59.9	31.2

Chapter 4 Experimental Results

The results from the separate stages of the performed tests will be discussed. The temperatures and exhaust flow rates for comparable tests from the ISM and ISL will differ from one another due to a change in testing strategy that was implemented during the test matrix. After completing a portion of the test matrix on the ISM, it was decided to set the engine speed and load during testing and then allow the engine and aftertreatment system to reach a steady state flow rate and temperature for that day. Previously adjustments were made to the engine operating conditions on each day of the test.

Since two emissions analyzers were used during testing, a comparison of these instruments will be presented so that the emissions values of the two engines can be better understood. A relation between the absolute humidity of the test cell and PM concentrations exiting the engine has been correlated allowing for a better estimate of loading times for tests. An investigation into the temperature distribution within the diesel oxidation catalyst (DOC) and catalyzed particulate filter (CPF) were performed in order to understand the gradients within these devices. Each stage of the test is discussed and conclusions are drawn when required. The discussion of the stages is separated into three parts. The gaseous emissions, pressure drop profiles across the CPF, and the PM reaction rates are discussed. The last section of this chapter compares the two catalyzed particulate filters that were used for testing on the ISM and ISL.

4.1 Emissions Analyzer Comparison

As discussed in Chapter 3, two gas analyzers were used on the performed experiments. Gaseous emissions during testing on the ISM were measured with both a Semtech DS and Pierburg AMA 4000 while only the Pierburg was used on the ISL. During testing on the ISM, the Semtech was used only for NO, NO₂ and NO_x measurements, all other values were measured by the Pierburg. For NO, NO₂ and NO_x measurements, the

analyzers use different measuring principles, the Pierburg uses a chemiluminescence detector (CLD) while the Semtech uses a non-dispersive ultraviolet (NDUV) analyzer.

The CLD analyzes the exhaust gas hot, which is termed a “wet” measurement while the Semtech has the exhaust gas passed through a heat exchanger which condenses the water out of the exhaust before it enters the analyzer. When the water is removed from the exhaust, the measurement is termed a “dry” measurement. Since the raw exhaust gas sample is conditioned by different methods and measured using different principles, the resultant concentration values are not directly comparable. To compensate for the analyzers measuring the exhaust gas with and without the water, all NO, NO₂ and NO_x measurements performed by the Semtech have been converted to wet measurements.

A comparison test was performed with the Semtech and Pierburg to determine if the resulting measurements of NO, NO₂ and total NO_x from the analyzers were comparable after correcting for the difference in measuring dry versus wet. Three engine operating conditions were selected for this test. The selected conditions cover the engine speed and load conditions during previous testing to give a wide range of temperatures and NO_x values for comparison.

There was approximately 9 months between testing on the ISM and this comparison test. During this time the Semtech was used offsite for several different tests. There is no certainty that when tested the Semtech was operating in the same manner as it was when testing was performed on the ISM. In addition to this, the CLD in the Pierburg malfunctioned and was sent to AVL for repair in between ISL 365 Test 4 and Test 5. During the repair, replacement parts were installed and AVL calibrated the CLD. Due to these changes there is uncertainty that the measured values before and after calibration would be the same.

Testing was performed post CLD repair on the Pierburg and NO, NO₂ and NO_x values were similar to prior values at the selected conditions as can be seen in Table 4.1. Some of the values do differ between pre and post repair, but the reader is directed to the CPF inlet temperature which differs by approximately 20°C to 40°C between the test

sessions. This difference in CPF inlet temperature likely means that the engine was operating in a different manner, even though the load and speed used for each test was the same.

Table 4.1: Post CLD repair Testing Engine Out Emissions

	Speed	Load	CPF Inlet Temp		NOx		NO		NO2	
	(rpm)	(Nm)	(deg C)		(ppm)		(ppm)		(ppm)	
	N/A	N/A	Pre	Post	Pre	Post	Pre	Post	Pre	Post
Point B	2100	195	272	251	82	76	51	55	31	21
Point F	1290	540	367	339	191	186	178	175	13	12
Point J	1650	1250	476	437	148	165	139	156	9	9

The three selected conditions used for the comparison test are engine operating points B, F, and H. The engine speed and load for these operating points can be found in Table 4.1. The results for the analyzer comparison can be seen in Table 4.2. NO accuracy values for the Pierburg are not available while the reported accuracy of the Semtech is $\pm 3\%$ of the analyzer reading or ± 15 ppm whichever is greater. Across the test conditions, the difference in measurements of NO concentrations varied from -11 ppm to +14 ppm. While the NO values do differ between analyzers, this is not expected to significantly affect the NO to NO₂ conversion efficiencies across the DOC. As an example, the conversion efficiency for Point F from the data in Table 4.2 is 52% for the ISM and 56% for the ISL.

Table 4.2: Emissions Analyzer Comparison Test Results (wet measurements)

		NO (ppm)			NO ₂ (ppm)			NO _x (ppm)		
		Pierburg	Semtech	Difference	Pierburg	Semtech	Difference	Pierburg	Semtech	Difference
Point B	UDOC	55	41	14	27	19	8	82	60	22
	DDOC	52	47	5	29	19	10	81	67	14
	DCPF	32	26	6	47	39	8	79	65	14
Point F	UDOC	203	215	-11	16	11	5	219	225	-6
	DDOC	98	95	2	120	103	17	217	198	20
	DCPF	104	97	7	113	99	14	217	195	21
Point H	UDOC	203	204	-1	16	7	9	219	211	8
	DDOC	140	143	-3	76	60	17	216	202	14
	DCPF	132	139	-7	76	66	11	208	204	4
		Average			Average			Average		
		1			11			12		

For NO₂, the accuracy values for the Pierburg are not available while the reported accuracy of the Semtech is $\pm 3\%$ of the analyzer reading or ± 10 ppm whichever is greater. The difference across all test conditions is from 8 to 17 ppm with an average of 11 ppm with the tendency of the Semtech to read lower than the Pierburg. Overall NO_x differences are just the sum of the prior two species so will not be discussed.

If the assumption is made that both analyzers were performing the same during the comparison test as they were during passive oxidation testing, although this is probably not a good assumption, the following could be implemented. Adjustments to the NO values for the testing on the ISM are hard to determine since the differences vary widely. The NO₂ values for testing on the ISM could be increased by 10 ppm if modeling efforts supported this increase. Simulations would need to be performed to determine if the modeling reaction rates provided for a better agreement with the measured PM masses.

4.2 PM Concentrations

PM concentrations were collected during each stage of the test. During stage 1 and 3, only one sample was collected upstream of the diesel oxidation catalyst (UDOC) due to the short duration of this stage. The number of samples collected during Stage 2 varied but a minimum of one sample downstream of the catalyzed particulate filter (DCPF) and five samples UDOC were collected. The UDOC samples from Stage 1, 2, and 3, which can be seen in Appendix I, were averaged to determine the PM concentration to be used in the mass balance for the loading portions of the tests. The tabulated results of the experimental PM concentrations are shown in Table 4.3. Also listed in Table 4.3 is the coefficient of variance (C.O.V.) for the samples collected for each test. The coefficient of variance is defined as the ratio of the standard deviation divided by the mean. ISM Test 5 was conducted at operating conditions different than the standard loading conditions and this is the reason PM concentrations within the table differ for this test.

Table 4.3: Experimental PM Concentrations

		ISM					ISL				
		Average PM Concentrations*									
		Test 1	Test 2	Test 3	Test 4	Test 5	Test 2	Test 1	Test 4	Test 5	Test 3
Loading Conditions	UDOC (mg/scm)	15.1	15.7	14.9	15.7	39.2	17.2	18.5	17.6	16.4	17.5
	UDOC C.O.V. (%)	7.2	3.1	4.0	2.5	9.9	2.3	1.4	3.7	2.8	5.0
	DCPF (mg/scm)	0.6	0.5	0.1	0.5	N/A	0.3	0.4	0.3	0.3	0.3
Passive Oxidation Conditions	UDOC (mg/scm)	32.1	30.6	5.4	7.1	39.2	6.9	6.0	6.3	13.3	7.0
	UDOC C.O.V. (%)	17.3	12.3	6.9	5.5	5.8	2.0	2.2	5.4	5.3	4.5

* Only one sample was collected DCPF

In reference [33] it was shown that PM concentrations can vary based upon ambient test cell conditions. Over the course of testing on the ISL, a correlation was demonstrated relating the absolute humidity of the test cell and engine out PM concentration. The test cell conditions that were recorded for the individual experiments can be seen in Table 4.4. The PM concentrations and absolute humidity are plotted in Figure 4.1 with the error bars representing one standard deviation of the samples from each test. Data acquired for the ISM does not display any visible trends but the ISL data does show an increasing trend as the absolute humidity increases. As discussed in Appendix G, this correlation has been used successfully for predicting the times required to reach a CPF PM loading 2.2 g/l. It is possible that there exists some lower threshold for the absolute humidity in order for this phenomenon to occur. This would explain why this trend was not shown with the ISM data due to testing taking place in the drier winter month of January.

Steady state filtration efficiencies are calculated using the PM mass measurements. This is discussed in section 3.2.6 and uses equation 3.1. A summary of the calculated filtration efficiencies for the ISM and ISL can be seen in Table 4.5. The average experimental filtration efficiencies were 97.3% and 98.1% for the ISM and ISL respectively. Since ISM Test 5 was performed using different conditions than the other

tests, a PM sample downstream of the CPF was not obtained preventing the calculation of the filtration efficiency.

Table 4.4: Test Cell Conditions during Passive Oxidation Testing

	Temperature	Relative Humidity	Atmospheric Pressure	Absolute Humidity	PM Concentration	PM Conc. Std Dev
Test	(°C)	(%)	(in Hg)	(kg water vapor/kg of dry air)	(mg/scm)	(mg/scm)
ISM Test 1	25.3	9.5	29.57	0.00191	15.1	1.1
ISM Test 2	25.5	6.2	29.73	0.00125	15.7	0.5
ISM Test 3	29.3	12.1	29.19	0.00312	14.9	0.6
ISM Test 4	26.5	19.5	28.39	0.00440	15.7	0.4
ISL Test 2	30.0	26.7	29.05	0.00725	17.2	0.4
ISL Test 1	33.5	31.5	29.27	0.01042	18.5	0.3
ISL Test 4	33.4	25.6	29.22	0.00842	17.6	0.7
ISL Test 5	29.4	23.8	29.33	0.00617	16.4	0.5
ISL Test 3	29.1	35.7	28.88	0.00929	17.5	0.9

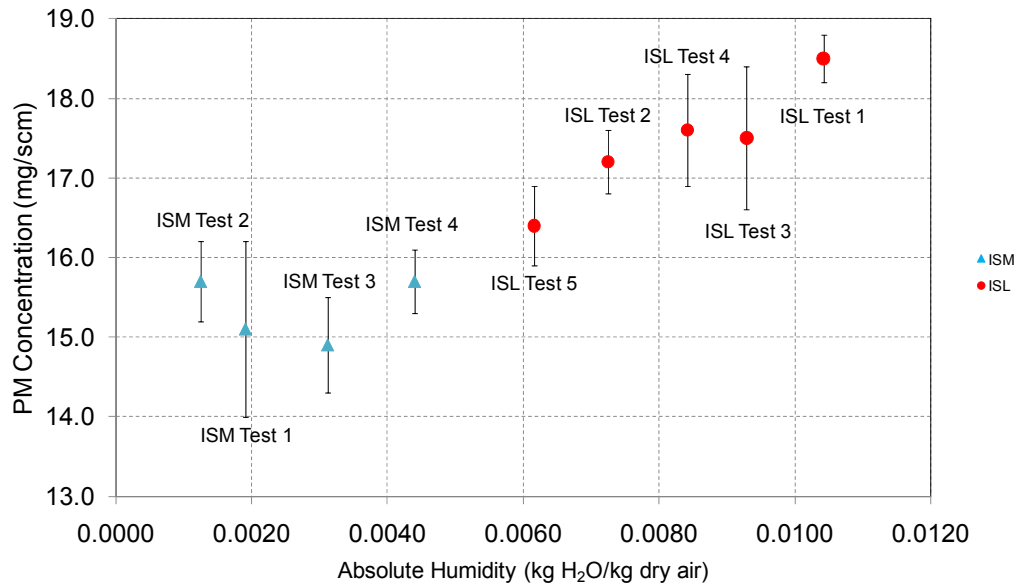


Figure 4.1: PM Concentration Variation Due to Absolute Humidity

Table 4.5: Calculated CPF Filtration Efficiencies

ISM CPF Filtration Efficiency						
Test 1	Test 2	Test 3	Test 4	Test 5	Average	Std. Dev
96.2	96.7	99.1	97.0	-	97.3	1.3

ISL CPF Filtration Efficiency						
Test 2	Test 1	Test 4	Test 5	Test 3	Average	Std. Dev
98.1	97.8	98.2	98.1	98.1	98.1	0.2

4.3 Gas Temperature Analysis

Since temperature plays such an important role in the passive oxidation of PM by NO₂, both through the production of NO to NO₂ and the dependence of the reaction rate on temperature, an effort was made to perform tests with additional thermocouples located within the DOC and CPF. This additional data collection has allowed for a better understanding of the thermal gradients located in the DOC and CPF and will be explained below. For the ISM tests, this was accomplished by increasing the number of thermocouples in the radial direction from three to five within quadrant II of the DOC as shown in Figure 3.5. A total of 16 thermocouples were used within the CPF to aid in this investigation.

4.3.1 DOC Temperatures

For ISL Test 1, 2, and 4, five thermocouples were also located in the radial direction within quadrant II of the DOC. The quadrant location was originally shown in Figure 3.4. The T/C layout of the DOC for the first three tests on the ISL can be seen in Figure 3.5. In addition, three more thermocouples were placed in quadrant III in order to determine if a temperature variation was present based upon the possibility of preferential heat transfer in one direction. The thermocouple layout for ISL Test 3 and 5 was changed to allow for the investigation of axial temperature gradients within the DOC. This layout can be seen in Figure 3.6. The additional radial thermocouples in quadrant II were removed

and placed along the same radial distance from the centerline of the DOC substrate while equally spacing them from the front to the back of the substrate.

Since five thermocouples were located in quadrant II for both the ISM and ISL, a direct comparison of the temperature gradients within the DOC can be performed. Several different operating conditions were chosen for comparison in order to provide a wide range of temperatures to investigate. The recorded temperatures used for this comparison can be seen in Figure 4.2. The overall shapes of the radial temperature profiles are similar for all operating conditions. As expected, at the peripheral of the DOC, the largest difference between any two thermocouples is present. This is a result of the convective and radiative heat transfer to the test cell.

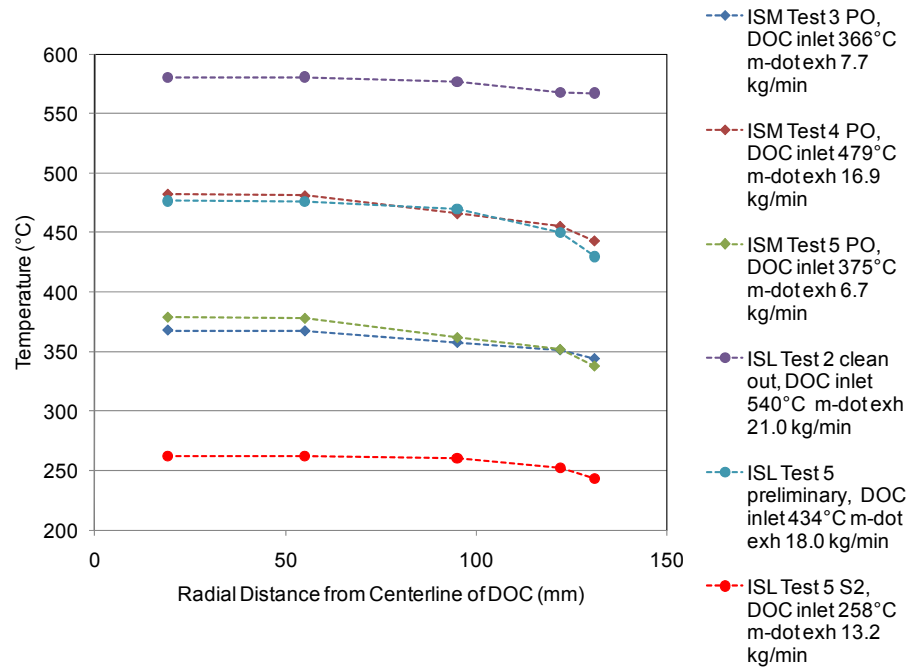


Figure 4.2: DOC Radial Temperature Distributions

The magnitudes of the temperature differences for the data in Figure 4.2 can be seen in Figure 4.3. This is the difference in temperature of the thermocouples at the radii of 45 mm and 131 mm. For all but one of the cases, as the inlet temperature of the DOC

increases the magnitude of the difference increases also. The lone exception is the CPF clean out performed during ISL Test 2 which has the highest inlet temperature and the smallest gradient. This is likely the result of the exothermic reaction taking place within the DOC due to the oxidation of hydrocarbons.

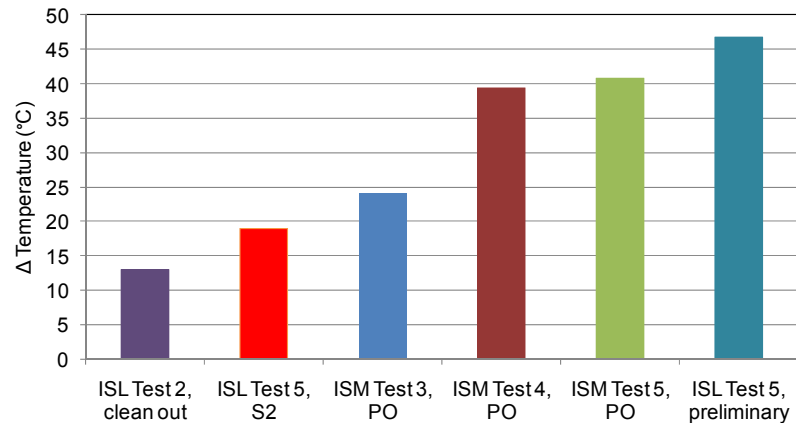


Figure 4.3: Magnitudes of Radial Temperature Differences in Quadrant II

The presence of radial temperature gradients will have an effect on NO to NO₂ conversion efficiency across the DOC. The magnitude of this effect depends upon the temperature of the system and which portion of the NO to NO₂ conversion efficiency plot the temperatures fall on. The overall effect of the gradients will then be different for each system and for each operating condition as it has been shown that the NO to NO₂ conversion efficiency of the DOC is both temperature and space velocity dependent which will change the shape of the conversion efficiency plot.

The data acquired for the analysis of the quadrant II and III temperatures can be seen in Figure 4.4. Three engine operating conditions were chosen to provide a range of temperatures to analyze. As can be seen in Figure 4.4, there is minimal temperature variation between quadrant II and III when the temperature measurements are recorded at the same radial distance. This is indicated by the close proximity of the data points taken at the same radial dimension. It therefore appears that the temperature is uniform

throughout the DOC at the same radial dimension but there are gradients present between two radial dimensions.

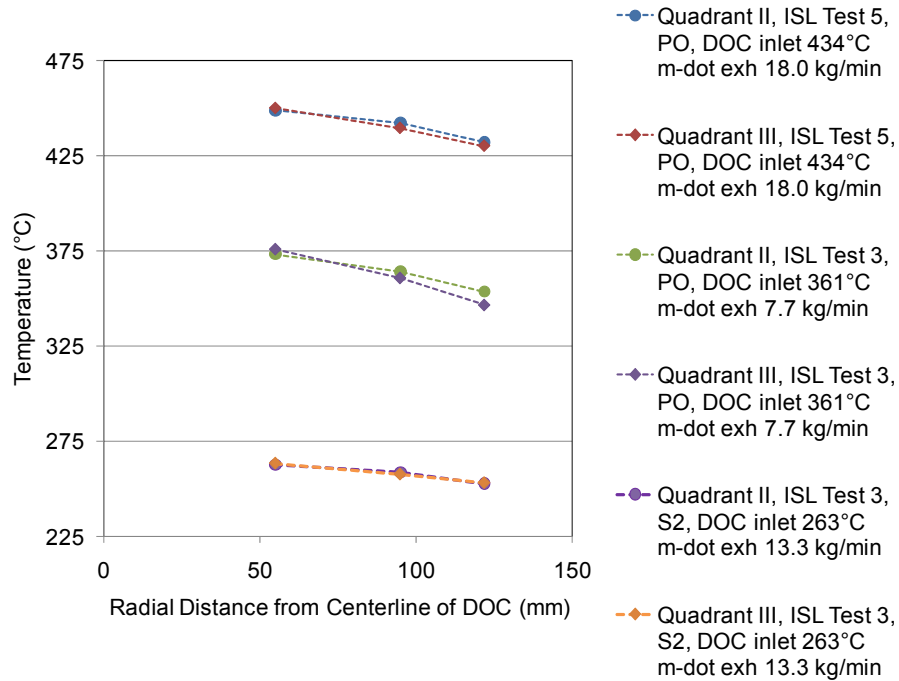


Figure 4.4: Comparison of Radial Temperature Profiles for DOC Quadrant II and III

Axial temperature gradients within the DOC were also investigated and can be seen in Figure 4.5. Again three engine operating conditions were selected to provide a range of temperatures to investigate. The three thermocouples used were placed at a radial distance of 95 mm from the centerline of DOC substrate. It can be seen in Figure 4.5 that there is minimal temperature variation along the length of the DOC during the selected operating conditions. Therefore, as long as the system is operating at steady state, it is valid to assume the axial temperature is constant at this radial distance. A good assumption would be that this holds at other radial distances but should be experimentally verified.

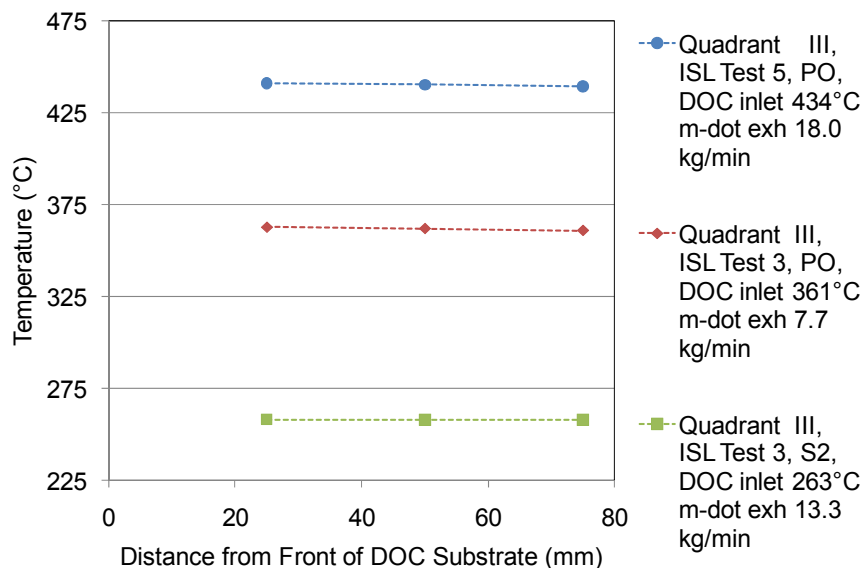


Figure 4.5: DOC Axial Temperature Profiles

4.3.2 CPF Temperatures

As shown in Figure 3.7, the current thermocouple layout in the CPF uses 16 thermocouples. This layout provides for the determination of the axial and radial temperature distribution within the CPF. An example of the data provided by these thermocouples, recorded during the passive oxidation portion of ISL Test 3, is shown in Figure 4.6. When the information is displayed in this manner, the transient response of the temperatures during the start of the passive oxidation portion of the test is visible. It takes approximately 20 minutes for the all of the temperatures to stabilize and this is a result of the thermal mass of the CPF. This long stabilization period is a driving factor in the calculation of an average reaction rate for experimental results as it would be difficult to account for this initial transient period accurately without the aid of a model.

The format used for the display of temperature data in Figure 4.6 is useful for an overall view of the temperatures within the CPF. It is however difficult to make direct comparisons of radial and axial temperatures when the data is displayed in this manner.

In order to determine axial temperature gradients within the CPF, the average temperature was calculated at each of the thermocouples for the passive oxidation portion of ISL Test 3. These data were then plotted based upon the location of the T/C within the CPF and can be visualized in Figure 4.7. Both the radial and axial location of the thermocouples were taken into account with the radial location indicated by the x-axis on the graph and the axial location being represented by the different markers and colored dotted lines.

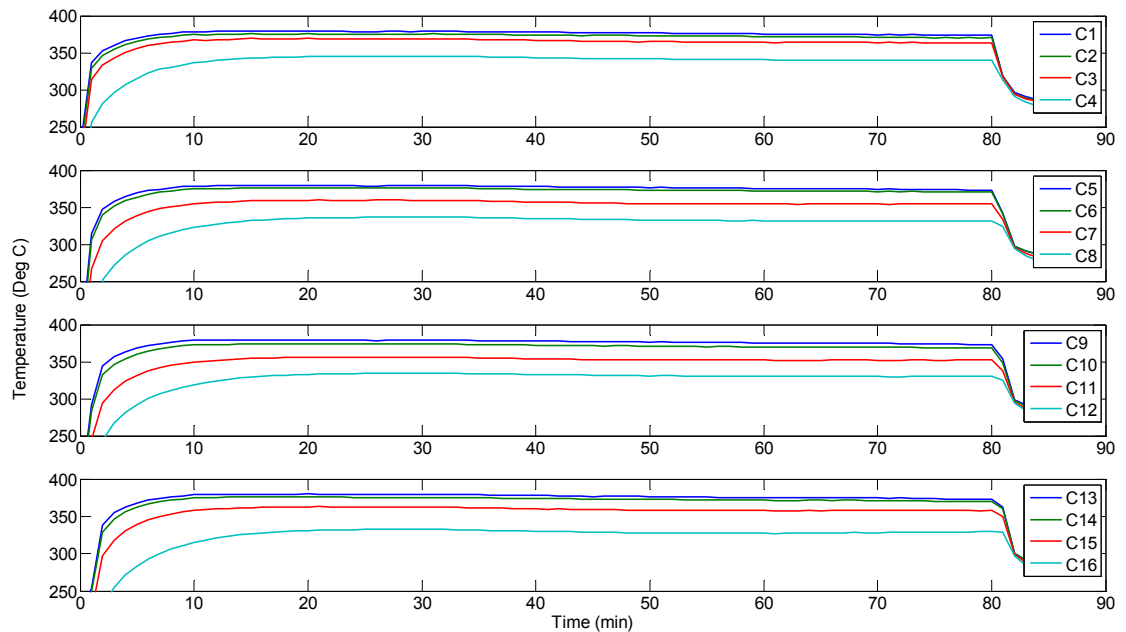


Figure 4.6: CPF Temperature Profiles during ISL Test 3 Passive Oxidation

When the temperatures are displayed as in Figure 4.7, the axial temperature gradients can be estimated by the proximity of the data points of the temperature measurements at each radial location. As an example, the temperature measurements at the radial location of 55 mm from the CPF centerline are superimposed upon one another indicating that there is no axial temperature gradient at the radial dimension of 55 mm. As the vertical dimension between temperature measurements increases, as can be seen at other radial dimensions in Figure 4.7, the axial temperature gradient increases. For ease of viewing, the average axial temperature difference has also been placed on

the plot and is indicated by the dotted orange line. Two additional examples of this method to display temperature data can be seen in Appendix J.

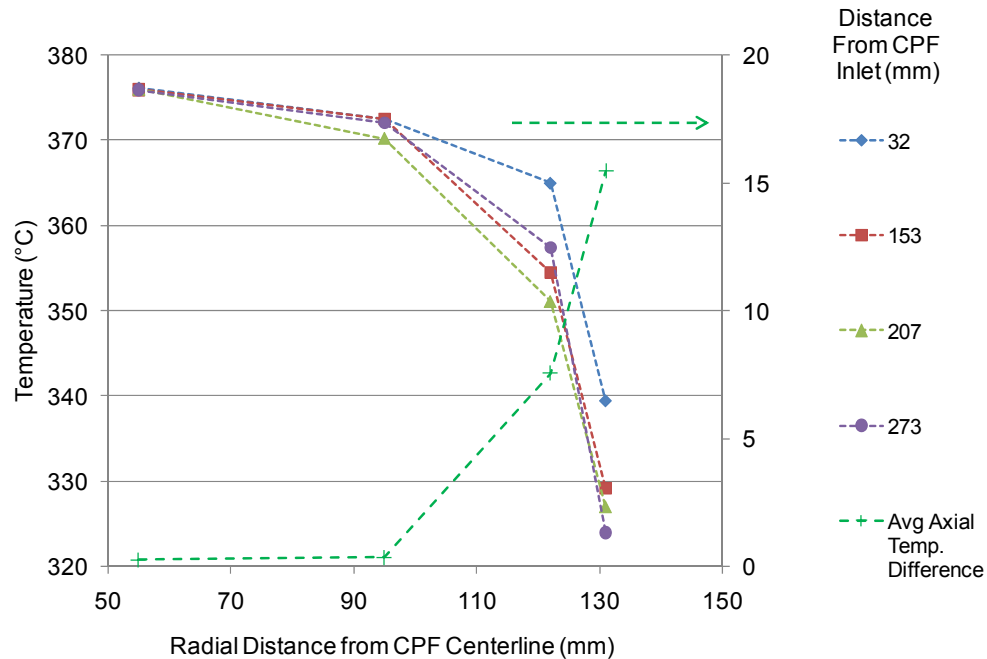


Figure 4.7: Average Temperature Profiles during Passive Oxidation for ISL Test 3

Along with the axial temperature gradients, radial temperature gradients are present within the CPF. The magnitudes of the radial temperature differences between thermocouples at the radii of 45 mm and 131 mm, measured during four engine operating conditions are shown in Figure 4.8. Of the four examples provided, the largest gradients occurred during the passive oxidation portion of ISL Test 3. When comparing the results shown in Figure 4.8 for ISL Test 2 and 5, similar gradients were measured even though the CPF inlet temperature differed by approximately 180°C. Since the large variation of CPF inlet temperature produced similar temperature gradients, the radial temperature gradients cannot solely be a function of CPF inlet temperature and are likely a function of several factors such as local reaction rate, exhaust mass flow rate and the inlet temperature of the CPF.

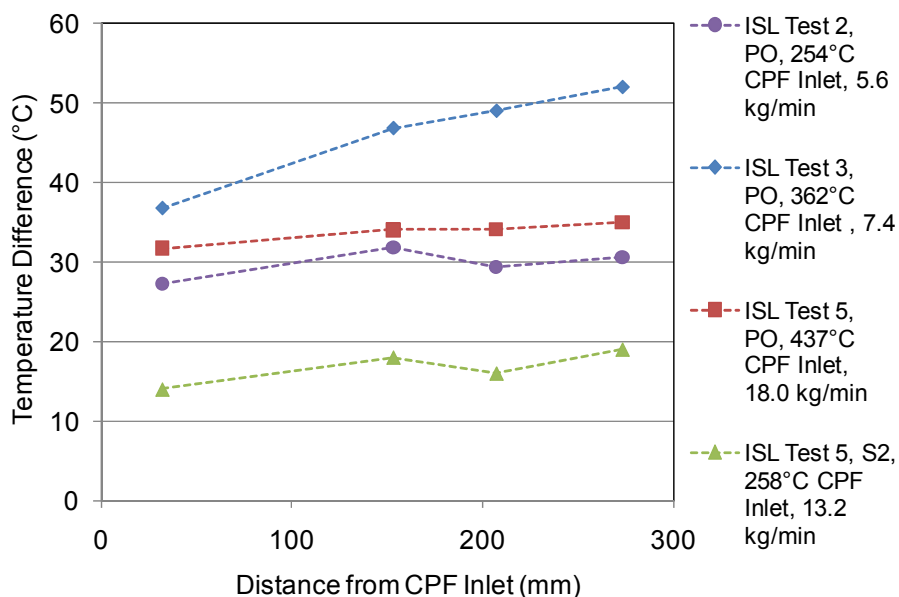


Figure 4.8: Radial Temperature Differences during Three Engine Operating Conditions

The thermocouples inserted in to the CPF provide a rich data set to investigate the temperatures during passive oxidation testing. Due to the large radial distance from the centerline of the CPF for the thermocouples labeled as C4, C8, C12, and C16 in Figure 3.7, these thermocouples cannot be used to facilitate the calculation of an average CPF temperature. It has been found that the best method to determine an average CPF temperature is the process used in references [33, 34] and this is the method that was used in the analysis of the CPF temperature data for this thesis. The temperatures from the listed thermocouples above would provide a good estimate of the surface temperature of the CPF and could be used while performing an energy balance across the CPF and DOC which can be used to estimate the DOC inlet HC concentrations during active regenerations.

The average CPF temperature was calculated by taking an area weighted average of the three thermocouple temperatures at the radial distances from the CPF centerline of 55, 95 and 122 mm. This is done at the four axial distances of 32, 153, 207, and 273 mm from the CPF inlet. After the average temperature is calculated at each location, the

average temperatures are plotted with the axial distance on the x-axis and the temperature on the y-axis. From these data points a linear trend line is applied and the equation for the line is obtained. From the linear equation of the trend line, the average CPF temperature is taken to be at the distance which signifies the midpoint of the CPF.

4.4 Stage 1 Loading

As discussed in section 3.3, Stage 1 loading consists of operating the engine at a specified engine speed and load for 30 minutes after the clean out of the CPF is performed. This allows the temperature of the CPF to stabilize. This is an important step in the mass balance process as it allows the CPF to be weighed at a similar temperature each time it is removed from the aftertreatment system.

4.4.1 Gaseous Emissions

A side by side comparison of the averaged gaseous emissions from Stage 1 loading of the CPF for testing performed on the ISM and ISL can be seen in Table 4.6. A summary of the gaseous emission testing for all of the reported experiments can be found in Appendix K. The data from Stage 1 and the variation of measurement during testing, represented by horizontal bars of one standard deviation, is also available in Figures 4.9 and 4.10 for the ISM and ISL respectively.

For the ISM, Stage 1, 2, and 3 loading consisted of running the engine at 1800 rpm and 300 Nm while the ISL was run at 2100 rpm and 200 Nm. The CO₂ and O₂ concentrations for both engines were comparable during the first stage of the test which can be seen in Table 4.6. For the specified engine operating conditions for this stage of the test it was not expected that the emissions values would be similar as the speed and load on the engines differ by 300 rpm and 100 Nm respectively.

Table 4.6: Comparison of Stage 1 Emissions from ISM (1800 rpm and 300 Nm) and ISL (2100 rpm and 195 Nm)

	O ₂ (%)		CO ₂ (%)		CO (ppm)		HC (ppmC)	
	ISM	ISL	ISM	ISL	ISM	ISL	ISM	ISL
UDOC	14.0	13.9	5.00	5.12	100	142	87	107
DDOC	14.0	13.9	5.02	5.10	0	0	17	21
DCPF	14.0	14.0	4.99	5.04	0	0	5	5

	NO* (ppm)		NO ₂ * (ppm)		NO _x * (ppm)	
	ISM	ISL	ISM	ISL	ISM	ISL
UDOC	164	56	26	27	190	83
DDOC	75	48	117	33	192	81
DCPF	48	26	142	51	190	76

*Measured with Semtech Analyzer

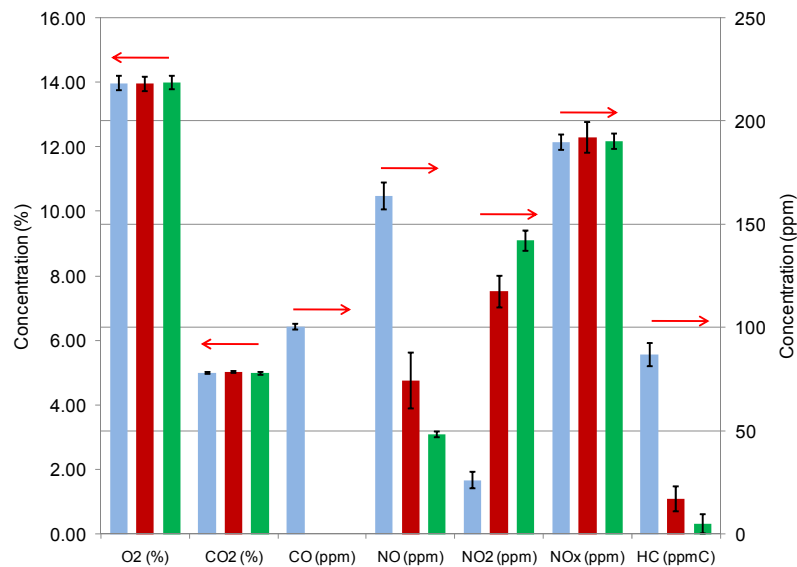


Figure 4.9: Summary of Gaseous Emissions during ISM Stage 1 Loading, 1800 rpm and 300 Nm

Engine out CO concentrations were higher on the ISL than the ISM, 140 ppm to 100 ppm, but on both engines the oxidation of CO to CO₂ was complete across the DOC resulting in no measurable CO entering the CPF. Total engine out HC concentrations were also slightly higher on the ISL as compared to the ISM, 107 ppmC to 87 ppmC. An 80% conversion efficiency of hydrocarbons was obtained during the operation of both

engines which left approximately 20 ppmC of HC to enter the CPF. Engine out NO_2 values were similar for both engines, but the NO_x from the ISM was more than two times greater than the NO_x coming from the ISL. CPF inlet NO_2 concentrations were also different since there was a larger quantity of NO for conversion to NO_2 on the ISM. Inlet CPF NO_2 concentrations were over 3 times higher on the ISM than the ISL.

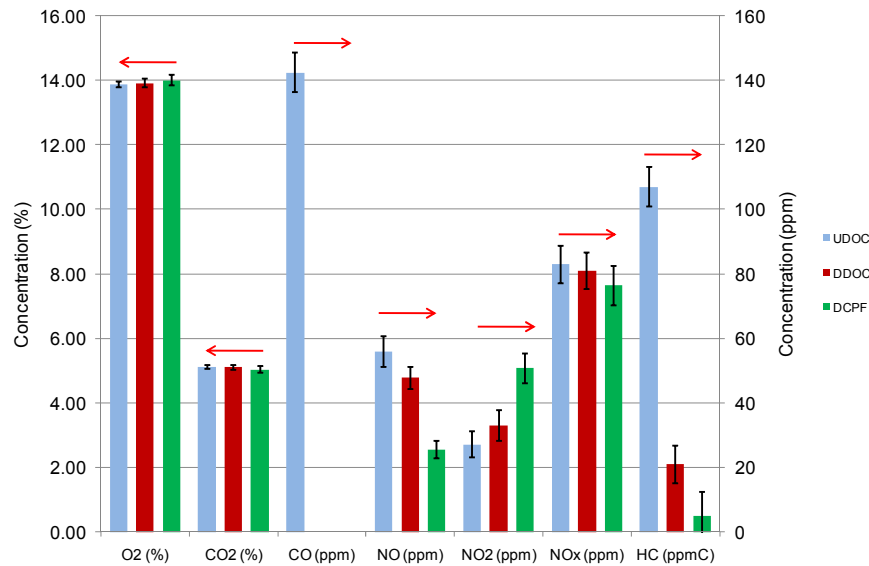


Figure 4.10: Summary of Gaseous Emissions during ISL 365 Stage 1 Loading, 2100 rpm and 195 Nm

The conversion efficiency of NO to NO_2 across the DOC varied between engines with the conversion efficiency on the ISM being significantly larger than that of the ISL as shown in Table 4.7. Average space velocities for Stage 1 loading on the ISM and ISL were comparable, 248 k h^{-1} and 240 k h^{-1} respectively. A small increase in NO to NO_2 conversion efficiency on the ISM would be expected due to the higher DOC inlet temperature, 279°C compared to 263°C on the ISL, but the difference should not be this large. The presence of additional reductants, HC and CO, in the ISL exhaust stream could decrease the efficiency of the DOC when compared to the ISM making the difference larger than it would be without the presence of HC and CO. As discussed in

section 2.2 the presence of reductants can result in the consumption of NO₂ thereby decreasing the overall conversion efficiency due to the simultaneous creation and consumption of NO₂.

Table 4.7: Conversions Efficiencies across the DOC for Stage 1 Loading

Stage 1 Conversion Efficiency (%)					
CO		NO to NO ₂		HC	
ISM	ISL	ISM	ISL	ISM	ISL
100	100	54	14	80	80

The calculated NO to NO₂ conversion efficiency for each stage of the performed tests can be seen in Table 4.8. Values for the passive oxidation stages of the tests on the ISM are reasonable and in most cases compare well with similar tests on the ISL.

Comparable passive oxidation tests can be seen in Table 4.9. The Stage 1 loading portions of testing on the ISM have values larger than expected for NO to NO₂ conversion efficiencies. This could be due to the higher DOC temperatures as the transition from the clean out of the CPF is made to Stage 1 or other variables. This trend is not consistent on the ISL but the higher efficiency during Stage 1 loading does occur during some tests.

Table 4.8: NO to NO₂ Conversion Efficiencies during Performed Testing

	ISM									
	Test 1		Test 2		Test 3		Test 4		Test 5	
	DOC Inlet Temp. (°C)	NO to NO ₂ Conv. Eff. (%)	DOC Inlet Temp. (°C)	NO to NO ₂ Conv. Eff. (%)	DOC Inlet Temp. (°C)	NO to NO ₂ Conv. Eff. (%)	DOC Inlet Temp. (°C)	NO to NO ₂ Conv. Eff. (%)	DOC Inlet Temp. (°C)	NO to NO ₂ Conv. Eff. (%)
	(°C)	(%)	(°C)	(%)	(°C)	(%)	(°C)	(%)	(°C)	(%)
Stage 1	277	51	280	51	280	52	277	65	371	54
Stage 2	276	39	277	39	275	38	276	41	373	56
Passive Regeneration	346	61	369	47	424	36	479	16	375	55
Stage 3	278	38	283	39	276	49	284	56	N/A	N/A

	ISL									
	Test 2		Test 1		Test 4		Test 5		Test 3	
	DOC Inlet Temp. (°C)	NO to NO ₂ Conv. Eff. (%)	DOC Inlet Temp. (°C)	NO to NO ₂ Conv. Eff. (%)	DOC Inlet Temp. (°C)	NO to NO ₂ Conv. Eff. (%)	DOC Inlet Temp. (°C)	NO to NO ₂ Conv. Eff. (%)	DOC Inlet Temp. (°C)	NO to NO ₂ Conv. Eff. (%)
	(°C)	(%)	(°C)	(%)	(°C)	(%)	(°C)	(%)	(°C)	(%)
Stage 1	270	18	269	14	265	8	255	19	257	12
Stage 2	271	13	273	10	269	8	258	10	263	14
Passive Regeneration	372	54	263	46	420	31	434	21	361	50
Stage 3	280	26	279	7	270	16	260	19	279	27

Table 4.9: Comparable Passive Oxidation Tests

Test #	ISM	ISL
	1,2,3	2,3
	3	4
	4	5

The conversion efficiencies during Stage 2 loading are closer to reported literature for the ISM. A plot of the conversion efficiencies is shown in Figure 4.11 with the data labels being the space velocities through the DOC. The values for the ISL are lower than the ISM for comparable tests as indicated by Figure 4.11. The conversion efficiencies for the passive oxidation portions of the test are shown in Figure 4.12. As mentioned previously these values do compare well between the tests performed on the ISM and ISL as demonstrated by the tests highlighted by the oval shape. The plots for Stage 1 and Stage 2 along with tabulated data on the NO to NO₂ conversion efficiencies can be found in Appendix L.

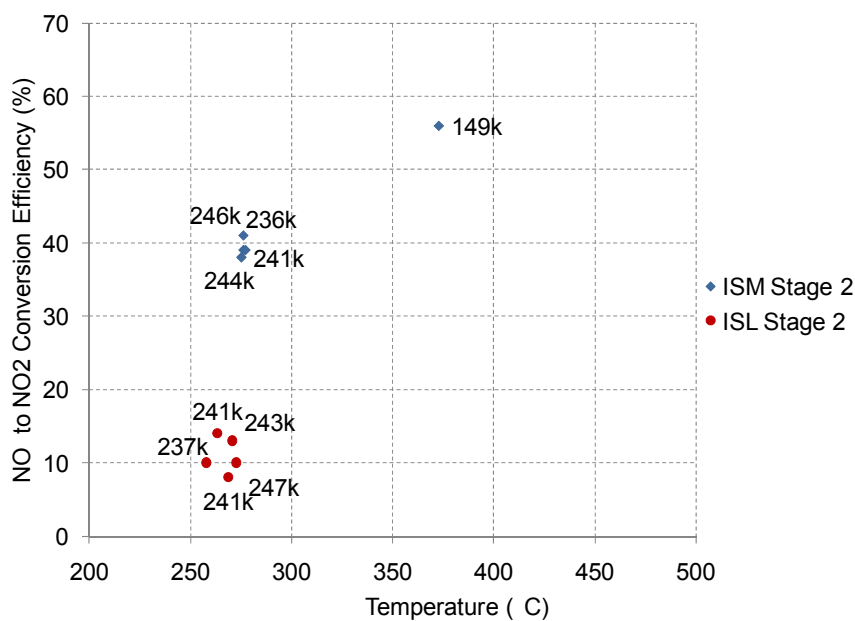


Figure 4.11: NO to NO₂ Conversion Efficiencies for Stage 2 Loading

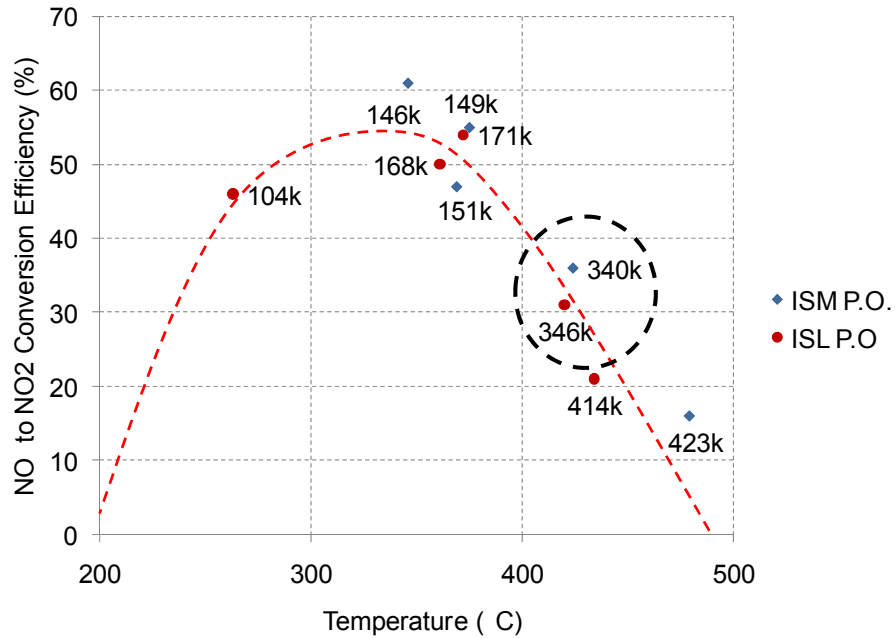


Figure 4.12: NO to NO2 Conversion Efficiencies for Passive Oxidation

4.4.2 Pressure Drop Profiles

A comparison of the pressure drop profiles of ISM Tests 1-4 for Stage 1 loading of the CPF can be seen in Figure 4.13 with an average actual volumetric flow rate of 0.320 act. m³/s. For the ISM, the tests are in chronological order by test number. ISM Test 5 is not included in this figure since it was performed at a different operating condition. The pressure drop profiles for this stage on the ISM were consistent with an average clean pressure drop of 2.5 kPa and a standard deviation of 0.1 kPa.

The pressure drop profiles for Stage 1 loading on the ISL can be seen in Figure 4.14 with an average actual volumetric flow rate of 0.322 act.m³/s. The tests were run in the order listed in the legend of Figure 4.14 with Test 2 being the first and Test 3 being the last test performed. The overall pressure drop profiles for Stage 1 testing on the ISL

were not as consistent as the pressure drop profiles for the ISM. As time progressed the profiles became more repeatable as can be seen from the profile of Test 5 and Test 3.

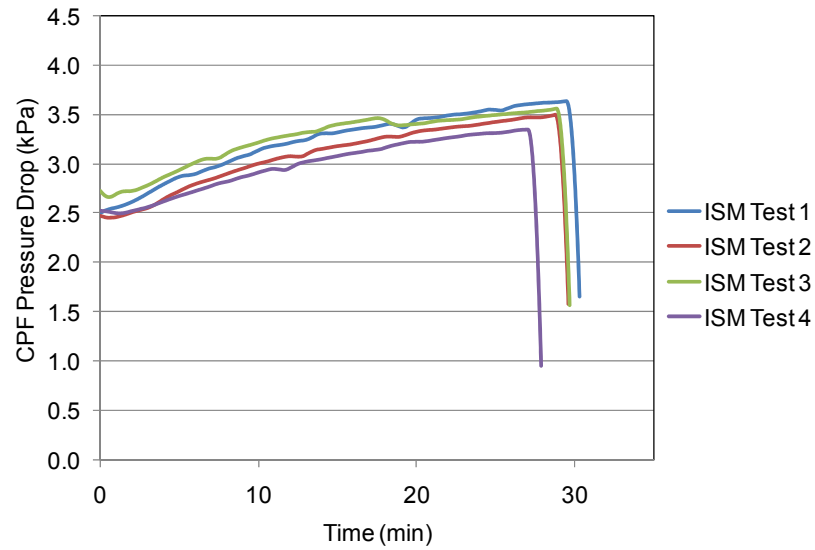


Figure 4.13: ISM CPF Pressure Drop Profiles during Stage 1

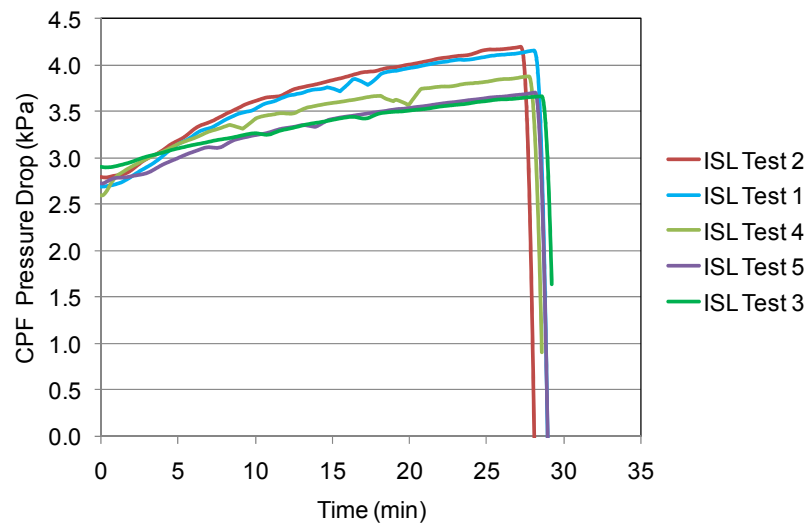


Figure 4.14: ISL CPF Pressure Drop Profiles during Stage 1

There are three possible explanations for this pressure drop variability. Although a de-greening procedure for the CPF was completed prior to performing the reported tests, the profiles become more consistent as time passes so the CPF could be continuing this process. The second possible cause is the PM concentration exiting the engine which affects the PM flow rate. If the variability associated with the measurement of the PM sample is taken into account, the variation in pressure drop could be due to the total mass deposited in the filter at the end of 30 minutes which would vary dependent upon the PM concentration. The third possibility is that an ash layer was forming a barrier against the CPF substrate wall.

Despite the variation in the pressure drop values at the end of Stage 1 for the ISL, the average clean pressure drop was 2.7 kPa with a standard deviation of 0.1 kPa. A statistical analysis to compare the clean pressure drop values for the ISM and ISL was performed. The two sample t-test was performed, with reference [40] as the source of the formulas, with a 0.01 significance level. The null hypothesis was that the mean clean pressure drop is the same from both engines, the alternative hypothesis is that the mean pressure drops are not the same. The results of this test are shown in Table 4.10 along with the 99% confidence interval associated with this statistic. The calculated t-value (T_o) was less than the critical t-value which results in a failure to reject the null hypothesis. Therefore when using a significance level of 0.01 the mean pressure drops come from the same population. The calculated 99% confidence interval includes zero which reinforces the above conclusion.

Table 4.10: T-Statistic and 99% Confidence Interval for Stage 1 Pressure Drop Comparison

Significance Level	$T_{0.005,7}$	T_o	99% Confidence Interval (kPa)
0.01	3.50	3.02	(-0.027,0.457)

The quantitative analysis performed above demonstrated that the clean pressure drop for Stage 1 loading on the ISM and the ISL were similar. In order to obtain a visual comparison of the results, two pressure drop profiles were superimposed. The pressure

drop from the ISM was selected at random, but since it is possible that the CPF used on the ISL was undergoing an extended de-greening process, as a precaution to obtain the best comparison, it was decided to use a profile from an experiment that was performed later in the test matrix. The plotted pressure drop profiles can be seen in Figure 4.15. The 0.2 kPa offset from the calculated means above is visible at the left side of the plot and is maintained throughout the profile. The curvature of both plots appears to be similar indicating the PM accumulation in the substrate wall and cake layer is occurring in a similar manner. This is not an expected result due to the differences in NO₂ and PM concentrations. The overall impression of the analysis from this section is that the two catalyzed particulate filters used on the ISM and ISL performed in the same manner during Stage 1 loading.

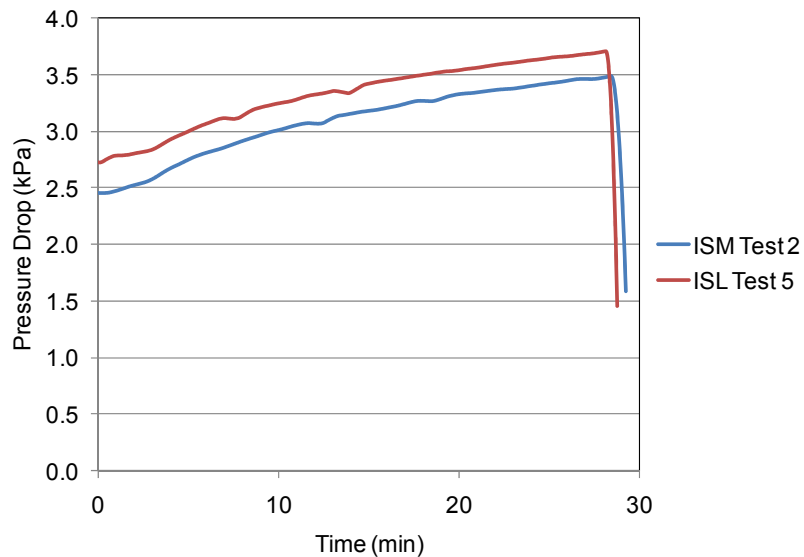


Figure 4.15: ISM vs. ISL Pressure Drop Comparison

4.5 Stage 2 Loading

Stage 2 loading consists of operating the engine at the specified loading conditions until a nominal CPF PM loading of 2.2 ± 0.2 g/g is achieved. For each engine, the first

experiment of the test matrix is performed by separating Stage 2 loading into two parts. This is done to ensure that the 2.2 g/L loading is met. The engine is operated for approximately half of the predicted loading time and the mass of the CPF is measured to obtain an accurate mass accumulation rate. From the calculation of this rate the required time to reach the specified CPF loading is determined.

4.5.1 Gaseous Emissions

A side by side comparison of the averaged gaseous emissions from Stage 2 loading of the CPF for testing performed on the ISM and ISL can be seen in Table 4.11. The data from Stage 2 and the variation of measurement during testing, represented by horizontal bars of one standard deviation, is also shown in Figures 4.16 and 4.17 for the ISM and ISL respectively.

The O₂ concentrations on the ISM were slightly higher than the ISL while the CO₂ concentrations were marginally lower on the ISM than the ISL. This can be seen in Table 4.11. Engine out CO concentrations were higher on the ISL than the ISM, 133 ppm to 100 ppm, but on both engines the oxidation of CO to CO₂ was complete across the DOC resulting in no CO entering the CPF. Total engine out HC concentrations were similar for the ISL and ISM. An 80% conversion efficiency of hydrocarbons was obtained during the operation of both engines which left approximately 20 ppmC of HC to enter the CPF. The calculated HC conversion efficiency across the DOC can be seen in Table 4.12 along with the CO and NO to NO₂ conversion efficiencies.

Engine out NO₂ values were similar for both engines, but the NO_x from the ISM was more than two times greater than the NO_x coming from the ISL. CPF inlet NO₂ concentrations were also different since there was a larger quantity of NO for conversion to NO₂ on the ISM. CPF Inlet NO₂ concentrations were 3 times higher on the ISM than the ISL. The conversion efficiency of NO to NO₂ across the DOC varied between engines with the conversion efficiency on the ISM being significantly higher than that of the ISL as shown in Table 4.12. Average space velocities for Stage 2 loading on the

ISM and ISL were 242 k h^{-1} for both engines. The DOC inlet temperatures were 276°C and 267°C for the ISM and ISL respectively. This discrepancy in efficiency could be the result of factors discussed during the Stage 1 loading emission analysis.

Table 4.11: Comparison of Stage 2 Emissions from ISM and ISL

	O ₂ (%)		CO ₂ (%)		CO (ppm)		HC (ppmC)	
	ISM	ISL	ISM	ISL	ISM	ISL	ISM	ISL
UDOC	14.0	13.8	5.00	5.13	100	133	90	92
DDOC	14.0	13.9	5.02	5.11	0	0	19	19
DCPF	14.0	13.9	4.98	5.07	0	0	3	0

	NO* (ppm)		NO ₂ * (ppm)		NO _x * (ppm)	
	ISM	ISL	ISM	ISL	ISM	ISL
UDOC	162	59	26	28	189	87
DDOC	99	53	93	31	192	84
DCPF	77	33	114	49	190	81

*Measured with Semtech Analyzer

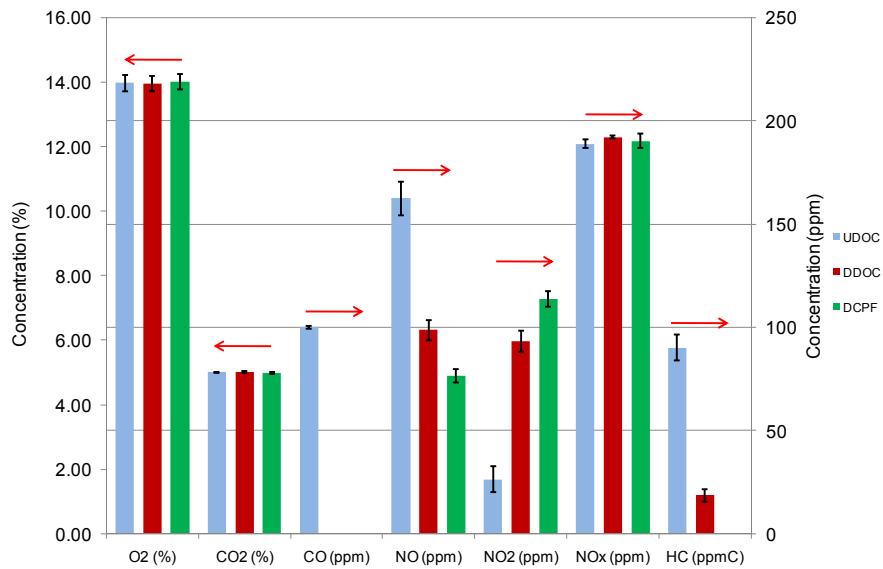


Figure 4.16: Summary of Gaseous Emissions during ISM Stage 2 Loading

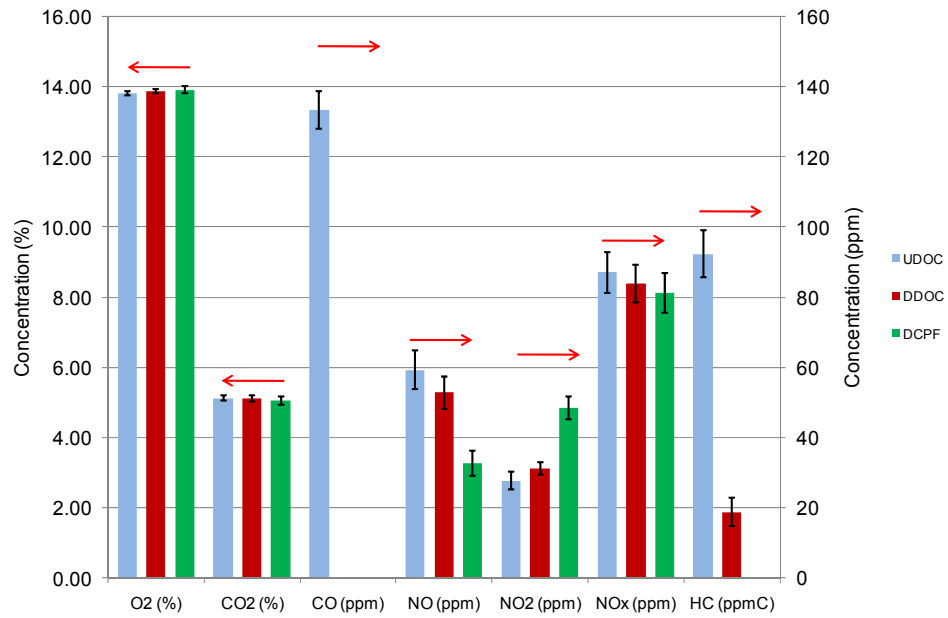


Figure 4.17: Summary of Gaseous Emissions during ISL Stage 2 Loading

Table 4.12: Conversions Efficiencies Across the DOC for Stage 2 Loading

Stage 2 Conversion Efficiency (%)					
CO		NO to NO ₂		HC	
ISM	ISL	ISM	ISL	ISM	ISL
100	100	39	11	79	80

4.5.2 Particle Size Distribution

For the completed tests on the ISM, an additional exhaust gas measurement was performed. The particle size distribution (PSD) of the exhaust gas was measured at three locations in the aftertreatment system. The three measurement locations were UDOC, DDOC, and DCPF. This measurement was not performed on the ISL due to the failure of the neutralizer in the electrostatic classifier. By using the measured values from

DDOC and DCPF, a steady state CPF filtration efficiency can be calculated using equation 4.1

$$\eta_{f-PSD} = \frac{PSD_{DDOC} - PSD_{DCPF}}{PSD_{DDOC}} * 100 \quad 4.1$$

η_{f-PSD} = Calculated filtration efficiency of the CPF using PSD values

PSD_{DDOC} = Particle size distribution DDOC, (particle/cm³ or nm³/cm³)

PSD_{DCPF} = Particle size distribution DCPF, (particle/cm³ or nm³/cm³)

Data are collected from the exhaust and then are post processed in order to represent the information in two different forms. When the sample is weighted by particle number, the post processed data represents the total number of particles at a certain diameter for a measured amount of flow. When weighted by volume, the data shows the total volume of those particles at each diameter for the same amount of flow. If the dilution ratio of the conditioning system is accurately accounted for as described in section 3.2.7, there is no visible differences in the distributions measured UDOC and DDOC. An example of this comparing the UDOC and DDOC PSD weighted by number can be seen in Figure 4.18.

During Stage 2 loading of ISM Test 1, the calculated filtration efficiency by particle number was 99.7% for this stage and is shown in the lower right corner of Figure 4.18. This value uses the total particle number DDOC and DCPF to determine the filtration efficiency. The PSD weighted by volume for ISM Test 1 during Stage 2 can be seen in Figure 4.19. This distribution displays the particle volume DDOC and DCPF which is then used to determine the CPF filtration efficiency. The calculated filtration efficiency for the data weighted by this method is 99.1%. The particle size distribution for tests performed on the ISM can be seen in Appendix M.

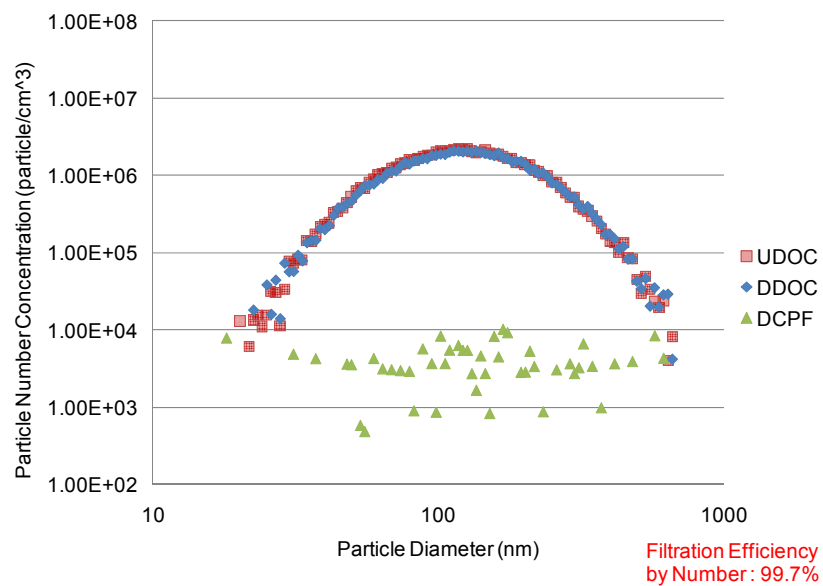


Figure 4.18: Particle Size Distribution Weighted by Number for the ISM at 1800 rpm and 300 Nm

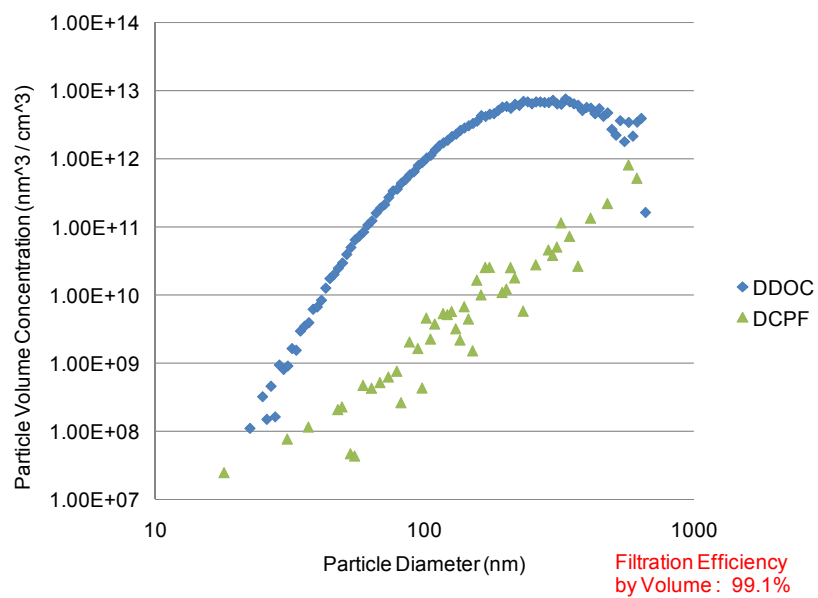


Figure 4.19: Particle Size Distribution Weighted by Volume for the ISM at 1800 rpm and 300 Nm

4.5.3 Reaction Rates and NO₂/PM Ratios

As discussed in section 3.4, the stoichiometric mass ratio of NO₂ to PM is 7.67 to 1. For discussion purposes, an uncatalysed diesel particulate filter (DPF) will be used for exhaust filtration for the following explanation. Assuming that the minimum temperature for NO₂ and PM to react is met and the temperature is below 400°C so there is no thermal oxidation of PM, at NO₂/PM ratios below the stoichiometric value there should be a gain of mass in the DPF during steady state loading conditions. Limited mass oxidation does occur at NO₂/PM ratios below the stoichiometric value since there is some NO₂ available to react with the PM but the reaction is limited by the availability of NO₂.

For ratios that are equal to the stoichiometric ratio, there should be neither net gain nor loss of mass in the DPF assuming that the reaction is not limited by kinetics or mass transfer. At ratios greater than 7.67 to 1 a quantity equal to the mass of PM coming into the DPF from the engine is oxidized and the excess NO₂ reacts with any remaining PM deposited in the DPF. This condition would result in a net loss of PM mass within the DPF assuming the reaction is not limited by kinetics or mass transfer. While an uncatalyzed DPF simplified the above discussion, a catalyzed particulate filter was used during the performed tests and adds additional complexity to the analysis of the PM oxidation within the filter which will be discussed below. The NO₂/PM ratios during Stage 2 for the performed tests can be seen in Table 4.13. A summary of the NO₂/PM ratios during each of the individual stages and the complete PM mass balances are shown in Appendix N.

The formulas used to calculate the reaction rates for the performed tests were initially introduced in section 2.7. Two stages during the test were chosen to perform a reaction rate calculation, Stage 2 loading and the passive regeneration portion of the test. The formula used to determine RRo is shown by equation 2.10. This equation is obtained from reference [31] and is used to determine the global reaction rate RR_o.

Table 4.13: Stage 2 Loading Reaction Rates

		Time	Avg CPF temp.	Avg CPF temp.	CPF inlet temp.	RRo	Percent PM Oxidized	Engine out PM Conc.	NO ₂ Conc. into CPF	NO ₂ into CPF	NO _x Conc. into CPF	NO _x into CPF	NO ₂ /PM ratio	NO _x /PM ratio
		min	°C	K	1000/K	(1/s)	%	mg/scm	ppm	mg/scm	ppm	mg/scm	-	-
ISM	Test 1	286.6	267	540	1.85	2.15E-05	11	15.1	94	176.7	192	361.0	11.7	23.9
	Test 2	271.8	270	543	1.84	2.83E-05	18	15.7	88	165.4	192	361.0	10.5	23.0
	Test 3	286.8	265	538	1.86	2.19E-05	15	14.9	95	178.6	191	359.1	12.0	24.1
	Test 4	288.0	271	544	1.84	2.61E-05	11	15.7	99	186.1	193	362.8	11.9	23.1
	Average	283.3	268	541	1.85	2.45E-05	14	15.4	94	176.7	192	361.0	11.5	23.5
ISL 365	Test 2	279.7	265	538	1.86	3.06E-05	17	17.2	30	63.9	85	159.8	3.7	9.3
	Test 1	280.6	270	543	1.84	3.29E-05	22	18.5	30	56.4	79	148.5	3.0	8.0
	Test 4	260.5	266	539	1.86	2.84E-05	18	17.6	33	56.4	80	150.4	3.2	8.5
	Test 5	284.2	258	531	1.88	3.08E-05	20	16.4	30	60.2	93	174.8	3.7	10.7
	Test 3	259.5	263	536	1.87	2.91E-05	18	17.5	31	56.4	83	156.0	3.2	8.9
	Average	272.9	264	537	1.86	3.04E-05	19	17.4	31	58.7	84	157.9	3.4	9.1

The components in the formula for RR_o can be seen in equation 2.11 and include several inputs such as NO₂ concentration, a pre-exponential factor (A), activation energy (E_a) and temperature. For the majority of the performed tests on the ISM and ISL the NO₂ concentration within the PM layer did not remain constant and therefore the calculation of E_a and A cannot be performed. A more detailed model such as the MTU 1-D CPF model will be required to accurately determine these values. While the parameter A and E_a cannot be accurately determined, this method does provide for an average reaction rate for the test.

The calculated reaction rates are listed in Table 4.13 along with the average CPF temperature, NO₂ and NO_x concentrations measured during the individual experiments. The reactions between the two engines, specifically from the different filters, are directly comparable due to the results of the testing discussed in section 4.9. The accuracy of the mass measurement in the heavy duty diesel lab is +/- 1g. In order to provide error bars for the calculated reaction rates, three reaction rates are calculated.

For the reported reaction rate (RR_o), the actual mass measurements recorded during the test are used in equation 2.10 for the calculation of the reaction rate. The lower bound for the error bar (RR_{oL}) is calculated by using a mass value for m_{Start} that is 1g less than measured while the measured value for m_{Stop} has an additional 1g added to it. This allows for the least amount of mass to be oxidized in the same time period as the

calculation for RRO which results in the lowest reaction rate. A visual interpretation of this calculation can be seen in Figure 4.20 with the available mass for oxidation represented by the vertical lines. RRO_H is calculated by using a mass value for m_{Start} that is 1g heavier than measured. While the value for m_{Stop} has 1g subtracted from it. This allows for the largest amount of mass to be oxidized in the same time period as the calculation for RRO which results in the highest reaction rate.

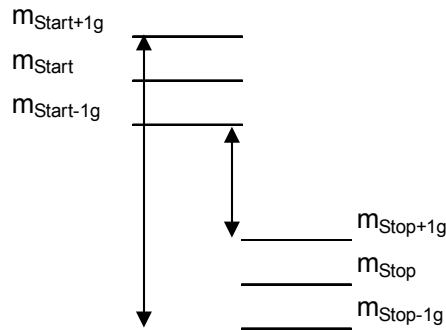


Figure 4.20: Mass Values Used in Determining Error Bars for the Reaction Rate Plot

After the three reaction rates are calculated, the lower and upper bounds for the error bars can be determined. The lower bound is determined by taking the value RRO and subtracting RRO_L from it. The difference from this calculation is then used as the magnitude of the lower error bar. The upper bound is determined by taking the value RRO and subtracting RRO_H from it and then using the absolute value of this number to represent the magnitude of the upper error bar. This then provides for RRO_H as the value for the upper error bar and RRO_L as the value for the lower error bar. For the average reaction rates on the ISM and ISL, the error bars represent one standard deviation which is calculated from the reaction rates on each engine. The calculated reaction rates for Stage 2 loading are displayed in Figure 4.21 with error bars.

A statistical analysis was performed to determine if the average of the calculated reaction rates for the ISM were different than the ISL. The null hypothesis was that the mean reaction rate during Stage 2 loading is the same for both engines, the alternative hypothesis is that the mean reaction rates are not the same. The results of this test are

shown in Table 4.14 along with the 99% confidence interval associated with this statistic. The calculated t-value (T_o) was less than the critical t-value which results in a failure to reject the null hypothesis. Therefore, when using a significance level of 0.01 the mean reaction rates come from the same population. The calculated 99% confidence interval includes zero which reinforces the above conclusion. The confidence interval can be used a check for the calculated T_o value. Since the value zero is included in the confidence interval and we are testing the difference in the means of the reaction rates, the reaction rate means could be the same.

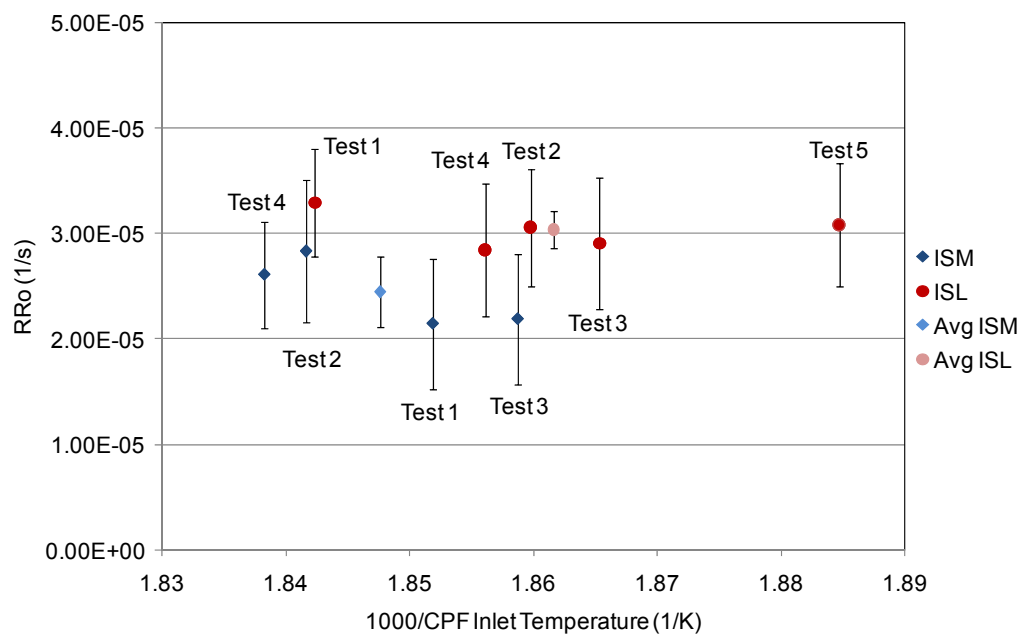


Figure 4.21: Stage 2 Loading Reaction Rates

Table 4.14 : T-Statistic and 99% Confidence Interval for Stage 2 Reaction Rate Comparison

Significance Level	$T_{0.005,7}$	T_o	99% Confidence Interval (1/s)
0.01	3.50	3.47	(-5.39E-8, 1.18E-5)

Testing performed on the ISM resulted in an average NO_2/PM ratio of 11.5 for Stage 2, while the average experimental values for the ISL were 3.4. The amount of PM that was oxidized after entering the CPF was 14% and 19% for the ISM and ISL respectively. The average CPF temperature for the individual tests along with additional information is listed in Table 4.13. An average CPF temperature for all of the tests performed on each engine was calculated and resulted in values of 268°C for the ISM and 264°C for the ISL. From the experimental NO_2/PM ratios and the similar CPF temperatures, the ISM should have a higher oxidation rate than the ISL. Since it does not, a hypothesis is that the structure or composition of the PM produced by the engines differs.

The information from the experimental results of Stage 2 loading is conflicting. For both engines the average CPF inlet temperature and exhaust mass flow rates were similar. The average calculated reaction rates are statistically from the same population but the experimental PM oxidation rates differed by 5%. The NO_2/PM ratio for the ISM during Stage 2 loading was approximately three times higher than the ISL. This should provide for a higher oxidation rate on the ISM and a larger percent oxidized of PM mass during this stage. Measured masses of the CPF indicate just the opposite effect. By exclusion of the other involved variables, one possible hypothesis is that the PM produced by the ISM probably has different physical characteristics than the ISL. To support this conclusion, in reference [23] the PM was analyzed from a Cummins 2004 and 2007 ISX and it was determined that the organic mass composition of the PM differed between the two engines. A second hypothesis is that the measured PM oxidation is not solely occurring by NO_2 oxidation.

4.6 Passive Regeneration

The passive regeneration portion of the test is initiated after the CPF has reached a PM loading of 2.2 ± 0.2 g/L. For the performed testing, a variety of exhaust mass flow rates and DOC inlet temperatures were selected for the test matrix. This allowed for a wide range of NO_2/PM ratios to be investigated and resulted in baseline data to calibrate the

MTU 1-D CPF model in order to further the understanding of the gaseous and PM oxidation reactions and the pressure drop components. The pressure drop components include contributions from the substrate wall, PM cake layer and substrate channel.

4.6.1 Gaseous Emissions

Due to the wide range of engine operating conditions used during passive regeneration, the recorded emissions data cannot be presented as compactly as in the previous sections. A summary of the emissions measured for this portion of the test can be found in Appendix K. Since NO_2 and NO_x concentrations are an integral part of the passive regeneration, these values will be presented in this section so a direct comparison between tests can be made.

4.6.2 Reaction Rates and NO_2 /PM Ratios

A summary of the most important variables during the performed passive regeneration testing, including a summary of the calculated reaction rates can be seen in Table 4.15. The complete PM mass balances are in Appendix N. Included in Table 4.15 are the average CPF temperatures and the NO_2 /PM ratios to facilitate the discussion. The experimental reaction rates are plotted with a log scale on the y-axis against $1000/\text{CPF}$ temperature on the x-axis in Figure 4.22. The error bars are calculated in the same manner as was discussed in the Stage 2 loading section. From this plot it can be seen that the temperature of the CPF plays an important role in the reaction rate and as expected, as the CPF temperature increases so does the reaction rate.

Table 4.16 shows the NO_2 concentration measurements during the passive regeneration portions of the tests. In addition, several other calculated values are available to aid in the following discussion. One of the critical values listed in Table 4.16 is the ratio of NO_2 consumed/ NO_2 into the CPF (C/A). The values for NO_2 consumed in Table 4.16 were calculated by taking the mass of PM oxidized for the stage and multiplying it by 7.67

which is the stoichiometric NO₂/PM ratio. For C/A values under one, assuming that only passive regeneration is occurring, there is an adequate supply of NO₂ available to oxidize the PM that was consumed during the completion of the test. When the value exceeds one, the CPF inlet NO₂ concentration cannot account for the total PM mass oxidized.

Table 4.15: Passive Oxidation NO₂/PM Ratios and Percent PM Oxidized

			Time	Avg CPF temp.	Avg CPF temp.	CPF inlet temp.	RRo	Percent PM Oxd.	Exh. Mass Flow Rate	Engine out PM Conc.	NO2 Conc. into CPF	NO2 into CPF	NOx Conc. into CPF	NOx into CPF	NO2/ PM ratio	NOx/ PM ratio
			min	°C	K	1000/K	(1/s)	%	kg/min	mg/scm	ppm	mg/scm	ppm	mg/scm	-	-
ISM	Test 1	81.1	327	600	1.67	0.99E-4	32	6.8	32.1	138	259.4	220	413.6	8.1	12.9	
	Test 2	89.9	348	621	1.61	1.48E-4	47	6.8	30.6	112	210.6	245	460.6	6.9	15.1	
	Test 3	48.9	411	684	1.46	7.79E-4	87	14.4	5.4	168	315.8	460	864.8	58.5	160.1	
	Test 4	22.3	463	736	1.36	11.34E-4	76	16.9	7.1	86	161.7	411	772.7	22.8	108.8	
	Test 5	120.1	358	631	1.58	1.30E-4	53	6.7	39.2	163	306.4	289	543.3	7.8	13.9	
ISL 365	Test 2	90.2	359	632	1.58	1.96E-4	63	7.7	6.9	117	220.0	206	387.3	31.9	56.1	
	Test 1	141.0	252	525	1.90	0.16E-4	12	5.6	6.0	151	283.9	283	532.0	47.3	88.7	
	Test 4	41.8	409	682	1.47	3.32E-4	54	15.1	6.5	73	137.2	200	376.0	21.1	57.8	
	Test 5	35.6	437	710	1.41	4.19E-4	53	18.0	13.3	45	84.6	174	327.1	6.4	24.6	
	Test 3	81.2	365	638	1.57	2.23E-4	64	7.7	7.0	116	218.1	223	419.2	31.2	59.9	

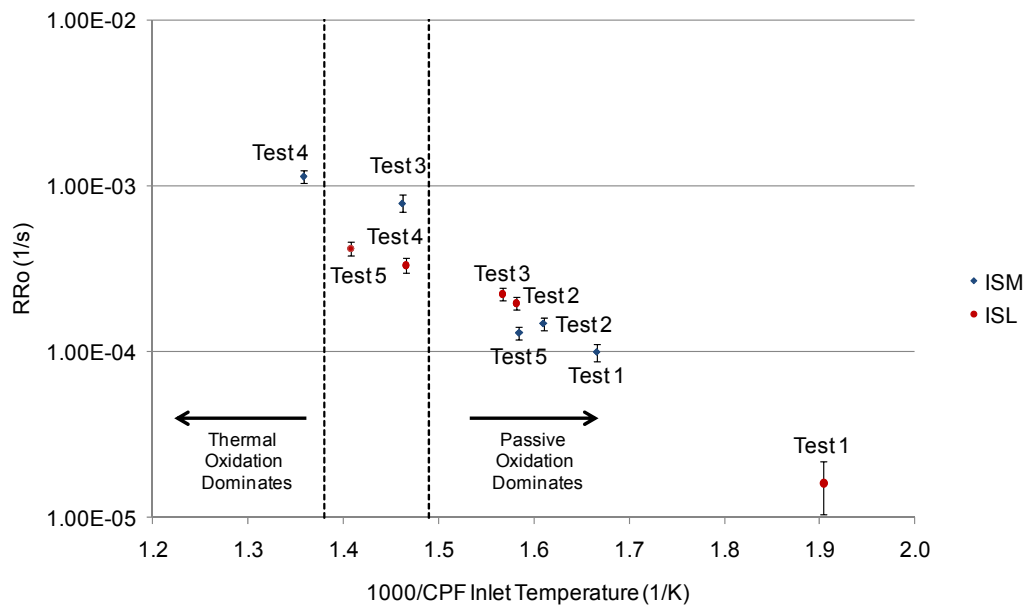


Figure 4.22: Average Particulate Matter Reaction Rates

Table 4.16: NO₂ Concentrations during Passive Regeneration Portions of Completed Tests.

		Avg. CPF Temp	t _{eff}	CPF Space Velocity	CPF Wall Velocity	Peclet #	PM Mass Oxd.	NO ₂ Conc. into CPF	NO ₂ into CPF	NO ₂ Conc. out of CPF	NO ₂ out of CPF	NO ₂ Consumed	NO ₂ Produced	NO ₂ Consumed / NO ₂ into CPF
		°C	min	1/h	m/s	-	g	ppm	g	ppm	g	g	g	-
ISM	Test 1	324	81.1	146k	0.012	0.073	16.4	138	116	122	103	126	112	1.08
	Test 2	345	89.9	151k	0.013	0.074	23.1	112	104	123	115	177	188	1.70
	Test 3	404	48.9	340k	0.028	0.165	34.4	168	180	172	184	264	268	1.47
	Test 4	461	22.3	423k	0.035	0.206	31.1	86	49	97	56	239	245	4.84
	Test 5	352	120.1	149k	0.013	0.077	23.1	163	201	146	180	177	156	0.88
ISL 365	Test 2	362	90.2	171k	0.015	0.088	27.1	117	125	111	119	208	201	1.66
	Test 1	254	141.0	104k	0.009	0.054	5.6	151	183	175	212	43	72	0.23
	Test 4	410	41.8	346k	0.031	0.181	22.6	73	70	71	68	173	171	2.48
	Test 5	437	35.6	414k	0.037	0.219	23.3	45	44	54	52	179	188	4.11
	Test 3	362	81.2	168k	0.015	0.090	26.8	116	110	109	104	206	199	1.86

There are two possibilities to account for C/A ratios above one. Thermal oxidation can be occurring in parallel with passive oxidation. An example of thermal oxidation occurring with passive oxidation can be seen in Table 4.16 for ISM Test 4 and ISL Test 5 where the average CPF temperature exceeds 430°C which is in the known thermal oxidation temperature range [25, 41]. For these two tests the C/A ratio exceeds four which is the result of the addition of thermal oxidation with passive. The second possibility to account for the increased PM oxidation is the back diffusion of NO₂ from the filter substrate which then oxidizes the PM. This topic was covered in Chapter 2 and was discussed in references [26, 27]. Calculation methods for other important variables within Table 4.16 are show in Appendix O.

The Péclet number and the variables involved in this calculation were initially discussed in section 2.5. This ratio is a dimensionless parameter group which relates the rate of advection of a substance to the rate of diffusion of the same substance which is driven by a concentration gradient. Péclet numbers were calculated for each of the passive oxidation tests. The Péclet number is not constant during the test and does change, however the values were calculated as a worst case scenario using values for the variables that would lessen the possibility of back diffusion occurring.

An effective NO_2 mass diffusion coefficient of $5.1\text{E-}6 \text{ m}^2/\text{s}$ was acquired from reference [26]. A PM thickness layer of $30 \text{ }\mu\text{m}$ was used which was obtained by simulating Point B loading conditions on the ISL (2100 rpm and 200 Nm) with the MTU 1-D CPF model for six hours and wall flow velocities were obtained from the 1-D CPF model. The formulas used for hand calculations of the filter wall velocity can be found in Appendix P. Through the use of these inputs the Péclet numbers in Table 4.16 were calculated. The calculated Péclet numbers for the performed passive regeneration testing are below one. This indicates that back diffusion of NO_2 from the CPF substrate dominates. This supports the calculated C/A ratios above and indicates that the additional PM oxidation is being accomplished through the back diffusion of NO_2 into the PM layer.

After the NO from the exhaust is converted to NO_2 in the catalyst on the CPF substrate wall, the NO_2 has the ability to diffuse from the area of high concentration (substrate wall) to areas of low concentrations (PM cake layer) if operating conditions are such that the Péclet number is under one. When the NO_2 consumed/ NO_2 into the CPF ratio is greater than one, the available NO_2 at the CPF inlet is reduced through the oxidation of PM before it reaches the substrate wall. This provides for a concentration gradient and allows the NO_2 generated at the CPF substrate to diffuse into the PM cake layer. This increased NO_2 concentration then promotes the oxidation of additional PM in the cake layer which increases the overall oxidation rate of the PM when compared to conditions when this diffusion process does not take place. A drawing of the hypothesized back diffusion process can be seen in Figure 4.23

The presence of back diffusion is an important finding. Under passive oxidation conditions the reaction rate does not only depend upon the NO_2 concentrations into the CPF but also on the NO available at the CPF inlet. The NO_x concentration then reflects the potential for PM oxidation since the NO contribution of this value can be oxidized to NO_2 and then diffuse back into the PM cake layer increasing the reaction rate. The production of NO_2 does follow an exponential trend when plotted vs temperature as seen in Figure 4.24.

Although not discernable by the reaction rate plot in Figure 4.22, it has been shown that increased NO_2 concentrations and flow rates into the CPF increases the oxidation of PM [10, 11, 25]. The importance of NO_2 in the oxidation of PM within the CPF can be verified experimentally by the ratio of NO_2 consumed/ NO_2 into the CPF (C/A). With C/A values greater than one, Péclet numbers under one, and at CPF temperatures under 400°C where passive oxidation is dominant, the experimentally calculated reaction rates during passive oxidation would not have been possible without the additional NO_2 provided by the back diffusion from the substrate wall. Therefore, C/A ratios above one indicate NO_2 production and the back diffusion of NO_2 from the substrate wall into the PM cake layer.

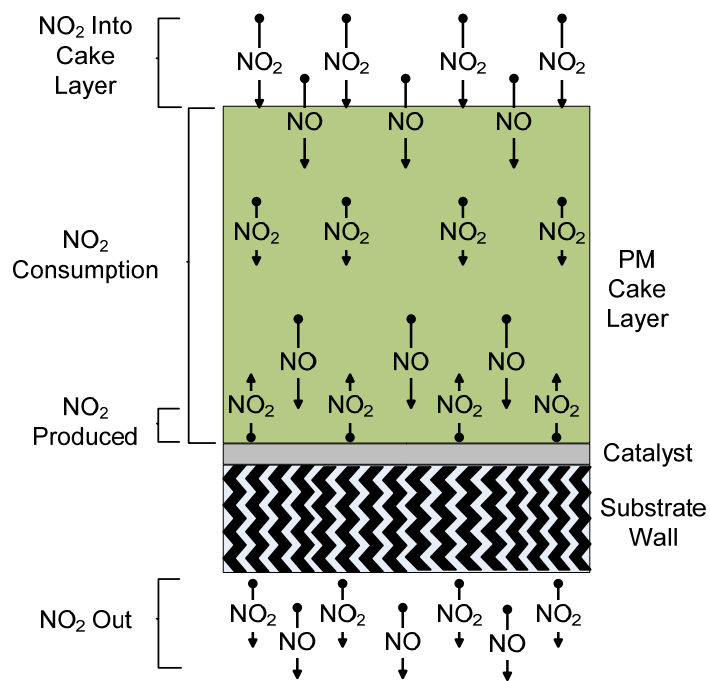


Figure 4.23: Visual Depiction of NO_2 Production

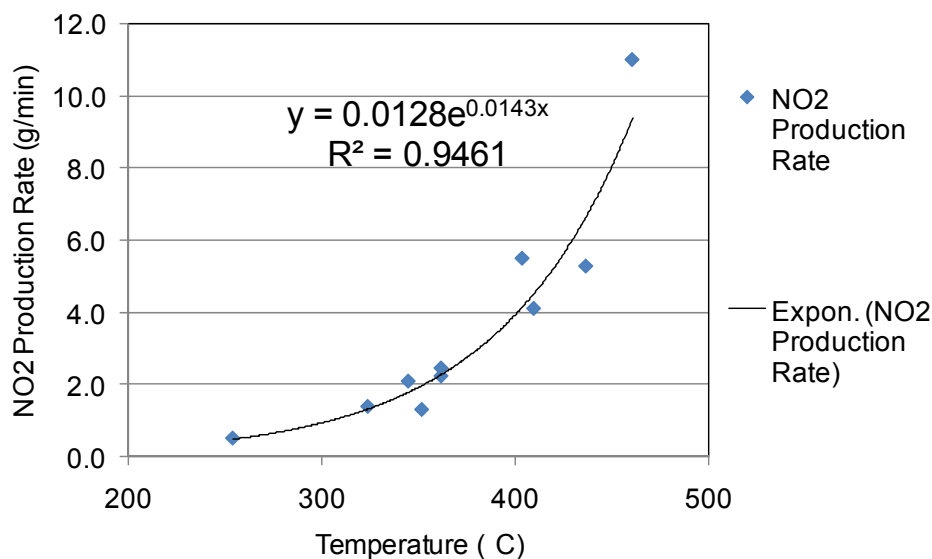


Figure 4.24: NO₂ Production Trend

One of the goals for this study was to determine if the PM created at different engine operating conditions reacted in the same manner. Two tests performed on the ISM allow this comparison. ISM Test 2 was performed in the usual manner. The CPF was loaded at 1800 rpm and 300 Nm with a DOC inlet temperature of 277°C until a CPF PM loading of 2.2 ± 0.2 g/L was obtained. The passive oxidation portion of the test was then performed at 1290 rpm at 560 Nm with a DOC inlet temperature of 369°C which allowed the determination of a reaction rate during passive regeneration. ISM Test 5 was performed as an extended loading at 1290 rpm and 560 Nm with a DOC inlet temperature of 373°C during the entire test. By performing the experiments in this manner, PM generated at two sets of engine operating conditions was oxidized at similar conditions and the reaction rates can be compared. The calculated reaction rates were $1.478\text{E-}4$ 1/s and $1.297\text{E-}4$ 1/s for ISM Test 2 and 5 respectively. When taking into account the accuracy of the CPF mass measurement and the resulting error on the calculated reaction rate, these rates are similar as can be seen by the error bars for the two tests shown in Figure 4.22.

While the NO_2/PM and NO_x/PM ratio are key parameters in the passive oxidation of PM, temperature also plays an important role as demonstrated by ISL Test 1. ISL Test 1 had one of the largest NO_2/PM ratios of the performed tests at 47.3:1 but had the lowest reaction rate of all tests. The average CPF temperature of 252°C limited the PM reaction even though there was an excess of NO_2 . Contrast this test with ISL Test 5 which had an NO_2/PM ratio of 6.4 which is under the stoichiometric ratio. The average CPF temperature for this test was 437°C which compensated for the low NO_2/PM ratio and provided for the largest calculated reaction rate on the ISM which is somewhat caused by the fact thermal oxidation starts at temperatures greater than 400°C .

Information presented at a Department of Energy project meeting from reference [41] is shown in Table 4.17. This table gives a breakdown of the separate passive and thermal reaction rates. It also demonstrates the temperature where thermal oxidation starts to become an important part of the total reaction rate. At 410°C during ISM Test 3, passive oxidation accounted for 96% of the total reaction rate. For ISL Test 5 with an average CPF temperature of 443°C the amount of passive oxidation was only 39% which is somewhat also related to the lower CPF inlet NO_2 concentration of 54ppm as compared to 180 ppm for ISM Test 3. From this information it can be determined that at temperatures below 400°C passive oxidation is dominant [11, 25].

In order to quantify the effect of NO_2 concentrations into the CPF, a comparison was performed between ISM Test 3 and ISL Test 4. Selected variables from this test can be seen in Table 4.18 with the remainder of the values for the tests found in Appendix N. The pressure drop profiles for the comparison of ISM Test 3 and ISL Test 4, along with the calculated reaction rates, can be seen in Figure 4.25. From the information in Table 4.18 and Figure 4.25 it can be seen that there is a large difference in NO_2 and NO_x concentrations between tests with the ISM having higher values. The remainder of the parameters of interest such as exhaust mass flow rate and temperature are similar.

Table 4.17: Simulation Results of Selected Passive Oxidation Testing from Reference [41]

Engine	Test		Exhaust Flow	Average CPF temp.	PM Concentration	CPF Inlet NO	CPF Inlet NO2	Experimental Reaction Rate	Total Model Reaction Rate	Model Passive Reaction Rate	Model Thermal Reaction Rate	Percent of Passive Oxidation
			kg/min	°C	mg/scm	ppm	ppm	1/s	1/s	1/s	1/s	%
ISM	1	Stage 2	13.1	270	15.1	86	115	0.21E-4	0.20E-4	0.20E-4	0	100
		Passive Ox.	6.8	327	32.1	87	146	1.00E-4	1.05E-4	1.05E-4	0	99
	2	Stage 2	13.2	272	15.7	86	91	0.28E-4	0.29E-4	0.29E-4	0	100
		Passive Ox.	6.8	348	30.6	142	120	1.48E-4	1.17E-4	1.15E-4	0.02E-4	99
	3	Stage 2	13.0	270	14.9	80	98	0.22E-4	0.24E-4	0.24E-4	0	100
		Passive Ox.	14.4	411	5.4	313	180	7.79E-4	7.13E-4	6.94E-4	0.02E-4	96
	4	Stage 2	12.7	272	15.7	57	103	0.26E-4	0.18E-4	0.18E-4	0	99
		Passive Ox.	16.9	463	7.1	351	93	11.34E-4	10.06E-4	3.53E-4	6.53E-4	35
ISL	2	Stage 2	12.9	266	17.2	45	36	0.25E-4	0.31E-4	0.31E-4	0	98
		Passive Ox.	7.7	359	6.9	88	117	1.96E-4	1.63E-4	1.35E-4	0.29E-4	82
	1	Stage 2	13.4	270	18.5	49	30	0.28E-4	0.28E-4	0.28E-4	0	98
		Passive Ox.	5.5	252	6.0	132	151	0.16E-4	0.13E-4	0.13E-4	0	98
	5	Stage 2	13.1	260	16.4	60	32	0.23E-4	0.33E-4	0.33E-4	0	98
		Passive Ox.	18.0	437	18.0	116	54	4.19E-4	4.87E-4	1.92E-4	2.95E-4	39

Table 4.18: Selected variables during ISM Test 3 and ISL Test 4 Comparison

	Average CPF temp.	Engine out PM Conc.	NO ₂ Conc. into CPF	NO _x Conc. into CPF	NO ₂ into CPF	NO _x into CPF	NO ₂ / PM ratio	NO _x / PM ratio
	°C	mg/scm	ppm	ppm	g	g	-	-
ISL Test 4	409	6.5	73	200	70	191	21.1	57.8
ISM Test 3	411	5.4	168	460	180	492	58.5	160.1

This difference of NO₂ and NO_x had a significant impact on the calculated average reaction rate. ISM Test 3 had an NO₂ concentration at the CPF inlet over two times higher than that of the ISL. This increased NO₂ concentration provided for a reaction rate that was over two times greater than the calculated reaction rate for ISL Test 4. The calculated reaction rates can be seen in Figure 4.25. Another indication of the difference in reaction rates is visible by the peak and slope of the pressure drop profiles. The slope is steeper for ISM Test 3 than ISL Test 4 indicating a higher reaction rate and the peak of the pressure drop profile for ISM Test 3 is narrower indicating that the reaction started to occur sooner than the reaction for ISL Test 4.

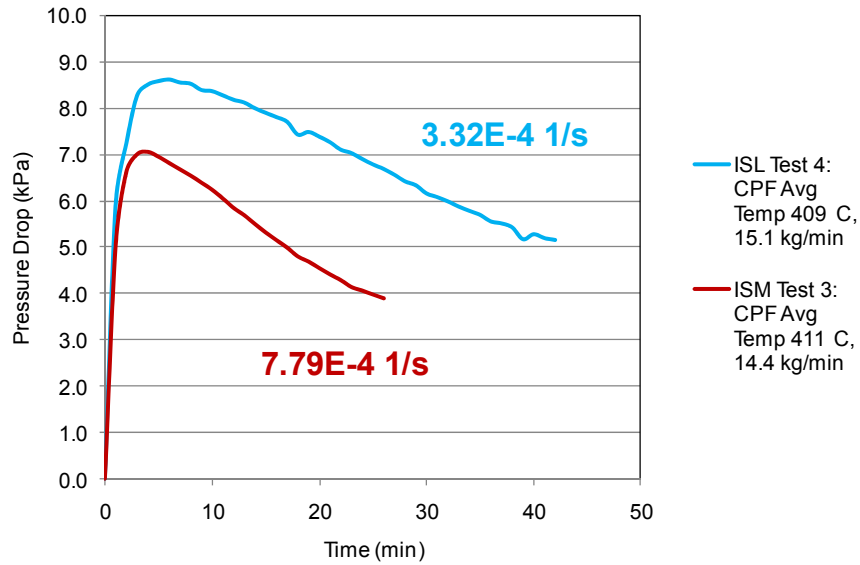


Figure 4.25: Pressure Drop Comparison of ISM Test 3 and ISL Test 4

4.6.3 Pressure Drop Profiles

The CPF temperatures and exhaust mass flow rates for the passive oxidation portion of the tests can be seen in Table 4.19 while the pressure drop profiles can be seen in Figures 4.26 and 4.27 for the ISM and ISL respectively. The complete pressure drop profile for the each of the tests can be seen in Appendix Q. For some of the performed tests on the ISM, similar tests were completed on the ISL. Comparable tests between the engines are indicated by the data in Table 4.19 having the same color font.

Table 4.19: Exhaust Mass Flow Rates and CPF Average Temperatures

		ISM					ISL 365				
		Test 1	Test 2	Test 3	Test 4	Test 5	Test 2	Test 1	Test 4	Test 5	Test 3
Average CPF temp.	°C	327	348	411	463	358	359	252	409	437	365
Exhaust volumetric flow rate	act m ³ /min	0.188	0.194	0.441	0.551	0.192	0.218	0.136	0.456	0.555	0.216

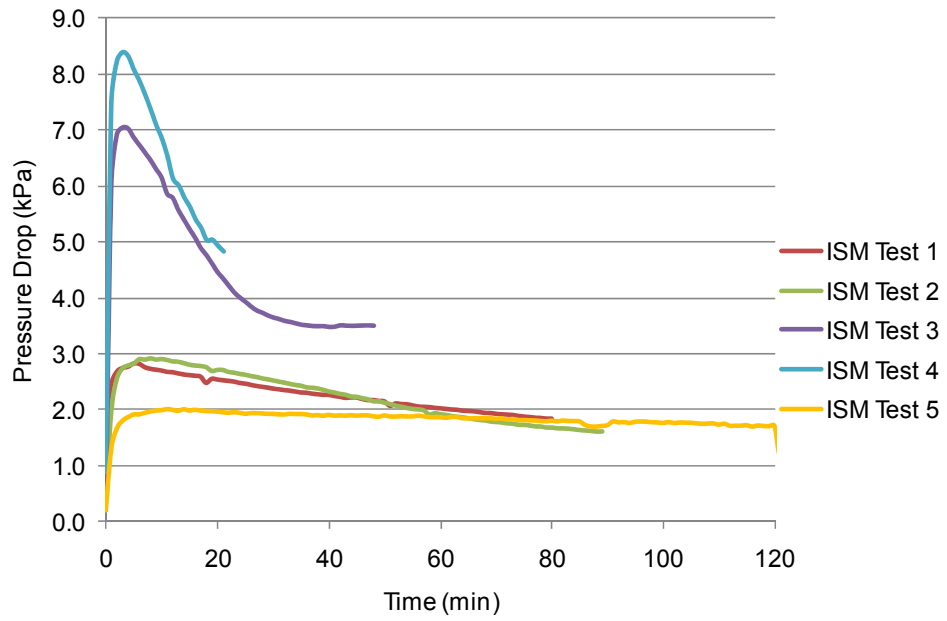


Figure 4.26: Pressure Drop Profiles during Passive Oxidation on the 2002 ISM

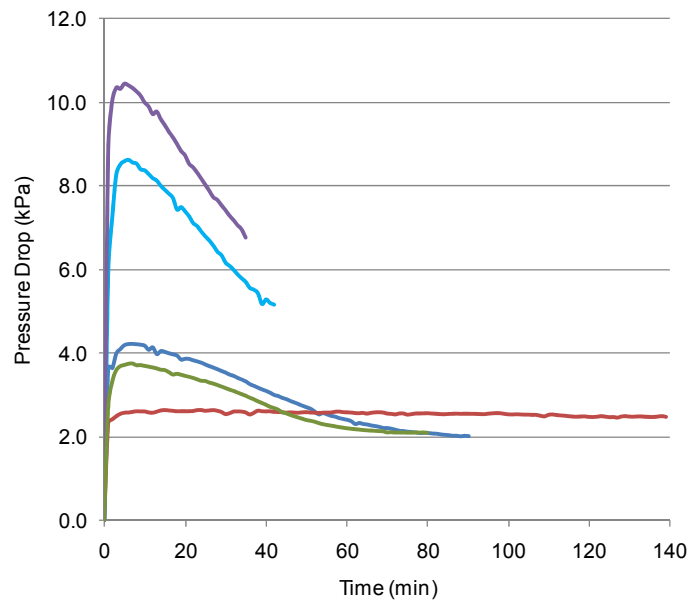


Figure 4.27: Pressure Drop Profiles during Passive Oxidation on the 2007 ISL

The maximum pressure drop across the CPF is greater for comparable tests performed on the ISL than it is for the ISM. This can be seen when comparing Figure 4.26 to Figure 4.27. This increased pressure drop is the result of higher actual volumetric flow rates as can be seen in Table 4.19. The peak of the pressure drop profiles for ISM Test 3 and 4 has a smaller radius which indicates the reaction initiated sooner. This trend is not visible on the lower temperature tests.

When comparing the pressure drop profiles of ISL Test 1 and Test 5, the slopes of the curves give an indication of how fast the reaction is occurring. ISL Test 1 had the lowest calculated reaction rate of the tests performed on the ISL and this is indicated by the horizontal pressure drop profile in Figure 4.27. ISL Test 5 had the highest reaction rate and this can be visualized by the pressure drop profile having the steepest slope. Due to this observation, the slope of the pressure drop profile which is a function of the PM cake permeability along with PM oxidation in the substrate wall and cake layer is a good indicator of the reaction rate during passive oxidation testing.

4.7 Stage 3 Loading

Stage 3 loading is the final stage of the test where the engine is operated at loading conditions for 30 minutes. This allows the CPF to reach to a repeatable temperature that is similar to Stage 2 loading which provides for the most accurate mass measurements between stages. With this mass measurement and value obtained from the MTU 1-D CPF model for the mass deposited within the CPF during Stage 3, the mass remaining in the CPF after the passive oxidation portion of the test can be calculated.

4.7.1 Gaseous Emissions

A side by side comparison of the averaged gaseous emissions from Stage 3 loading of the CPF for testing performed on the ISM and ISL can be seen in Table 4.20. The data from Stage 3 and the variation of measurement during testing, represented by horizontal

bars of one standard deviation, is shown in Figures 4.28 and 4.29 for the ISM the ISL respectively. The O₂ concentrations on the ISM were slightly higher than the ISL while the CO₂ concentrations were marginally lower on the ISM than the ISL, as can be seen in Table 4.20. Total engine out HC concentrations were also similar for both engines.

Table 4.20: Comparison of Stage 3 Emissions from ISM and ISL

	O ₂ (%)		CO ₂ (%)		CO (ppm)		HC (ppmC)	
	ISM	ISL	ISM	ISL	ISM	ISL	ISM	ISL
UDOC	14.0	13.8	4.97	5.10	102	132	87	88
DDOC	13.9	13.8	5.00	5.14	0	0	16	13
DCPF	13.9	13.9	5.00	5.07	0	0	0	0

	NO* (ppm)		NO ₂ * (ppm)		NO _x * (ppm)	
	ISM	ISL	ISM	ISL	ISM	ISL
UDOC	157	58	27	29	185	86
DDOC	86	47	101	37	187	84
DCPF	59	31	131	52	190	82

*Measured with Semtech Analyzer

Engine out CO concentrations were higher on the ISL than the ISM, approximately 130 ppm to 100 ppm, but on both engines the oxidation of CO to CO₂ was complete across the DOC resulting in no CO entering the CPF. Tabulated conversion efficiencies across the DOC can be seen in Table 4.21. A hydrocarbon conversion efficiency higher than 80% was obtained during the operation of both engines which left approximately 15 ppmC of HC to enter the CPF. Engine out NO₂ values were similar for both engines, but the total NO_x from the ISM was more than two times greater than the NO_x coming from the ISL. CPF inlet NO₂ concentrations were also different since there was a larger quantity of NO for conversion to NO₂ on the ISM. Inlet NO₂ values were over 2 times higher on the ISM than the ISL.

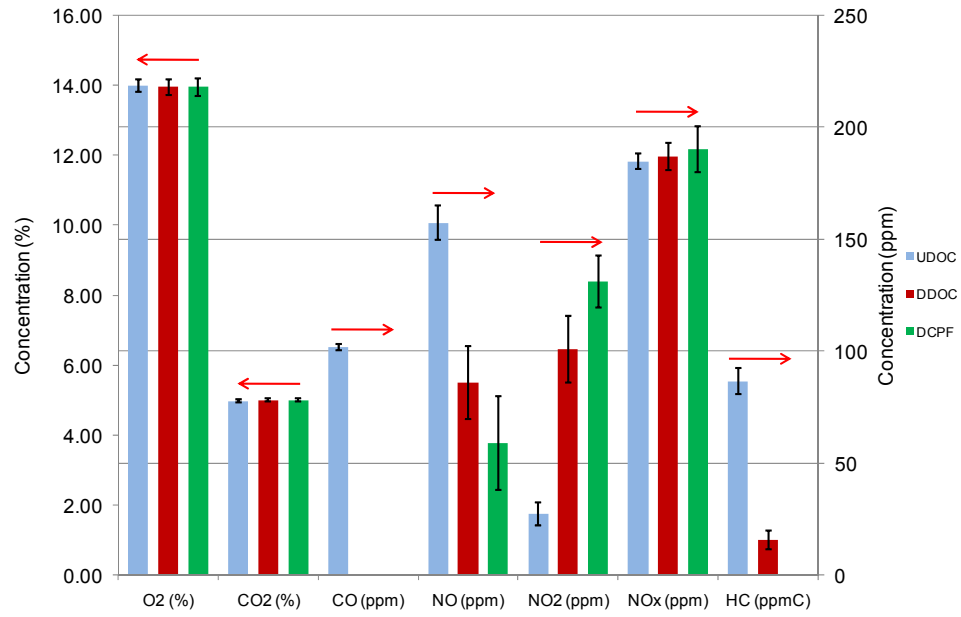


Figure 4.28: Summary of Gaseous Emissions during ISM Stage 3 Loading

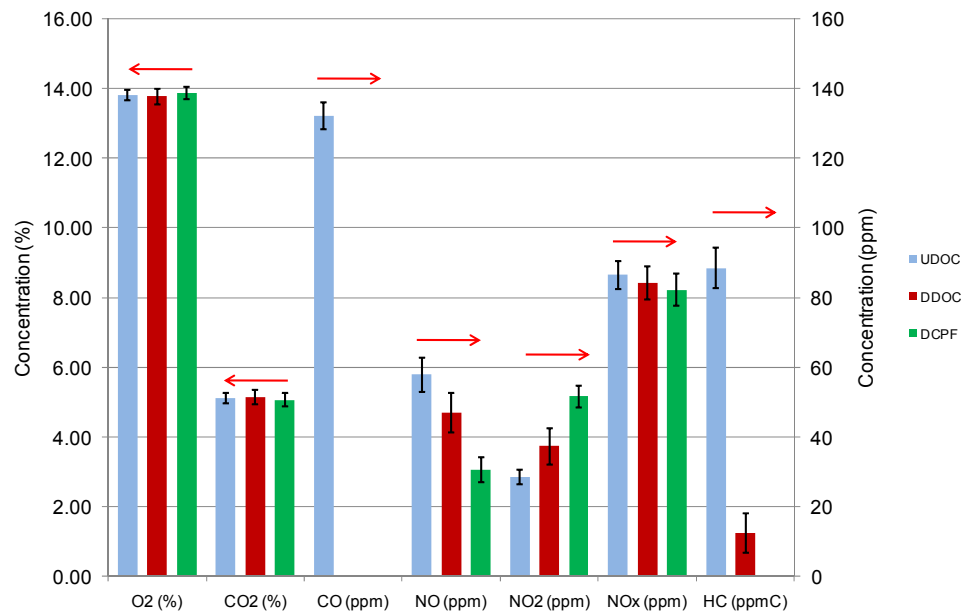


Figure 4.29: Summary of Gaseous Emissions during ISL Stage 3 Loading

Table 4.21: Conversions Efficiencies across the DOC for Stage 3 Loading

Stage 3 Conversion Efficiency (%)					
CO		NO to NO ₂		HC	
ISM	ISL	ISM	ISL	ISM	ISL
100	100	45	19	82	86

4.7.2 Pressure Drop Profile

The pressure drop profiles for Stage 3 loading of the performed tests can be seen in Figures 4.30 and 4.31 for the ISM and ISL respectively. Due to the initial transient period as the exhaust flow and temperatures stabilize after the passive oxidation portion of the test, there is not a smooth transition for the pressure drop profile between stages. The profiles shown below have been shortened at the beginning of the stage to see only the portions that are steady in nature. By observing the slope of the pressure drop profile, an estimate can be made as to whether the CPF is accumulating PM at the same rate for the displayed tests.

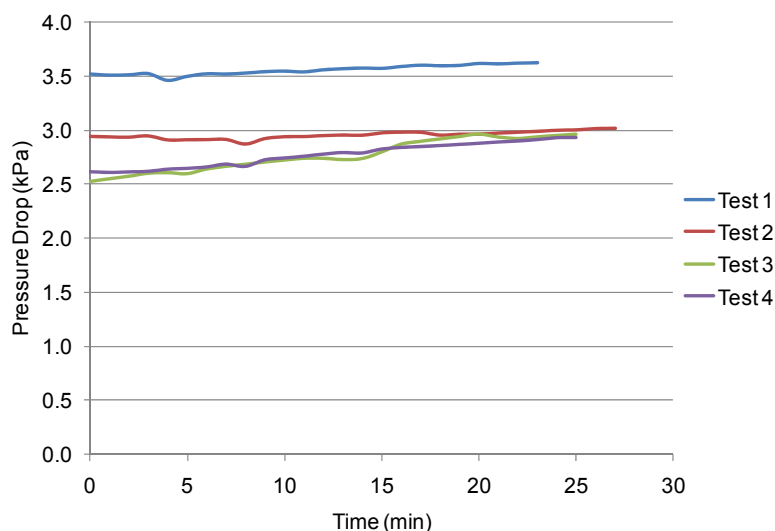


Figure 4.30: CPF Pressure Drops for ISM Stage 3 Loading

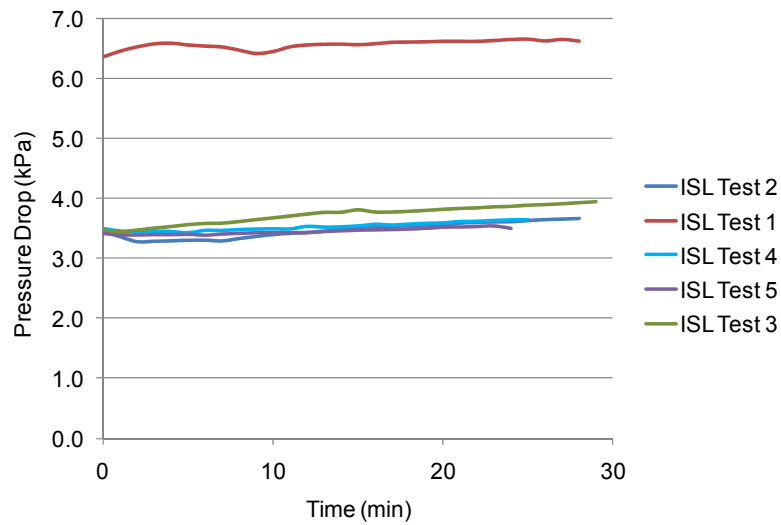


Figure 4.31: CPF Pressure Drops for ISL Stage 3 Loading

In Figure 4.30 for the ISM, there are two slopes associated with Stage 3 loading. ISM Test 1 and 2 have similar slopes while Test 3 and 4 have a different slope. The engine was operated at the same conditions of 1800 rpm and 300 Nm during Stage 3 for each of these tests. The PM flow rate is a possible cause of the differing mass accumulation. Evidence for this is not definitive however since as can be seen in Table 4.22 the concentration for Test 4 is only slightly higher than the other tests and the total variation between tests, excluding Test 3 is less than 1 mg/scm. The value for Test 3 is likely from a mishandled or torn filter. Another possible reason for this difference in slope could be the engine conditions prior to Stage 3 as ISM Test 3 and 4 were performed at average CPF temperatures above 410°C.

Table 4.22: PM Concentrations for Stage 3 Loading

		ISM					ISL				
	Location	Test 1	Test 2	Test 3	Test 4	Test 5	Test 2	Test 1	Test 4	Test 5	Test 3
Stage 3	UDOC	15.4	15.2	12.2	16.1	-	16.8	16.6	16.0	16.0	16.2

*Measurements in mg/scm

Results for testing on the ISL are repeatable as seen in Figure 4.31. All five tests have similar slopes for Stage 3. The pressure drop for Test 1 is approximately 3 kPa higher than the rest of the tests since the PM loading of the filter was higher than the other tests at 2.4 g/L. The variation of the PM concentrations for all of the tests on the ISM is less than 1 mg/scm when excluding Test 3. This indicates that the small variation of concentrations and the resultant effect on PM flow rates is not likely the cause of the different slopes on the ISM.

4.8 Overall Pressure Drop Profiles

It has been demonstrated in references [33, 34] that after an active regeneration is performed on a CPF that the resulting pressure drop across the CPF is less than pressure drop before the regeneration was initiated. This is a result of the PM within the wall and cake layer oxidizing which decreases the flow restriction across the CPF. As long as a complete regeneration is not performed or there is not a breakthrough of the PM cake layer, this reduced flow restriction is maintained due to the filtration efficiency of the PM cake layer. Therefore, a CPF with the same PM loading should exhibit an overall lower pressure drop across the CPF after a partial passive or active regeneration when compared to a similar CPF which has only been operated under loading conditions if the wall PM has been oxidized significantly during the regeneration process.

Some of the performed passive oxidation experiments have a significant portion of thermal oxidation which contributes to the overall reaction rate. Due to this fact, it was expected that this pressure drop phenomenon would be experienced on at least some of the performed tests. The procedure used during the performed tests differs slightly from [33, 34] in that at the beginning of the passive oxidation tests, the filter is completely clean. As a result of this test procedure, the post regeneration pressure drop cannot be below the initial pressure drop value during Stage 1 loading when operating at the same conditions.

The complete pressure drop profiles from ISM Test 3 and 4 are shown in Figure 4.32. As can be seen in this figure, the pressure drop across the CPF during post passive regeneration operation does decrease from the end of Stage 2 loading due to PM oxidation in the wall and cake layer. When evaluating pressure drop profiles from other tests, similar results are seen. In Figure 4.33, the pressure drop profiles for ISL Test 2 and 3 also exhibit this pressure drop reduction after post regeneration. It is possible that at a lower temperature range during passive regeneration that the PM within the wall might not be oxidized completely.

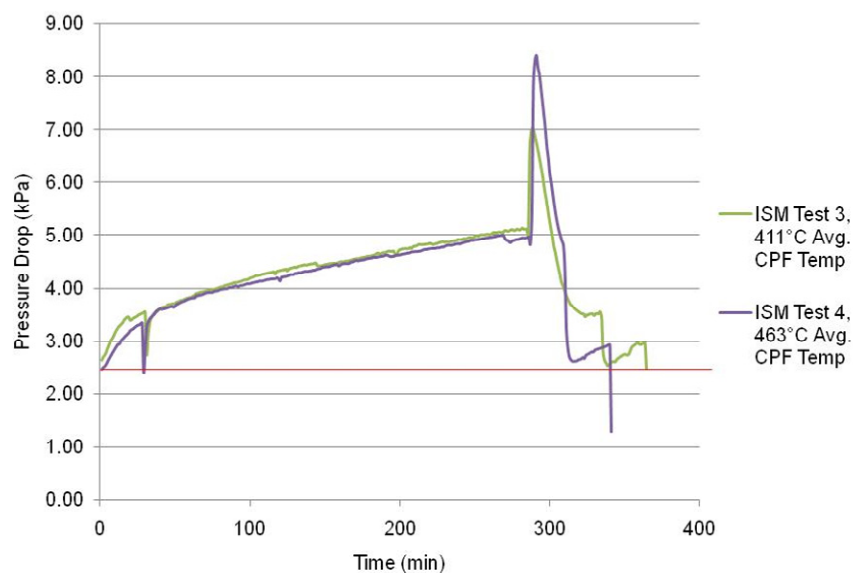


Figure 4.32: ISM Test 3 and 4 Pressure Drop Profile

During ISL Test 1 only a small decrease in the overall pressure drop was measured after the passive regeneration portion of the test as can be seen in Figure 4.34. To determine how much of the oxidized PM was within the wall, an analysis would be required using the MTU 1-D CPF model. The PM mass in the CPF after regeneration and the measured pressure drop across the CPF is shown in Figure 4.35. These data were collected for all of the tests except for ISM Test 5 which was carried out at a different operating condition. This shows that the total pressure drop across the CPF is not a reliable

indicator of the PM within the CPF since the wall pressure drop is a function of how much PM in the wall was oxidized during the passive oxidation stage and the cake permeability. Several tests have a CPF pressure drop of approximately 3.5 kPa but the PM within the CPF when this pressure drop was recorded varies from 19g - 33 g.

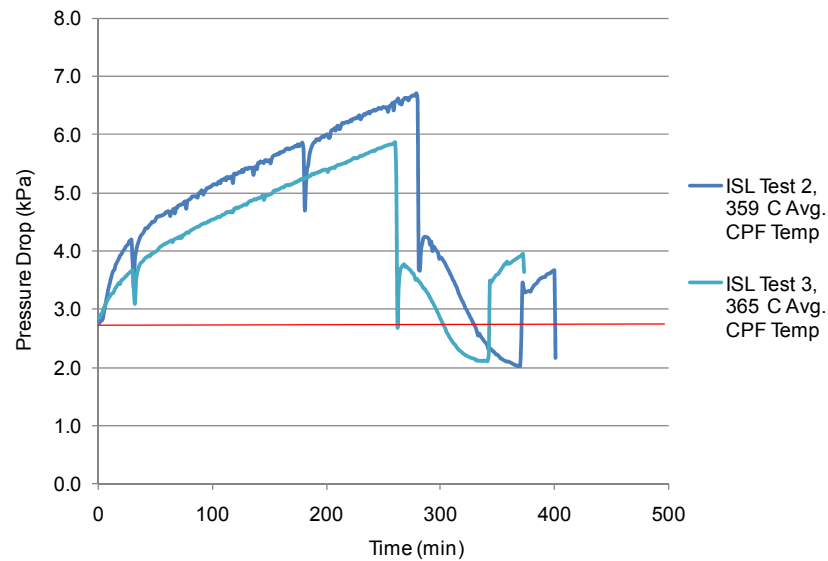


Figure 4.33: ISL Test 2 and 3 Pressure Drop Profile

In order to determine if the PM mass within the wall was oxidized during the passive oxidation portions of the test, data provided by the MTU 1-D CPF model was analyzed. The pressure drop during Stage 2 loading was obtained for a selected PM mass within the CPF which is visible at the top of the columns for each test in Figure 4.36. The model data were then used to determine the pressure drop during Stage 3 for the same amount of mass in the CPF. If there is a difference in the pressure drops between Stage 2 and 3 when the same amount of mass is present, this difference in pressure drop is caused by the oxidation of PM within the wall during the passive oxidation stage. As can be seen in Figure 4.36, the pressure drop difference between Stage 2 and 3 loading ranges from 0.2 to 2.0 kPa indicating that PM within the wall has been oxidized for most of the tests.

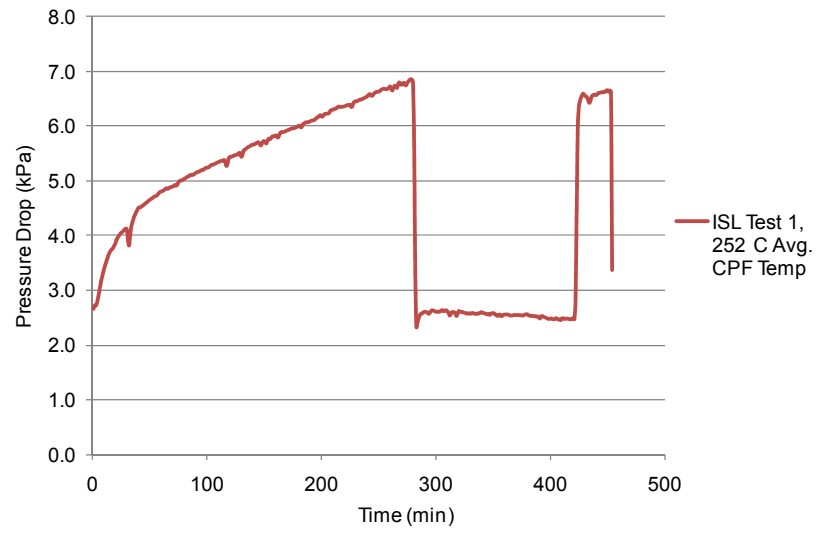


Figure 4.34: ISL Test 1 Pressure Drop Profile

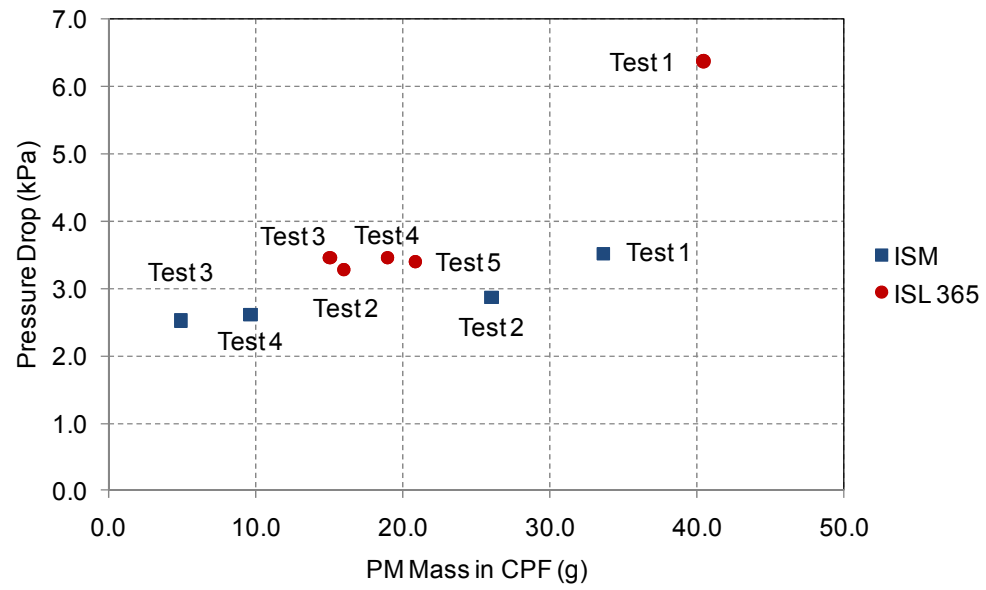


Figure 4.35: PM Mass Retained after Regeneration

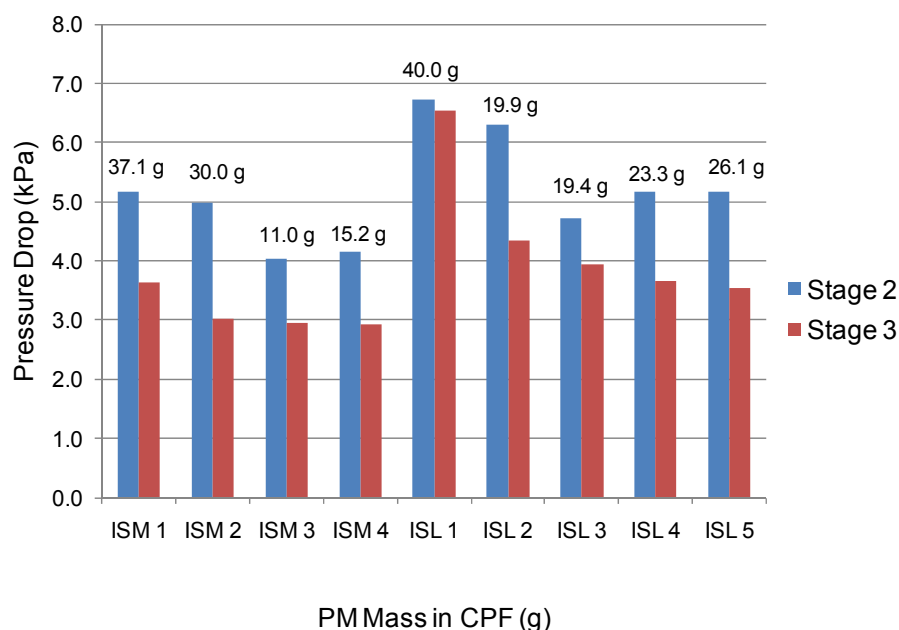


Figure 4.36: Pressure Drop Comparison of Stage 2 and 3 Loading

4.9 CPF Comparison Test

Two catalyzed particulate filters were used during the performed testing. One filter was dedicated to the ISM and the second filter to the ISL. In order to determine if the oxidation characteristics were comparable from the different filters, ISL Test 3 was performed as a CPF comparison test with a DOC inlet temperature of 361°C and an exhaust mass flow rate of 7.7 kg/min. ISL Test 2 was performed with the CPF used during testing on the ISL so the results from this test were available for comparison when testing the CPF from the ISM. In order to determine if using the CPF from experiments performed on the ISM would result in similar reaction rates, the conditions from ISL Test 2, shown in Table 4.23, were recreated.

Preliminary testing showed that this could be accomplished with an engine speed of 1290 rpm and load of 560 Nm. ISL 365 Test 3 would then be conducted with a CPF inlet

temperature of 351°C and an exhaust mass flow rate of 7.7 kg/min. Experimental results with an engine speed of 1290 rpm and 560 Nm resulted in a CPF inlet temperature of 362°C and exhaust flow rate of 7.7 kg/min. The targeted DOC inlet temperature and exhaust mass flow rate for Point F are 371°C and 6.8 kg/min respectively. The predicted load and speed for Point F are 1290 rpm and 540 Nm.

Table 4.23: Summarized Passive Oxidation Values

	Variable	Time	CPF inlet temp.	Average CPF temp.	DOC NO to NO2 Conv Eff.	Exhaust Mass flow rate	Actual Exhaust Volumetric flow rate	Engine out PM Conc.	Percent PM oxidized	NO2 Conc. into CPF	NO2 Conc. into CPF	NO2/PM ratio
Engine	Test/Units	minutes	°C	°C	%	kg/min	m ³ /sec	mg/scm	%	ppm	mg/scm	-
ISL 365	Test 2	90.2	362	351	54	7.7	0.223	6.9	64	117	220.0	31.9
	Test 3	81.2	362	355	50	7.7	0.226	7.0	65	116	218.1	31.2

An abbreviated table of the important variables during passive oxidation can be seen in Table 4.23. Except for Stage 1 loading, the values throughout the test compare reasonably well which can be seen by the emissions data and PM mass balances in Appendix K and Appendix N respectively. The experimentally determined reaction rate for ISL Test 3 was $2.229\text{E-}04\text{ s}^{-1}$ while the reaction rate for Test 2 was $1.961\text{E-}04\text{ s}^{-1}$. While these values are not identical, when considering the accuracy of the mass measurements and the subsequent error bars that this accuracy generates during the calculation of the reaction rate, the values are close enough to determine that the filters oxidized PM at a similar rate.

The experimental pressure drop profiles from ISL Test 2 and 3 are shown in Figure 4.37. As can be seen from the figure, the slopes of the curves appear similar but the magnitude of the pressure drops differ by approximately 0.5 - 0.75 kPa. In order to better analyze this difference, the plots of the passive oxidation portion of the test were time aligned and can be seen in Figure 4.38. This shows that the difference of the pressure drop profiles during passive oxidation is approximately 0.5 kPa. The exhaust volumetric flow rates values for the two tests are in Table 4.23 and the actual volumetric flow rate for ISL Test 2 and Test 3 were 0.223 and 0.226 act. m³/s respectively.

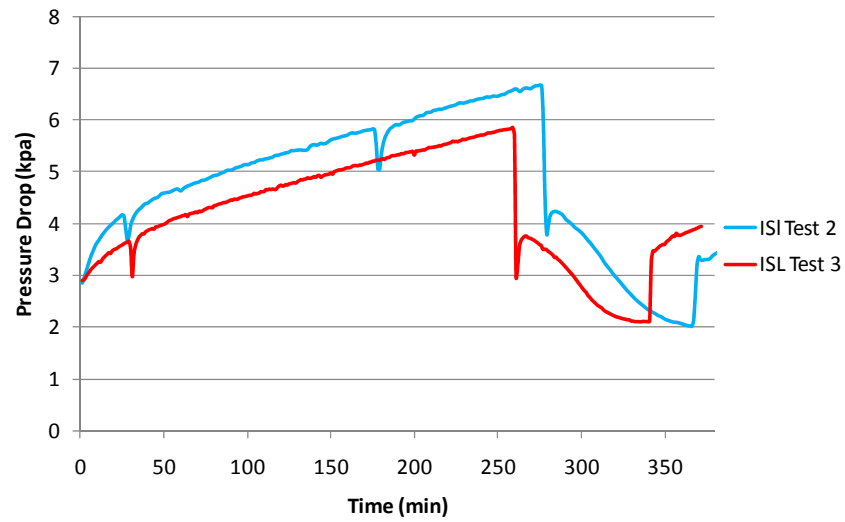


Figure 4.37: ISL Test 2 and ISL Test 3 Pressure Drop Comparisons

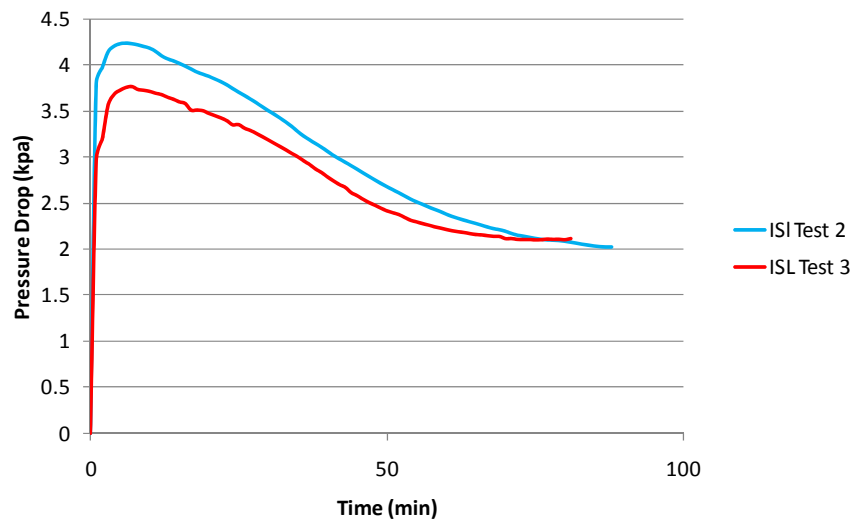


Figure 4.38: ISL Test 2 and ISL Test 3 Aligned for Data during Passive Oxidation (Test 2 data was moved 21 min. earlier) Pressure Drop Comparisons

Upon reviewing the equation for the total pressure drop across the CPF, shown by equation 4.5 obtained from reference [42], it can be seen that the pressure drop across

the CPF has the actual volumetric exhaust flow rate as a term within the equation. This equation assumes that the permeability of the cake and wall are constant. In order to account for the different exhaust flow rates, the pressure drop profiles were scaled by the ratio of the actual exhaust volumetric flow rates. Each flow rate from the test was divided by the flow rate for Test 2 which resulted in scaling factors of 1 and 1.01 for Test 2 and Test 3 respectively. The scaling factor was then multiplied by the recorded pressure drop values from each test. The plot of these data can be seen in Figure 4.39. After this procedure the pressure drop values changed very little and there is still a 0.42 kPa difference between the peaks.

$$\Delta P_{\text{Total}} = \Delta P_{\text{Friction}} + \Delta P_{\text{Cake}} + \Delta P_{\text{Wall}} \quad 4.5$$

$$\Delta P_{\text{Total}} = \frac{4}{3} * \frac{\mu \dot{V} (a + w_s^2) F L^2}{V_{\text{Trap}}^2 a^4} + \frac{\mu}{k_p} v_w w + \frac{\mu}{k_s} v_w w_s$$

ΔP_{Total} = Pressure drop across CPF (pa)

μ = Dynamic viscosity (kg/m*s)

\dot{V} = Actual volumetric flow rate (m³/s)

a = Width of channel (m)

w_s = Substrate wall thickness (m)

$F = 2C_f \text{Re}$

$C_f \text{Re} = 14.227$ for a square type channel geometry

L = Effective filter channel length (m)

V_{Trap} = Volume of the filter (m³)

w = PM layer thickness (m)

v_w = Wall flow velocity (m/s)

k_s = Instantaneous permeability of the filter wall (m²)

k_p = Permeability of the cake layer (m²)

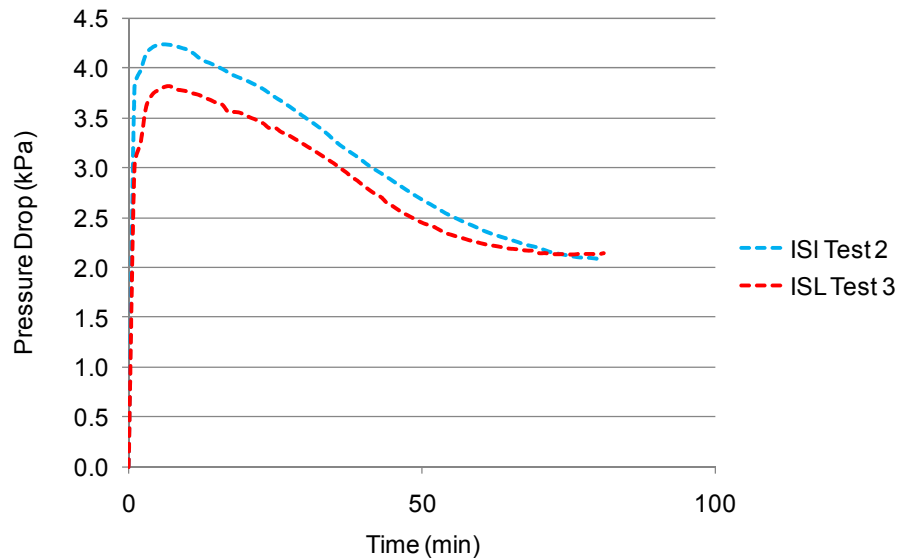


Figure 4.39: ISL Test 2 and ISL Test 3 Normalized Pressure Drops

As can be seen in Table 4.23, the average experimental values for the test are similar so it was decided to investigate the individual temperatures within the CPF. The sixteen individual temperatures recorded within the CPF substrate are shown in Figure 4.40 for ISL Test 2 and Figure 4.41 for ISL Test 3. From these figures it can be seen the temperature distribution is different between tests. Specifically, the radial temperature distributions are different between the tests. This could be a partial explanation for the difference in total pressure drop across the CPF. From the comparison test it has been shown that the reaction rates were similar from both of the filters but pressure drop characteristics differ by approximately 0.5 kPa due to an undeterminable cause.

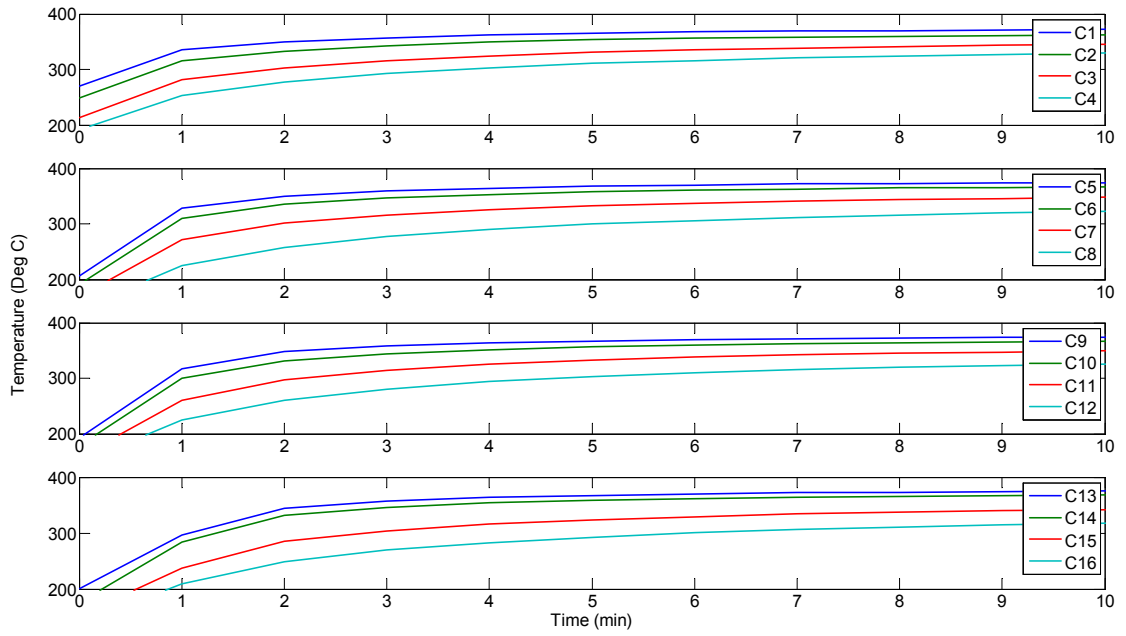


Figure 4.40: ISL Test 2 CPF Temperatures

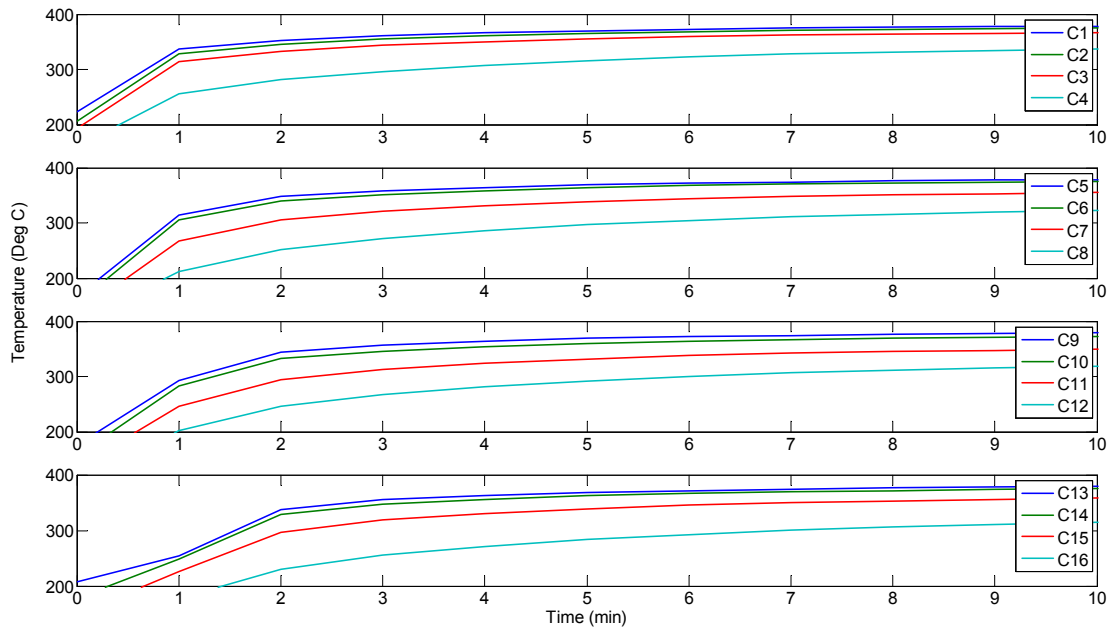


Figure 4.41: ISL Test 3 CPF Temperatures

Chapter 5 Summary and Conclusions

5.1 Summary

A series of tests have been performed on two engines, a Cummins 2002 256 kW (330 hp) ISM and Cummins 2007 272 kW (365hp) ISL. The experiments consisted of operating the engines at a specified set of conditions to obtain a CPF PM loading of 2.2 ± 0.2 g/L and then changing engine operating conditions to investigate the passive regeneration characteristics of the PM in the CPF. By changing the engine operating conditions, the CPF inlet exhaust temperature, exhaust flow rate, NO₂ concentration, NO₂ flow rate, and NO₂/PM ratio were varied in order to promote different reaction rates and to investigate the effect of changing these variables on the reaction rates. These data will also be used for the calibration of the MTU 1-D CPF model.

5.1.1 NO and NO₂ Emissions Measurement

Two emissions analyzers were used for the performed passive oxidation testing. For all of the performed tests on the ISM a Semtech DS (Sensors Inc.) was used to measure NO, NO₂ and total NO_x concentration in the exhaust. The remainder of the gaseous emissions were recorded by a Pierburg AMA 4000 emissions bench (AVL). Testing performed on the ISL used the Pierburg bench for all gaseous emissions.

The operating principles for the two NO_x analyzers within the emission benches differ as the Semtech measures “dry” concentrations while the Pierburg Measures “wet”. All NO, NO₂ and NO_x measurements reported in this document have been converted to wet concentrations. When a comparison test of the two analyzers was performed, the analyzers reported NO₂ concentrations that were different within the exhaust. On average over the tested conditions, the Pierburg measured NO₂ concentrations that were 11 ppm higher than the Semtech.

In order to compensate for this difference, the NO₂ values for testing on the ISM could be increased by 10 ppm if modeling efforts supported this increase. Simulations would need to be performed to determine if the modeled reaction rates provided for a better agreement with the measured PM masses. Across the test conditions, the difference in measurements of NO concentrations varied from -11 ppm to +14 ppm. While the NO values do differ between analyzers, this is not expected to significantly affect the NO to NO₂ conversion efficiencies across the DOC. Adjustments to the NO values for the testing on the ISM are hard to determine since the differences vary widely.

5.1.2 PM Concentrations and CPF Filtration Efficiency

PM concentrations were collected during each stage of the test. During Stage 1 and 3, only one sample was collected upstream of the diesel oxidation catalyst (UDOC) due to the short duration of this stage. The number of samples collected during Stage 2 varied but a minimum of one sample downstream of the catalyzed particulate filter (DCPF) and five samples UDOC were collected. The UDOC samples from Stage 1, 2, and 3 were averaged to determine the PM concentration to be used in the mass balance for the loading portions of the tests and a CPF filtration efficiency calculation. The average PM concentrations for the loading portions of the test were 15.4 and 17.4 mg/scm for the ISM and ISL respectively. The average PM concentration for the test and the DCPF sample were used to determine CPF filtration efficiency. The average calculated filtration efficiencies were 97.3 and 98.1% for the ISM and ISL respectively.

A correlation between engine out PM concentrations and ambient test cell absolute humidity has been demonstrated. As the absolute humidity in the test cell increases there is an increase in engine out PM concentrations. There might be a lower limit for this correlation as testing on the ISM at low humidity's did not show any visible trends.

5.1.3 Temperature Analysis

A total of nine thermocouples were placed in the DOC substrate to investigate both radial and axial temperature gradients. Samples were taken once every three seconds on the ISM and once every second on the ISL. For the investigation of radial temperature gradients, the thermocouple layout consisted of five thermocouples at different radial dimensions from the centerline of the DOC substrate. Results from testing on both engines showed that the radial temperature distributions followed the same pattern on both engines and at different temperatures. As the radial dimension is increased, the temperature difference between thermocouples increases. The magnitude of the radial temperature gradient varies based upon DOC inlet temperature and engine operating strategy. As discussed in section 4.3.1, during a clean out of the CPF the radial temperature gradients were less than when operating at passive oxidation conditions. It is hypothesized that the oxidation of hydrocarbons within the DOC creates different temperature gradients and therefore the temperature distribution is dependent upon the operating strategy of the engine.

An analysis of the temperature in different quadrants of the DOC was performed by using three thermocouples in each of two quadrants of the DOC and then analyzing the temperature measurements. This showed that at the same radial dimension, temperatures were similar from the two quadrants. Three thermocouples were placed at a radial distance of 95 mm from the DOC centerline and equally space from the front to the rear of the substrate to investigate axial gradients. Testing showed minimal axial gradients at three different DOC inlet temperatures.

Sixteen thermocouples were used to measure temperature variation within the CPF. These were positioned at four axial dimensions measured from the front of the CPF substrate. At the prescribed axial dimensions, four thermocouples were placed at different radial dimensions from the centerline of the CPF and three of these thermocouples were placed at the centroid of three equal areas to facilitate the calculation of a volume averaged temperature.

CPF temperature analysis showed that, dependent on CPF inlet temperature, steady state temperatures are not reached within the CPF for up to 20 minutes during passive oxidation testing. Radial and axial temperature gradients are present within the CPF. These gradients differ between the performed tests and are a function of local reaction rate, exhaust mass flow rate and inlet temperature of the CPF. Average CPF temperatures should be calculated using the thermocouples at the radial distances of 55, 95 and 122 mm.

5.1.4 Stage 1 and Stage 2 Loading

Stage 1 loading consisted of operating the engine for 30 minutes for the specified loading conditions. For the ISM, Stage 1 and 2 loading consisted of operating the engine at 1800 rpm and 300 Nm while the ISL was run at 2100 rpm and 200 Nm. Stage 2 consisted of operating the engine at the above conditions until a nominal CPF loading of 2.2 ± 0.2 g/L was achieved. Gaseous emissions of CO₂ and O₂ were similar for both engines with CO and HC concentrations on the ISL being slightly higher than the ISM.

On average, the ISM had NO₂ concentrations that were approximately three times larger than the ISL. Average PM concentrations and NO₂/PM ratios on the ISM were 15.4 mg/scm and 11.5 respectively. The ISL average PM concentrations and NO₂/PM ratios were 17.4 mg/scm and 3.2. During Stage 2 the higher NO₂/PM ratios on the ISM should have provided for a higher reaction rate since the average CPF temperatures were similar at 268°C for the ISM and 264°C for the ISL. The average calculated reaction rate for the ISL is 3.04E-5 1/s while the average calculated reaction rate for the ISM is 2.45E-05 1/s.

Although the reaction rate for the ISM is lower than the ISL, the values are not statistically different. The higher reaction rate for the ISL does provide for an oxidation rate that is on average 5% higher than the ISM. From the experimental NO₂/PM ratios and the similar CPF temperatures, the ISM should have a higher oxidation rate than the

ISL. Since it does not, this indicates the most likely difference is the composition or structure of the PM produced by the engines.

The clean pressure drop across the CPF was investigated for both engines with average actual volumetric flow rates through the CPF being 0.320 act.m³/s and 0.322 act.m³/s for the ISM and ISL respectively. The average clean pressure drop across the CPF for the ISM was 2.5 kPa with a standard deviation of 0.1 kPa. For the ISL, the average pressure drop was 2.7 kPa with a standard deviation of 0.1 kPa. After performing a statistical two sided t-test, the clean pressure drops were determined to be from the same population which indicates that they are statistically the same.

5.1.5 Passive Oxidation

The passive regeneration portion of the test is initiated after the CPF has reached a PM loading of 2.2 ± 0.2 g/L. For the performed testing, a variety of exhaust mass flow rates and DOC inlet temperatures were selected for the test matrix. This allowed for a wide range of NO₂/PM ratios to be investigated. CPF average temperatures ranged from 262° to 463°C while experimental NO₂/PM ratios varied from 6 to 59.

An important calculated value during the passive oxidation portion of the test is the ratio NO₂ consumed/NO₂ available at the inlet of the CPF. For ratios over one, more NO₂ is consumed than what is present at the CPF inlet. This indicates that the production of NO₂ is occurring within the CPF at the filter substrate and the NO₂ is back diffusing into the PM cake layer. To confirm this finding, Péclet numbers were calculated for the passive oxidation portions of the tests. Values less than one were calculated for each test confirming that the transport of NO₂ within the PM cake layer is diffusion dominated.

The presence of back diffusion is an extremely important finding. Under passive oxidation conditions the reaction rate does not only depend upon NO₂ concentrations but the NO_x concentrations at the inlet of the CPF. The NO_x concentration then reflects the

potential for PM oxidation since the NO contribution of this value can be oxidized to NO₂ and then diffuse back into the PM cake layer increasing the reaction rate.

The experimental reaction rates varied based upon the average CPF temperature, NO₂ concentrations, NO₂ flow rates into the CPF and the NO₂/PM ratios. Due to the limited data for the reaction rate model, the pre-exponential factor and activation energy for passive oxidation cannot be calculated. Also, the effect of NO₂ concentrations cannot be quantified directly from the experimental data. The calculated reaction rates do provide for an indication of how the combinations of the involved variables affect the rate of PM oxidation. They also allow for a comparison with the reaction rates simulated within the MTU 1-D CPF model. The simulated reaction rates compare well with the experimental rates. The model has the additional benefit of being able to identify what portion of the reaction rate is from passive oxidation and what percentage is from thermal oxidation. This is useful in determining the temperatures for future tests to ensure that the test is performed at temperatures where passive oxidation is dominant.

Temperature played a large role in the experimental reaction rate. As temperatures increased the reaction rates also went up. This was the result of two contributions. As the temperature increased, the NO to NO₂ conversion efficiency of the DOC increased thereby increasing the NO₂ at the CPF inlet in some cases. In cases where higher temperatures are involved, the DOC NO to NO₂ conversion efficiency can decrease with an increase in temperature. The second reason is that the higher temperature promoted an increased reaction between NO₂ and PM. While NO₂ concentrations are important, the temperature of the CPF is the dominant effect in the reaction rate. As an example, ISL Test 1 had one of the highest NO₂/PM ratios at 47.3:1. The average CPF temperature was the lowest of all testing and as a result the calculated reaction rate was the lowest of the performed tests.

The maximum pressure drop profiles during the testing on the ISL were higher than on tests performed on the ISM due to higher actual volumetric flow rates. The slope of the pressure drop profile is an indicator of the reaction rate occurring in the CPF. Steeper pressure drop profiles would indicate a reaction rate that is larger than a profile which is

flat. When reviewing the peak of the pressure drop profile from ISM Test 4 and 5 it can be seen that the passive oxidation of PM was initiated sooner than on the comparable test on the ISL. This is visualized by the smaller radius of the peak.

5.1.6 Stage 3 Loading

Stage 3 loading consisted of operating the engine at the specified loading conditions used during Stage 1 and 2. This was done to ensure that the CPF temperature cooled to a repeatable value in order to provide for the most accurate mass measurements between the stages of the test. Measured gaseous emissions and PM concentrations for this stage were similar to values reported for Stage 1 and 2. The accumulated mass for this stage is obtained from the MTU 1-D CPF model. With this mass value and the measurement of the CPF mass at the end of Stage 3, the PM present in the CPF at the end of the passive oxidation stage can be determined. The average reaction rate for the passive oxidation portion of the test can then be calculated.

A comparison of the pressure drops across the CPF both before and after the passive oxidation portion of the test was performed. This was done with the same mass of PM in the filter to determine if the pressure drop prior to passive regeneration of the filter would be higher than the post regeneration pressure drop value. The post passive oxidation pressure drops were compared to pre-regeneration values ensuring that the mass of PM within the CPF was the same to determine if PM oxidation within the substrate wall was occurring. This comparison showed the pressure drop across the CPF did decrease for all tests and the PM within the substrate wall was being oxidized.

The pressure drop across the CPF for Stage 3 loading was less than the end of Stage 2 loading for the performed tests. This is due to the reduction of the PM cake layer and the PM within the substrate wall. During ISL Test 1 however the total mass oxidized from the CPF was only 1.8 g which allows for the possibility of some mass remaining in the catalyst wall. This trend could be possible for other temperatures in the passive oxidation realm.

During Stage 3 loading, the slope of the pressure drop profiles on the ISM differed between tests. ISM Test 1 and 2 has similar slopes while Test 3 and 4 were alike. Possible causes for this difference are the PM flow rates or the engine operating conditions prior to Stage 3. The pressure drop profiles for Stage 3 on the ISL were repeatable. The pressure drop for ISL Test 2 was higher than all other tests due to the high PM loading of the filter of 2.4 g/L.

5.1.7 CPF Comparison Test

In order to determine if the results from the testing performed on the ISM and ISL could be compared directly, a test was performed to compare the catalyzed particulate filters used on each engine. ISL Test 2, 372°C DOC inlet temperature and 7.7 kg/min exhaust flow rate, was used as the baseline test. ISL Test 3, 361°C DOC inlet temperature and 7.7 kg/min exhaust flow rate, was performed using the CPF from the ISM to determine if the filters oxidized PM in a similar manner.

The experimental values from both tests were similar. Important test values such as NO₂ flow rates, NO₂ concentrations, CPF average temperatures and NO₂/PM ratios were within 5% for both tests. The experimental reaction rates for the performed tests were 1.961E-4 1/s and 2.229E-4 1/s for ISL Test 2 and 3 respectively. When considering the accuracy of the CPF mass measurements and the subsequent error this provides when calculating the reaction rates, it has been determined that the filters oxidize PM in a similar manner.

After scaling the pressure drop profiles by a ratio of the actual volumetric flow rates, the CPF pressure drop characteristics appear similar but the pressure drop from ISL Test 2 is higher than Test 3 by 0.42 kPa. This could be a result of the different temperature distributions within the CPF during the two tests. After reviewing the results of this comparison test it has been determined that the filters oxidize PM in a similar manner. The pressure drop profiles have the same slope but are offset by 0.42 kPa. While the

pressure drop profiles are different it is felt that the results from testing on the ISM and the ISL can be directly compared.

5.2 Conclusions

The overall goal of this thesis was to characterize the passive oxidation of PM within the CPF and determine the impact of using different engine technologies on this process. This goal has been met through the performed testing and the subsequent analysis of the data collected. Conclusions from analysis of the collected data are as follows.

Test Procedure Development

- Operating the engine for 30 minutes after the clean out of the CPF and after the passive oxidation portion of the test allows the CPF to cool to a repeatable temperature providing for the most accurate mass measurements between stages. The accuracy of the CPF mass measurements are ± 1 g.
- The absolute humidity of the test cell affects the engine out PM concentrations. As the absolute humidity of the test cell increases the PM concentration increases for test cell conditions experienced during testing. The engine out PM concentration varied from 16.4 to 18.5 mg/scm for test cell absolute humidity's ranging from 0.062 kg to 0.010 kg water vapor/kg of dry air. The absolute humidity measured during tests can be used to help predict loading times.
- The temperature throughout the DOC at different radial dimensions is the same in different quadrants. The axial temperature gradient within the DOC at a radial dimension of 95 mm is less than 3°C during the performed experiments. With this information it is a good assumption that the DOC temperature is uniform throughout at steady state operation.

Loading

- The average reaction rates for the ISM ($2.45\text{E-}5$ 1/s) and ISL ($3.04\text{E-}5$ 1/s) during Stage 2 loading were not statistically different for similar average CPF temperatures of 268°C and 264°C respectively. The ISM had an NO_2/PM ratio that on average was three times greater than that of the ISL which should have resulted in a higher reaction rate if all other things were equal.
- Due to the average CPF temperatures and reactions rates being similar during loading for both engines while the ISM had higher NO_2/PM ratios, an unmeasured experimental value differed between engines. The most likely difference is the composition or structure of the PM produced by the engines.
- The clean pressure drop across the CPF used on the ISM and the CPF used on the ISL were statistically the same for Stage 1 loading.

Passive Oxidation

- Due to the limited test matrix and the variation of temperatures, NO_2 concentrations, NO_2 flow rates into the CPF and NO_2/PM ratios between comparable passive oxidation tests for each engine, a direct comparison of the reaction rates between engines is not possible for this stage of the test.
- The reaction rates during passive oxidation showed a strong temperature dependence. Due to limited data for the reaction rate model, the direct effect of NO_2 concentrations on the oxidation of PM is not obtainable. An increased data set or a detailed model such as the MTU 1-D CPF will be required for further analysis.
- The reaction rates simulated with the MTU 1-D CPF model agree well with the experimentally determined rates.
- The particulate matter generated at two different engine operating conditions, loading point B (1800 rpm, 300 Nm) and loading point F (2100 rpm and 200 Nm), passively oxidized in the same manner for testing on the ISM.

- The NO_2 consumed during passive oxidation was in most cases greater than the NO_2 available at the CPF inlet. This indicates the production of NO_2 at the CPF catalyst on the substrate and the diffusion upstream into the PM cake layer.
- In addition to NO_2 concentrations at the CPF inlet, NO_x concentrations are also important as the contribution of NO to this value indicates the potential for PM oxidation as the result of the oxidation of NO to NO_2 at the substrate wall and the back diffusion into the PM cake layer.
- Calculated Péclet values for the passive oxidation portions of the test were less than one indicating that the transport of NO_2 within the CPF cake layer is diffusion dominated.

Stage 3 Loading

- The pressure drop across the CPF after a passive oxidation event has occurred is not a good indicator of the amount of PM within the CPF. It has been shown that at a pressure drop across the CPF of approximately 3.5 kPa the PM mass with the CPF varied from 19 to 35 g.
- A comparison of the pressure drop from Stage 2 and 3 was performed when the CPF was loaded with the same amount of PM mass. The pressure drop decreased from 0.2 to 2.0 kPa after the passive oxidation stage of the test. This decrease in pressure drop was caused by the oxidation of PM within the wall.

5.3 Recommendations

- Due to the amount of down time that was experienced during the testing due to the emissions analyzer, it is recommended that funding be secured to replace the current emissions bench.
- Testing should be performed in order to characterize the reactivity of the PM with NO_2 in order to determine experimental activation energies

- The current global reaction rate model is of limited use due to the varying NO₂ concentrations within the PM layer which prevents the calculation of A and Ea. Before performing more tests, additional discussion should be undertaken in order to determine what information is needed to better understand the process of back diffusion of NO₂ within a CPF and the best methods to collect the required information.
- When testing resumes, additional passive oxidation testing should include additional tests at temperatures below 400°C.
- In order to determine if uniform temperatures exist throughout the DOC, the axial thermocouple layout used for testing on the ISL should be repeated at different radial dimensions.
- In order to experimentally verify NO₂ back diffusion within the CPF, measurements of NO₂ concentration downstream of the CPF should be performed continuously.
- A NO to NO₂ conversion efficiency test across the DOC should be performed at different space velocities and temperatures to determine the NO conversion efficiencies of the DOC.
- The amount of mass retained within the CPF at the end of the passive oxidation portion of the test should be a targeted value. This value should be maintained consistent throughout testing to ensure directly comparable results between tests.
- An evaluation of the comparison tests, tests where the passive oxidation portion of the test was performed at Point F (1290 rpm, 540 Nm) after a CPF PM loading of 2.2 g/L was obtained, should be performed to determine if the measured temperature distributions within the CPF affect the pressure drop across the CPF.

References

1. Steve Charlton, Thomas Dollmeyer and Thomas Grana, "Meeting the US Heavy-Duty EPA 2010 Standards and Providing Increased Value for the Customer", SAE Technical Paper No. 2010-01-1934, 2010
2. David B. Kittelson, "Engines and Nanoparticles: A Review", J. Aerosol Sci. Vol. 29, No. 5/6, pp. 575-588, 1998
3. Z. Gerald Liu, Devin R. Berg, James J. Schauer, "Detailed Effects of a Diesel Particulate Filter on the Reduction of Chemical Species Emissions", SAE Technical Paper No. 2008-01-0333, 2008
4. Krishna Pradeep Chilumukuru, Rohith Arasappa, John H. Johnson and Jeffrey D. Naber, "An Experimental Study of Particulate Thermal Oxidation in a Catalyzed Filter During Active Regeneration", SAE Technical Paper No. 2009-01-1474, 2008
5. Ingo Mikulic, Reggie Zhan, Scott Eakle, "Dependence of Fuel Consumption on Engine Backpressure Generated by a DPF", SAE Technical Paper No. 2010-01-0535, 2010
6. G. C. Koltsakis, O. A. Haralampous, C. K. Dardiotis and Z. C. Samaras, C.-D. Vogt and E. Ohara, Y. Watanabe, T. Mizutani, "Performance of Catalyzed Particulate Filters without Upstream Oxidation Catalyst", SAE Technical Paper No. 2005-01-0952, 2005
7. Antonio P. Triana, John H. Johnson and Song L. Yang, Kirby J. Baumgard, "An Experimental and Numerical Study of the Performance Characteristics of the Diesel Oxidation Catalyst in a Continuously Regenerating Particulate Filter", SAE Technical Paper No. 2003-01-3176, 2003
8. Santhoji R. Katare, Joseph E. Patterson and Paul M. Laing, "Aged DOC is a Net Consumer of NO₂: Analyses of Vehicle, Engine-dynamometer and Reactor Data", SAE Technical Paper No. 2007-01-3984, 2007
9. Robert K. Miller, Cheng G. Li, "Effect of Catalyst Support Structure on Conversion Efficiency", SAE Technical Paper No. 2000-01-0183, 2000

10. O. A. Haralampous, G. C. Koltsakis, Z. C. Samaras, C.-D. Vogt, E. Ohara, Y. Watanabe, T. Mizutani, "Reaction and Diffusion Phenomena in Catalyzed Diesel Particulate Filters", SAE Technical Paper No. 2004-01-0696, 2004
11. Mejdí Jeguirim, Valerie Tschamber and Jean Francois Brillhac, "Kinetics of Catalyzed and Non-Catalyzed Soot Oxidation with Nitrogen Dioxide Under Regeneration Particle Trap Conditions", J Chem Technol Biotechnol; 84: 770–776, 2009
12. M. Schejbal, J. Stepanek, M. Marek, P. Koci, M. Kubicek, "Modelling of soot oxidation by NO₂ in various types of diesel particulate filters", Fuel 89: 2365–2375, 2010
13. T. Maunula, P. Matilainen, M. Louhelainen, P. Juvonen and T. Kinnunen, "Catalyzed Particulate Filters for Mobile Diesel Applications", SAE Technical Paper No. 2007-01-0041, 2007
14. Arvind Suresh, Aleksey Yezerets, Neal Currier, Jim Clerc, "Diesel Particulate Filter System – Effect of Critical Variables on the Regeneration Strategy Development and Optimization", SAE Technical Paper No. 2008-01-0329, 2008
15. Rayomand H. Dabhoiwala, John H. Johnson, Jeffrey D. Naber and Susan T. Bagley, "Experimental and Modeling Results Comparing Two Diesel Oxidation Catalyst – Catalyzed Particulate Filter Systems", SAE Technical Paper No. 2008-01-0329, 2008
16. Gregory Austin, Jeffrey Naber, John Johnson, Chris Hutton, "Effects of Biodiesel Blends on Particulate Matter Oxidation in a Catalyzed Particulate Filter during Active Regeneration", SAE Technical Paper No. 2010-01-0557, 2010
17. Hasan Mohammed, Antonio P. Triana, Song-Lin Yang and John H. Johnson, "An Advanced 1D 2-Layer Catalyzed Diesel Particulate Filter Model to Simulate: Filtration by the Wall and Particulate Cake, Oxidation in the Wall and Particulate Cake by NO₂ and O₂, and Regeneration by Heat Addition", SAE Technical Paper No. 2006-01-0467, 2006
18. Kristian M. Bodek, Victor V. Wong, "The Effects of Sulfated Ash, Phosphorus and Sulfur on Diesel Aftertreatment Systems – A Review", SAE Technical Paper No. 2007-01-1922, 2007

19. Paramjot Singh, Abishek M. Thalagavara, Jeffrey D. Naber, John H. Johnson, Susan T. Bagley, "An Experimental Study of Active Regeneration of an Advanced Catalyzed Particulate Filter by Diesel Fuel Injection Upstream of an Oxidation Catalyst" SAE Technical Paper No. 2006-01-0879, 2006
20. Ronny Allansson, Philip G. Blakeman, Barry J. Cooper, Howard Hess, Peter J. Silcock, Andrew P Walker. "Optimising the Low Temperature Performance and Regeneration Efficiency of the Continuously Regenerating Diesel Particulate Filter (CR-DPF) System", SAE Technical Paper No. 2002-01-0428, 2002
21. Navtej Singh, Christopher J. Rutland, David E. Foster, Kushal Narayanaswamy, Yongsheng He, "Investigation into Different DPF Regeneration Strategies Based on Fuel Economy Using Integrated System Simulation", SAE Technical Paper No. 2009-01-1275, 2009
22. Seung Yang, Kyeong Lee, Hwansoo Chong, "Characterization of Oxidation Behaviors and Chemical-Kinetics Parameters of Diesel Particulates Relevant to DPF Regeneration", SAE Technical Paper No. 2010-01-2166, 2010
23. Z. Gerald Liu, Devin R. Berg, Thaddeus A. Swor, James J. Schauer, Barbara Zielinska, "A Study on the Emissions of Chemical Species from Heavy-Duty Diesel Engines and the Effects of Modern Aftertreatment Technology", SAE Technical Paper No. 2009-01-1084, 2009
24. Markus Maly, Michael Claussen, Otto Carlowitz, Peter Kroner, Marco Ranalli, Stefan Schmidt, "Influence of the Nitrogen Dioxide Based Regeneration on Soot Distribution", SAE Technical Paper No. 2004-01-0823, 2004
25. Antonio P. Triana, John H. Johnson, Song L. Yang, Kirby J. Baumgard, "An Experimental and Computational Study of the Pressure Drop and Regeneration Characteristics of a Diesel Oxidation Catalyst and a Particulate Filter", SAE Technical Paper No. 2006-01-0266, 2006
26. Andrew P.E. York, Mehrdad Ahmadijad, Timothy C. Watling, Andrew P. Walker, Julian P. Cox, Jane Gast, Philip G. Blakeman, Ronny Allansson, "Modeling of the Catalyzed Continuously Regenerating Diesel Particulate Filter (CCR-DPF) System: Model Development and Passive Regeneration Studies", SAE Technical Paper No. 2007-01-0043, 2007

27. Nickolas Vlachos, Giorgos Patrianakos, Margaritis Kostoglou, Athanasios G. Konstandopoulos, "Micro-Simulation of NO-NO₂ Transport and Reaction in the Wall of a Catalyzed Diesel Particulate Filter", SAE Technical Paper No. 2008-01-0442, 2008
28. A. Messerer, R. Niessner, U. Poschl, "Comprehensive Kinetic Characterization of the Oxidation and Gasification of Model and Real Diesel Soot by Nitrogen Oxides and Oxygen Under Engine Exhaust Conditions: Measurement, Langmuir–Hinshelwood, and Arrhenius parameters", Carbon 44: 307–324, 2006
29. Ken Kimura, Mike Lynskey, Eric R. Corrigan, David L. Hickman, Jerry Wang, Howard L. Fang, Sougato Chatterjee, "Real World Study of Diesel Particulate Filter Ash Accumulation in Heavy-Duty Diesel Trucks", SAE Technical Paper No. 2007-01-1922 2007
30. Athanasios G. Konstandopoulos, Margaritis Kostoglou, Souzana Lorentzou, Chrysa Pagkoura, Eleni Papaioannou, Kazushige Ohno, Kazutake Ogyu, Tomokazu Oya, "Soot Oxidation Kinetics in Diesel Particulate Filters", SAE Technical Paper No. 2007-01-1129, 2007
31. A. Awara, C. Opris, J. Johnson, "A theoretical and Experimental Study of the Regeneration Process in a Silicon Carbide Particulate Trap Using a Copper Fuel Additive", SAE Technical Paper No. 970188, 1997
32. Jinwoo Jung, Soonho Song and Kwang Min Chun, "Characterization of Catalyzed Soot Oxidation with NO₂, NO and O₂ using a Lab-Scale Flow Reactor System", SAE Technical Paper No. 2008-01-0482, 2007
33. Greg Austin, "Effects of Biodiesel Blends on Particulate Matter Oxidation in a Catalyzed Particulate Filter during Active Regeneration", Master's Thesis, Michigan Technological University, 2010
34. Krishna P. Chilumukuru, "An Experimental Study of Particulate Thermal Oxidation in a Catalyzed Filter during Active Regeneration", Master's thesis, Michigan Technological University, 2008
35. Ioannis P. Kandylas, Onoufrios A. Haralampous, Grigorios C. Koltsakis, "Diesel Soot Oxidation with NO₂: Engine Experiments and Simulations". Ind. Eng. Chem. Res. 41, 5372-5384, 2002

36. K. Yamamoto, S. Oohori, H. Yamashita, S. Daido, "Simulation on Soot Deposition and Combustion in Diesel Particulate Filter", Proceedings of the Combustion Institute 32, pg 1965-1972, 2009
37. Venkata R. Lakkireddy. "The Effect of an Advanced Oxidation Catalytic Converter and a Catalyzed Particulate Filter on the Emissions from a Heavy Duty Diesel Engine". Master's thesis, Michigan Technological University, 2005.
38. H. Burtscher et al, "Separation of Volatile and Non-Volatile Aerosol Fractions by Thermodesorption: Instrumental Development and Applications". Aerosol Science 32: 427-442, 2001
39. S. Abdul-Khalek, D. B. Kittelson, B. R. Graskow and Q. Wei, "Diesel Exhaust Particle Size: Measurement Issues and Trends", SAE Technical Paper No. 980525, 1998
40. Geoffery Vining and Scott Kowalski, "Statistical Methods for Engineers" second edition, Thomson Brooks/Cole, Belmont, CA. 2006
41. Harsha Shankar, "Modeling Study of Passive Oxidation Experimental Data", Department of Energy Partner Presentation, October 10, 2010
42. Kiran C. Premchand, "An Experimental and Modeling Study of the Filtration and Oxidation Characteristics of a Diesel Oxidation Catalyst and a Catalyzed Particulate Filter", Master's Thesis, Michigan Technological University, 2006

Appendix A. CPF Mass Balance

The mass balance for the CPF starts with a control volume as shown in Figure A.1. The process used for this mass balance was obtained from reference [31]. The assumptions used for the derivation of this equation are as follows.

1. The temperature of the system remains constant
2. The gaseous species at the inlet of the CPF remain constant
3. The reaction rate during PM oxidation remains constant
4. The PM concentration in the exhaust remains constant
5. The exhaust volumetric flow rate remains constant
6. The filtration efficiency of the CPF remains constant

Therefore the change in mass within the CPF over time is given by equation A1. With substitution of the appropriate variables, equation A1 becomes A2. Further simplification of the equation and separation of variables leads to equation A3.

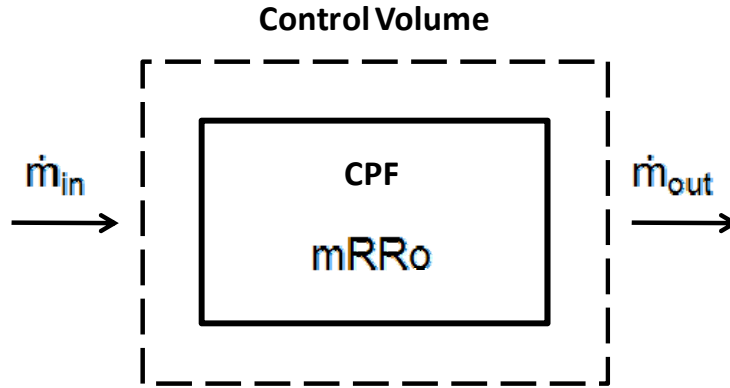


Figure A.1: Control Volume for CPF Mass Balance

$$\frac{dm}{dt} = \dot{m}_{in} - \dot{m}_{out} - m_{start} RRo \quad \mathbf{A1}$$

$\frac{dm}{dt}$ = Change in mass within the CPF over time (g/s)

\dot{m}_{in} = PM mass into the CPF (g/s) = $Q \cdot C_{in}$

Q = Volumetric flow rate (std. m^3/s)

C_{in} = PM concentration into CPF (mg/std. m^3)

\dot{m}_{out} = PM mass out of the CPF g/s = $Q \cdot C_{in} (1 - \eta_f)$

η_f = Filtration efficiency of the CPF

RRo = Prevalent reaction rate (1/s)

m_{start} = PM mass in CPF (g)

$m_{start} RRo$ = Oxidation of mass within the CPF

$$\frac{dm}{dt} = Q \cdot C_{in} - Q \cdot C_{in} (1 - \eta_f) - m_{start} RRo \quad \mathbf{A2}$$

$$\frac{dm}{dt} = Q \cdot C_{in} (1 - (1 - \eta_f)) - m_{start} RRo$$

$$\frac{dm}{dt} = Q \cdot C_{in} \eta_f - m_{start} RRo$$

$$\frac{1}{Q \cdot C_{in} (1 - (1 - \eta_f)) - m_{start} RRo} dm = dt \quad \mathbf{A3}$$

$$\int_{m_{\text{start}}}^{m_{\text{stop}}} \frac{1}{Q \cdot C_{\text{in}} (1 - (1 - \eta_f)) - m_{\text{start}} RR_o} dm = \int_0^t dt$$

Integration of equation A3 and simplification of the results yields equation A4

$$m_{\text{Stop}} = \frac{Q_{\text{exh}} \cdot C_{\text{in}} \cdot \eta_f}{RR_o \cdot 1000} \left[1 - e^{(-RR_o \cdot t_{\text{eff}})} \right] + m_{\text{Start}} \cdot e^{(-RR_o \cdot t_{\text{eff}})} \quad \mathbf{A4}$$

m_{stop} = The mass in the CPF at the end of time t (g)

t_{eff} : Time of passive oxidation, (s)

Appendix B. Engine Dynamometer Supplementary Data

This information was obtained directly from Dyne Systems (Jackson, WI)

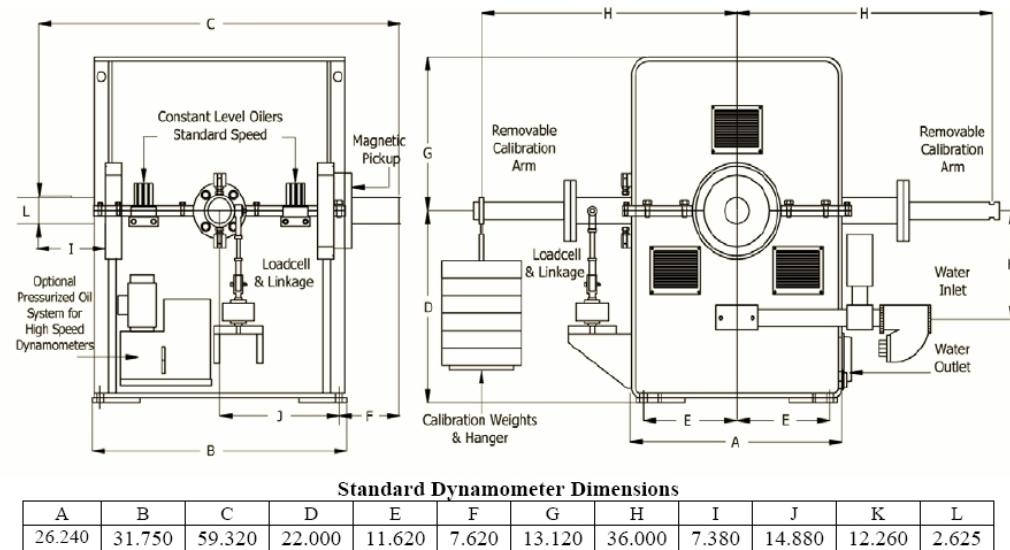


Figure B.1: Engine Dynamometer Dimensions (in.)

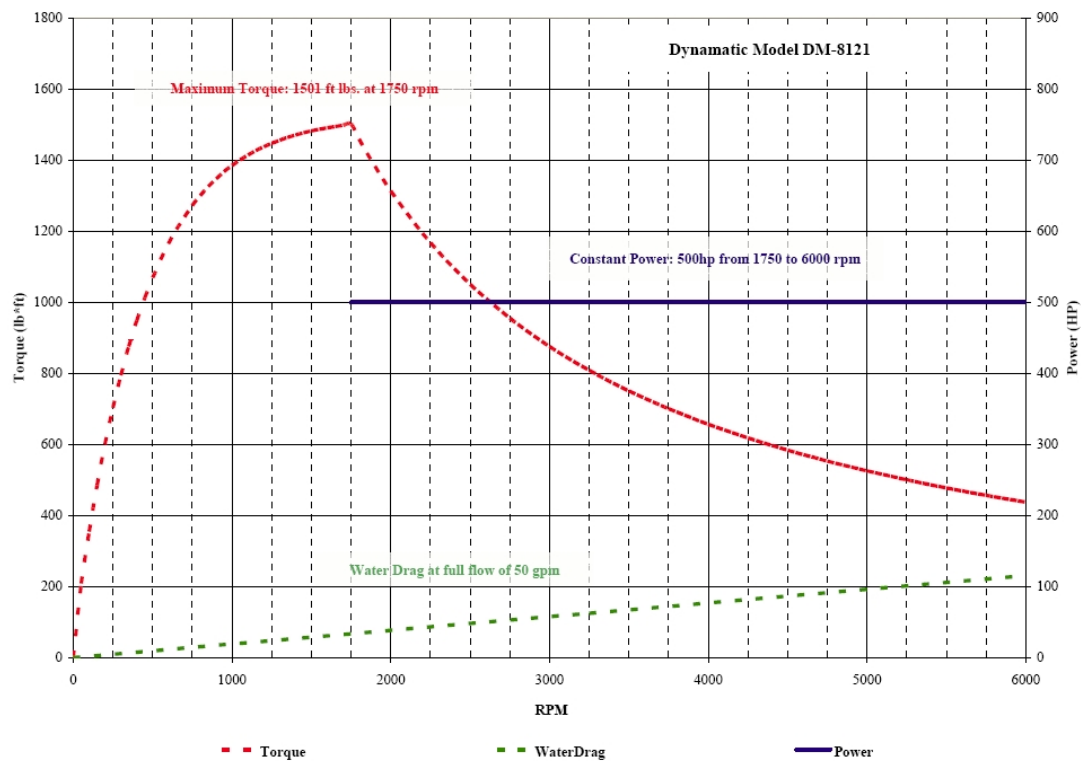


Figure B.2: Engine Dynamometer Torque (red) and Power Curve (blue)

Appendix C. Differential Pressure Transducer Calibration

Through the course of validating the engine and dynamometer installation, it was discovered that the flow rates being calculated through the use of the laminar flow element (LFE) were in error. This has been addressed by performing a calibration on the differential pressure sensor used for the LFE. This calibration occurred in stages, first concentrating on the sensor itself.

The differential pressure (DP) sensor was calibrated using a u-type manometer using a working fluid of distilled water. This was a simple calibration only using National Instruments Signal Express and the u-type manometer. The output of the program was a voltage with no scaling factors included. This voltage was used to determine the calibration factor for the sensor which was experimentally determined to be 1.001 mV/V. This is the identical value on the certification certificate dated 7/7/2003. Confident that the sensor itself was performing properly a calibration was performed through the current Labview program.

The results of the initial values from testing with the manometer are shown in Figure C.1. Three separate calibration runs were performed to determine if the calibration of the sensor through the program was correct, these runs are identified by the “(U)” within the legend. It was important to determine the repeatability of the technique, so the test was performed more three times. This initial information showed that the DP was reading approximately 18% high.

A second series of three tests were performed after adjusting the scaling factor within Labview, these data can be viewed in Figure C.1, identified by “(C)” in the legend. A linear regression was performed on the data obtained using the uncorrected and corrected scaling factor. The x-axis in the displayed graphs shows the manometer reading while the y-axis shows the value recorded by Labview. The liner interpolation is used to show how well the readings agree. It can be seen from these equations that the slopes differ between the data sets and that the corrected data now agrees within 1% of the manometer reading. Since there was such a large difference in the actual pressures

to the pressures displayed and recorded in the Labview program, it was decided to calibrate the two other DP sensors used in the test cell.

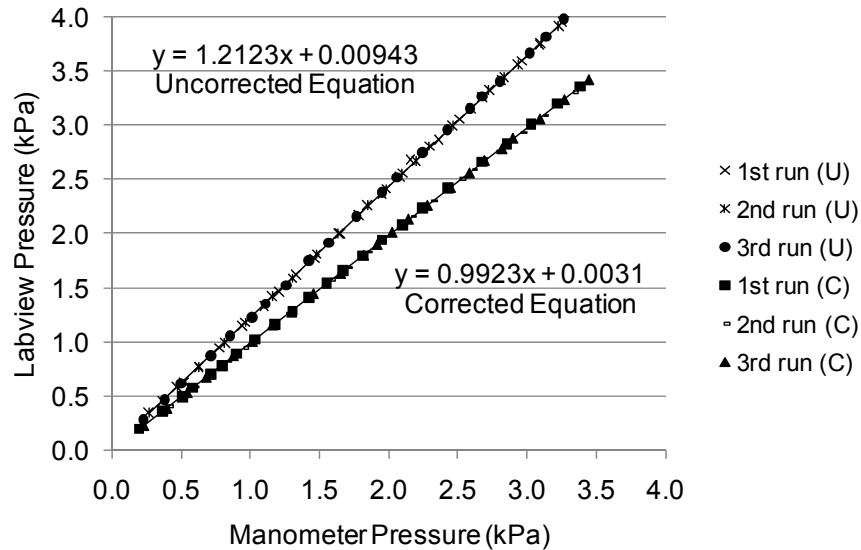


Figure C.1: Calibration of LFE Differential Pressure Transducer through Labview

A similar set of experiments were performed for the differential pressure sensors used on the CPF and DOC. Testing on the DP for the DOC used the same manometer for calibration but due to the larger values required for the DP of the CPF, a digital pressure gauge was chosen as the calibration device. This pressure gauge had a range of 0-207 kPa (0-30 psi) with a readability of 0.7 hPa (.01 psi). The data collected for the DP used on the CPF can be seen in Figure C.2. Again, linear regression was performed and it showed that the original scaling factor was producing values that were approximately 15% too high. Data were collected after the scaling factor was changed and the values produced by Labview now agree with 1% of the pressure gauge readings. Using the same method for the DP DOC demonstrated an initial reading that was approximately 17% too high. Corrected values now agree within 1%. The data gathered during the calibration procedure for the DP DOC can be seen in Figure C.3.

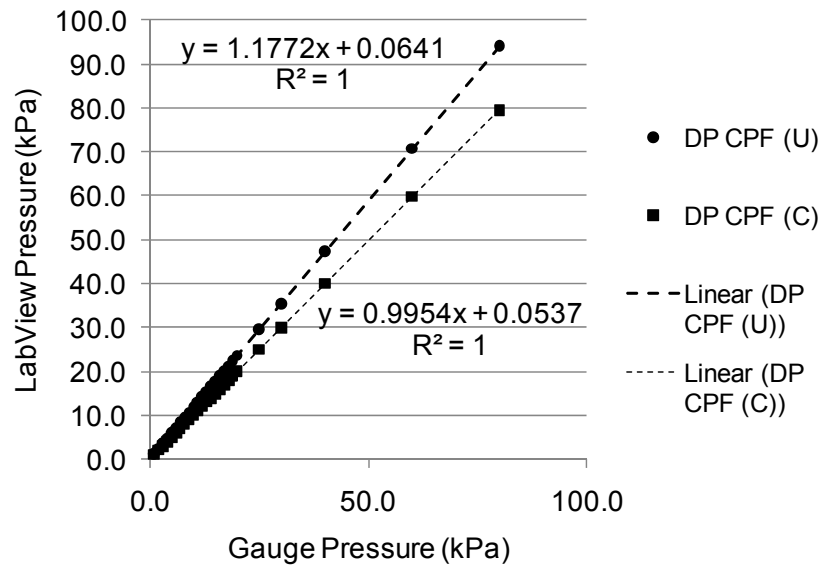


Figure C.2: Calibration of CPF Differential Pressure Transducer through Labview

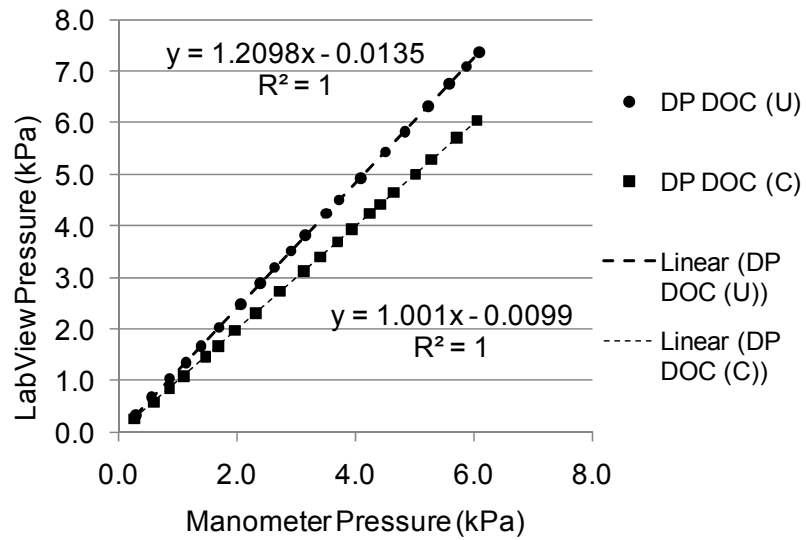


Figure C.3: Calibration of DOC Differential Pressure Transducer through Labview

The scaling factors and y-intercepts used within the current Labview program can be seen in Table C.1.

Table C.1: Differential Pressure Transducer Scaling Factors

Sensor	Range	Scale Factor	Y-intercept
DP across LFE	0.0-3.5 kPa	2823	0
DP across DOC	0.0-13.8 kPa	7613	0
DP across CPF	0.0-68.9 kPa	29109	0

Appendix D. Air Flow Calculations Using the Laminar Flow Element (LFE)

Formulas are provided by the Meriam Instruments (Cleveland, Ohio) operating manual for the LFE. Several of the formulas shown below are not used within the Labview program but were used in the development of the final three formulas used within the program. The formulas implemented within the program are the calculations used to determine actual volumetric flow rate for flowing humid air ($AVFR_{Wet}$), standard volumetric flow rate for flowing humid air ($SVFR_{Wet}$), and mass air flow rate ($m_{exhaust}$). The equations used for these calculations are D1, D2 and D3 respectively. Equations D1 and D2 are calculated in ft^3/min but need to be converted to m^3/s .

General Equation (Dry gas flow rate)

$$(B*DP)+(C*DP^2)=Flow$$

B = 127.151, calibration constant #1

C = -1.03714, calibration constant #2

DP= Differential Pressure Drop across the LFE (in. H_2O @ $4^\circ C$)

Actual Volumetric Flow Rate Equation for Flowing Dry Air (AVFR_{Dry}), ft³/min

$$AVFR_{Dry} = (B \cdot DP + C \cdot DP^2) \cdot \frac{\mu_{Std}}{\mu_{flow}}$$

μ_{Std} = 181.87 micropoise (viscosity as standard conditions)

Correction Factor for Air Temperature

$$\mu_{Flow} = \frac{14.58 \cdot (K)^2}{110.4 + (K)}$$

K = Temperature in Kelvin

$$\text{Correction Factor} = \left(\frac{529.67}{459.67 + ^\circ F} \right) \cdot \frac{181.87}{\left(\frac{14.58 \cdot (K)^2}{110.4 + (K)} \right)} = \frac{\mu_{Std}}{\mu_{Flow}}$$

Units for viscosity are Micropoise

$$AVFR_{Dry} = 127.151 \cdot DP - 1.03714 \cdot DP^2 \cdot \left[\left(\frac{529.67}{459.67 + ^\circ F} \right) \cdot \frac{181.87}{\left(\frac{14.58 \cdot (K)^2}{110.4 + (K)} \right)} \right]$$

Actual Volumetric Flow Rate Equation for Flowing Humid Air (AVFR_{Wet}), ft³/min

Correction factor for Viscosity When Flowing Wet Air

$$\mu_{\text{Flow (wet)}} = \frac{14.58 \cdot K^2}{110.4 + K} \cdot \frac{\mu_{\text{wet}}}{\mu_{\text{dry}}}$$

Where $\mu_{\text{wet}}/\mu_{\text{dry}}$ is obtained from Figure D1 below

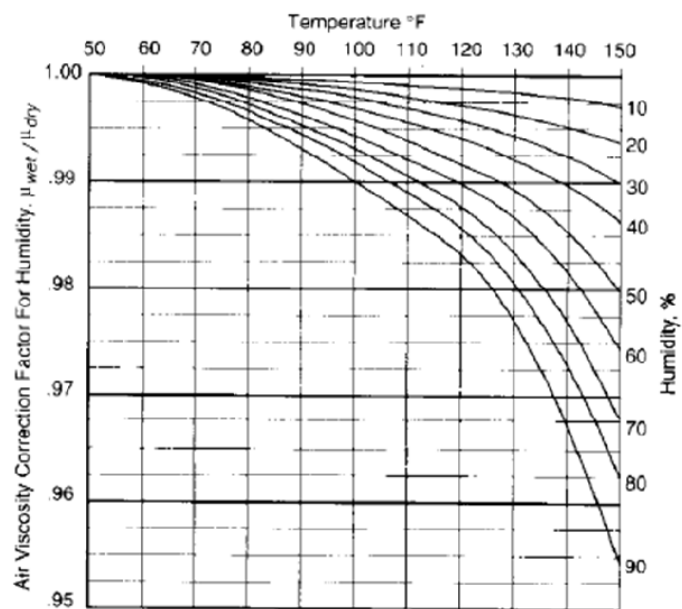


**Figure2: Relative humidity correction factor
for air viscosity. A-35500
Kestin & Whitelaw**

Figure D.1: Viscosity Correction Factor Plot

This provides for the correction factor below,

$$\text{Correction Factor} = \left(\frac{529.67}{459.67 + ^\circ\text{F}} \right) * \left[\frac{181.87}{\left(\frac{14.58 * (K)^2}{110.4 + (K)} * \frac{\mu_{\text{wet}}}{\mu_{\text{Dry}}} \right)} \right] = \frac{\mu_{\text{Std}}}{\mu_{\text{Flow(Wet)}}}$$

$$\text{AVFR}_{\text{Wet}} = (127.151 * \text{DP} - 1.03714 * \text{DP}^2) * \left(\frac{529.67}{459.67 + ^\circ\text{F}} \right) * \left[\frac{181.87}{\left(\frac{14.58 * (K)^2}{110.4 + (K)} * \frac{\mu_{\text{wet}}}{\mu_{\text{Dry}}} \right)} \right] \quad \mathbf{D1}$$

Standard Volumetric Flow Rate for Flowing Humid Air (SVFR_{Wet}), ft³/min

$$\text{SVFR}_{\text{Wet}} = (B * \text{DP} + C * \text{DP}^2) * \frac{\mu_{\text{Std}}}{\mu_{\text{Flow(wet)}}} * \frac{T_{\text{Std}}}{T_{\text{Flow}}} * \frac{P_{\text{Flow}}}{P_{\text{Std}}} * \frac{\rho_{\text{wet}}}{\rho_{\text{dry}}}$$

Where $\frac{\rho_{\text{wet}}}{\rho_{\text{dry}}}$ is obtained from Table D.1 below.

Table D.1: Density Correction Factor Table for Humid Air (Meriam Instruments Manual)

Temperature (deg F)	% Relative Humidity				
	20%	40%	60%	80%	100%
40	0.9993	0.9987	0.9981	0.9975	0.9969
50	0.9990	0.9981	0.9973	0.9964	0.9955
60	0.9986	0.9973	0.9960	0.9948	0.9934
70	0.9981	0.9962	0.9944	0.9925	0.9907
80	0.9974	0.9948	0.9922	0.9895	0.9870
90	0.9964	0.9928	0.9892	0.9855	0.9818
100	0.9951	0.9902	0.9854	0.9805	0.9756

$$SVFR_{Wet} = (127.151 \cdot DP - 1.03714 \cdot DP^2) \left(\frac{529.67}{459.67 + ^\circ F} \right) \left[\frac{181.87}{\left(\frac{14.58 \cdot (K)^2 + \mu_{Wet}}{110.4 + (K) \mu_{Dry}} \right)} \right] \left[\frac{T_{Std}}{T_{Flow}} \right] \left[\frac{P_{Flow}}{P_{Std}} \right] \left[\frac{\rho_{Wet}}{\rho_{dry}} \right] \quad \mathbf{D2}$$

Mass Air Flow Rate ($m_{Exhaust}$), kg/min

$$\text{Mass Flow Rate} = SVFR \cdot \rho_{Std} \quad \mathbf{D3}$$

$\rho_{Std} = 1.18537 \text{ kg/m}^3$ (density at standard conditions, 25°C and 101.325 kpa)

Conversion from cu. ft/min to cu m/sec

$$\frac{\text{ft}^3}{\text{min}} \cdot \frac{(12 \text{ in})^3}{(\text{ft})^3} \cdot \frac{(25.4 \text{ mm})^3}{(\text{in})^3} \cdot \frac{(\text{m})^3}{(1000 \text{ mm})^3} \cdot \frac{\text{min}}{60 \text{ sec}} = 0.000472 \frac{\text{m}^3}{\text{sec}}$$

Appendix E. Development of Particle Size Distribution Measurement Technique

A series of tests were performed on the 2002 Cummins ISM to investigate particle size distribution (PSD) of the PM exiting the CPF. This testing lead to the development of an improved technique for measuring the PSD during experiments. The first step was to replace the activated carbon used within the thermodenuder (TD) to ensure that this instrument was performing as designed. With the arrival of the new activated carbon that is used within the TD, testing was completed to see if there was a significant change in values recorded by the condensation particle counter (CPC) when compared with previous tests using the old carbon. The results from this test can be seen in Figure E.1. The graph shows an identical pattern for both tests and with similar magnitudes it can be concluded that the values gathered with the TD after it was repaired will be accurate even though the old carbon was being used.

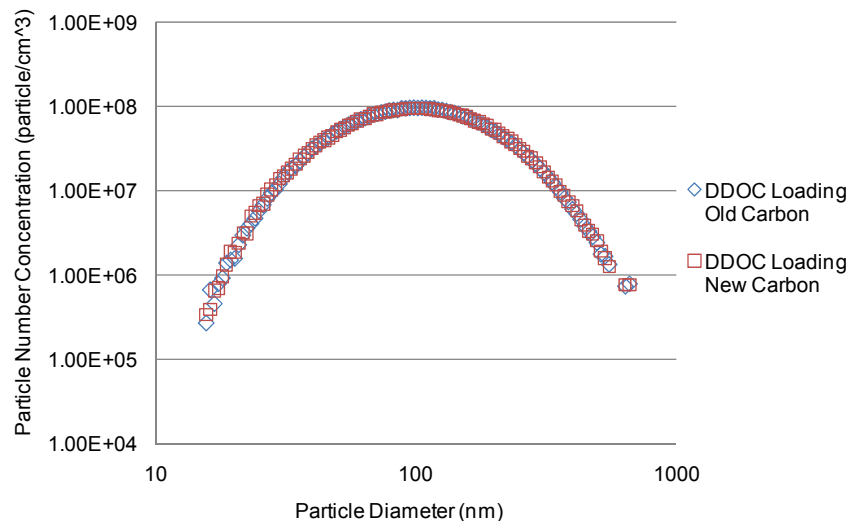


Figure E.1: Comparison of Old and New Carbon

Since the use of a dilution system is an important part of the process used for the measurement of PSD, testing was completed to ensure that reported dilution ratio of the

system was still within specifications. The gaseous emissions bench was used to record the CO₂ concentration of the exhaust gas while the engine was running at steady state without using the dilution system. After this value was recorded, the pressure regulator was adjusted on the dilution system and a second measurement was made of the exhaust gas while diluting the sample. The dilution ratio was then determined by taking a ratio of the two values.

To facilitate additional testing, a series of different dilution ratios were used in order to develop an equation relating the input pressure to the dilution ratio. Four pressures were used to vary the dilution ratio and the values used during this test sequence can be seen in Figure E.2. The corresponding dilution function generated by this information can be also seen in Figure E.2 and is the result of applying a liner trend line to the recorded data points which were acquired while sampling DDOC. To verify the accuracy of this function over time, periodic calibration checks should be done on the dilution system as it has been shown that as the components of the dilution system become dirty, the dilution ratio changes. Through additional testing it has been shown that the dilution ratio of the system changes dependent upon the sampling location in the aftertreatment system.

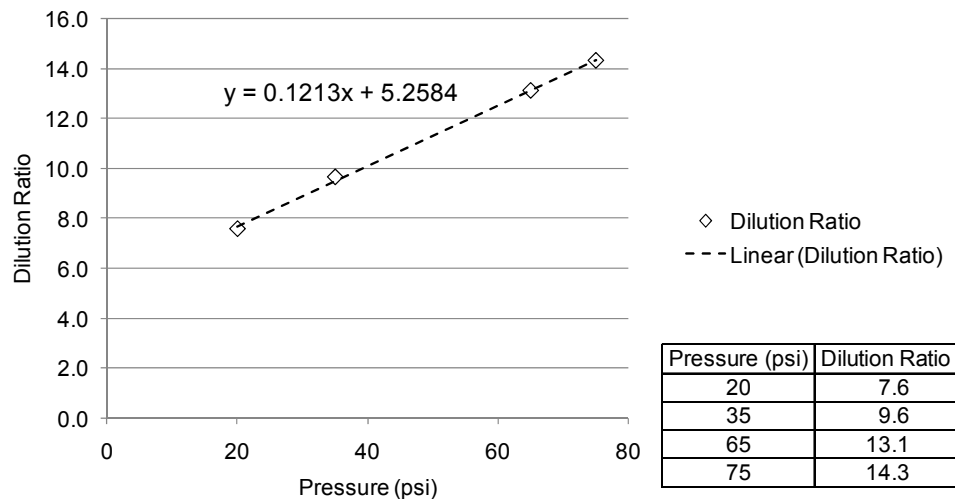


Figure E.2: Dilution Ratio Function

While maintaining a constant value of 35 psig for the compressed air used by the dilution system, additional testing was performed to quantify the change of dilution ratio based upon sampling location. Two different testing conditions were used during the experiment because it was hypothesized that it was the actual exhaust flow rate and pressure drop across the aftertreatment components which was the driving factor for the dilution ratio change and the not necessarily the sampling location.

The dilution ratio values gathered while using a 20% load (2100 rpm, 224 Nm) and 40% (2100 rpm, 448 Nm) on the 2002 ISM can be seen in Table E.1 and the data can be seen in graphical form in Figure E.3. In addition to the dilution ratio, the exhaust pressure and mass flow rate during the experiment were calculated and are also shown in Table E.1. From the comparison of the 20 and 40% load data, it can be seen that when the exhaust mass flow rate changes, the dilution ratio changes when remaining at the same sampling location. When looking at the magnitude of the dilution ratio changes, it can be observed that the largest change occurs DCPF. Since the outlet of the CPF is assumed to be at atmospheric pressure but in reality is held at a constant vacuum, approximately 3.5 in. H₂O, the driving factor for this change in dilution ratio must be the magnitude of the pressure drop across the various components of the aftertreatment system and the exhaust mass flow rate.

Table E.1: Dilution Ratios Based upon Sample Location

	20% Load Summary			40% Load Summary		
	Exhaust Flow (kg/min)	Pressure (kpa)	Dilution ratio —	Exhaust Flow (kg/min)	Pressure (kpa)	Dilution ratio —
UDOC	16.1	112.6	9.7	18.8	115.8	9.8
DDOC	16.1	110.7	10.0	18.8	113.6	10.1
DCPF	16.1	101.3	10.7	18.8	101.3	11.4

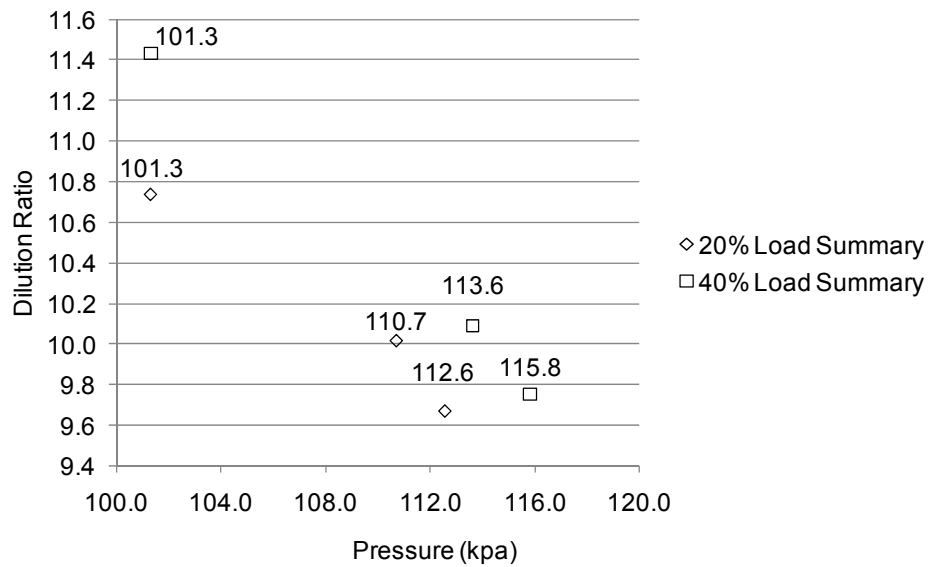


Figure E.3: Variation of Dilution Ratio Dependent upon Sampling Location

Since an exact correlation cannot be determined, the recommended procedure is as follows.

- Maintain the filtered compressed air used for the dilution system at one constant pressure.
- Use the method detailed above to determine the dilution ratio for each of the sampling locations to be used during testing. This will need to be performed at the engine speed and load conditions, along with filter loading if possible, which will be used during the actual test.
- After the actual test, post process the PSD data using the calculated dilution ratio from the method above using the formulas described below.

The dilution process itself also needs to be accounted for when evaluating the data recorded for PSD. An example of the dilution process can be seen in Figure E.4. The dilution ratio of 10:1 used in this example corresponds to a pressure of approximately 39 psig when sampling DDOC. The air used for dilution is conditioned before use by

removing moisture through the use of a desiccant system. Also two separate filters are used in series that remove debris down to a size of 5 μm and 10 nm respectively. The 10 nm filter also incorporates an oil removal feature.

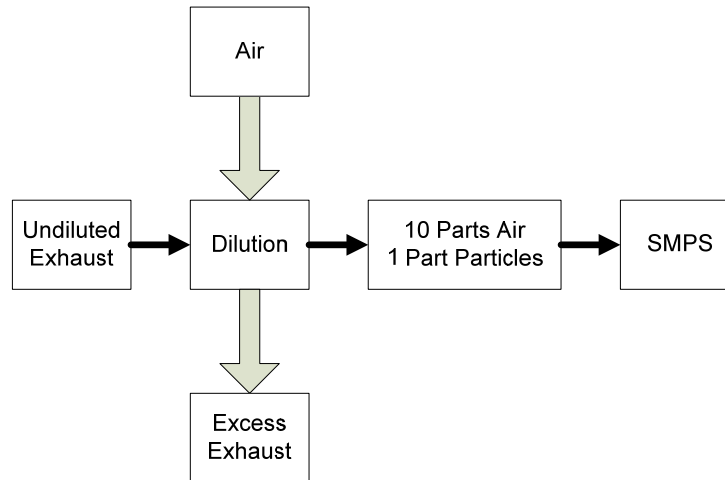


Figure E.4: Dilution Process

Since a sizable portion of the sample received by the CPC is compressed air, it was important to determine the number of particles contributed to the measurement from this source. Even though the dilution air is dried, heated, and filtered, the CPC displayed the PSD shown in Figure E.5. Although the specifications for the device indicate that it can detect particle quantities in the single digits, the distribution displayed could be due to approaching the lower limits of detection for the device. Regardless of the source, it is felt that these particles should be accounted for and a method was developed to correct for them.

In order to correct for the dilution ratio, the particles present within the compressed air and the experienced losses due to the use of the TD, the following procedure should be followed.

1. Correct the data recorded by the CPC to account for TD losses and background particles

2. Incorporate the dilution ratio to obtain accurate particle numbers, which is varies dependent upon sampling location, on samples that are obtained using the dilution system.

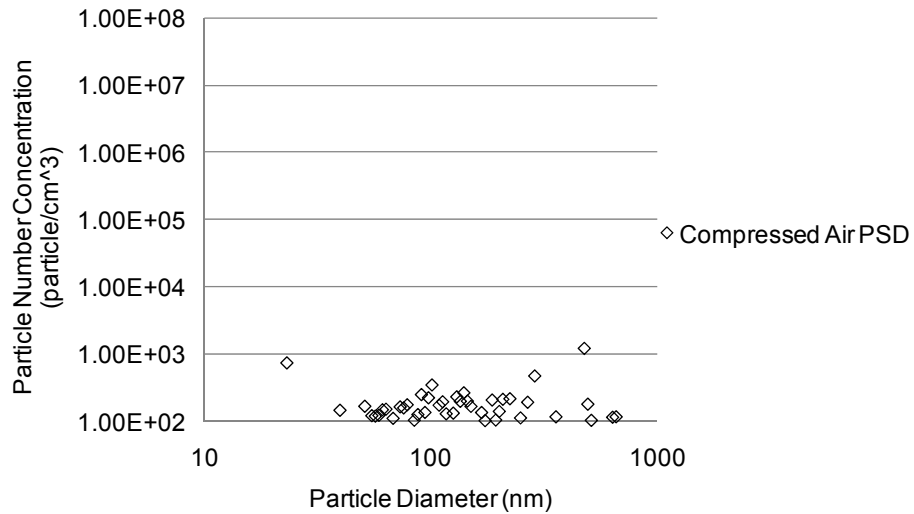


Figure E.5: Background Particles in the Compressed Air

To correct for dilution and TD losses requires the use of the formula below for non-diluted and diluted samples respectively.

For No Dilution

$$D_{cpc} = C_{Exhaust} - (C_{Exhaust} * T_{Loss})$$

$$C_{Exhaust} = \frac{D_{cpc}}{(1 - T_{Loss})}$$

E1

D_{cpc} = Displayed value on CPC counter

$C_{Exhaust}$ = Particle concentration in the exhaust, (particle/cm³ or nm³/cm³)

T_{Loss} = Thermodenuder losses in fraction form from eqn. C5, “.9 not 90%”

For Dilution

$$D_{cpc} = \left(\frac{1}{(D_R+1)} C_{Exhaust} + \frac{D_R}{(D_R+1)} C_{CA} \right) - \left(\frac{1}{(D_R+1)} C_{Exhaust} + \frac{D_R}{(D_R+1)} C_{CA} \right) * T_{Loss}$$

$$D_{cpc} = \left(\frac{1}{(D_R+1)} C_{Exhaust} + \frac{D_R}{(D_R+1)} C_{CA} \right) * [1 - T_{Loss}]$$

$$\frac{1}{(D_R+1)} C_{Exhaust} + \frac{D_R}{(D_R+1)} C_{CA} = \frac{D_{cpc}}{[1 - T_{Loss}]}$$

$$\frac{1}{(D_R+1)} C_{Exhaust} = \frac{D_{cpc}}{[1 - T_{Loss}]} - \frac{D_R}{(D_R+1)} C_{CA}$$

$$C_{Exhaust} = \frac{(D_R+1)D_{cpc}}{[1 - T_{Loss}]} - D_R C_{CA}$$

E2

C_{CA} = Concentration of particles in compressed air used for dilution,
(particle/cm³ or nm³/cm³)

D_R = Dilution Ratio

Through review of the previous recorded values when measuring PSD with and without the TD and through information gained while performing a literature review, it was determined that there are some losses attributed to using the TD. In reference [38], TD losses were determined by using a particle generator which created particles composed of NaCl. This is the ideal method for determining losses because the NaCl is non volatile and any reduction in particle concentration is due only to losses caused by the TD and not from absorption due to the activated carbon. At the time of testing no method was available to create particles of this nature so an alternate experimental procedure was developed.

After careful consideration it was determined to use dilution with and without the TD to determine a numerical value for the observed losses. Dilution can accomplish similar results to the TD if a high enough dilution ratio is used. Therefore it was hypothesized that by using dilution, most if not all of the particles removed by the TD would be absent when the sample reached the TD and only losses caused by the TD would be observed by the CPC. Sampling was performed to validate this theory.

An incorrect method for determining losses can be seen in Figure E.6. This method takes samples without dilution, with and without the TD. The difficulty when using this method is determining the actual losses caused by the TD. There is no specific way to differentiate between particle losses and particles adsorbed by the TD. This results in a significant error when performing loss calculations resulting in a value of 85.22%.

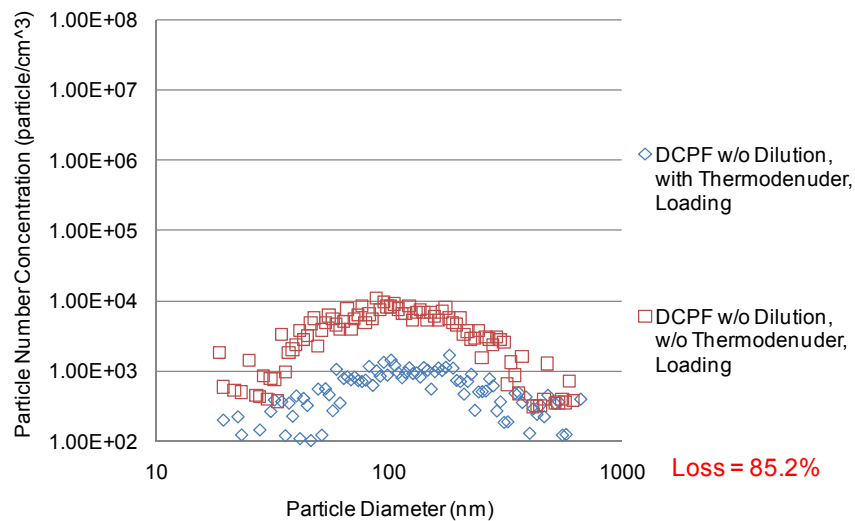


Figure E.6: Incorrect Method for Determining Thermodenuder Losses

A more correct method can be viewed in Figure E.7. This method allows for the removal of the volatile particles through dilution therefore allowing the determination of losses by using the CPC. While using a high dilution ratio, the majority of particles that are recorded at this point will be solid particles and will therefore allow for a good estimate of the losses. By using this method, the loss due to using the TD DCPF is 7.5%. This procedure was used for the other two sampling locations, upstream of the UDOC and downstream of the DDOC, which provided the calculated losses seen in Figure E.8 and Figure E.9 respectively.

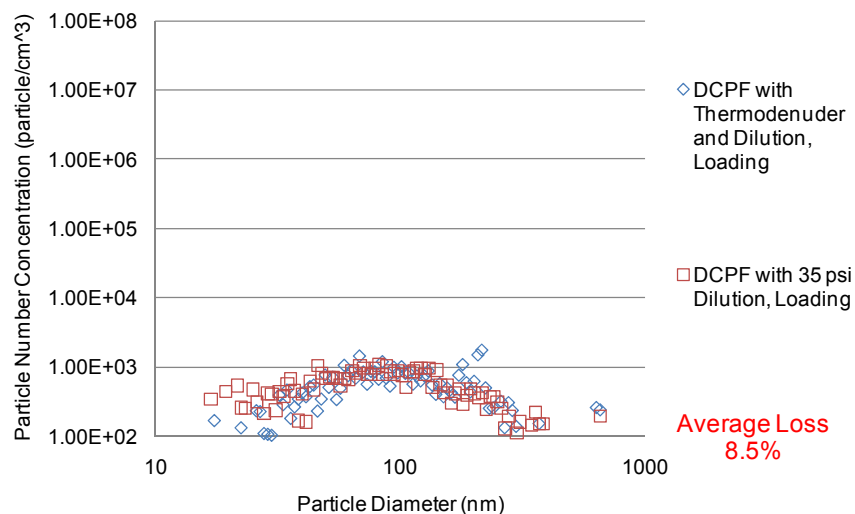


Figure E.7: Method for Determining Thermodenuder Losses DCPF, Not Compensating for Dilution Ratio

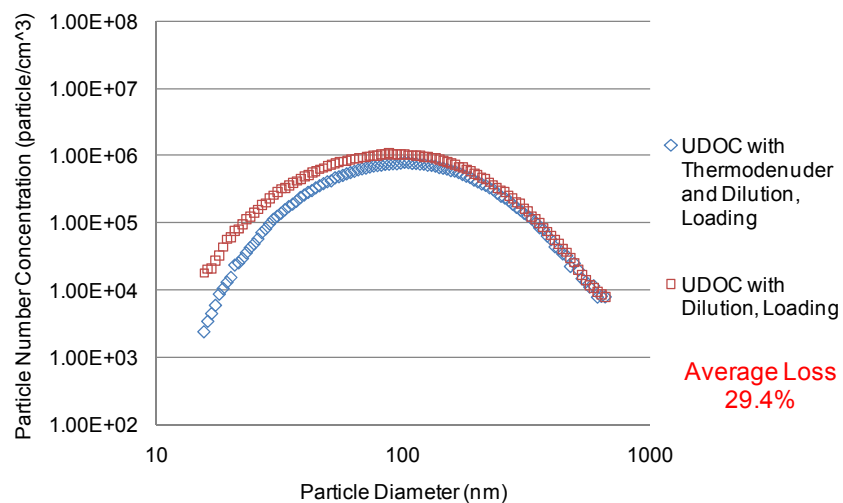


Figure E.8: Method for Determining Thermodenuder Losses UDOC, Not Compensating for Dilution Ratio

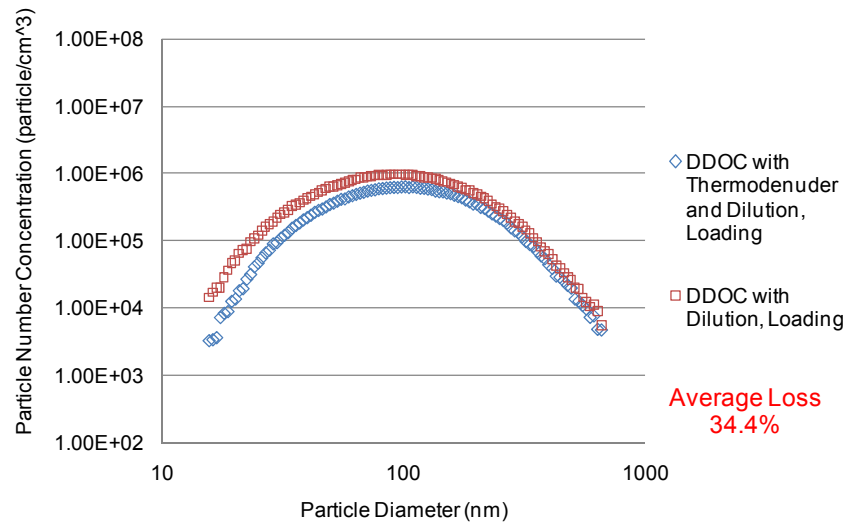


Figure E.9: Method for Determining Thermodenuder Losses DDOC, Not Compensating for Dilution Ratio

The mathematical formula used to calculate the losses in Figure D9 can be seen in equation E3.

$$\frac{A-B}{A} * 100 = \% \text{ Loss} \quad \mathbf{E3}$$

A = Sum of Particles DDOC with Dilution

B = Sum of Particles DDOC with Thermodenuder and Dilution

This method was also used at the other two sampling locations in determining the losses. Follow up testing revealed similar numbers for other tests. The values obtained downstream seem to be lower than documented experiments in the literature, so a further review of previous research was performed. A formula was developed by reference [38] to determine losses when using a TD. This formula was dependent on temperature of the TD and the specific diameter of the particle. This formula which can

be seen in equation E4 will be used to determine the losses experienced by the TD since it appears to be more consistent than the experimental losses calculated from previous tests. If a consistent method can be developed here by the researchers, equation E4 will be substituted by that method.

$$TP(\%) = a \cdot T(^{\circ}C) + b \cdot D(nm) + c \quad \text{E4}$$

$$T_{Loss} = 1 - TP \quad \text{E5}$$

TP= % of particles passing through thermodenuder

a = -0.0864 ($^{\circ}C^{-1}$)

b = 0.0108 (nm^{-1})

c = 91.9

D = diameter of the particle (nm)

T_{Loss} = Thermodenuder losses in fraction form. “.9 not 90%”

The total procedure for taking PSD measurements is as follows.

1. Prior to measuring PSD data, determine the experimental dilution ratios that are being used at each of the three sample locations, UDOC, DDOC and DCPF.
2. These dilution ratios should be measured while using the identical engine operating conditions that are to be used during the steady state testing.
3. Determine the concentration of particles in the compressed air (C_{CA}) used for the dilution system by measuring the size distribution within the air.

4. Record the PSD data during testing using the dilution system and thermodenuder at all sampling locations when measuring a “dry” sample. This method allows for consistent conditioning of the sample before measurement.
5. After the collection of raw data has been performed, the first step of post processing is accounting for losses created by the use of the thermodenuder using equation E4 and E5 [38].
6. Then finish post processing the data by taking into account the dilution ratio and number of particles contained in the compressed air, equation E2.

Appendix F. CPF Weighing Procedure

During different portions of the test, the CPF is removed from the aftertreatment system for weighing. The complete aftertreatment assembly is shown in Figure F.1. In order to allow for clear communication, the individual parts are listed below and are correlated by number listed on the picture.

1. Inlet Cone
2. Diesel Oxidation Catalyst (DOC)
3. Catalyzed Particulate Filter (CPF)
4. Exit Cone

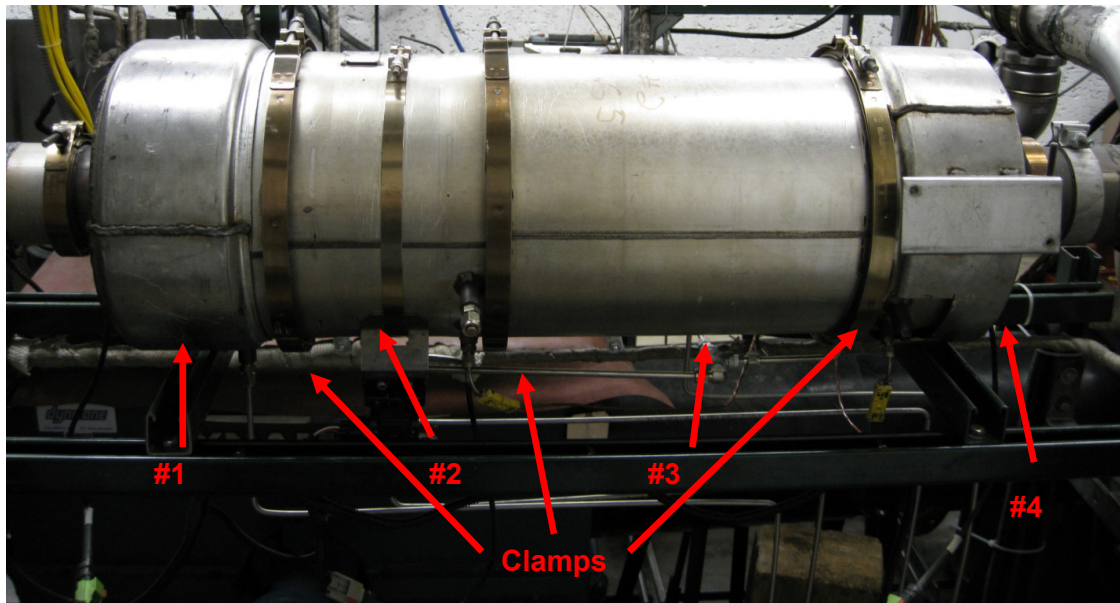


Figure F.1: Cummins 2007 ISL After-treatment System

Disassembly and weighing of the CPF takes place a minimum of three times for each of the passive oxidation tests. The filter and associated hardware are removed from the system hot, with surface temperatures up to and exceeding 300°C. The weighing is done at elevated temperatures for two main reasons. First, as the CPF cools there is the possibility that the CPF will gain mass due to moisture absorption from the ambient air. Second, it has been shown that the weighing procedure is a dynamic process with the

CPF appearing to gain mass as it cools due to the reduction of the buoyancy effect provided by the temperature of the filter. Therefore filter weighing takes place at similar temperatures during the different portions of the test. A detailed analysis investigating the variability of the mass measurement due to temperature variations is discussed in reference [33].

The weighing procedure is detailed below.

1. The entire after-treatment system, parts 1-4 in Figure F.1, are removed from the exhaust system fully assembled.
2. The system is lowered to the ground and rests on Part #4 which then puts the system in a vertical orientation.
3. The clamp between Part #2 and #3 is removed, the DOC and Inlet Cone are then removed as an assembly.
4. A steel cover is placed over the inlet of the CPF and fastened to the filter by the previously removed clamp.
5. The filter is then rotated to rest on the steel cover and the clamp between Part #3 and #4 is removed.
6. The exit cone is then removed and a separate steel cap is placed over the exit of the CPF. This cap is fastened to the filter by the previously removed clamp.
7. The filter is then brought to the scale and temperatures are recorded throughout the filter and caps.
8. The scale is zeroed prior to each mass measurement.
9. A calibration weight is measured to ensure scale accuracy.
10. The CPF is weighed three times, with the temperatures recorded throughout the CPF prior to the first weighing, an average of the mass measurements is then calculated.
11. It would be nice to specify a temperature that we follow every time, the actual temperature may vary from day to day somewhat based on ambient temperature. What I try to maintain consistent is the temperatures between weighings on the same test day. I try not to let the individual temperature measurements (at each

thermocouple) vary by more than ± 15 deg C. The actual separate T/C temperatures can be anywhere from 180 deg C to 290 deg C

12. The reassembly process is the reverse of the disassembly process.

Appendix G. Passive Oxidation Test Procedure

G.1 Loading Prediction Times

In order to be as efficient as possible, loading times were predicted for the passive oxidation testing using two different methods. The first method consisted of taking preliminary test data collected on the engine and using this information as input to the MTU 1-D CPF model. This method was used the primary reference for the first few tests and then was supplemented with the second method during subsequent testing. As was discussed in reference [33], a relationship exists between the PM concentration exiting the engine and the ambient test cell conditions. During testing on the ISL this phenomenon was experienced which allowed for the development of the second method to estimate CPF loading times during passive oxidation testing.

Prior to the start of the test, the test cell temperature, relative humidity and barometric pressure were recorded. These values were then used to calculate the absolute humidity of the test cell on that day. The calculated absolute humidity value was then compared with the humidity present in the test cell during previous tests. Once the closest match available was found, loading times from that test were used for the scheduled experiment. The formulas used to convert relative humidity to absolute humidity can be found in Appendix R. The calculated humidity values and a discussion of the correlation between absolute humidity and PM concentrations can be found in paragraph 4.2.

G.2 Engine Start Up

For the first start up of the day, the engine is started and brought to idle using SOP-S1 which can be found in Appendix S. This is performed through the test cell trapline which includes the engine exhaust and complete aftertreatment system. The engine is allowed

to idle for approximately one minute and then the engine load and speed are adjusted in steps to bring the engine up to operating temperature. The engine load, speed and times used for this incremental warm up are listed in Table G.1. The final warm up point is used until the DOC inlet temperature stabilizes to approximately $380^{\circ}\text{C} \pm 10^{\circ}\text{C}$.

Table G.1: Engine Speed and Load for Initial Engine Warm Up

Engine Speed	Engine Load	Time
(rpm)	(Nm)	(min)
750	0	1
1200	220	5
1800	220	5
2100	440	5
2100	840	5

G.3 Catalyzed Particulate Filter Clean Out

After the engine is brought up to 2100 rpm and 840 Nm, the DOC inlet temperature is allowed to stabilize to approximately 380°C . When the DOC inlet temperature stabilizes, the auxiliary fuel dosing injector shown in Figure 3.2 is turned on and the duty cycle of the injector is adjusted until a CPF inlet temperature of 600°C is reached. The CPF inlet temperature is allowed to stabilize for five minutes at 600°C and then a countdown timer is started. The clean out of the filter is performed for approximately 15 minutes ensuring that a constant pressure drop across the CPF is observed on the monitor. If 15 minutes passes and the pressure drop has not stabilized, the clean out of the filter is continued until a stable pressure drop is achieved.

G.4 Stage 1 Loading of the CPF

After it has been determined that the CPF is clean by monitoring the pressure drop profile, but before the dosing injector is turned off, the emissions analyzer bench is turned on and connected to the sample port downstream of the CPF (DCPF) shown in Figure 3.2. After this occurs, the dosing injector is turned off and the pressure drop profile across the CPF is allowed to stabilize. When this condition is reached, the engine speed and load are changed to allow for the specified DOC inlet temperature and exhaust mass flow rate. The DOC inlet temperature is maintained at $\pm 10^{\circ}\text{C}$ of the set point while the exhaust mass flow rate is kept at $\pm 5\%$ of the specified value for that day.

The engine is run at this speed and load setting for approximately 30 minutes. This is to allow the temperature of the CPF to stabilize. This temperature stabilization period is an important aspect of the weighing procedure. By weighing the CPF at a similar temperature during all portions of the test, the buoyancy effect that results from the thermal mass of the filter is maintained at a consistent level. This technique minimizes variability during CPF mass measurements.

While the engine is operating during Stage 1 loading, several measurements are performed and recorded. Gaseous emissions are collected from three locations, DCPF, downstream the DOC (DDOC) and upstream the DOC (UDOC). Each location is sampled for 10 minutes with five minutes being used to collect NO_x values and the remainder of the time being used to measure NO. The other gaseous emissions collected are HC, CO, CO_2 and O_2 . After sampling DCPF is completed, the sampling location is changed to DDOC. The last gaseous emission sampling location is UDOC. This strategy has been selected because it has been shown with the emissions bench at MTU, that sampling gaseous emissions at locations of high HC concentrations (UDOC or DDOC) and transitioning to a location of low concentration (DCPF) provides the opportunity for HC hang up in the sample lines and the FID. The result of this hang up is the incorrect measurement of HC concentrations.

One particulate matter (PM) concentration sample is collected UDOC for five minutes during Stage 1 loading along with the continuous monitoring of temperature, exhaust flow, fuel flow and pressure drops across the DOC and CPF. After 30 minutes of Stage 1 loading, the engine out exhaust is switched to the bypass line which diverts the exhaust flow around the aftertreatment system. The engine is then shut down and the aftertreatment assembly is disassembled to allow the weighing of the CPF which is explained in detail in Appendix F.

The weighing of the CPF provides for the mass measurement m_{stage1} which is used with $m_{\text{Ret-S1}}$ to determine the clean weight of the filter (m_c) using equation G1. The value $m_{\text{Ret-S1}}$ is obtained twice, once prior to the start of the experiment using preliminary test data. This value is used to predict the CPF PM loading during the test. After the test has been completed, the MTU 1-D model is then run a second time using the experimental gaseous and PM concentrations in order to provide a more accurate mass estimate to be used in the final mass balance.

$$m_c = m_{\text{stage1}} - m_{\text{Ret-S1}} \quad \textbf{G1}$$

m_c = Calculated clean weight of the CPF, [g]

m_{stage1} = Measured mass of the CPF after Stage 1 loading, [g]

$m_{\text{Ret-S1}}$ = MTU 1-D model predicted PM added during Stage 1 loading, [g]

G.5 Stage 2 Loading of the CPF

After the aftertreatment system is reassembled and installed in the exhaust system, the engine is started and brought to idle. A stepwise warm up strategy is used to allow the

engine to reach a steady state operating condition before the exhaust is switched back to the trapline. The engine operating conditions for this warm up are shown in Table G.2 with the times shown being approximate. Warm up is complete when a steady temperature is achieved at the exhaust manifold for the specified operating conditions.

Table G.2: Engine Speed and Load for Stage 2 Engine Warm Up

Engine Speed	Engine Load	Time
(rpm)	(Nm)	(min)
750	0	1
1200	195	5
1800	195	5
2100	195	5

Stage 2 loading takes place at the same engine operating conditions as Stage 1. Stage 2 loading is performed until nominal CPF loading of 2.2 ± 0.2 g/l is reached. The time required to reach this loading has been shown to vary based upon the engine out PM concentration. During Stage 2 loading, the same measurements are performed as in Stage 1 but on a more frequent basis. Five PM concentration measurements are performed UDOC along with one DCPF. Only one measurement is collected DCPF due to the amount of time required to collect a measurable amount of mass, 1 hr, compared to UDOC which only takes five minutes. The average of the UDOC PM concentrations and the single DCPF measurement are used to calculate steady state filtration efficiency. A detailed explanation of the filtration efficiency calculation can be found in [19].

The strategy for gaseous sampling is modified from Stage 1 with initial sampling occurring DDOC. This location was given first priority in order to facilitate the modeling effort as it was deemed important from a modeling perspective to record the CPF inlet concentrations during the start of Stage 2 loading. The second sampling location is DCPF with the final location being UDOC. Gaseous sampling is cycled through these locations during the test with the time at each location split equally dependent upon the length of the test. This sampling strategy is used for the remainder the experiment since

the analyzer hang-up which results from HC dosing during active regenerations is not present.

After a predetermined amount of loading time has passed, which is based upon the preliminary modeling predictions, the exhaust is diverted to the bypass line and the engine is shut down. The aftertreatment system is removed from the exhaust system and then disassembled for CPF weighing. The weighing of the CPF provides for the mass measurement m_{Load} which is used with m_c in equation G2 to determine the amount of PM mass deposited in the filter (m_{Ret-Ld}) and subsequently the CPF loading of the filter after Stage 2 has been completed.

$$m_{Ret-Ld} = m_{Load} - m_c \quad \mathbf{G2}$$

m_{Ret-Ld} = Calculated PM mass retained in the CPF at end of Stage 2 loading, [g]

m_{Load} = Measured mass of the CPF after a nominal CPF loading of 2.2 g/l is achieved at end of Stage 2, [g]

m_c = Calculated clean weight of the CPF, from eqn. G1, [g]

The PM loading of the filter is verified by using the value m_{Ret-Ld} , which is the mass of the accumulated PM in the filter, and dividing this mass value by the volume of the CPF. After verifying that the CPF loading of 2.2 ± 0.2 g/l has been achieved, the aftertreatment system is reassembled and reinstalled into the exhaust system. Time is critical in the weighing procedure at this stage of the test due to the high temperatures that are sometimes experienced during the PO portions of the test. An attempt is made to limit the amount of cool-down time experienced between Stage 2 and PO portions of the experiment to reduce the thermal shock that the filter experiences at the beginning of the PO stage of the test.

G.6 Passive Oxidation

In order to ensure steady-state operation, the engine is operated in a stepwise warm up procedure that is similar to Stage 2. The engine operating conditions that are used for the warm up procedure vary based upon the predetermined conditions for the test, but ensure that the engine is operating at a steady state before the PO portion of the test is initiated. After steady-state is confirmed by the exhaust manifold temperature, the engine exhaust is switched to the trapline which marks the beginning of the test. Collection of experimental data is performed in the same manner as Stage 2 except that no DCPF PM concentrations are collected due to the lack of time necessary to acquire the data.

In order to determine the amount of time that the engine is operated at PO conditions, preliminary modeling predictions are acquired through the use of the MTU 1-D CPF model. The time estimates provided by the modeling efforts are used as a first estimate, but the pressure drop profile across the CPF is monitored to provide a real time approximation of the PO of PM within the CPF. The time of the passive oxidation portion of the experiment is closely regulated to ensure that the CPF does not reach its balance point. When the system reaches the balance point, the rate of change of PM within the CPF is zero which prevents the calculation of an accurate reaction rate. After a predetermined amount of time or prior to the pressure drop profile across the CPF becoming horizontal, the PO portion of the experiment is halted and the transition is made to Stage 3 loading.

G.7 Stage 3 Loading of the CPF

After the determination has been made to stop the PO portion of the test, Stage 3 loading begins. The engine operating conditions are changed to the same values that were used within Stage 1 and Stage 2 loading. The collection of experimental data occurs in the same manner as the PO stage of the test with no PM concentration sampling being performed DCPF but one sample being collected UDOC. This portion of

the test is approximately 30 minutes long which allows the temperature of the CPF to stabilize to the values that were experienced in Stage 1 and Stage 2 loading. Weighing the CPF at this temperature allows for the best calculation of mass oxidized.

After 30 minutes of operation at Stage 1 loading conditions for Stage 3 operation, the exhaust is switched to the baseline bypassing the aftertreatment system. The engine is then brought to idle and shut down. The aftertreatment assembly is removed from the exhaust system and disassembled for mass measurement. The weighing of the CPF provides for the mass measurement m_{stage3} which is used with m_c in equation G3 to determine the remaining amount of PM mass in the filter ($m_{\text{Ret-s3}}$) and subsequently the PM loading of the filter after Stage 3 has been completed.

$$m_{\text{Ret-s3}} = m_{\text{stage3}} - m_c \quad \mathbf{G3}$$

$m_{\text{Ret-s3}}$ = Calculated PM mass retained in the CPF after Stage 3 loading, [g]

m_{stage3} = Measured mass of the CPF after Stage 3 loading, [g]

m_c = Calculated clean weight of the CPF, from eqn. G1, [g]

In order to determine the amount of mass present in the filter after the PO portion of the experiment, the MTU 1D CPF model is used to calculate the amount of PM mass that is added during Stage 3 (m_{s3}) which is used with equation G4 to determine the amount of PM present in the filter ($m_{\text{Ret-P.O.}}$) after the PO portion of the experiment. A detailed visual representation of the four main stages of the test can be seen in Figure G.1.

$$m_{\text{Ret-PO}} = m_{\text{Ret-s3}} - m_{\text{s3}}$$

G4

$m_{\text{Ret-PO}}$ = Calculated PM mass retained in the CPF after Passive Oxidation, [g]

$m_{\text{Ret-s3}}$ = Measured PM mass retained in the CPF after Stage 3 loading, [g]

m_{s3} = MTU 1-D model predicted PM mass added to the CPF during Stage 3 loading, [g]

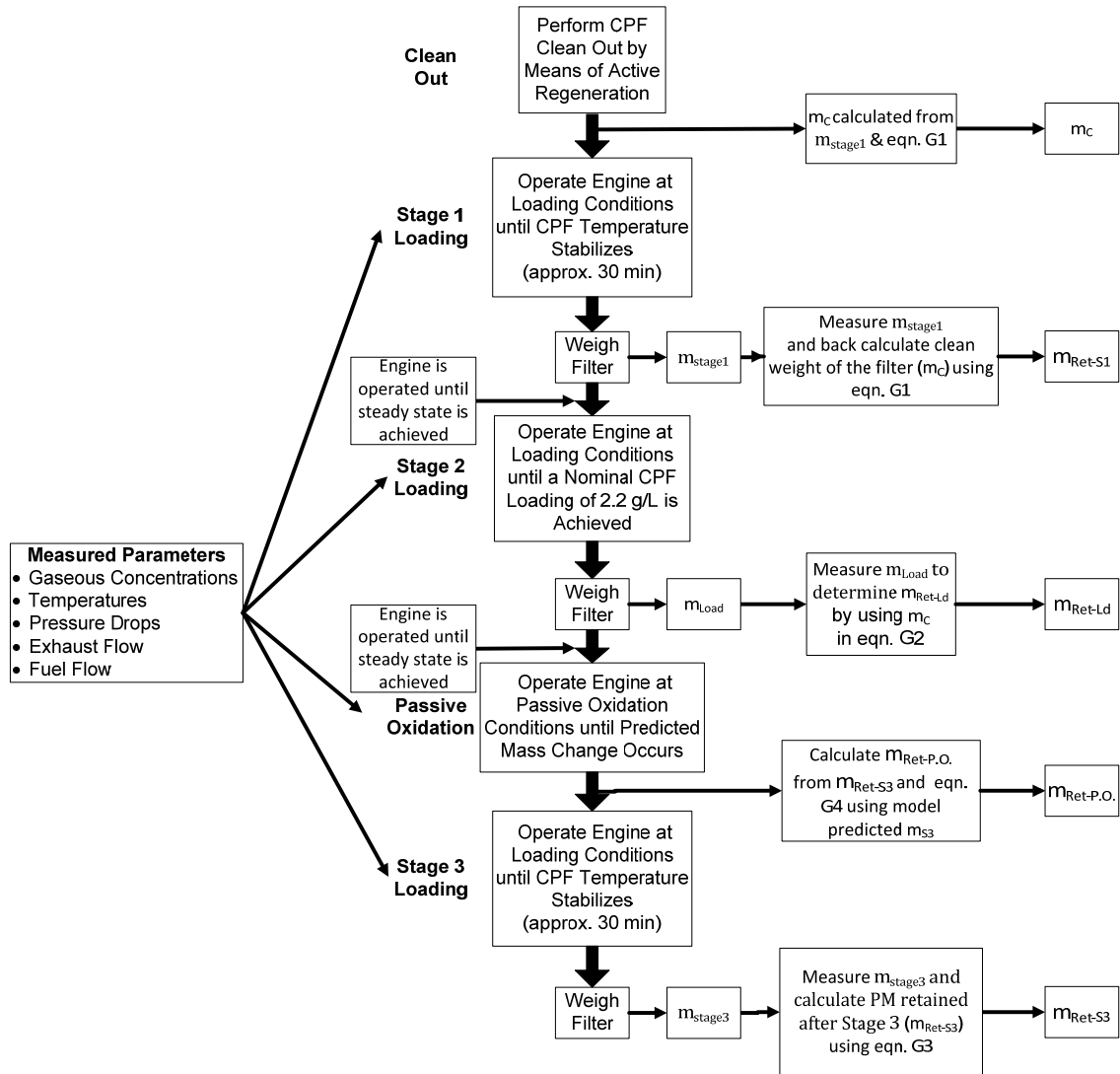


Figure G.1: Schematic Overview of Passive Oxidation Test Procedure

Appendix H. NO₂ Stoichiometric Reaction with Carbon

The stoichiometric reaction for gaseous NO₂ reacting with carbon is shown below in equation H1.



The left hand side of equation H1 when converting the moles to mass is shown by equation H2.

$$12 \text{ kg(C)} + 92 \text{ kg (NO}_2\text{)} \quad \text{H2}$$

The ratio of the mass is the shown below.

$$\frac{92 \text{ kg}}{12 \text{ kg}} = 7.67$$

The conversion of the concentration of NO₂ in ppm to mg is shown by equation H3.

$$C_{\text{NO}_2} * \rho_{\text{NO}_2, \text{Std}} * \frac{\text{m}^3}{(100 \text{ cm})^3} * \frac{1\text{E}^6 \text{mg}}{\text{kg}} = \text{mg NO}_2 \quad \text{H3}$$

C_{NO_2} = Concentration of NO₂ in ppm

$\rho_{\text{NO}_2, \text{Std}}$ = Density of NO₂ at standard conditions (25°C, 101.325 kPa) = 1.88 kg/m³

Appendix I. PM Concentrations

	Location	ISM					ISL				
		Test 1	Test 2	Test 3	Test 4	Test 5	Test 2	Test 1	Test 4	Test 5	Test 3
Stage 1	UDOC	13.8	16.2	14.0	16.2	-	17.0	18.8	17.9	16.2	18.5
Stage 2	UDOC	16.4	15.7	15.4	15.2	45.7	17.0	17.7	17.9	17.0	17.6
	UDOC	15.5	16.2	14.9	15.8	48.6	17.6	18.7	18.3	16.8	17.9
	UDOC	14.9	15.6	14.5	15.6	39.9	17.9	18.5	18.1	16.6	18.6
	UDOC	14.8	15.1	15.4	15.5	-	17.4	18.7	17.6	16.4	16.9
	UDOC	-	-	15.5	-	-	17.3	18.5	16.5	15.7	17.1
	UDOC	-	-	-	-	-	16.9	-	17.1	-	-
	DCPF	0.6	0.5	0.1	0.5	-	0.3	0.4	0.3	0.3	0.3
Passive Regeneration	UDOC	31.1	30.3	5.1	6.5	40.2	7.1	5.8	6.6	14.0	7.3
	UDOC	32.7	35.4	5.3	7.4	41.6	6.9	5.9	6.4	13.3	6.8
	UDOC	33.1	26.2	5.8	7.0	37.1	6.8	6.1	5.9	12.6	6.7
	UDOC	-	30.6	-	7.3	-	-	-	-	-	-
Stage 3	UDOC	15.4	15.2	12.2	16.1	-	16.8	16.6	16.0	16.0	16.2
Average Loading	UDOC	15.1	15.7	14.6	15.7	44.7	17.2	18.2	17.4	16.4	17.5
Std Dev	-	0.9	0.5	1.2	0.4	4.4	0.4	0.8	0.8	0.5	0.9
Average Passive Regeneration	UDOC	32.3	30.6	5.4	7.1	39.6	6.9	5.9	6.3	13.3	6.9
Std Dev	-	1.1	3.8	0.4	0.4	2.3	0.2	0.2	0.4	0.7	0.3
CPF Filtration Efficiency	-	96.2	96.7	99.1	97.0	-	98.1	97.8	98.2	98.1	98.1

* ISM Test 5 was performed as an extended loading

** Measurements in mg/scm

Appendix J. Additional Temperature Profiles

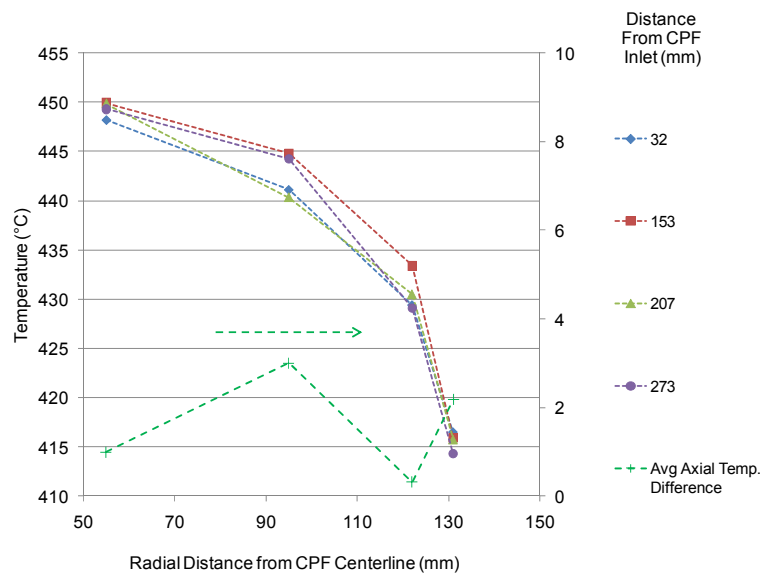


Figure J.1: Radial Temperature Profiles during Passive Oxidation for ISL Test 5

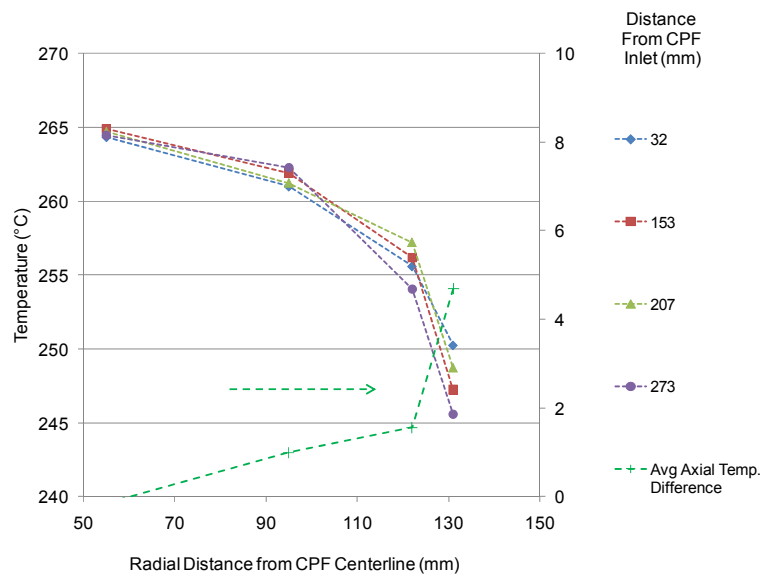


Figure J.2: Radial Temperature Profiles during Stage 2 for ISL Test 5

Appendix K. Gaseous Emissions Summary

ISM Test 1 Gaseous Emissions Summary

Stage 1							
	O2 (%)	CO2 (%)	CO (ppm)	NO (ppm)	NO2 (ppm)	NOx (ppm)	HC (ppm)
UDOC	13.64	4.99	101	169	23	192	87
DDOC	13.62	5.00	0	83	111	194	18
DCPF	13.70	4.97	0	48	142	190	3

Stage 2							
	O2 (%)	CO2 (%)	CO (ppm)	NO (ppm)	NO2 (ppm)	NOx (ppm)	HC (ppm)
UDOC	13.64	4.99	101	162	24	187	87
DDOC	13.62	5.00	0	101	91	191	18
DCPF	13.70	4.97	0	72	113	185	3

Stage 2-2							
	O2 (%)	CO2 (%)	CO (ppm)	NO (ppm)	NO2 (ppm)	NOx (ppm)	HC (ppm)
UDOC	13.63	5.00	98	167	24	191	85
DDOC	13.64	5.00	0	100	92	192	16
DCPF	13.69	4.96	0	81	107	188	1

Passive Oxidation							
	O2 (%)	CO2 (%)	CO (ppm)	NO (ppm)	NO2 (ppm)	NOx (ppm)	HC (ppm)
UDOC	9.63	7.97	128	210	10	220	97
DDOC	9.59	8.01	0	82	138	220	3
DCPF	9.81	7.86	0	93	122	215	0

Stage 3							
	O2 (%)	CO2 (%)	CO (ppm)	NO (ppm)	NO2 (ppm)	NOx (ppm)	HC (ppm)
UDOC	13.78	4.90	101	159	23	182	82
DDOC	13.71	4.95	0	99	87	186	13
DCPF	13.69	4.95	0	73	120	193	0

Note: NO and NO2 values from Semtech DS all other values are from Pierburg
Used Stage 2 emissions data (O2,CO2,CO and HC) for Stage 1
O2, CO2, and CO measured dry, NO, NO2, NOx, and HC measured wet

ISM Test 2 Gaseous Emissions Summary

Stage 1*							
	O2 (%)	CO2 (%)	CO (ppm)	NO (ppm)	NO2 (ppm)	NOx (ppm)	HC (ppm)
UDOC	14.04	4.98	101	169	23	192	80
DDOC	14.02	5.00	0	83	111	194	12
DCPF	14.10	4.94	0	48	142	190	3

Stage 2							
	O2 (%)	CO2 (%)	CO (ppm)	NO (ppm)	NO2 (ppm)	NOx (ppm)	HC (ppm)
UDOC	14.00	5.00	100	173	18	191	84
DDOC	13.99	5.02	0	105	88	192	16
DCPF	14.03	4.98	0	81	111	191	3

Passive Oxidation							
	O2 (%)	CO2 (%)	CO (ppm)	NO (ppm)	NO2 (ppm)	NOx (ppm)	HC (ppm)
UDOC	9.02	8.62	125	249	6	255	91
DDOC	9.00	8.65	0	133	112	245	3
DCPF	9.15	8.54	0	126	123	249	1

Stage 3							
	O2 (%)	CO2 (%)	CO (ppm)	NO (ppm)	NO2 (ppm)	NOx (ppm)	HC (ppm)
UDOC	13.94	5.00	103	167	23	190	85
DDOC	13.89	5.04	0	101	92	193	14
DCPF	13.86	5.05	0	81	123	203	1

Note: NO and NO2 values from Semtech DS all other values are from Pierburg

* Used Test #1 NO2 values due to inaccurate values during Test #2

O2, CO2, and CO measured dry, NO, NO2, NOx, and HC measured wet

ISM Test 3 Gaseous Emissions Summary							
--------------------------------------	--	--	--	--	--	--	--

Stage 1							
	O2 (%)	CO2 (%)	CO (ppm)	NO (ppm)	NO2 (ppm)	NOx (ppm)	HC (ppm)
UDOC	14.19	5.01	98	160	31	191	94
DDOC	14.11	5.06	0	77	121	198	25
DCPF	14.15	5.04	0	47	149	195	12

Stage 2							
	O2 (%)	CO2 (%)	CO (ppm)	NO (ppm)	NO2 (ppm)	NOx (ppm)	HC (ppm)
UDOC	14.24	4.98	100	155	31	186	95
DDOC	14.22	5.00	0	96	95	191	22
DCPF	14.28	4.98	0	72	117	189	5

Passive Oxidation							
	O2 (%)	CO2 (%)	CO (ppm)	NO (ppm)	NO2 (ppm)	NOx (ppm)	HC (ppm)
UDOC	8.75	8.96	49	456	7	463	61
DDOC	8.71	8.99	1	292	168	460	9
DCPF	8.73	8.98	0	289	172	460	3

Stage 3							
	O2 (%)	CO2 (%)	CO (ppm)	NO (ppm)	NO2 (ppm)	NOx (ppm)	HC (ppm)
UDOC	14.24	4.98	100	149	33	182	95
DDOC	14.22	5.00	0	75	104	179	22
DCPF	14.28	4.98	0	41	139	180	5

Note: NO and NO2 values from Semtech DS all other values are from Pierburg
Used Stage 2 emissions data (O2,CO2,CO and HC) for Stage 3
O2, CO2, and CO measured dry, NO, NO2, NOx, and HC measured wet

ISM Test 4 Gaseous Emissions Summary							
--------------------------------------	--	--	--	--	--	--	--

Stage 1							
	O2 (%)	CO2 (%)	CO (ppm)	NO (ppm)	NO2 (ppm)	NOx (ppm)	HC (ppm)
UDOC	14.02	5.02	102	156	28	184	87
DDOC	14.06	4.99	0	55	126	181	13
DCPF	14.02	5.02	0	50	137	187	2

Stage 2							
	O2 (%)	CO2 (%)	CO (ppm)	NO (ppm)	NO2 (ppm)	NOx (ppm)	HC (ppm)
UDOC	13.99	5.03	101	157	32	189	96
DDOC	13.97	5.05	0	93	99	193	20
DCPF	14.01	5.01	0	77	117	194	2

Passive Oxidation							
	O2 (%)	CO2 (%)	CO (ppm)	NO (ppm)	NO2 (ppm)	NOx (ppm)	HC (ppm)
UDOC	6.91	10.22	85	388	11	399	45
DDOC	6.95	10.18	0	324	86	411	5
DCPF	7.00	10.14	0	309	97	406	1

Stage 3							
	O2 (%)	CO2 (%)	CO (ppm)	NO (ppm)	NO2 (ppm)	NOx (ppm)	HC (ppm)
UDOC	14.01	5.00	103	154	31	185	84
DDOC	13.96	5.03	0	68	121	189	14
DCPF	13.98	5.01	0	41	144	185	0

Note: NO and NO2 values from Semtech DS all other values are from Pierburg
O2, CO2, and CO measured dry, NO, NO2, NOx, and HC measured wet

ISM Test 5 Gaseous Emissions Summary

Stage 1							
	O2 (%)	CO2 (%)	CO (ppm)	NO (ppm)	NO2 (ppm)	NOx (ppm)	HC (ppm)
UDOC	8.81	8.79	202	264	11	275	104
DDOC	8.75	8.84	0	122	152	274	7
DCPF	9.11	8.60	0	98	167	264	4

Stage 2							
	O2 (%)	CO2 (%)	CO (ppm)	NO (ppm)	NO2 (ppm)	NOx (ppm)	HC (ppm)
UDOC	8.77	8.80	160	276	6	282	94
DDOC	8.72	8.82	0	123	158	281	4
DCPF	8.88	8.70	0	132	146	278	1

Passive Oxidation							
	O2 (%)	CO2 (%)	CO (ppm)	NO (ppm)	NO2 (ppm)	NOx (ppm)	HC (ppm)
UDOC	8.86	8.78	151	280	9	290	91
DDOC	8.81	8.80	0	125	163	289	3
DCPF	8.99	8.67	0	135	149	284	0

Note: NO and NO2 values from Semtech DS all other values are from Pierburg
O2, CO2, and CO measured dry, NO, NO2, NOx, and HC measured wet

ISL 365 Test 2 Gaseous Emissions Summary
--

Stage 1							
	O2 (%)	CO2 (%)	CO (ppm)	NO (ppm)	NO2 (ppm)	NOx (ppm)	HC (ppm)
UDOC	13.91	5.16	147	54	31	86	116
DDOC	14.08	5.05	0	45	36	80	22
DCPF	14.04	5.07	0	25	55	80	18

Stage 2-01							
	O2 (%)	CO2 (%)	CO (ppm)	NO (ppm)	NO2 (ppm)	NOx (ppm)	HC (ppm)
UDOC	13.82	5.12	139	57	32	88	102
DDOC	13.83	5.12	0	51	34	85	27
DCPF	13.92	5.04	0	31	51	82	7

Stage 2-01							
	O2 (%)	CO2 (%)	CO (ppm)	NO (ppm)	NO2 (ppm)	NOx (ppm)	HC (ppm)
UDOC	13.77	5.18	133	60	29	89	99
DDOC	13.93	5.09	0	51	34	85	24
DCPF	13.95	5.06	0	31	51	82	5

Passive Oxidation							
	O2 (%)	CO2 (%)	CO (ppm)	NO (ppm)	NO2 (ppm)	NOx (ppm)	HC (ppm)
UDOC	9.17	8.54	61	191	16	207	67
DDOC	9.17	8.55	0	88	117	206	8
DCPF	9.28	8.46	0	91	111	202	3

Stage 3							
	O2 (%)	CO2 (%)	CO (ppm)	NO (ppm)	NO2 (ppm)	NOx (ppm)	HC (ppm)
UDOC	13.78	5.14	134	56	30	86	95
DDOC	13.75	5.15	0	42	41	83	20
DCPF	13.87	5.07	0	28	53	81	4

Note: O2, CO2, and CO measured dry, NO, NO2, NOx, and HC measured wet

ISL 365 Test 1 Gaseous Emissions Summary
--

Stage 1							
	O2 (%)	CO2 (%)	CO (ppm)	NO (ppm)	NO2 (ppm)	NOx (ppm)	HC (ppm)
UDOC	13.85	5.08	147	51	26	77	99
DDOC	13.87	5.08	0	44	31	75	15
DCPF	14.02	4.98	0	22	46	69	0

Stage 2							
	O2 (%)	CO2 (%)	CO (ppm)	NO (ppm)	NO2 (ppm)	NOx (ppm)	HC (ppm)
UDOC	13.79	5.12	139	55	27	82	93
DDOC	13.82	5.10	0	49	30	79	17
DCPF	13.91	5.03	0	30	46	76	0

Passive Oxidation							
	O2 (%)	CO2 (%)	CO (ppm)	NO (ppm)	NO2 (ppm)	NOx (ppm)	HC (ppm)
UDOC	12.68	5.86	72	246	38	284	88
DDOC	12.73	5.84	0	132	151	283	4
DCPF	12.79	5.79	0	102	175	277	0

Stage 3							
	O2 (%)	CO2 (%)	CO (ppm)	NO (ppm)	NO2 (ppm)	NOx (ppm)	HC (ppm)
UDOC	13.65	5.10	129	60	30	90	88
DDOC	13.54	5.19	0	56	30	86	15
DCPF	13.80	4.99	0	35	47	82	0

Note: O2, CO2, and CO measured dry, NO, NO2, NOx, and HC measured wet

ISL 365 Test 4 Emissions Summary

Stage 1							
	O2 (%)	CO2 (%)	CO (ppm)	NO (ppm)	NO2 (ppm)	NOx (ppm)	HC (ppm)
UDOC	13.97	5.10	146	53	28	81	105
DDOC	14.02	5.07	0	48	32	80	22
DCPF	14.20	4.94	0	24	49	73	3

Stage 2							
	O2 (%)	CO2 (%)	CO (ppm)	NO (ppm)	NO2 (ppm)	NOx (ppm)	HC (ppm)
UDOC	13.93	5.06	134	54	29	83	95
DDOC	13.96	5.06	0	50	30	80	18
DCPF	14.06	4.97	0	30	47	77	1

Passive Oxidation							
	O2 (%)	CO2 (%)	CO (ppm)	NO (ppm)	NO2 (ppm)	NOx (ppm)	HC (ppm)
UDOC	7.46	9.77	62	184	21	204	31
DDOC	7.51	9.77	0	127	73	200	2
DCPF	7.80	9.53	0	116	71	187	0

Stage 3							
	O2 (%)	CO2 (%)	CO (ppm)	NO (ppm)	NO2 (ppm)	NOx (ppm)	HC (ppm)
UDOC	14.00	4.98	137	51	29	80	93
DDOC	14.02	4.97	0	43	35	78	13
DCPF	14.10	4.91	0	26	49	76	0

Note: O2, CO2, and CO measured dry, NO, NO2, NOx, and HC measured wet

ISL 365 Test 5 Emissions Summary

Stage 1							
	O2 (%)	CO2 (%)	CO (ppm)	NO (ppm)	NO2 (ppm)	NOx (ppm)	HC (ppm)
UDOC	13.85	5.06	133	62	29	92	109
DDOC	13.85	5.07	0	51	40	90	16
DCPF	13.95	5.00	0	29	56	85	0

Stage 2							
	O2 (%)	CO2 (%)	CO (ppm)	NO (ppm)	NO2 (ppm)	NOx (ppm)	HC (ppm)
UDOC	13.80	5.06	125	67	29	96	82
DDOC	13.85	5.04	0	60	32	93	15
DCPF	13.87	5.01	0	38	53	90	0

Passive Oxidation							
	O2 (%)	CO2 (%)	CO (ppm)	NO (ppm)	NO2 (ppm)	NOx (ppm)	HC (ppm)
UDOC	6.03	10.73	82	164	18	181	14
DDOC	6.01	10.78	0	129	45	174	0
DCPF	6.27	10.55	0	116	54	170	0

Stage 3							
	O2 (%)	CO2 (%)	CO (ppm)	NO (ppm)	NO2 (ppm)	NOx (ppm)	HC (ppm)
UDOC	13.93	4.97	134	58	30	87	82
DDOC	13.95	4.95	0	47	37	84	4
DCPF	13.91	4.97	0	30	53	83	0

Note: O2, CO2, and CO measured dry, NO, NO2, NOx, and HC measured wet

ISL 365 Test 3 Emissions Summary

Stage 1							
	O2 (%)	CO2 (%)	CO (ppm)	NO (ppm)	NO2 (ppm)	NOx (ppm)	HC (ppm)
UDOC	13.77	5.21	139	59	21	80	106
DDOC	13.74	5.24	0	52	27	79	30
DCPF	13.76	5.19	0	28	47	75	3

Stage 2							
	O2 (%)	CO2 (%)	CO (ppm)	NO (ppm)	NO2 (ppm)	NOx (ppm)	HC (ppm)
UDOC	13.78	5.26	133	62	24	86	91
DDOC	13.80	5.26	0	53	30	83	19
DCPF	13.76	5.28	0	35	45	81	1

Passive Oxidation							
	O2 (%)	CO2 (%)	CO (ppm)	NO (ppm)	NO2 (ppm)	NOx (ppm)	HC (ppm)
UDOC	8.80	8.89	60	213	15	228	62
DDOC	8.76	8.93	0	107	116	223	2
DCPF	8.79	8.91	0	111	109	219	0

Stage 3							
	O2 (%)	CO2 (%)	CO (ppm)	NO (ppm)	NO2 (ppm)	NOx (ppm)	HC (ppm)
UDOC	13.73	5.34	128	64	25	89	84
DDOC	13.57	5.46	0	47	43	90	11
DCPF	13.61	5.42	0	33	55	89	0

Note: O2, CO2, and CO measured dry, NO, NO2, NOx, and HC measured wet

Appendix L. DOC NO to NO₂ Conversion Efficiencies

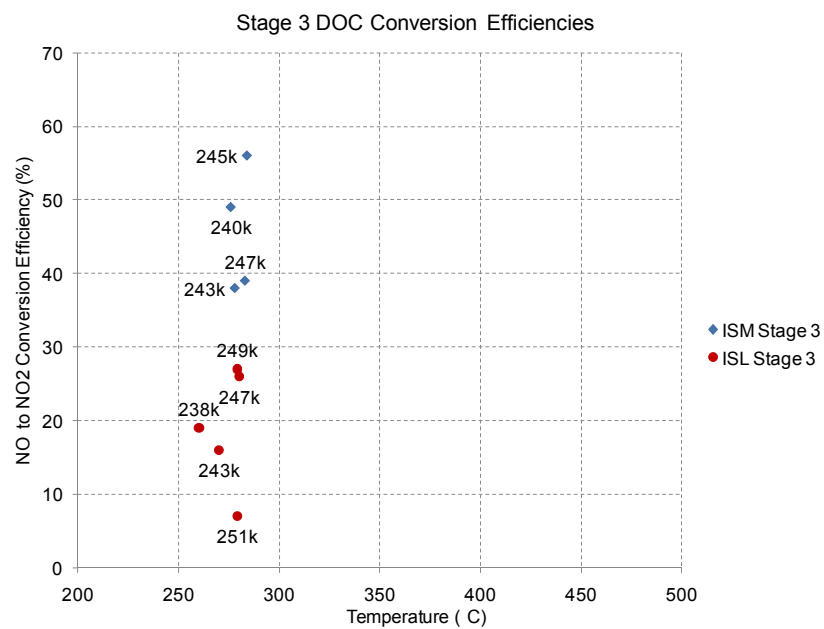
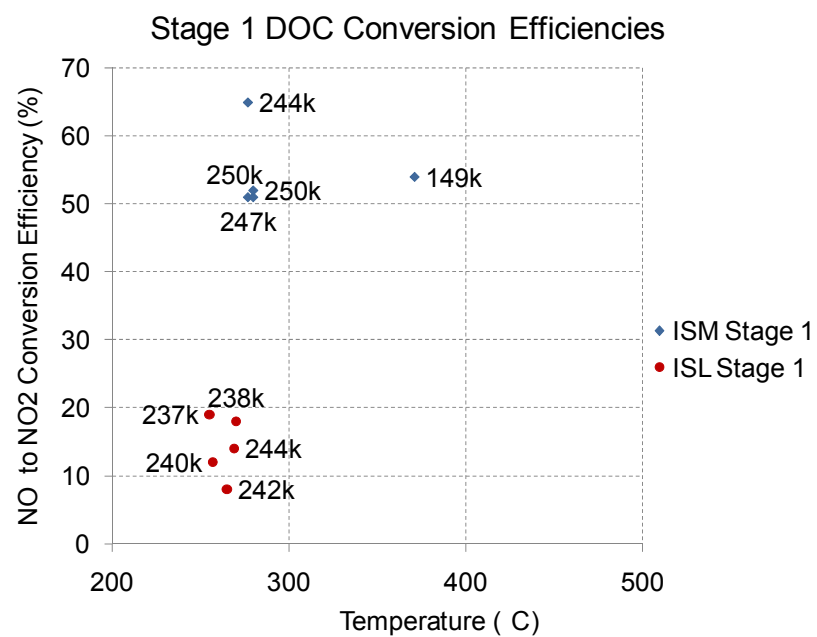


Table L.1: Tabulated DOC NO to NO₂ Conversion Efficiencies

	ISM Stage 1		
	DOC Inlet Temp.	NO to NO ₂ Eff	DOC Space Velocity
	°C	%	1/h
Test 1	277	51	247k
Test 2	280	51	250k
Test 3	280	52	250k
Test 4	277	65	244k
Test 5	371	54	149k

	ISL Stage 1		
	DOC Inlet Temp.	NO to NO ₂ Eff	DOC Space Velocity
	°C	%	1/h
Test 2	270	18	238k
Test 1	269	14	244k
Test 4	265	8	242k
Test 5	255	19	237k
Test 3	257	12	240k

	ISM Stage 2		
	DOC Inlet Temp.	NO to NO ₂ Eff	DOC Space Velocity
	°C	%	1/h
Test 1	276	39	244k
Test 2	277	39	246k
Test 3	275	38	241k
Test 4	276	41	236k
Test 5	373	56	149k

	ISL Stage 2		
	DOC Inlet Temp.	NO to NO ₂ Eff	DOC Space Velocity
	°C	%	1/h
Test 2	271	13	243k
Test 1	273	10	247k
Test 4	269	8	241k
Test 5	258	10	237k
Test 3	263	14	241k

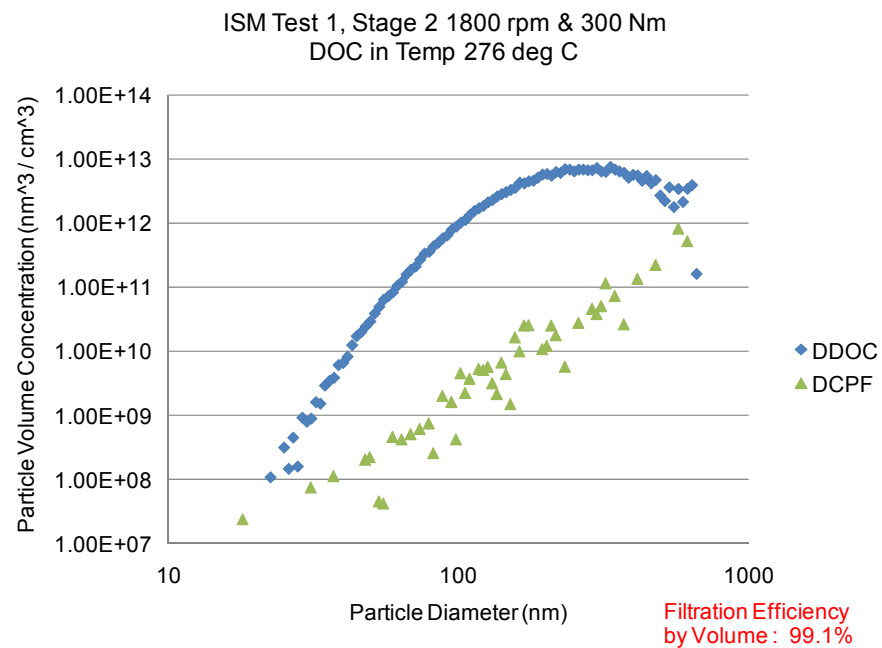
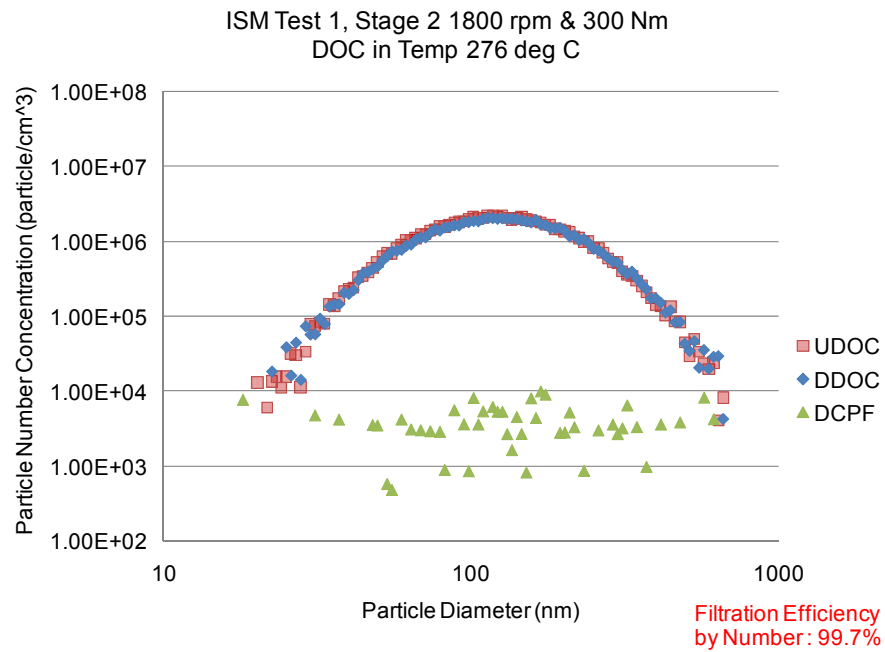
	ISM P.O.		
	DOC Inlet Temp.	NO to NO ₂ Eff	DOC Space Velocity
	°C	%	1/h
Test 1	346	61	146k
Test 2	369	47	151k
Test 3	424	36	340k
Test 4	479	16	423k
Test 5	375	55	149k

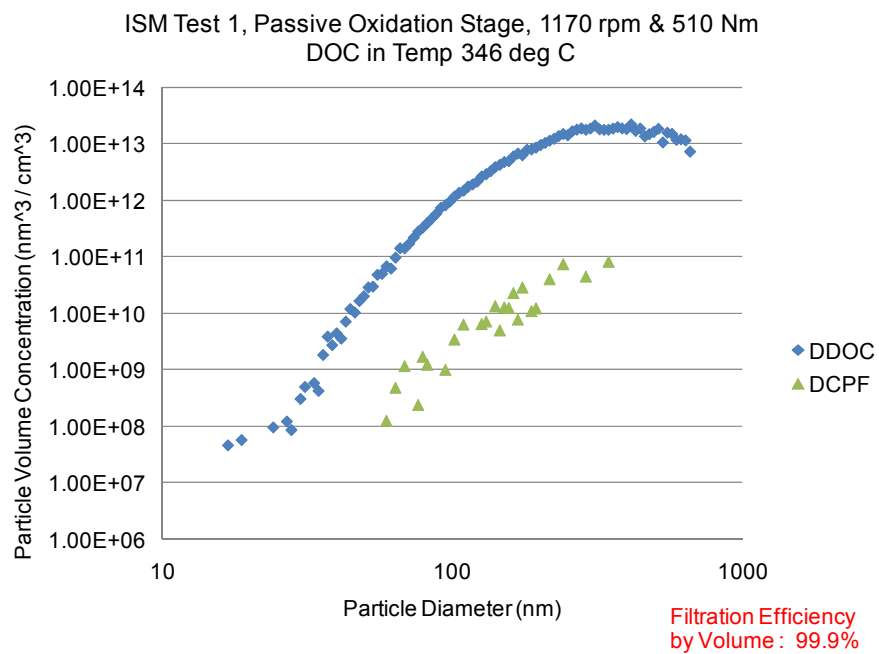
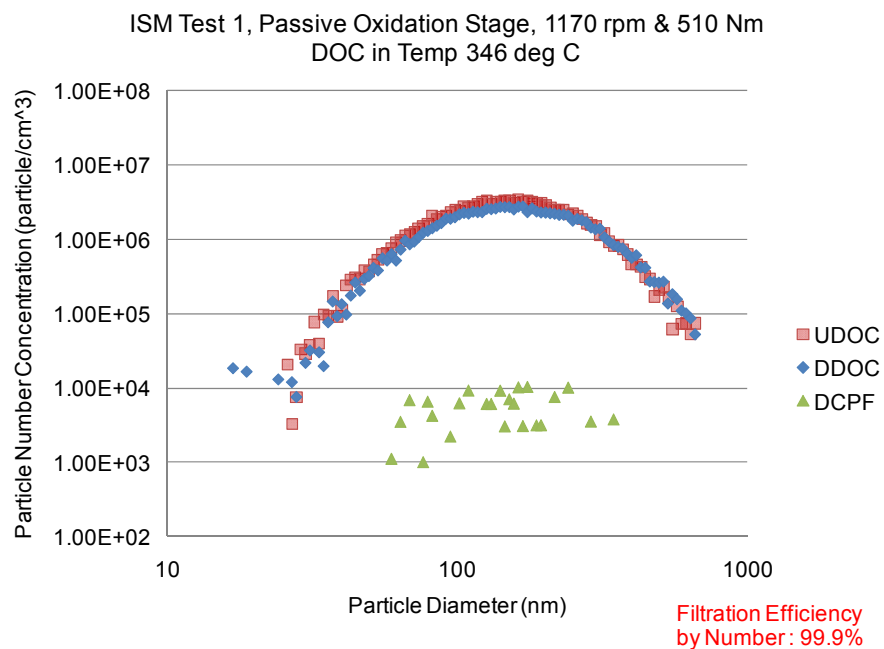
	ISL P.O.		
	DOC Inlet Temp.	NO to NO ₂ Eff	DOC Space Velocity
	°C	%	1/h
Test 2	372	54	171k
Test 1	263	46	104k
Test 4	420	31	346k
Test 5	434	21	414k
Test 3	361	50	168k

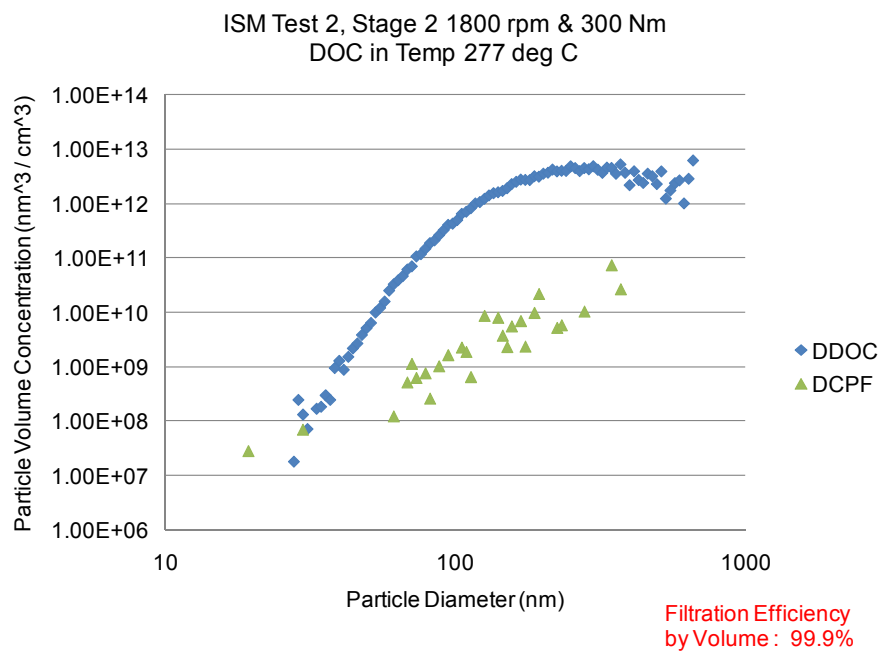
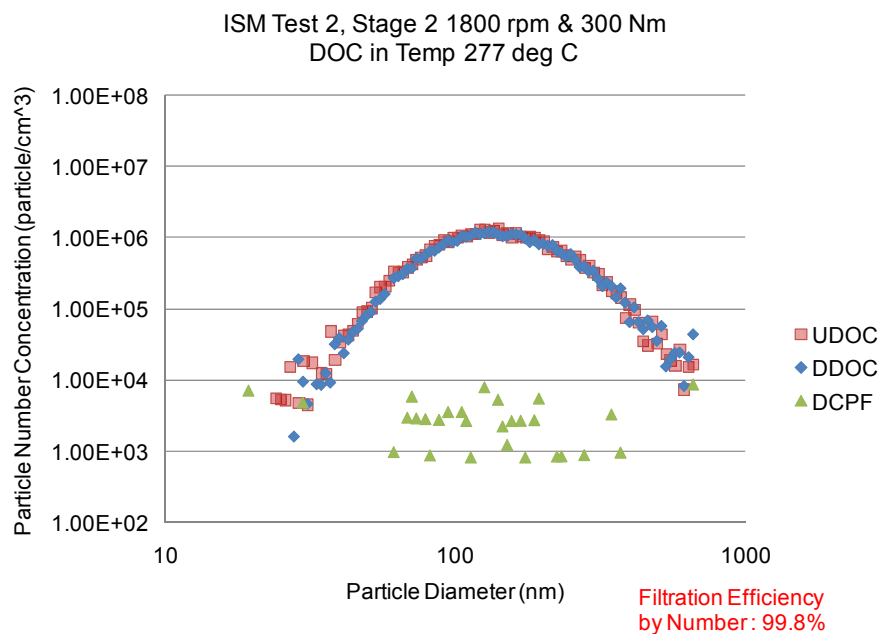
	ISM Stage 3		
	DOC Inlet Temp.	NO to NO ₂ Eff	DOC Space Velocity
	°C	%	1/h
Test 1	278	38	243k
Test 2	283	39	247k
Test 3	276	49	240k
Test 4	284	56	245k
Test 5	N/A	N/A	N/A

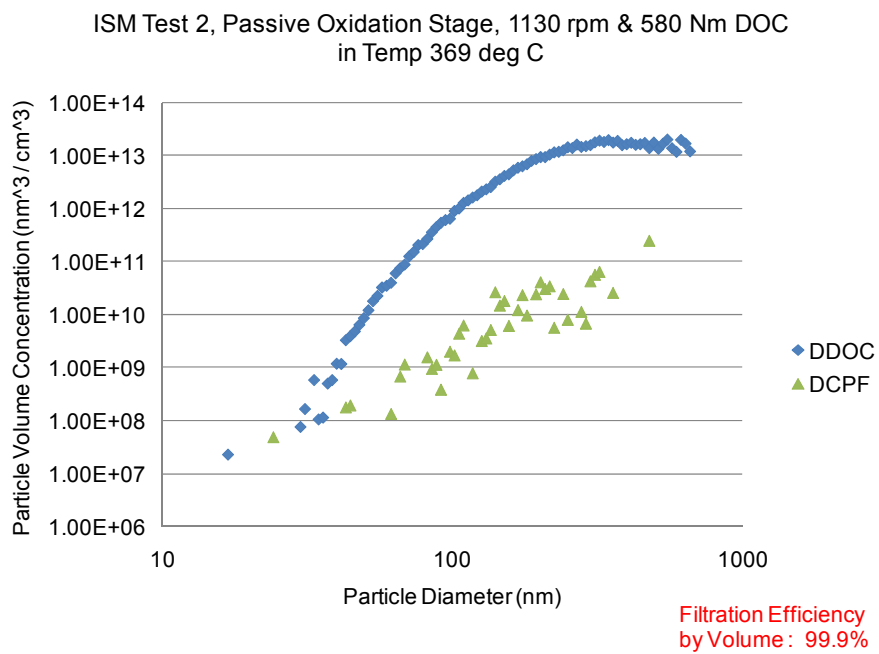
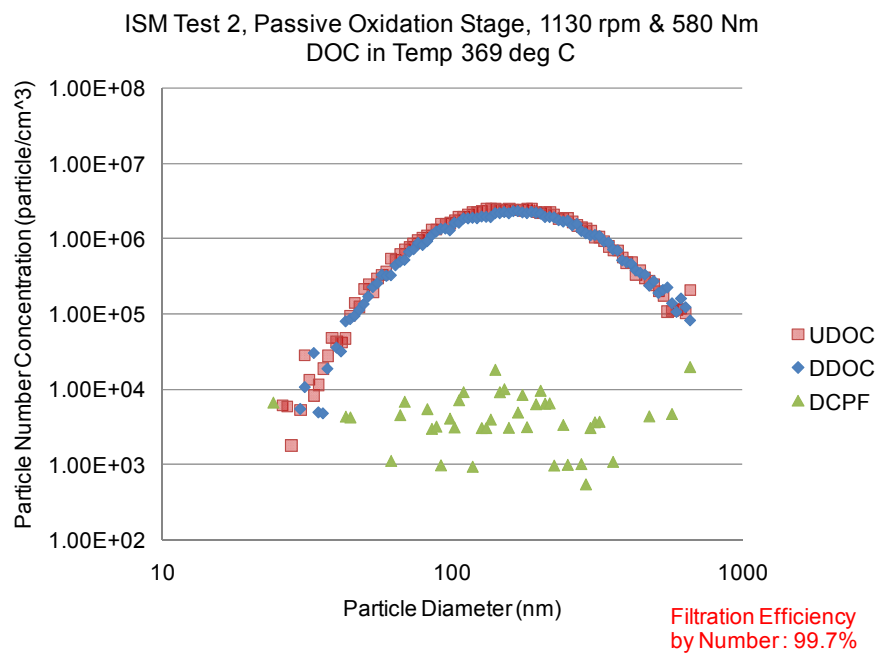
	ISL Stage 3		
	DOC Inlet Temp.	NO to NO ₂ Eff	DOC Space Velocity
	°C	%	1/h
Test 2	280	26	247k
Test 1	279	7	251k
Test 4	270	16	243k
Test 5	260	19	238k
Test 3	279	27	249k

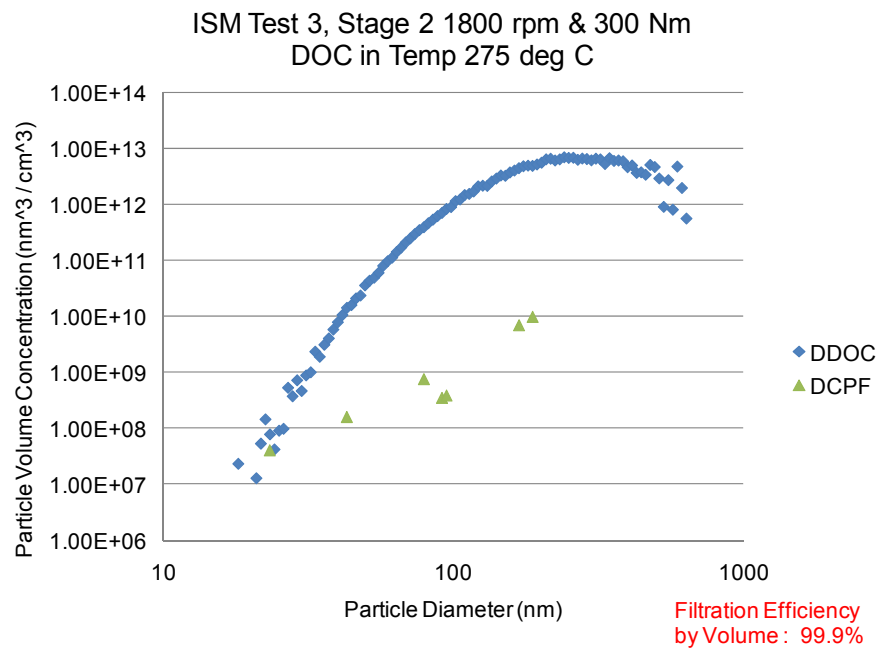
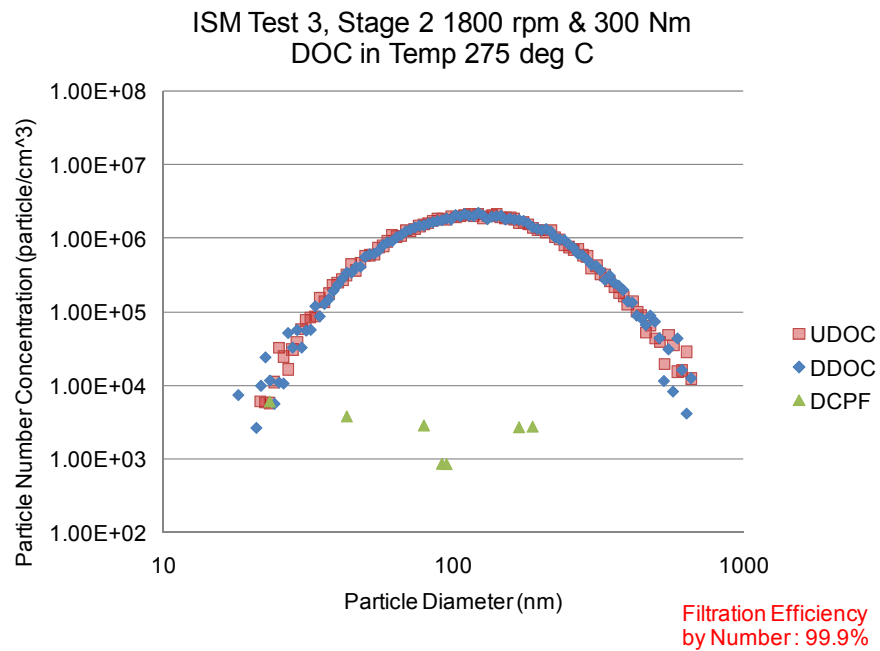
Appendix M. Particle Size Distribution Data

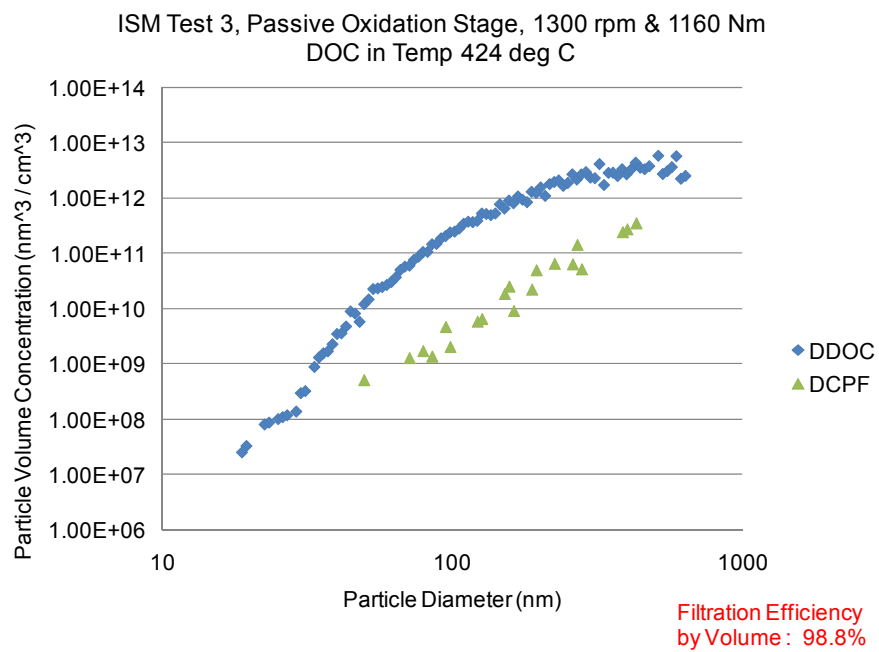
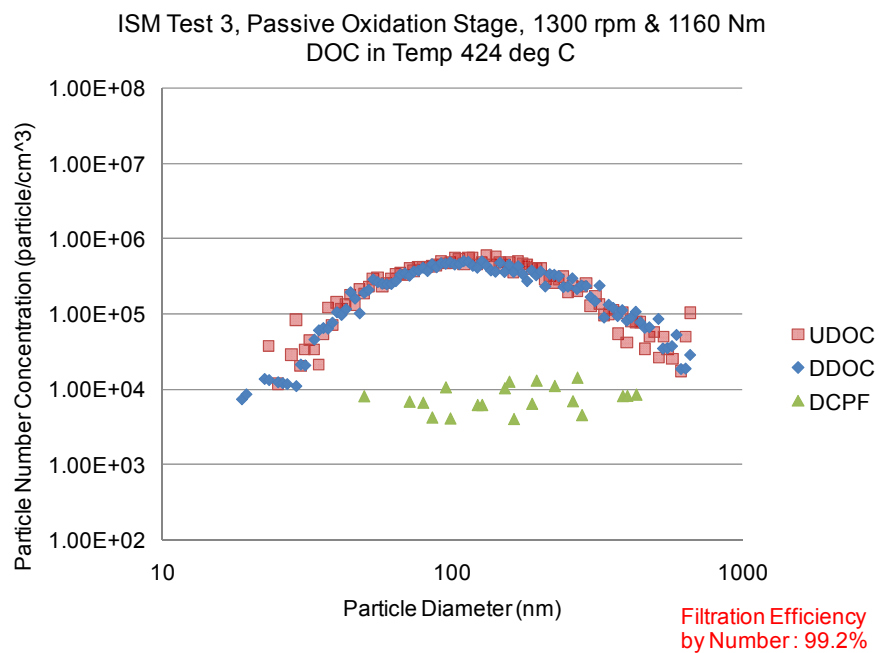


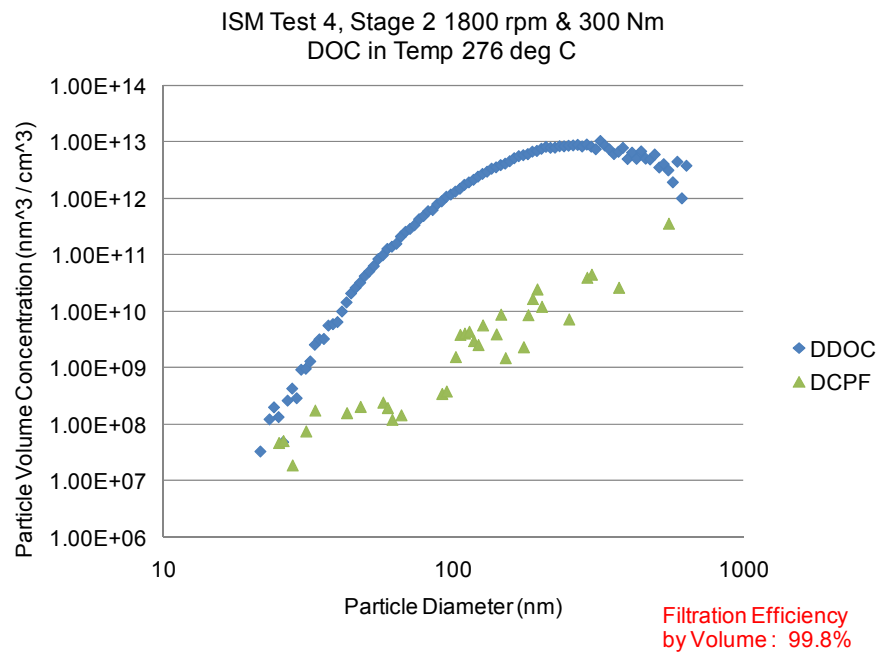
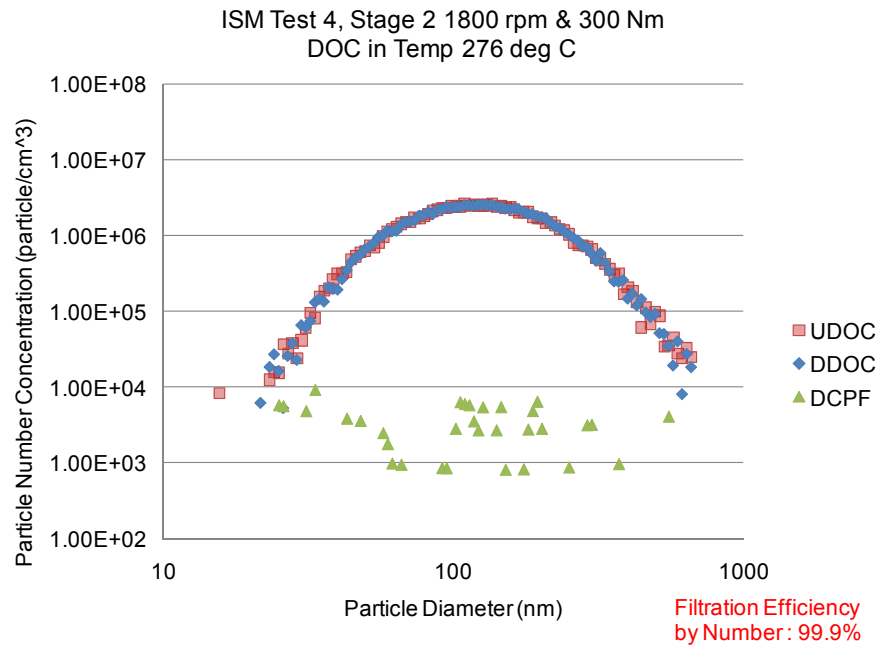


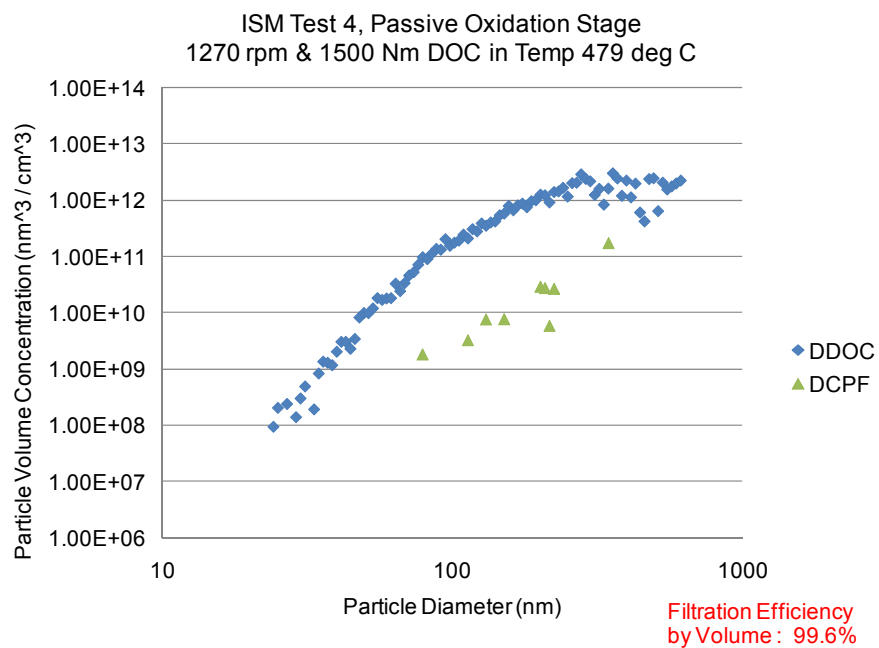
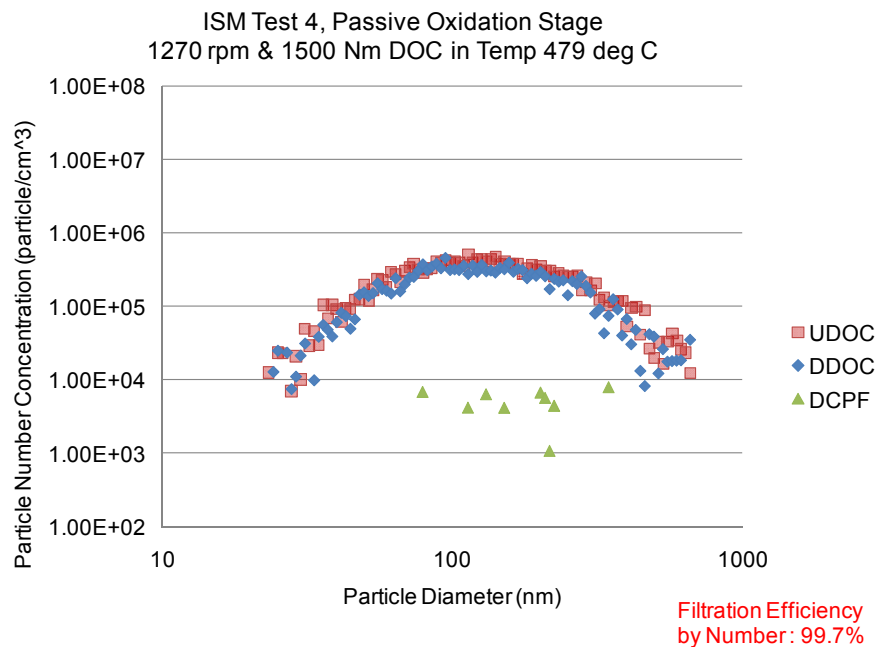


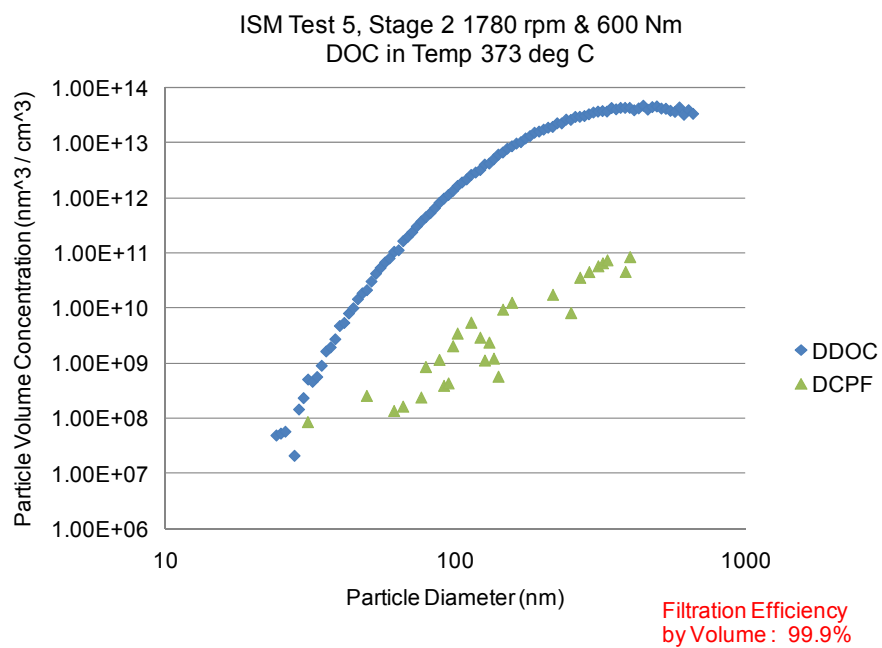
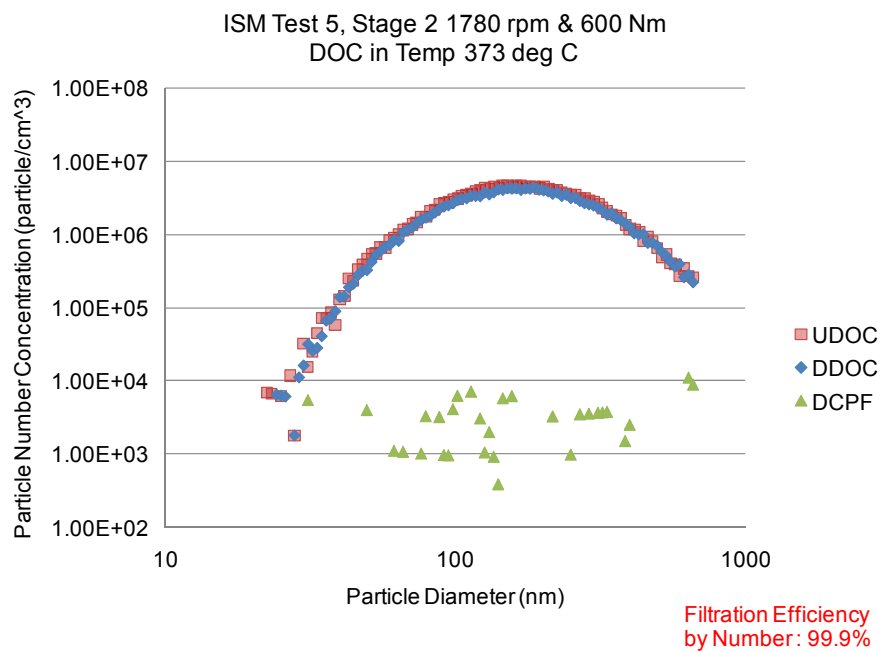




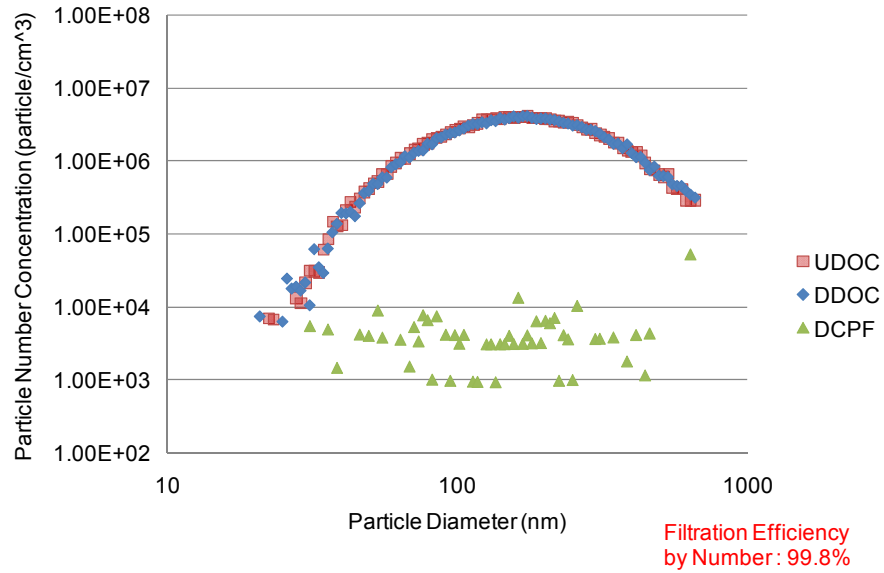




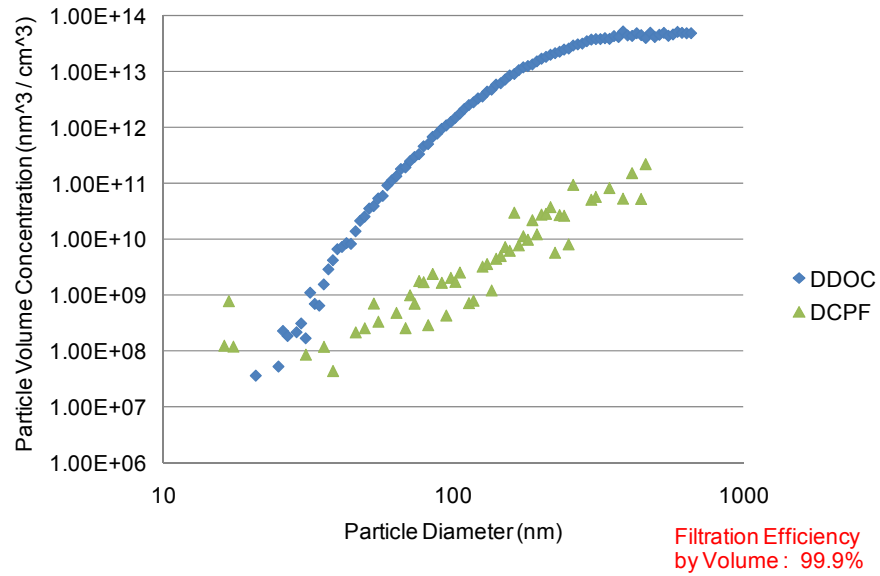




ISM Test 5, Passive Oxidation Stage 1780 rpm & 600 Nm
DOC in Temp 375 deg C



ISM Test 5, Passive Oxidation Stage 1780 rpm & 600 Nm
DOC in Temp 375 deg C



Appendix N. Mass Balances

Stage 1 Loading**																	
	Variable	Stage 1 Load Time	DOC inlet temp.	CPF inlet temp.	Exhaust Volumetric flow rate	Exhaust Mass flow rate	Engine out PM Conc.	Engine out PM mass	PM mass retained in CPF	Mass Oxidized	Percent PM oxidized	Mass Out	CPF Loading	NO2 Conc. into CPF	NO2 into CPF	NO2 into CPF	NO2/PM ratio
	Abbreviation	t _{S1}	T _{DOC IN-S1}	T _{CPF IN-S1}	Q _{exh-S1}	m _{dot-exh-S1}	C _{in}	m _{E.O.-S1}	m _{Ret-S1}	m _{Oxd-S1}	PM _{% oxd-S1}	m _{Out-S1}	m _{cpf-S1}	Y _{NO2-S1}	X _{NO2-S1}	NO _{2-into CPF}	NO ₂ Ratio-S1
Engine	Test/Units	minutes	°C	°C	scm/sec	kg/min	mg/scm	g	g	g	%	g	g/l	ppm	mg/scm	g	-
ISM	Test 1	31.6	277	273	0.183	13.3	15.1	5.1	2.8	0.0	1	2.3	0.2	111	208.7	72.4	13.8
	*Test 2	31.7	280	277	0.184	13.4	15.7	5.2	3.0	0.0	1	2.2	0.2	111	208.7	73.0	13.3
	Test 3	31.7	280	277	0.184	13.4	14.9	4.9	2.7	0.0	1	2.2	0.2	121	227.5	79.6	15.3
	Test 4	29.3	277	274	0.179	13.1	15.7	5.0	2.9	0.0	1	2.2	0.2	126	236.9	74.5	15.1
	Test 5	30.6	371	356	0.092	6.8	39.2	6.5	4.5	0.3	1	1.7	0.3	152	285.8	48.3	7.3
ISL 365	Test 2	29.4	270	269	0.177	12.9	17.2	5.6	4.0	0.0	0	1.6	0.2	36	67.7	21.1	3.9
	Test 1	30.2	269	268	0.182	13.2	18.5	6.1	4.5	0.1	0	1.6	0.3	31	58.3	19.2	3.2
	Test 4	30.3	265	264	0.181	13.2	17.6	5.5	3.8	0.0	0	1.6	0.2	32	60.2	19.8	3.4
	Test 5	28.9	255	254	0.181	13.2	16.4	5.8	2.8	0.0	0	1.6	0.2	40	75.2	23.6	4.6
	Test 3	29.4	257	256	0.181	13.2	17.5	5.7	4.0	0.0	0	1.6	0.2	27	50.8	16.2	2.9

*Used Test #1 NO2 values due to inaccurate values during Test #2

** Stage 1 loading consists of operating the engine at the loading conditions specified for the test, for approximately 30 minutes after clean out of the CPF

	Variable	NOx Conc. into CPF	NOx into CPF	NOx into CPF	NOx/PM ratio	NO2 Consumed	NO2 Consumed / NO2 into CPF	CPF Wall Velocity	Peclet Number	NO2 Conc. out of CPF	NO2 Out of CPF	NO2 Available at Exit of CPF	NO2 production	Filtration Efficiency by Mass
	Abbreviation	Y _{NOx-P.O.}	X _{NOx-P.O.}	NO _{x-into CPF}	NO _{x ratio-P.O.}	NO _{2-Cons.}	NO _{2-Cons/Into}	V _w	Pe	NO _{2-Out-ppm}	NO _{2-Out-mg}	NO _{2-Avail}	NO _{2-Prod}	-
Engine	Test/Units	ppm	mg/scm	g	-	g	-	m/s	-	ppm	mg/scm	g	g	%
ISM	Test 1	194	364.7	126.5	24.2	0.1	0.00	0.022	0.131	142	267.0	92.6	20.3	96.2
	*Test 2	194	364.7	127.6	23.2	0.1	0.00	0.022	0.132	142	267.0	93.4	20.5	96.7
	Test 3	198	372.2	130.3	25.0	0.1	0.00	0.022	0.132	149	280.1	98.0	18.5	99.1
	Test 4	181	340.3	107.1	21.7	0.1	0.00	0.022	0.128	137	257.6	81.0	6.6	97.0
	Test 5	274	515.1	87.0	13.1	2.5	0.05	0.011	0.066	167	314.0	53.0	7.2	-
SL 365	Test 2	80	150.4	47.0	8.7	0.4	0.02	0.022	0.127	51	95.9	29.9	9.2	98.1
	Test 1	75	141.0	46.5	7.6	0.4	0.02	0.022	0.130	46	86.5	28.5	9.7	97.8
	Test 4	80	150.4	49.5	8.5	0.3	0.01	0.022	0.129	49	92.1	30.3	10.8	98.2
	Test 5	90	169.2	53.1	10.3	0.3	0.01	0.022	0.129	56	105.3	33.0	9.8	98.1
	Test 3	79	148.5	47.4	8.5	0.2	0.01	0.022	0.129	47	88.4	28.2	12.2	98.1

Stage 2-01																	
	Variable	Loading Time	DOC inlet temp.	CPF inlet temp.	Exhaust Volumetric flow rate	Exhaust Mass flow rate	Engine out PM Conc.	Engine out PM mass	PM mass retained in CPF	Mass Oxidized	Percent PM oxidized	Mass Out	Total CPF Loading	NO2 Conc. into CPF	NO2 into CPF	NO2 into CPF	NO2/PM ratio
	Abbreviation	t	T _{DOC IN}	T _{CPF IN}	Q _{exh}	m _{dot-exh}	C _{in}	m _{E.O.}	m _{Ret}	m _{Oxd}	PM% oxd	m _{Out}	m _{cpf}	Y _{NO2}	X _{NO2}	NO ₂ -Into CPF	NO ₂ -ratio
Engine	Test/Units	minutes	°C	°C	scm/sec	kg/min	mg/scm	g	g	g	%	g	g/l	ppm	mg/scm	g	-
ISM	Test 1	210.2	276	267	0.181	13.1	15.1	39.6	31.2	4.6	12	3.8	1.8	91	171.1	390.5	11.3
	Test 2	240.1	277	270	0.181	13.2	15.7	46.1	34.5	7.9	17	3.7	2.0	88	165.4	431.4	10.5
	Test 3	255.1	275	265	0.179	13.0	14.9	45.8	36.3	6.8	15	2.6	2.1	95	178.6	489.3	12.0
	Test 4	258.7	276	271	0.174	12.7	15.7	47.5	38.7	5.2	11	3.6	2.3	99	186.1	502.7	11.9
	Test 5	120.2	373	349	0.091	6.8	39.2	32.2	17.9	11.6	36	2.8	1.0	158	297.0	194.9	7.6
SL 365	Test 2	150.4	269	263	0.182	13.2	17.2	33.9	25.8	5.9	17	2.2	1.5	34	63.9	105.0	3.7
	Test 1	250.4	273	270	0.184	13.4	18.5	57.3	42.2	12.2	21	2.9	2.5	30	56.4	155.9	3.0
	Test 4	230.2	269	266	0.181	13.1	17.6	49.5	38.3	8.7	18	2.5	2.2	30	56.4	141.0	3.2
	Test 5	255.3	258	258	0.182	13.2	16.4	51.5	37.5	11.5	22	2.6	2.2	32	60.2	167.7	3.7
	Test 3	230.1	264	264	0.183	13.3	17.5	49.9	38.4	9.0	18	2.5	2.2	30	56.4	142.5	3.2

*This is a running Mass Balance and takes into account the Pre Load Portion of the test

	Variable	NOx Conc. into CPF	NOx into CPF	NOx into CPF	NOx/PM ratio	NO2 Consumed	NO2 Consumed / NO2 into CPF	CPF Wall Velocity	Peclet Number	NO2 Conc. out of CPF	NO2 Out of CPF	NO2 Available at Exit of CPF	NO2 production	Filtration Efficiency by Mass	Filtration Efficiency by PSD
	Abbreviation	Y _{NOx-P.O.}	X _{NOx-P.O.}	NOx-Into CPF	NOx ratio-P.O.	NO ₂ -Cons.	NO ₂ -Cons/Into	V _w	Pe	NO ₂ -Out-ppm	NO ₂ -Out-mg	NO ₂ -Avail	NO ₂ -Prod	η _{Mass}	η _{Ipsd-vol}
Engine	Test/Units	ppm	mg/scm	g	-	g	-	m/s	-	ppm	mg/scm	g	g	%	%
ISM	Test 1	191	359.1	819.7	54.3	35.1	0.09	0.022	0.129	113	212.4	485.0	129.6	96.2	99.1
	Test 2	192	361.0	941.2	59.9	60.7	0.14	0.022	0.129	111	208.7	544.1	173.5	96.7	99.9
	Test 3	191	359.1	983.8	66.0	52.4	0.11	0.022	0.128	117	220.0	602.6	165.7	99.1	99.9
	Test 4	193	362.8	980.0	62.4	39.6	0.08	0.021	0.124	117	220.0	594.1	131.0	97.0	99.8
	Test 5	281	528.3	346.7	8.8	88.8	0.46	0.011	0.065	146	274.5	180.1	74.0	-	99.9
SL 365	Test 2	85	159.8	262.5	15.3	45.2	0.43	0.022	0.130	51	95.9	157.5	97.6	98.1	N/A
	Test 1	79	148.5	410.6	22.2	93.3	0.60	0.022	0.132	46	86.5	239.1	176.5	97.8	N/A
	Test 4	80	150.4	376.0	21.4	66.7	0.47	0.022	0.129	47	88.4	220.9	146.6	98.2	N/A
	Test 5	93	174.8	487.4	29.7	87.9	0.52	0.022	0.130	53	99.6	277.8	198.0	98.1	N/A
	Test 3	83	156.0	394.2	22.5	68.7	0.48	0.022	0.131	45	84.6	213.7	140.0	98.1	N/A

Stage 2-02																	
	Variable	Loading Time	DOC inlet temperature	CPF inlet temp.	Exhaust Volumetric flow rate	Exhaust Mass flow rate	Engine out PM Conc.	Engine out PM mass	PM mass retained in CPF	Mass Oxidized	Percent PM oxidized	Mass Out	Total CPF Loading	NO2 Conc. into CPF	NO2 into CPF	NO2 into CPF	NO2/PM ratio
	Abbreviation	t	T _{DOC IN} °C	T _{CPF IN} °C	Q _{exh} scm/sec	m _{dot-exh} kg/min	C _{in} mg/scm	m _{E.O.} g	m _{Ret} g	m _{Oxd} g	PM _{% oxd} %	m _{Out} g	m _{cpf} g/l	Y _{NO2} ppmv	X _{NO2} mg/scm	NO _{2-into CPF} g	NO _{2-ratio} -
Engine	Test/Units	minutes	°C	°C	scm/sec	kg/min	mg/scm	g	g	g	%	g	g/l	ppmv	mg/scm	g	-
ISM	Test 1	44.8	276	276	0.179	13.1	15.1	46.8	36.3	5.0	11	5.6	2.1	92	173.0	83.2	11.5
	Test 2	N/A															
	Test 3	N/A															
	Test 4	N/A															
	Test 5	N/A															
ISL 365	Test 2	99.9	273	266	0.182	13.2	17.2	52.6	39.3	10.2	19	3.2	2.3	34	63.9	69.7	3.7
	Test 1	N/A															
	Test 4	N/A															
	Test 5	N/A															
	Test 3	N/A															

*This is a running Mass Balance and takes into account the Pre Load Portion of the test

	Variable	NOx Conc. into CPF	NOx into CPF	NOx into CPF	NOx/PM ratio	NO2 Consumed	NO2 Consumed/ NO2 Available	CPF Wall Velocity	Peclet Number	NO2 Conc. out of CPF	NO2 Out of CPF	NO2 Available at Exit of CPF	NO2 production	Filtration Efficiency by Mass
	Abbreviation	Y _{NOx-P.O.}	X _{NOx-P.O.}	NO _x -Into CPF	NO _x ratio-P.O.	NO ₂ -Cons.	NO ₂ -Cons/Into	V _w	Pe	NO ₂ -Out-ppm	NO ₂ -Out-mg	NO ₂ -Avail	NO ₂ -Prod	η _{Mass}
Engine	Test/Units	ppm	mg/scm	g	-	g	-	m/s	-	ppm	mg/scm	g	g	%
ISM	Test 1	191	359.1	172.8	23.8	38.4	0.46	0.022	0.128	110	206.8	99.5	54.6	96.2
	Test 2	N/A												
	Test 3	N/A												
	Test 4	N/A												
	Test 5	N/A												
ISL 365	Test 2	85	159.8	174.3	9.3	77.9	1.12	0.022	0.130	51	95.9	104.6	112.7	98.1
	Test 1	N/A												
	Test 4	N/A												
	Test 5	N/A												
	Test 3	N/A												

Total Stage 2 Loading**																	
	Variable	Total Loading Time	DOC inlet temp.	CPF inlet temp.	Average CPF temp.	Exhaust Volumetric flow rate	Exhaust Mass flow rate	Engine out PM Conc.	Engine out PM mass	PM mass retained in CPF During Loading	Mass Oxidized	Percent PM oxidized	Mass Out	CPF Loading	NO2 Conc. into CPF	NO2 into CPF	NO2/PM ratio
	Abbreviation	t _{total-Ld}	T _{DOC IN-Ld}	T _{CPF IN-Ld}	T _{CPF-avg-s2}	Q _{exh-Ld}	m _{dot-exh-Ld}	C _{in-Ld}	m _{E.O.-Ld}	m _{Ret-Ld}	m _{Oxd-Ld}	PM% _{oxd-Ld}	m _{Out-Ld}	m _{cpf-Ld}	Y _{NO2-Ld}	X _{NO2-Ld}	NO2 _{ratio-Ld}
Engine	Test/Units	minutes	°C	°C	°C	scm/sec	kg/min	mg/scm	g	g	g	%	g	g/l	ppm	mg/scm	-
ISM	Test 1	286.6	276	267	270	0.181	13.1	15.1	46.8	36.3	5.0	11	5.6	2.1	94	176.7	11.7
	Test 2	271.8	277	270	272	0.181	13.2	15.7	46.1	34.5	7.9	17	3.7	2.0	88	165.4	10.5
	Test 3	286.8	275	265	270	0.179	13.0	14.9	45.8	36.3	6.8	15	2.6	2.1	95	178.6	12.0
	Test 4	288.0	276	271	272	0.174	12.7	15.7	47.5	38.7	5.2	11	3.6	2.3	99	186.1	11.9
	Test 5	150.8	373	349	351	0.091	6.8	39.2	32.2	17.9	11.6	36	2.8	1.0	158	297.0	7.6
ISL 365	Test 2	279.7	271	265	266	0.181	13.2	17.2	52.6	39.3	10.2	17	3.2	2.3	34	63.9	3.7
	Test 1	280.6	273	270	270	0.184	13.4	18.5	57.3	42.2	12.2	21	2.9	2.5	30	56.4	3.0
	Test 4	260.5	269	266	266	0.181	13.1	17.6	49.5	38.3	8.7	18	2.5	2.2	30	56.4	3.2
	Test 5	284.2	258	258	260	0.182	13.2	16.4	51.5	37.5	11.5	22	2.6	2.2	33	60.2	3.7
	Test 3	259.5	263	263	265	0.183	13.3	17.5	49.9	38.4	9.0	18	2.5	2.2	30	56.4	3.2

*This is a running Mass Balance and takes into account the Stage 1 Loading

**Stage 2 loading is the portion of the test where a nominal loading of 2.2 g/l is achieved while operating the engine at the specified engine speed and load used for loading

	Variable	NOx Conc. into CPF	NOx into CPF	NOx into CPF	NOx/PM ratio	NO2 Consumed	NO2 into CPF	NO2 Consumed / NO2 into CPF	CPF Wall Velocity	Peclet Number	NO2 Conc. out of CPF	NO2 Conc. of CPF	NO2 Available at Exit of CPF	NO2 production	Filtration Efficiency by Mass	Filtration Efficiency by PSD
	Abbreviation	Y _{NOx-P.O.}	X _{NOx-P.O.}	NOx _{into CPF}	NOx _{ratio-P.O.}	NO2 _{Cons.}	NO2 _{into CPF}	NO2 _{Cons/into}	V _w	Pe	NO2 _{Out-ppm}	NO2 _{Out-mg}	NO2 _{Avall}	NO2 _{Prod}	η _{Mass-Ld}	η _{psd-vol-Ld}
Engine	Test/Units	ppm	mg/scm	g	-	g	g	-	m/s		ppm	mg/scm	g	g	%	%
ISM	Test 1	192	361.0	1123	23.9	38	549.8	0.07	0.039	0.230	110	206.8	388.8	122.6	96.2	99.1
	Test 2	192	361.0	1068	23.0	61	489.3	0.12	0.040	0.233	111	208.7	392.3	36.3	96.7	99.9
	Test 3	191	359.1	1106	24.1	52	550.1	0.10	0.039	0.228	117	220.0	413.5	84.2	99.1	99.9
	Test 4	193	362.8	1091	23.1	40	559.6	0.07	0.038	0.224	117	220.0	413.5	106.5	97.0	99.8
	Test 5	281	528.3	435	13.5	89	244.6	0.36	0.023	0.137	146	274.5	516.0	360.3	-	99.9
ISL 365	Test 2	85	159.8	487	9.3	78	194.7	0.40	0.039	0.230	51	95.9	180.3	63.4	98.1	N/A
	Test 1	79	148.5	460	8.0	93	174.5	0.53	0.040	0.235	46	86.5	162.6	81.4	97.8	N/A
	Test 4	80	150.4	425	8.5	67	159.6	0.42	0.039	0.229	47	88.4	166.1	73.2	98.2	N/A
	Test 5	93	174.8	542	10.7	88	186.6	0.47	0.039	0.228	53	99.6	187.3	88.7	98.1	N/A
	Test 3	83	156.0	444	8.9	69	160.5	0.43	0.039	0.231	45	84.6	159.0	67.3	98.1	N/A

Passive Oxidation																	
	Variable	Time	DOC inlet temp.	CPF inlet temp.	Average CPF temp.	Exhaust Volumetric flow rate	Exhaust Mass flow rate	Engine out PM Conc.	Engine out PM mass During Passive Ox.	PM mass retained in CPF During Loading	Decrease of PM Mass in CPF	PM mass retained in CPF	Total Mass Available for OX	Total Mass of PM Oxidized	Percent PM oxidized	Mass Out	CPF Loading
	Abbreviation	t	T _{DOC IN-P.O.}	T _{CPF IN-P.O.}	T _{CPF-avg-P.O.}	Q _{exh-P.O.}	m _{dot-exh-P.O.}	C _{in-P.O.}	m _{E.O.-P.O.}	m _{Ret-Ld}	m _{dec-P.O.}	m _{Ret-P.O.}	m _{Available-P.O.}	m _{oxd-tot-P.O.}	PM% oxd-P.O.	m _{Out-P.O.}	m _{cpf-P.O.}
Engine	Test/Units	minutes	°C	°C	°C	scm/sec	kg/min	mg/scm	g	g	g	g	g	g	%	g	g/l
ISM	Test 1	81.1	346	324	327	0.092	6.8	32.1	14.4	36.3	2.6	33.7	50.6	16.4	32	0.5	2.0
	Test 2	89.9	369	345	348	0.092	6.8	30.6	15.2	34.5	8.4	26.0	49.6	23.1	47	0.5	1.5
	Test 3	48.9	424	404	411	0.194	14.4	5.4	3.1	36.3	31.4	4.9	39.4	34.4	87	0.0	0.3
	Test 4	22.3	479	461	463	0.228	16.9	7.1	2.2	38.7	29.0	9.6	40.8	31.1	76	0.1	0.6
	Test 5	120.1	375	352	358	0.091	6.7	39.2	25.7	17.9	-1.7	19.6	43.6	23.1	53	0.8	1.1
ISL 365	Test 2	90.2	372	362	359	0.105	7.7	6.9	3.9	39.3	23.2	16.0	43.2	27.1	63	0.1	0.9
	Test 1	141.0	263	254	252	0.076	5.6	6	3.9	42.2	1.8	40.4	46.1	5.6	12	0.1	2.4
	Test 4	41.8	420	410	409	0.203	15.1	6.5	3.3	38.3	19.4	18.9	41.6	22.6	54	0.1	1.1
	Test 5	35.6	434	437	437	0.241	18.0	13.3	6.8	37.5	16.6	20.8	44.3	23.3	53	0.1	1.2
	Test 3	81.2	361	362	365	0.104	7.7	7.0	3.5	38.4	23.3	15.1	41.9	26.8	64	0.1	0.9

	Variable	NO2 Conc. into CPF	NO2 into CPF	NO2 into CPF	NO2/PM ratio	NOx Conc. into CPF	NOx into CPF	NOx into CPF	NOx/PM ratio	NO2 Consumed	NO2 Consumed / NO2 into CPF	CPF Wall Velocity	Peclet Number	NO2 Conc. out of CPF	NO2 Out of CPF	NO2 Available at Exit of CPF	NO2 production	Filtration Efficiency by Mass
	Abbreviation	Y _{NO2-P.O.}	X _{NO2-P.O.}	NO ₂ -into CPF	NO ₂ ratio-P.O.	Y _{NOx-P.O.}	X _{NOx-P.O.}	NO _x -into CPF	NO _x ratio-P.O.	NO ₂ -Cons.	NO ₂ -Cons./into	V _w	Pe	NO ₂ -Out-ppm	NO ₂ -Out-mg	NO ₂ -Avail	NO ₂ -Prod	η _{Mass-Ld}
Engine	Test/Units	ppm	mg/scm	g	-	ppm	mg/scm	g	-	g	-	m/s	-	ppm	mg/scm	g	g	%
ISM	Test 1	138	259.4	116.1	8.1	220	413.6	185.0	12.9	125.9	1.08	0.012	0.073	122	229.4	102.6	112.5	96.2
	Test 2	112	210.6	104.4	6.9	245	460.6	228.4	15.1	177.2	1.70	0.013	0.074	123	231.2	114.7	187.5	96.7
	Test 3	168	315.8	179.8	58.5	460	864.8	492.2	160.1	264.2	1.47	0.028	0.165	172	323.4	184.1	268.5	99.1
	Test 4	86	161.7	49.3	22.8	411	772.7	235.7	108.8	238.8	4.84	0.035	0.206	97	182.4	55.6	245.1	97.0
	Test 5	163	306.4	200.9	7.8	289	543.3	356.3	13.9	177.4	0.88	0.013	0.077	146	274.5	180.0	156.4	-
ISL 365	Test 2	117	220.0	125.0	31.9	206	387.3	220.1	56.1	207.7	1.66	0.015	0.088	111	208.7	118.6	201.3	98.1
	Test 1	151	283.9	182.5	47.3	283	532.0	342.1	88.7	42.7	0.23	0.009	0.054	175	329.0	211.5	71.8	97.8
	Test 4	73	137.2	69.9	21.1	200	376.0	191.4	57.8	173.3	2.48	0.031	0.181	71	133.5	68.0	171.4	98.2
	Test 5	45	84.6	43.6	6.4	174	327.1	168.4	24.6	179.0	4.11	0.037	0.219	54	101.5	52.3	187.7	98.1
	Test 3	116	218.1	110.5	31.2	223	419.2	212.4	59.9	205.6	1.86	0.015	0.090	109	204.9	103.8	198.9	98.1

*This Mass Balance is just for the Passive Oxidation portion of the test

Stage 3 Loading																	
	Variable	Time	DOC inlet temp.	CPF inlet temp.	Exhaust Volumetric flow rate	Exhaust Mass flow rate	Engine out PM Conc.	Engine out PM mass	PM mass retained in CPF, S3	Total PM mass retained in CPF	Mass Oxidized	Percent PM oxidized	Mass Out	CPF Loading	NO2 Conc. into CPF	NO2 into CPF	NO2 into CPF
	Abbreviation	t _{S3}	T _{DOC IN-S3}	T _{CPF IN-S3}	Q _{exh-S3}	m _{dot-exh-S3}	C _{in-S3}	m _{E.O.-S3}	m _{Ret-S3}	m _{Ret-Total}	m _{Oxd-S3}	PM% oxd-S3	m _{Out-S3}	m _{cpf-S3}	Y _{NO2-S3}	X _{NO2-S3}	NO ₂ Into CPF
Engine	Test/Units	minutes	°C	°C	scm/sec	kg/min	mg/scm	g	g	g	g	%	g	g/l	ppm	mg/scm	g
ISM	Test 1	30.9	278	271	0.179	13.0	15.1	5.0	4.2	37.9	0.7	14	0.0	2.2	87	163.6	54.2
	Test 2	31.2	283	276	0.180	13.1	15.7	5.3	4.1	30.1	1.0	19	0.0	1.8	92	173.0	58.3
	Test 3	30.9	276	272	0.176	12.9	14.9	4.9	4.0	8.9	0.7	15	0.0	0.5	104	195.5	63.8
	Test 4	31.0	284	282	0.179	13.0	15.7	5.2	4.3	13.9	0.6	12	0.0	0.8	121	227.5	75.7
	Test 5	N/A															
ISL 365	Test 2	30.4	280	279	0.181	13.2	17.2	5.7	4.7	20.8	1.0	18	0.0	1.2	41	77.1	25.4
	Test 1	31.4	279	275	0.184	13.4	18.5	6.4	5.1	45.5	1.3	20	0.0	2.7	30	56.4	19.6
	Test 4	30.5	270	269	0.181	13.2	17.6	5.8	4.7	23.6	0.7	13	0.0	1.4	35	65.8	21.8
	Test 5	30.8	260	258	0.181	13.2	16.4	5.5	4.5	25.4	1.2	22	0.0	1.5	37	69.6	23.3
	Test 3	31.0	279	277	0.183	13.3	17.5	6.0	4.9	19.9	0.8	14	0.0	1.2	43	80.8	27.5

*Assumption: Oxidation rate during Post Loading is the same as total loading oxidation rate.

** Stage 3 loading consists of operating the engine at the loading conditions specified for the test, for approximately 30 minutes after passive oxidation

	Variable	NOx Conc. into CPF	NOx into CPF	NOx into CPF	NOx/PM ratio	NO2 Consumed	NO2 Consumed / NO2 into CPF	CPF Wall Velocity	Peclet Number	NO2 Conc. out of CPF	NO2 Out of CPF	NO2 Available at Exit of CPF	NO2 production	Filtration Efficiency by Mass
	Abbreviation	Y _{NOx-P.O.}	X _{NOx-P.O.}	NO _x Into CPF	NO _x ratio-P.O.	NO ₂ -Cons.	NO ₂ -Cons/Into	V _w	Pe	NO ₂ -Out-ppm	NO ₂ -Out-mg	NO ₂ -Avail	NO ₂ -Prod	η _{Mass-Ld}
Engine	Test/Units	ppm	mg/scm	g	-	g	-	m/s	-	ppm	mg/scm	g	g	%
ISM	Test 1	186	349.7	115.9	7.7	5.2	0.10	0.022	0.128	120	225.6	74.7	25.7	96.2
	Test 2	193	362.8	122.3	7.8	7.6	0.13	0.022	0.129	123	231.2	77.9	27.3	96.7
	Test 3	179	336.5	109.8	7.4	5.7	0.09	0.021	0.126	139	261.3	85.3	27.2	99.1
	Test 4	189	355.3	118.3	7.5	4.8	0.06	0.022	0.128	144	270.7	90.1	19.2	97.0
	Test 5	N/A												
ISL 365	Test 2	83	156.0	51.5	3.0	9.7	0.38	0.022	0.129	53	99.6	32.9	17.1	98.1
	Test 1	86	161.7	56.0	3.0	5.6	0.29	0.022	0.132	47	88.4	30.6	16.7	97.8
	Test 4	78	146.6	48.6	2.8	9.2	0.42	0.022	0.129	49	92.1	30.5	17.9	98.2
	Test 5	84	157.9	52.8	3.2	9.2	0.40	0.022	0.129	53	99.6	33.3	19.3	98.1
	Test 3	90	169.2	57.6	3.3	6.2	0.23	0.022	0.131	55	103.4	35.2	13.9	98.1

Appendix O. NO₂ Calculations

The calculation of NO₂ consumed is performed by taking the mass of PM oxidized during the stage and multiplying it by 7.67 which is the stoichiometric ratio of NO₂ to PM by mass. This value will not be accurate when passive and thermal oxidation are occurring in parallel and assumes that the PM is being oxidized solely by equation O1.



The conversion of either the inlet or outlet concentration of NO₂ in the concentration of parts per million (ppm) to mg/scm is shown below by equation O2.

$$m_{NO_2} = (C_{NO_2}) \left(\rho_{NO_2, std} \right) \left(\frac{m^3}{(100cm)^3} \right) \left(\frac{1 \cdot 10^6 mg}{kg} \right) \quad \text{O2}$$

m_{NO_2} = Mass concentration of NO₂, (mg/scm)

C_{NO_2} = Concentration of NO₂, (ppm)

$\rho_{NO_2, std}$ = Density of NO₂ @ standard conditions, 25 °C, 101 kpa = 1.88, $\left(\frac{kg}{m^3} \right)$

The calculation of the NO₂ mass that flows into the CPF during the time of passive oxidation (t_{eff}) is shown by equation O3. The calculation of the NO₂ mass that flows out of the CPF during the time of passive oxidation (t_{eff}) is performed in the same manner.

$$NO_{2, Into} = Q_{exh} * t_{eff} * m_{NO_2} * \frac{60}{1000} \quad \text{O3}$$

$NO_{2, Into}$ = NO₂ mass that flows into the CPF during t_{eff} , (g)

Q_{Exh} = Standard volumetric flow rate of exhaust, (scm/sec)

t_{eff} : Time of passive oxidation, (min)

m_{NO_2} = Mass concentration of NO_2 , (mg/scm)

NO_2 production is calculated by equation O4.

$$\text{NO}_{2,\text{Produced}} = \text{NO}_{2,\text{Into}} - \text{NO}_{2,\text{out}} - \text{NO}_{2,\text{Consumed}}$$

O4

Appendix P. Filter Wall Velocities

Assumptions:

1. Flow is uniform throughout CPF.
2. Exhaust flow is perpendicular to wall as it passes through the wall.
3. Porosity of the filter is 52% and this is the only restriction to flow.

Specifications for CPF: 200 CPSI

$$\frac{200 \text{ cells}}{\text{in}^2} * \frac{\text{in}^2}{(2.54 \text{ cm})^2} * \frac{(100 \text{ cm})^2}{\text{m}^2} = 310,001 \frac{\text{cells}}{\text{m}^2} \quad \text{P1}$$

Diameter of CPF: 0.2667m

$$\text{Frontal Area} = \frac{\pi}{4} (0.2667 \text{ m})^2 = 0.0559 \text{ m}^2 \quad \text{P2}$$

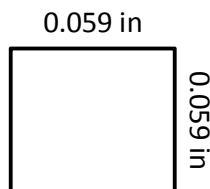
Number of Cells:

$$\# \text{ of Cells} = \frac{310,001 \text{ cells}}{\text{m}^2} * 0.0559 \text{ m}^2 = 17,318 \text{ cells} \quad \text{P3}$$

Since it is the inlet of the CPF one half of the cells are plugged

$$17,318 \text{ cells} * \frac{1}{2} = 8659 \text{ cells} \quad \text{P4}$$

Cell width:



Perimeter of Cell:

$$\text{Perimeter of cell} = 4 * 0.059 \text{ in} * \frac{2.54 \text{ cm}}{\text{in}} * \frac{\text{m}}{100 \text{ cm}} = 0.005994 \text{ m} \quad \mathbf{P5}$$

Total Open Filtration Area:

Length of CPF: 0.3048 m

$$\frac{0.005994 \text{ m}}{\text{cell}} * 8659 \text{ cell} * 0.3048 \text{ m} = 15.82 \text{ m}^2 \quad \mathbf{P6}$$

Taking into account porosity

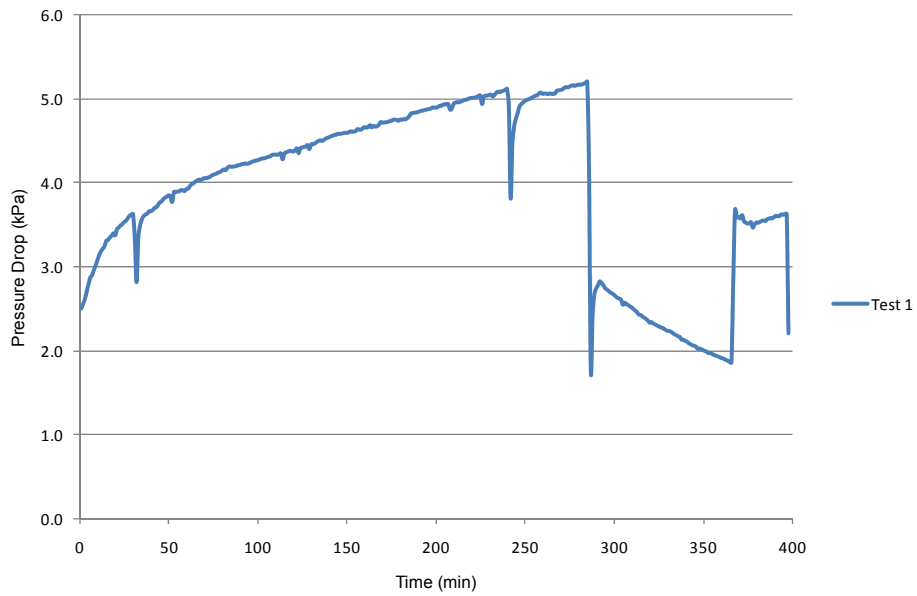
$$15.82 \text{ m}^2 * 0.52 = 8.2264 \text{ m}^2 \quad \mathbf{P7}$$

Amount of open substrate wall that exhaust can flow through: 8.2264 m²

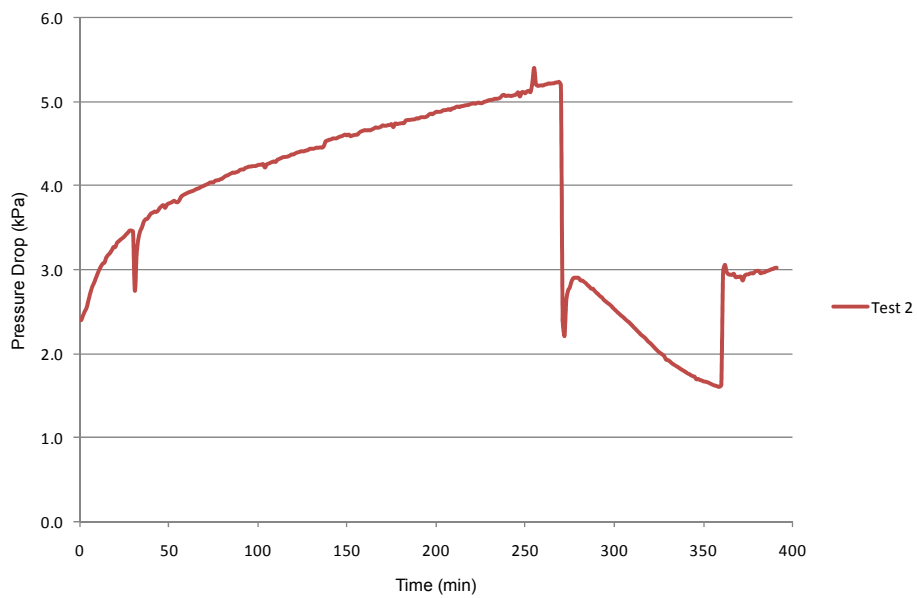
$$\text{Filter Wall Velocity} = \frac{\text{Actual Volumetric Flow Rate (m}^3/\text{s)}}{8.2264 \text{ m}^2} \quad \mathbf{P8}$$

Appendix Q. Pressure Drop Profiles

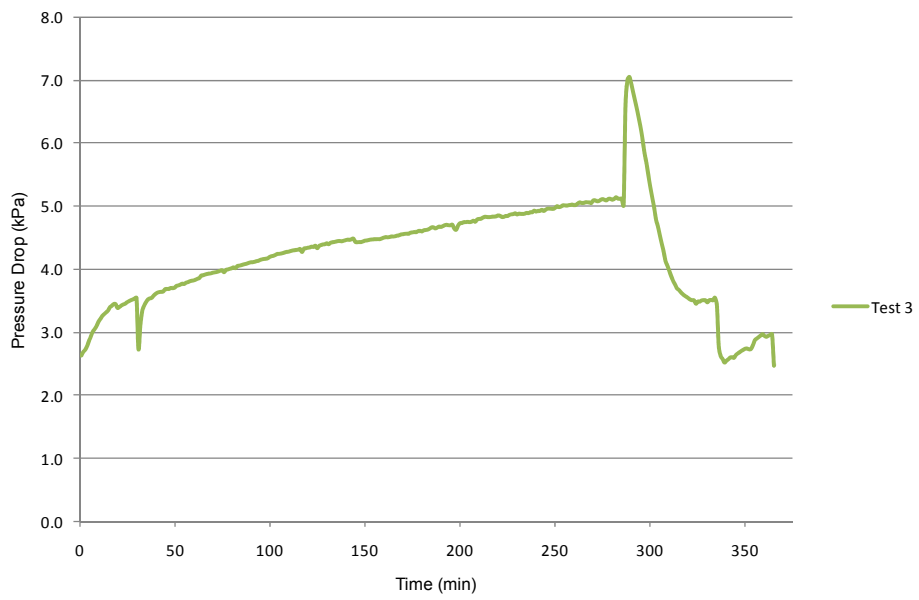
ISM Test 1



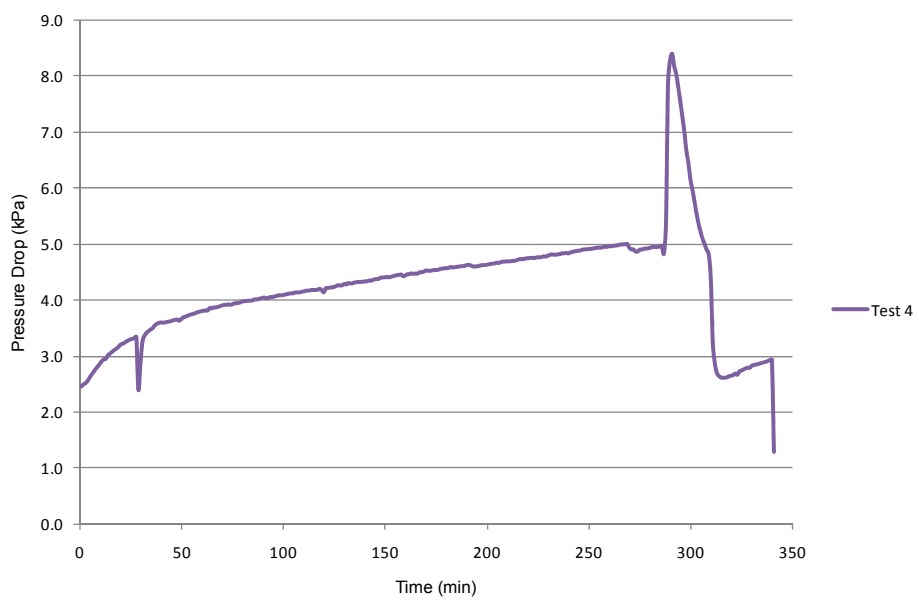
ISM Test 2



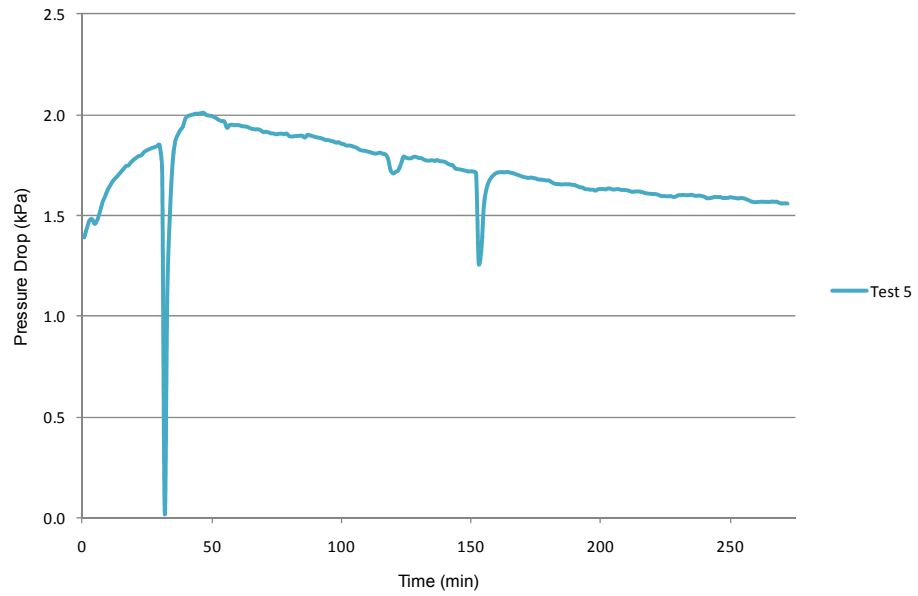
ISM Test 3



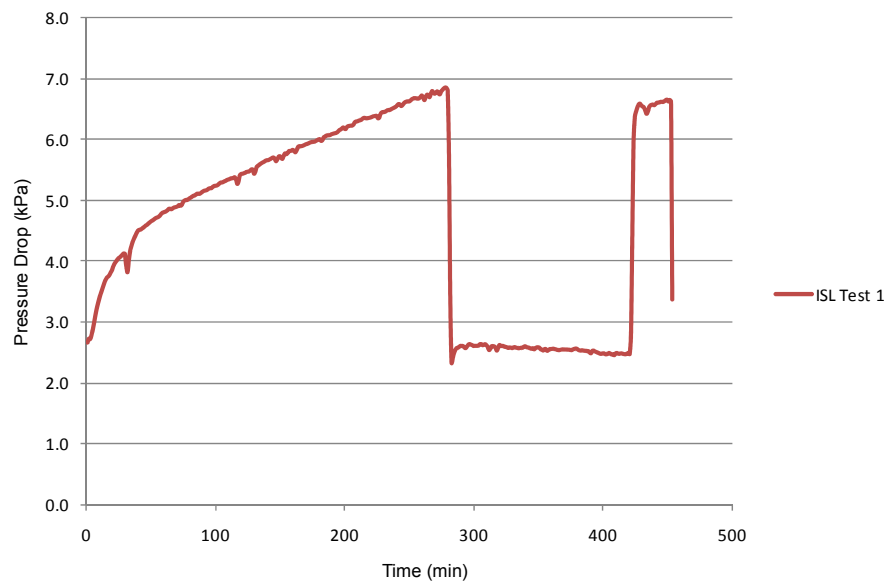
ISM Test 4



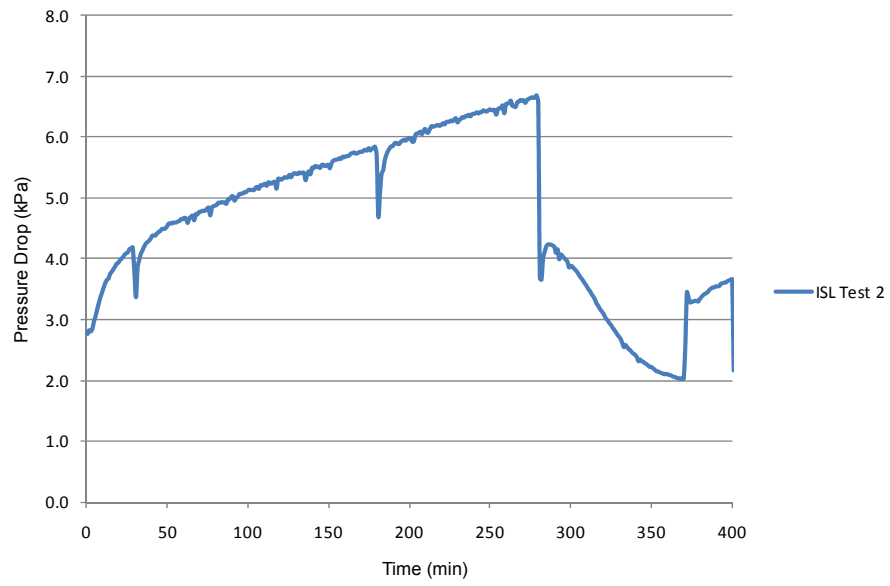
ISM Test 5



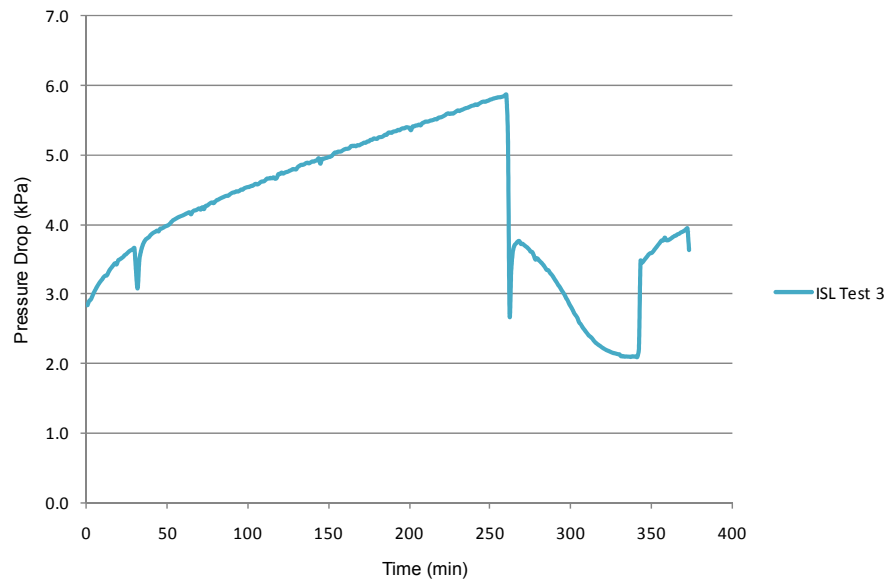
ISL Test 1



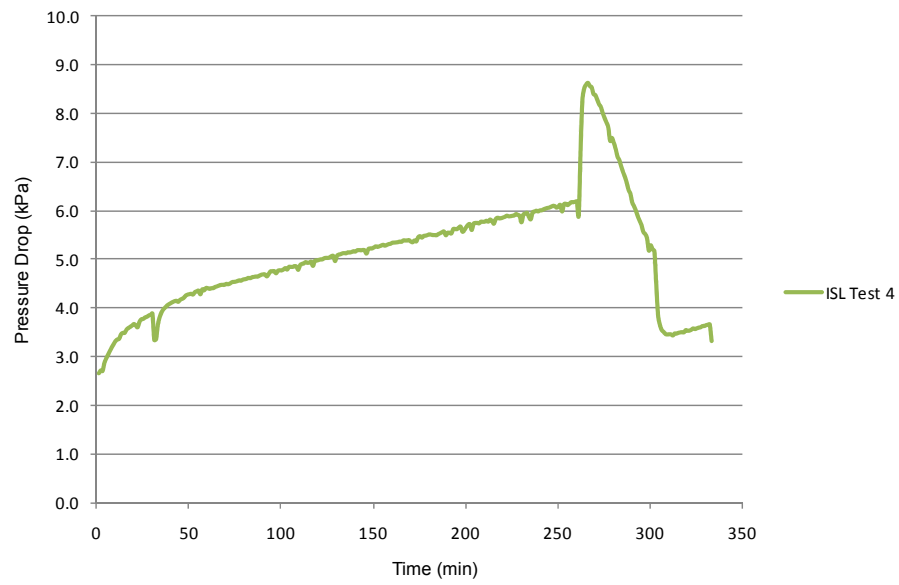
ISL Test 2



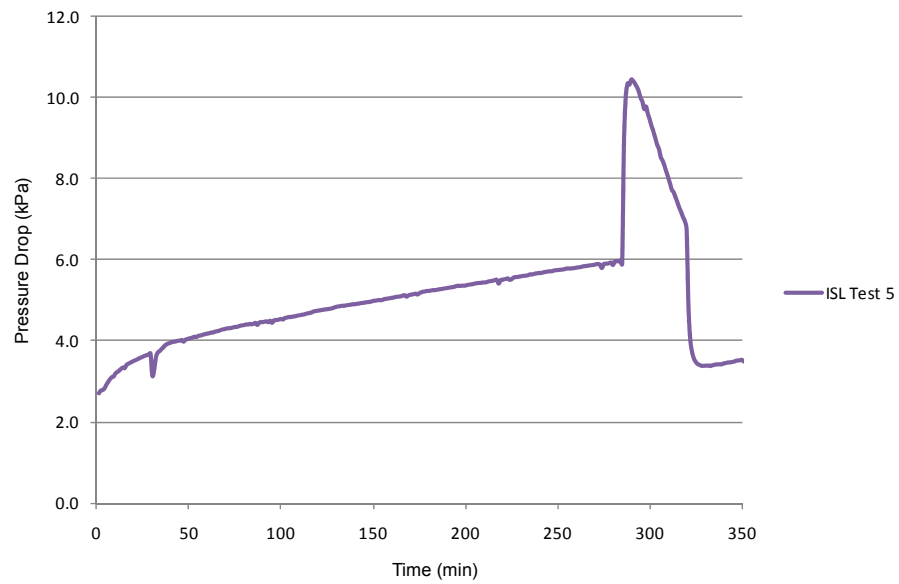
ISL Test 3



ISL Test 4



ISL Test 5



Appendix R. Relative Humidity to Absolute Humidity

Relative Humidity

$$\phi = \frac{m_v}{m_g} = \frac{\left(\frac{P_v V}{R_v T}\right)}{\left(\frac{P_g V}{R_v T}\right)} = \frac{P_v}{P_g}$$

ϕ =Relative Humidity

P_v =Partial pressure of water vapor in air

P_g =The saturation pressure of water at temperature $T=P_{\text{sat}@T}$

Absolute Humidity

$$\omega = \frac{0.622 P_v}{P - P_v}$$

ω =Absolute Humidity

P =Atmospheric pressure

$$\omega = \frac{(0.622)(\phi)(P_{\text{sat}@T})}{P - (\phi)(P_{\text{sat}@T})}$$

Reference: Cengel and Boles, Thermodynamics, An engineering Approach, 6th edition

Appendix S. Standard Operating Procedures

Standard Operating Procedure for ISL Engine Start-Up (SOP-S1)

Dyno Room

1. Check engine dynamometer lube oil, add if necessary
2. Check engine oil level, add oil in necessary
3. Check engine coolant level, add coolant if necessary
4. Open fuel supply and return valves
5. Open engine dynamometer cooling water valve
6. Open fuel heat exchanger valve on west wall
7. Open fuel barrel and insert fuel supply hose into barrel
8. Turn on the heaters for the gaseous emissions sampling lines
9. Plug in the air compressor
10. Turn on power supply to ECM and National Instruments hardware

Control Room

1. Turn on room and exhaust ventilation, see SOP- EF1
2. Toggle the engine fuel switch to the right side
3. Ensure “Day Tank” fuel switch is on
4. AVL controls
5. Turn on power switch (E2)
6. Weight switch (0.4 kg)
7. Repeat to “on”
8. Turn on “Controller” and “Dyno” switches
9. Set switches on front of dyno controller panel
10. MAN/EXT = in the “out” position

11. TORQUE/CURRENT = in the “out” position
12. MAN/EXT = in the “out” position
13. RPM/LOAD = in the “out” position
14. “MAN RSP” : 1200 RPM
15. “MAN LSP” : 200 N-m
16. Ensure that the dyno is on the “Load “ readout
17. Start up the LabView, Calterm and Emissions program simultaneously
18. Push “Ignition” button to start the engine
19. After Calterm start up adjust the necessary parameters
20. Connect “X7” connector within Pierburg bench
21. Do a visual inspection of the test cell to ensure that no problems are present
22. Perform test based on predetermined test plan.

Appendix T. Permissions to Use Copyrighted Material

Chris,
Yes, you have my permission.
Thanks,
Greg Austin

----- Original Message -----

From: "Christopher Hutton" <crhutton@mtu.edu>

To: "Greg Austin" <gtaustin@mtu.edu>

Sent: Tuesday, December 7, 2010 6:48:43 AM GMT -06:00 US/Canada Central

Subject: Thesis Figure

Greg,

I am asking permission to use figure 9 from your thesis
for my thesis. Please leave this text in your reply.

Thanks

Chris

Christopher Hutton
Michigan Technological University
Graduate Student Mechanical Engineering
MEEM B008
crhutton@mtu.edu
Office: [906-487-2886](tel:906-487-2886)
Cell: [906-369-3040](tel:906-369-3040)

Dear Christopher,

Thank you for your correspondence requesting permission to reprint several figures (noted below) from SAE paper to include in your thesis at Michigan Technological University.

Permission is hereby granted, and we request the following credit statement appear directly below the figures:

“Reprinted with permission from SAE Paper No. XXXXXX* © 200X* SAE International.” *please insert the paper number and **year of publication

Permission is for this one-time use only in print format only, and does not cover any third party copyrighted work which may appear in the material requested.

2007-01-3984, figures 3 & 10

2007-01-0041, figure 5

2008-01-0329, figure 7

2002-01-0428, figure 4

2006-01-0266, figure 22

Again, thank you for contacting SAE for this permission.

Regards,

Terri Kelly

Intellectual Property Rights Administrator

SAE International

Phone: 001.[724.772.4095](tel:724.772.4095); Fax: 001.[724.776.9765](tel:724.776.9765)

E-mail: terri@sae.org

-----Original Message-----

From: Christopher Hutton [<mailto:crhutton@mtu.edu>]

Sent: Sunday, November 14, 2010 9:42 PM

To: copyright

Subject: Request for permission to use copyrighted figures

Hello,

Attached please find a Microsoft Word document with a request to use a total of 6 figures from 5 different S.A.E. publications in my Master's thesis. I did not realize that there was a 4-6 week lead time and I am planning to finish my degree December 17, 2010. If there is anything that could be done to expedite the process it would be greatly appreciated. If you have any question please do not hesitate to contact me at the listed information below.

Sincerely

Christopher Hutton

Christopher Hutton
Michigan Technological University
Graduate Student Mechanical Engineering
MEEM B008
crhutton@mtu.edu
Office: [906-487-2886](tel:906-487-2886)
Cell: [906-369-3040](tel:906-369-3040)

ELSEVIER LICENSE
TERMS AND CONDITIONS

Dec 12, 2010

This is a License Agreement between Christopher R Hutton ("You") and Elsevier ("Elsevier") provided by Copyright Clearance Center ("CCC"). The license consists of your order details, the terms and conditions provided by Elsevier, and the payment terms and conditions.

All payments must be made in full to CCC. For payment instructions, please see information listed at the bottom of this form.

Supplier

Elsevier Limited
The Boulevard, Langford Lane
Kidlington, Oxford, OX5 1GB, UK

Registered Company Number

1982084

Customer name

Christopher R Hutton

Customer address

210 Vivian St

Hancock, MI 49930

License number

2547970468215

License date

Nov 14, 2010

Licensed content publisher

Elsevier

Licensed content publication

Fuel

Licensed content title

Modeling of soot oxidation by NO₂ in various types of diesel particulate filters

Licensed content author

M. Schejbal, J. Štěpánek, M. Marek, P. Kočí, M. Kubíček

Licensed content date

September 2010

Licensed content volume number

89

Licensed content issue number

9

Number of pages

11

Start Page

2365

End Page

2375

Type of Use

reuse in a thesis/dissertation

Portion

figures/tables/illustrations

Number of figures/tables/illustrations

1

Format

print

Are you the author of this Elsevier article?

No

Will you be translating?

No

Order reference number

Title of your thesis/dissertation

An Experimental Investigation Into The Passive Oxidation Of Particulate Matter
In A Catalyzed Particulate Filter

Expected completion date

Dec 2010

Estimated size (number of pages)

150

Elsevier VAT number

GB 494 6272 12

Permissions price

0.00 USD

Value added tax 0.0%

0.0 USD / 0.0 GBP

Total

0.00 USD

Terms and Conditions

INTRODUCTION

1. The publisher for this copyrighted material is Elsevier. By clicking "accept" in connection with completing this licensing transaction, you agree that the following terms and conditions apply to this transaction (along with the Billing and Payment terms and conditions established by Copyright Clearance Center, Inc. ("CCC"), at the time that you opened your Rightslink account and that are available at any time at <http://myaccount.copyright.com>).

GENERAL TERMS

2. Elsevier hereby grants you permission to reproduce the aforementioned material subject to the terms and conditions indicated.

3. Acknowledgement: If any part of the material to be used (for example, figures) has appeared in our publication with credit or acknowledgement to another source, permission must also be sought from that source. If such permission is not obtained then that material may not be included in your publication/copies. Suitable acknowledgement to the source must be made, either as a footnote or in a reference list at the end of your publication, as follows:

"Reprinted from Publication title, Vol /edition number, Author(s), Title of article / title of chapter, Pages No., Copyright (Year), with permission from Elsevier [OR APPLICABLE

SOCIETY COPYRIGHT OWNER].” Also Lancet special credit - “Reprinted from The Lancet, Vol. number, Author(s), Title of article, Pages No., Copyright (Year), with permission from Elsevier.”

4. Reproduction of this material is confined to the purpose and/or media for which permission is hereby given.

5. Altering/Modifying Material: Not Permitted. However figures and illustrations may be altered/adapted minimally to serve your work. Any other abbreviations, additions, deletions and/or any other alterations shall be made only with prior written authorization of Elsevier Ltd. (Please contact Elsevier at permissions@elsevier.com)

6. If the permission fee for the requested use of our material is waived in this instance, please be advised that your future requests for Elsevier materials may attract a fee.

7. Reservation of Rights: Publisher reserves all rights not specifically granted in the combination of (i) the license details provided by you and accepted in the course of this licensing transaction, (ii) these terms and conditions and (iii) CCC's Billing and Payment terms and conditions.

8. License Contingent Upon Payment: While you may exercise the rights licensed immediately upon issuance of the license at the end of the licensing process for the transaction, provided that you have disclosed complete and accurate details of your proposed use, no license is finally effective unless and until full payment is received from you (either by publisher or by CCC) as provided in CCC's Billing and Payment terms and conditions. If full payment is not received on a timely basis, then any license preliminarily granted shall be deemed automatically revoked and shall be void as if never granted. Further, in the event that you breach any of these terms and conditions or any of CCC's Billing and Payment terms and conditions, the license is automatically revoked and shall be void as if never granted. Use of materials as described in a revoked license, as well as any use of the materials beyond the scope of an unrevoked license, may constitute copyright infringement and publisher reserves the right to take any and all action to protect its copyright in the materials.

9. Warranties: Publisher makes no representations or warranties with respect to the licensed material.

10. Indemnity: You hereby indemnify and agree to hold harmless publisher and CCC, and their respective officers, directors, employees and agents, from and against any and all claims arising out of your use of the licensed material other than as specifically authorized pursuant to this license.

11. No Transfer of License: This license is personal to you and may not be sublicensed, assigned, or transferred by you to any other person without publisher's written permission.

12. No Amendment Except in Writing: This license may not be amended except in a writing signed by both parties (or, in the case of publisher, by CCC on publisher's behalf).

13. Objection to Contrary Terms: Publisher hereby objects to any terms contained in any purchase order, acknowledgment, check endorsement or other writing prepared by you, which terms are inconsistent with these terms and conditions or CCC's Billing and Payment terms and conditions. These terms and conditions, together with CCC's Billing and Payment terms and conditions (which are incorporated herein), comprise the entire agreement between you and publisher (and CCC) concerning this licensing transaction. In the event of any conflict between your obligations established by these terms and conditions and those established by CCC's Billing and Payment terms and conditions, these terms and conditions shall control.

14. Revocation: Elsevier or Copyright Clearance Center may deny the permissions described in this License at their sole discretion, for any reason or no reason, with a full refund payable to you. Notice of such denial will be made using the contact information provided by you. Failure to receive such notice will not alter or invalidate the denial. In no event will Elsevier or Copyright Clearance Center be responsible or liable for any costs, expenses or damage incurred by you as a result of a denial of your permission request, other than a refund of the amount(s) paid by you to Elsevier and/or Copyright Clearance Center for denied permissions.

LIMITED LICENSE

The following terms and conditions apply only to specific license types:

15. Translation: This permission is granted for non-exclusive world English rights only unless your license was granted for translation rights. If you licensed translation rights you may only translate this content into the languages you requested. A professional translator must perform all translations and reproduce the content word for word preserving the integrity of the article. If this license is to re-use 1 or 2 figures then permission is granted for non-exclusive world rights in all languages.

16. Website: The following terms and conditions apply to electronic reserve and author websites:

Electronic reserve: If licensed material is to be posted to website, the web site is to be password-protected and made available only to bona fide students registered on a relevant course if:

This license was made in connection with a course,

This permission is granted for 1 year only. You may obtain a license for future website posting,

All content posted to the web site must maintain the copyright information line on the bottom of each image,

A hyper-text must be included to the Homepage of the journal from which you are licensing at <http://www.sciencedirect.com/science/journal/xxxxx> or the Elsevier homepage for books at <http://www.elsevier.com> , and

Central Storage: This license does not include permission for a scanned version of the material to be stored in a central repository such as that provided by Heron/XanEdu.

17. Author website for journals with the following additional clauses:

All content posted to the web site must maintain the copyright information line on the bottom of each image, and

the permission granted is limited to the personal version of your paper. You are not allowed to download and post the published electronic version of your article (whether

PDF or HTML, proof or final version), nor may you scan the printed edition to create an electronic version,

A hyper-text must be included to the Homepage of the journal from which you are licensing at <http://www.sciencedirect.com/science/journal/xxxxx> , As part of our normal production process, you will receive an e-mail notice when your article appears on Elsevier's online service ScienceDirect (www.sciencedirect.com). That e-mail will include the article's Digital Object Identifier (DOI). This number provides the electronic link to the published article and should be included in the posting of your personal version. We ask that you wait until you receive this e-mail and have the DOI to do any posting.

Central Storage: This license does not include permission for a scanned version of the material to be stored in a central repository such as that provided by Heron/XanEdu.

18. Author website for books with the following additional clauses:

Authors are permitted to place a brief summary of their work online only.

A hyper-text must be included to the Elsevier homepage at <http://www.elsevier.com>

All content posted to the web site must maintain the copyright information line on the bottom of each image

You are not allowed to download and post the published electronic version of your chapter, nor may you scan the printed edition to create an electronic version.

Central Storage: This license does not include permission for a scanned version of the material to be stored in a central repository such as that provided by Heron/XanEdu.

19. Website (regular and for author): A hyper-text must be included to the Homepage of the journal from which you are licensing at <http://www.sciencedirect.com/science/journal/xxxxx> or for books to the Elsevier homepage at <http://www.elsevier.com>

20. Thesis/Dissertation: If your license is for use in a thesis/dissertation your thesis may be submitted to your institution in either print or electronic form. Should your thesis

be published commercially, please reapply for permission. These requirements include permission for the Library and Archives of Canada to supply single copies, on demand, of the complete thesis and include permission for UMI to supply single copies, on demand, of the complete thesis. Should your thesis be published commercially, please reapply for permission.

21. Other Conditions:

v1.6

Gratis licenses (referencing \$0 in the Total field) are free. Please retain this printable license for your reference. No payment is required.

If you would like to pay for this license now, please remit this license along with your payment made payable to "COPYRIGHT CLEARANCE CENTER" otherwise you will be invoiced within 48 hours of the license date. Payment should be in the form of a check or money order referencing your account number and this invoice number RLNK10882847.

Once you receive your invoice for this order, you may pay your invoice by credit card. Please follow instructions provided at that time.

Make Payment To:
Copyright Clearance Center
Dept 001
P.O. Box 843006
Boston, MA 02284-3006

If you find copyrighted material related to this license will not be used and wish to cancel, please contact us referencing this license number 2547970468215 and noting the reason for cancellation.

Questions? customercare@copyright.com or +1-877-622-5543 (toll free in the US) or +1-978-646-2777.